Investigation of heavy-light four-quark systems by means of Lattice QCD

Dissertation
zur Erlangung des Doktorgrades der Naturwissenschaften

vorgelegt beim Fachbereich Physik der Goethe-Universität Frankfurt am Main

von Antje Peters aus Westerland

Frankfurt 2017 (D 30)

Zusammenfassung

Die Suche nach dem Allerkleinsten und Unteilbaren ist ein wichtiger Aspekt der menschlichen Kultur. Das Konzept eines Grundbausteins aller Materie reicht bis in das antike Griechenland zurück. Die Suche nach dem Unteilbaren wird, seit es die technischen Voraussetzungen dazu gibt, unermüdlich und mit großem Aufwand betrieben. Hielt man zunächst das Atom, dann seinen Kern und schließlich dessen Bestandteile für unteilbar, wissen wir heute, dass es etwas gibt, was noch kleiner ist: das Quark.

Aus Quarks zusammengesetzte Objekte werden Hadronen genannt. Es gibt zwei Arten von Hadronen: Baryonen, die einen halbzahligen Spin tragen und aus einer ungeraden Anzahl von Quarks zusammengesetzt sind, und Mesonen mit ganzzahligem Spin, die aus Paaren von Quark und Antiquark bestehen. Die bekanntesten Vertreter der Baryonen sind das Proton und das Neutron. Anders als Proton und Neutron, die im Atomkern eine lange Lebensdauer aufweisen, sind andere Baryonen und Mesonen extrem instabil und können nur in Teilchendetektoren beobachtet werden. Das Verständnis der hadronischen Systeme schafft letztendlich ein Verständnis des Aufbaus der Materie, aus der der Mensch und die Umwelt, die ihn umgibt, aufgebaut sind. Bisher wurden sechs verschiedene Arten von Quarks, die sogenannten Flavors, beobachtet. Die sechs Flavors werden in drei Gruppen sortiert, die Generationen genannt werden. Die beiden leichtesten Quarks, u und d bzw. up and $down$, gehören der ersten Generation an. Die zweite Generation wird von den mittelschweren Quarks gebildet, die s und c, bzw. $strange$ und $charm$ genannt werden. Ihre Masse ist einige hundert Mal größer als die der leichten Quarks. Der dritten Generation gehören die schwersten Quarks an, deren Namen b oder $bottom/beauty$ und t oder top lauten. Ihre Masse liegt um einige tausend Mal höher als die der leichten Quarks. Der Grund dafür, dass es ausgerechnet drei Generationen gibt und nicht mehr oder weniger oder dass sich die Massen der Quarks so stark unterscheiden, ist bisher nicht bekannt. Das Standardmodell der Teilchenphysik, das alle gängigen Theorien der Elementarteilchen zusammenfasst, kann diese Frage nicht beantworten. Unter anderem deswegen ist es wichtig, das Standardmodell laufend infrage zu stellen, um anhand möglicherweise auftretender Widersprüche auf Erweiterungen zu stoßen, im Rahmen derer offene Fragen beantwortet werden können. Quarks haben eine Reihe ungewöhnlicher Eigenschaften. So nimmt beispielsweise ihre elektrische Ladung nichtganzzahlige Werte an. Neben einer elektrischen Ladung tragen sie noch einer weitere Art der Ladung, die Farbladung genannt wird. Auch Gluonen, die Kraftteilchen, die die Wechselwirkung zwischen Quarks vermitteln, tragen Farbladung. Farbgeladene Objekte wechselwirken miteinander. Die heute gängige Theorie der Quarks und Gluonen wird Quantenchromodynamik (QCD) genannt. Eine wichtige Anforderung an die Quantenchromodynamik ist, dass sie die Selbstwechselwirkung der Gluonen aufgrund ihrer Farbladung beschreibt. Diese Selbstwechselwirkung sorgt dafür, dass niederenergetische Observablen wie Hadronenmassen nicht im Rahmen der Störungstheorie beschrieben werden können, was eine analytische Berechnung der Gleichungen, die diese Observablen beschreiben, ohne weitere Annahmen unmöglich macht. Ein möglicher Ansatz zu Lösung dieses Problems bietet die Gittereichtheorie, auch Gitter-QCD oder Lattice QCD genannt. Sie geht von einer Diskretisierung der Raumzeit und der Objekte der Feldtheorie aus. Im Rahmen des sogenannten Pfadintegralformalismus können die Gleichungen der QCD numerisch gelöst werden. Im Allgemeinen sind diese Rechnungen sehr aufwändig, sodass sie nur auf Hochleistungsrechnern durchgeführt werden können. Ein Vorteil der Gittereichtheorie ist, dass neben der puren QCD keine weiteren Annahmen

in die Berechnungen einfließen. Nimmt man an, dass die QCD die Natur perfekt beschreibt, kann man bei der Ausführung von Gitter-QCD-Rechnungen folglich von Experimenten am Computer sprechen. In diesem Sinne kann man Gitter-QCD als Mischung aus theoretischer Physik, Experimentalphysik und Computational Science verstehen. Ein weiterer Vorteil der Gitter-QCD ist, dass sie eine quantitative Bestimmung aller systematischen Fehler ermöglicht. Bei diesen Fehlern handelt es sich zum Beispiel um die endliche Ausdehnung des vierdimensionalen Gitters, den nichtverschwindenden Gitterabstand und die häufig verwendeten unphysikalisch hohen Quarkmassen, die aus numerischen Gründen verwendet werden müssen. Nach Extrapolation zu unendlich großen Gittervolumina, zum Kontinuumsgrenzwert und zu physikalischen Quarkmassen lassen sich physikalische Werte mit genau bestimmten Fehlern angeben.

In den 1950er-Jahren belief sich die Anzahl der mit Hilfe von Teilchendetektoren entdeckten Hadronen auf eine derartige Menge, dass von einem regelrechten „Teilchenzoo" die Rede war. Je genauer man suchte, desto mehr Teilchen fand man. Mit Hilfe des Konzepts des Quarks wurde ein Schema entwickelt, nach dem die vielen verschiedenen Baryonen und Mesonen, die bei Messungen mit Teilchendetektoren gemessen worden waren, klassifiziert werden konnten. Dieses Schema trägt den Namen *constituent quark model* oder kurz *quark model*, also Quarkmodell. Im Rahmen des Quarkmodells können Baryonen und Mesonen in sogenannte $SU(N)$-Multipletts eingeordnet werden, wobei N die anzahl der berücksichtigten Flavors benennt. Dadurch wurde es z.B. möglich, neue Teilchen vorherzusagen, die kurz darauf tatsächlich in Teilchendetektoren gefunden wurden. Dies beweist die weitgehende Gültigkeit des Quarkmodells. Das Modell beschreibt Mesonen als gebundene Zustände, die aus einem Quark und einem Antiquark beliebigen Flavors zusammengesetzt sind, kurz $q\bar{q}$. Baryonen werden als gebundene Systeme von drei Quarks qqq beschrieben. Dies sind jedoch nicht die einzigen beiden Arten von Hadronen, die im Rahmen der QCD erlaubt sind. Jenseits des Quarkmodells sind zahlreiche weitere Strukturen denkbar. Möglich wären unter anderem auch Zustände, die nur aus Gluonen bestehen (*Glueballs*), Zustände aus einem Quark-Antiquark-Paar und einem angeregten Gluon (*Hybrids*) und baryonische und mesonische Multiquark-Systeme wie $\bar{q}qqqq$ (*Pentaquarks*) und $\bar{q}\bar{q}qq$ (*Tetraquarks*).

Im Fokus dieser Arbeit steht das Tetraquark. In Teilchendetektoren wie dem LHCb in der Schweiz oder Belle in Japan wurden in jüngerer Zeit mesonische Zustände gefunden, die für Tetraquark-Kandidaten gehalten werden. Ihre Masse und ihre Zerfallsprodukte belegen, dass sie schweres Quarkonium beinhalten, also Paare von b- oder c-Quark und -Antiquark. Darüber hinaus tragen sie eine elektrische Ladung, die nicht vom ungeladenen Quarkonium rühren kann. Somit liegt der Schluss nahe, dass die Zustände noch ein weiteres, leichtes Quark-Antiquark-Paar enthalten. Aus diesem Grund sind die gefundenen Zustände Kandidaten für sogenannte Tetraquarks. Diese Arbeit befasst sich mit der Beschreibung und Untersuchung solcher Tetraquark-Zustände. Es werden die Eigenschaften und Symmetrien der Zustände ermittelt sowie Techniken zur numerischen Berechnung bereitgestellt. Es wird ein bisher noch nicht beobachteter Zustand postuliert und ein Erklärungsansatz für einen weiteren bisher noch nicht hinreichend verstandenen Zustand geliefert. Die Systeme, um die es in dieser Arbeit hauptsächlich geht, enthalten vier Quarks unterschiedlicher Masse. Zwei Quarks sind im Verhältnis zu den anderen so schwer, dass die Annahme einer unendlich großen Masse eine sinnvolle Näherung darstellt. Die beiden anderen sind leicht und voll dynamisch. In dieser statisch-leichten Näherung ist es möglich, das Potential der schweren Quarks in Anwesenheit
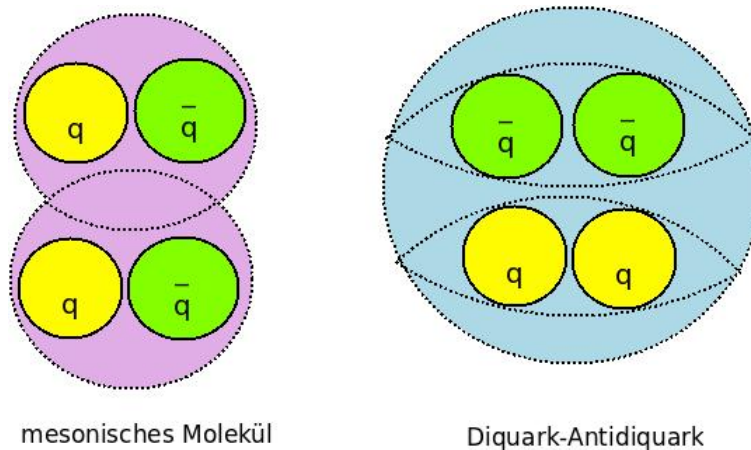
Abbildung 0.1.: Skizzen zweier der bekanntesten möglichen Tetraquark-Strukturen: Das mesonische Molekül und der Diquark-Antidiquark-Zustand.

der leichten Quarks zu bestimmen und zu überprüfen, ob es attraktiv genug ist, um dafür zu sorgen, dass die vier Quarks einen gebundenen Zustand bilden. Dieses Vorgehen ist als Born-Oppenheimer-Approximation bekannt. Die wesentliche Observable, die berechnet werden muss, ist das Vier-Quark-Potential. Die Berechnung erfolgt unter Verwendung von Werkzeugen der Hadronenspektroskopie. Zentraler Gegenstand der Hadronspektroskopie ist die Ermittlung des dem Potential zugrunde liegenden Objektes, der Korrelationsfunktion. Es gilt, den numerischen Rechenaufwand durch Anwendung diverser Techniken möglichst gering zu halten und die Genauigkeit der Berechnung dabei zu maximieren.

Mesonen, die aus einem schweren b-Quark und einem leichteren u-,d-,s- oder c-Quark bestehen, werden B-Mesonen genannt. Ein Molekül aus zwei B-Mesonen ist eine mögliche Struktur, in der ein Tetraquark vorliegen kann. Eine andere Möglichkeit ist eine sogenannte Diquark-Antidiquark-Struktur. In Abbildung 0.1 sind beide Fälle skizziert. Der Fall des mesonischen Moleküls ist Gegenstand dieser Arbeit. Folglich ist die Beschreibung von B-Mesonen und ihrer Eigenschaften und Symmetrien in der statisch-leichten Näherung ein wichtiger erster Schritt für die Untersuchung von Tetraquark-Zuständen. Die Wechselwirkung verschiedener B-Mesonen erzeugt verschiedene Vier-Quark-Zustände. So können zwei B-Mesonen zusammen einen BB-Zustand, eine mögliche Struktur des $\bar{b}\bar{b}ud$-Zustandes, beschreiben und ein B und ein $\bar{B}$-Meson einen $B\bar{B}$-Zustand, also eine mögliche Manifestation eines $b\bar{b}u\bar{d}$-Zustandes.

Die Doktorarbeit enthält drei Ergebnisteile. Im ersten Ergebnisteil der Arbeit werden die verschiedenen Potentiale aufgeführt, die zu einem $\bar{b}\bar{b}ud$- oder BB-Zustand gehören, und die jeweiligen Quantenzahlen genannt. Es werden zwei verschiedene attraktive Grundzustandskanäle identifiziert, die anhand ihrer Isospin-Quantenzahl unterschieden werden können: $I = 0$ und $I = 1$. Die Attraktivität des Potentials ist dabei zwingend notwendig für die mögliche Bildung eines gebundenen Zustands. Jeder der identifizierten Kanäle wird auf seine Fähigkeit untersucht, einen gebundenen Zustand zu bilden. Dabei wird die Abhängigkeit der Bindung von der Masse der dynamischen Quarks einbezogen. Man findet, dass die Attraktivität der Potentiale größer wird, je leichter die dynamischen Quarks sind. Außerdem sind

Potentiale mit $I = 0$ attraktiver als Potentiale mit $I = 1$. Eine ausführliche systematische und statistische Analyse liefert den eindeutigen Befund, dass Bindung nur für $I = 0$ und dynamische u- und d-Quarks möglich ist. Im Falle von $I = 1$ oder dynamischen s- und c-Quarks ist kein gebundener Zustand zu erwarten. Schließlich wird für dynamische u- und d-Quarks eine Extrapolation zu physikalischen Quarkmassen durchgeführt. Dazu werden drei unterschiedliche Quarkmassen verwendet. Es zeigt sich, dass für $I = 1$ keine Abhängigkeit der Bindung von der Quarkmasse vorliegt. Anders verhält es sich für $I = 0$: Die Bindung wird mit abnehmender Quarkmasse stärker. Am physikalischen Punkt wird eine Bindungsenergie von $E_B = -90^{+43}_{-36}$ MeV festgestellt. Damit wird für Quantenzahlen $I(J^{\mathcal{P}}) = 0(1^+)$ ein gebundener BB-Zustand postuliert.

Im zweiten Ergebnisteil wird die statisch-leichte Näherung aufgehoben. An die Stelle unendlich schwerer b-Quarks treten b-Quarks endlicher Masse. Auf diese Weise kann, anders als im statisch-leichten Fall, der Spin der schweren Quarks einbezogen werden. Dies führt unter anderem dazu, dass B- und B^*-Mesonen unterscheidbar werden, was im statisch-leichten Fall nicht möglich ist. Ein Nachteil dessen, dass vier Quarks endlicher Masse verwendet werden, ist der, dass es nun nicht mehr möglich ist, das Potential der schweren Quarks in Gegenwart der leichten zu bestimmen. Stattdessen wird aus der Korrelationsfunktion des Vier-Quark-Zustands direkt die Masse bestimmt. Liegt die Masse des Vier-Quark-Zustand unterhalb des B/B^*-Schwellenwerts, ist dies ein Hinweis auf einen gebundenen Vier-Quark-Zustand. Da es sich in den meisten Fällen nicht anbietet, die schweren Quarks wie die leichten Quarks auf dem Gitter voll dynamisch zu behandeln, wird zur Beschreibung der schweren Quarks der Ansatz der nichtrelativistischen QCD (NRQCD) gewählt. NRQCD ist eine effektive Theorie für schwere Quarks. In ihrem Rahmen wird die Lagrangedichte der schweren Quarks in Ordnungen ihrer räumlichen Geschwindigkeit entwickelt. Auf diese Weise ist es möglich, relativistische Korrekturen beliebiger Ordnung einzubeziehen. Die leichten Quarks werden voll dynamisch behandelt. Wir verwenden NRQCD zur Untersuchung des aus dem ersten Teil bekannten $\bar{b}\bar{b}ud$-Zustands mit Quantenzahlen $I(J^{\mathcal{P}}) = 0(1^+)$. Die Quantenzahlen des Zustandes können durch ein BB^*-Molekül realisiert werden. In einem ersten Schritt berechnen wir die Masse dieses Moleküls und vergleichen sie mit der Summe der Massen des B- und des B^*-Moleküls. Es stellt sich heraus, dass die Masse des Moleküls so knapp unterhalb des B/B^*-Schwellenwerts liegt, dass eine Aussage über einen gebundenen Zustand nicht möglich ist. Die Situation verändert sich, wenn man außer dem BB^*-Molekül auch das B^*B^*-Molekül in die Untersuchung mit einbezieht und mit Hilfe des generalisierten Eigenwertproblems den Grundzustand bestimmt. In diesem Fall liegt die Masse des Grundzustands deutlich unterhalb des Schwellenwerts, was ein Hinweis auf die Existenz eines gebundenen Zustands ist. Dieses Verhalten bestätigt die Vorhersage einer Untersuchung mit statisch-leichten Quarks, nämlich dass der $\bar{b}\bar{b}ud$-Zustand im $I(J^{\mathcal{P}}) = 0(1^+)$-Kanal eher eine Superposition aus BB^* und B^*B^* ist als ein reiner BB^*-Zustand. Insgesamt bekräftigt der gefundene Zustand unterhalb des Schwellenwerts das im ersten Teil der Arbeit gefundene Resultat, die Vorhersage eines bisher nicht gemessenen Tetraquark-Zustandes, qualitativ.

Im dritten Ergebnisteil geht es um $\bar{b}bu\bar{d}$-Systeme, die ein schweres Quark und ein schweres Antiquark sowie ein leichtes Quark und ein leichtes Antiquark enthalten. Eine mögliche Struktur dieser Systeme ist das $B\bar{B}$-Molekül. Neben dem $B\bar{B}$-Molekül kann noch eine Reihe weiterer Strukturen auftreten: Der Diquark-Antidiquark-Zustand, ein Zwei-Teilchen-Zustand aus B-Meson und ungebundenem $\bar{B}$-Meson sowie ein Bottomonium-Zustand und ein Pi-

on. Der Impuls des Pions kann dabei einen endlichen Wert annehmen oder verschwinden. Die Möglichkeit der Bildung eines solchen Zustanden macht die theoretische Beschreibung des Systems ungleich schwieriger als die Beschreibung des BB-Zustandes. Die experimentelle Erzeugung des Zustandes hingegen ist weniger aufwändig. So wurden experimentell bereits Kandidaten für einen $b\bar{b}u\bar{d}$-Tetraquark gemessen. Es handelt sich um die geladenen Zustände $Z_b(10610)$ und $Z_b(10650)$. In dieser Arbeit beschränken wir uns auf den positiv geladenen Fall mit den Quantenzahlen $I(J^{\mathcal{P}}) = 1(1^+)$. Zunächst wird schematisch skizziert, in welcher Reihenfolge die zu den verschiedenen Strukturen gehörenden Potentiale vorliegen können. So handelt es sich bei dem Grundzustandspotential des Systems um das Potential eines unangeregten Bottomonium-Zustands und eines Pions in Ruhe. Darüber liegen zahlreiche Bottomonium-Zustände mit Pionen mit endlichem Impuls, wobei deren genaue Lage und Anzahl vom verwendeten Gittervolumen abhängt. Inmitten dieser Potentiale wird das gesuchte Tetraquark-Potential erwartet. Es gilt also, einen Weg zu finden, die Bottomonium-und-Pion-Potentiale und das Tetraquark-Potential voneinander zu unterscheiden. Der erste Schritt in diese Richtung ist festzustellen, ob das Tetraquark-Potential überhaupt attraktiv ist, sodass ein gebundener Tetraquark-Zustand prinzipiell möglich ist. Dazu wird der Bottomonium-und-Pion-Grundzustand aus dem System entfernt. Dies wird durch die Lösung des generalisierten Eigenwertproblems unter Einbeziehung des Bottomonium-und-Pion-Zustandes und eines molekülähnlichen Tetraquark-Zustandes erreicht. Der erste angeregte Zustand ist im Anschluss daran weitgehend frei von Einflüssen des Grundzustands. Man findet, dass das Potential des ersten angeregten Zustandes attraktiv ist, sodass die Bildung eines Tetraquark-Zustandes nicht ausgeschlossen ist. Um den ersten angeregten Zustand weiter zu untersuchen, wird die Volumenabhängigkeit der verschiedenen Strukturen untersucht. Man kann zeigen, dass sich Zwei-Teilchen-Strukturen wie die Bottomonium-und-Pion-Struktur bei Vergrößerung des Gittervolumens anders verhalten als Einteilchen-Strukturen wie der Tetraquark-Zustand. So ist es prinzipiell möglich, unter Zuhilfenahme mehrerer Gittervolumina eine Aussage über die Struktur des ersten angeregten Zustands zu treffen.

Die Arbeit liefert die folgenden Vorschläge für weitere Schritte:

- Statisch-leichte BB-Systeme: Untersuchung der Abhängigkeit der Ergebnisse von kleinen Gitterabständen, die bisher nicht mit einbezogen wurden. Dazu könnten entweder Berechnungen mit kleineren Gitterabständen durchgeführt oder bei der Ermittlung des Potentials auch Nichtdiagonal-Abstände einbezogen werden.

- Statisch-leichte $b\bar{b}u\bar{d}$-Systeme: Weitere Untersuchung des ersten angeregten Zustands zur Ermittlung des Tetraquark-Zustands. Durchführung der Berechnungen zur Volumenabhängigkeit mit hinreichend großer Statistik.

- $b\bar{b}ud$-Zustand mit NRQCD: Rechnungen mit einer größeren Basis von Strukturen.

Zusammenfassend lässt sich sagen, dass im Rahmen der Doktorarbeit Beispiele für die verschiedenen Möglichkeiten des Zusammenspiels zwischen theoretischer Physik und Experimentalphysik präsentiert werden. Einerseits kann die Theorie Vorhersagen treffen, wonach im Experiment gesucht werden soll. Andererseits kann die Theorie experimentelle Befunde deuten und anhand von möglicherweise auftretenden Widersprüchen zum Experiment gängige Erklärungsmuster korrigieren oder anhand von Übereinstimmungen bestätigen. So gelingt in dieser Arbeit die Vorhersage eines bisher nicht beobachteten Tetraquark-Zustands mit der

Struktur $\bar{b}\bar{b}ud$. Eine ausführliche Analyse im Rahmen der statisch-leichten Approximation liefert eine Bindungsenergie von $E_B = -90^{+43}_{-36}$ MeV im $I(J^{\mathcal{P}}) = 0(1^+)$-Kanal. Dieser Befund kann unter Verwendung von schweren Quarks endlicher Masse und unter Einbeziehung des schweren Quarkspins qualitativ bestätigt werden. An dieser Stelle sei auf eine weitere Untersuchung verwiesen, in der auf Grundlage der Ergebnisse dieser Arbeit eine $\bar{b}\bar{b}ud$-Resonanz im $I(J^{\mathcal{P}}) = 0(1^-)$-Kanal postuliert wird [1]. Weiterhin gelingt im Rahmen der Arbeit ein erster Schritt zur Bestätigung des Z_b^+-Zustands als Tetraquark-Kandidat. In der statisch-leichten Approximation werden Hinweise auf einen gebundenen $b\bar{b}u\bar{d}$-Zustand mit den Quantenzahlen $I(J^{\mathcal{P}}) = 1(1^+)$ gefunden.

Contents

1. Introduction

Quarks are the fundamental constituents of matter. Composites of quarks, the so-called hadrons, come in two types: Baryons, which are systems with a half-integer spin composed of odd numbers of quarks and mesons, which are built of quark and antiquark pairs and which have an integer spin. u and d quarks form the most well-known baryons, protons and neutrons. In the atomic nucleus these baryons are stable. All other hadrons have a short lifetime and can only be detected in particle detectors. Very often, large particle accelerator facilities are necessary to deliver the energy that is needed for the formation of these particles. Quarks come in six types, the so called flavors. The flavors are ordered in three groups, the so-called generations: u and d quark build the lightest generation. The next generation, which is made of s and c quark, is heavier by a few hundred times. Finally, b and t quark, which form the third generation, have a mass that is a few thousand times heavier than the quarks of the first generation. Why there are three generations and not more or less and why there are these large mass differences is still an open question. The Standard Model of particle physics which provides the theory of all known elementary particles has no answer to this question. Among others, this is a reason why it has to be tested continuously in order to find indications for a possible extension that clarifies the open questions.

Quarks have some very special properties. They are point-like particles without any known sub-structure. Their electric charge assumes non-integer values. Despite the electromagnetic charge they carry a second kind of charge, the so-called color charge. Color charge is also carried by gluons, the particles that transmit the interaction between quarks. The currently most widely accepted theory of quarks gluons and the forces between them is called Quantum Chromodynamics (QCD). Due to the color charge, self interaction between the gluons is possible which makes quark interaction rather complicated. For this reason it is not possible to solve equations that describe low-energy observables of QCD analytically without further assumptions. One way to deal with this problem is an approach called Lattice QCD, which is also used in this thesis. The idea is to discretize the space-time continuum and obtain a finite four-dimensional space-time lattice with a finite lattice spacing. Using the path integral approach it is possible to solve equations of QCD numerically by means of special algorithms and high performance computers.

In the time when scientists started to build large facilities to measure hadrons and their properties, very soon more and more particles were discovered. To categorize these hadrons, a classification scheme was developed: the so-called constituent quark model or simply quark model [2]. According to the quark model, baryons and mesons can be grouped into $SU(N)$ flavor multiplets. By means of this scheme it was possible to predict particles which where indeed found in particle detectors soon after. The quark model describes mesons as bound $q\bar{q}$ pairs with q any quark flavor. Baryons are described as bound qqq composites of quarks. However, according to QCD various additional structures beyond the quark model are allowed. There may be e.g. composites of bound gluons (glueballs), $q\bar{q}$ structures in combination with

excited gluons (hybrids), baryonic or mesonic multiquark states such as $\bar{q}qqqq$ (pentaquarks) or $\bar{q}\bar{q}qq$ (often referred to as tetraquarks). Prominent examples for tetraquark candidates are the charmonium-like X(3872) state found in 2003 [3] and the bottomonium-like $Z_b(10610)$ and $Z_b(10650)$ states found in 2012 [4].

In this thesis, heavy-light four-quark systems are investigated. The thesis comprises two parts: a preparatory part where concepts and techniques are introduced (Chapters 2 to 4) and a discussion of physics results (Chapters 5 to 7). Each of the three chapters of the discussion part contains sections in which essentially self-contained investigations are presented. Each of these chapters closes with a short summary of the obtained results. In the following, we give more details on the individual chapters.

In Chapter 2 we give a short introduction to Lattice QCD. We present the idea of the path integral formalism as well as some possibilities to discretize quark and gluon fields. Most importantly, we introduce two approaches to deal with heavy quarks on the lattice: Heavy Quark Effective Field Theory (HQET) and nonrelativistic QCD (NRQCD).

In Chapter 3 we present concepts of hadron spectroscopy used in this work. By means of detailed calculations, methods to effectively implement quark propagators are explained. Moreover, techniques to improve the signal quality of a lattice computation are briefly introduced.

Chapter 4 collects properties of heavy-light four-quark states in the static approximation. Symmetries and quantum numbers of these systems are listed. An important part is the introduction of the so-called Born-Oppenheimer approximation on which most of the computations in this work are based.

Chapter 5 focuses on $\bar{b}\bar{b}qq$ systems with $q \in \{u, d, s, c, \}$ in the Born-Oppenheimer approximation. We list results for all possible channels. We report on a detailed statistical and systematic analysis to identify a candidate for a bound state. Finally we perform an extrapolation to the physical pion mass and calculate the binding energy of the bound state.

In Chapter 6 we report on a study of $\bar{b}\bar{b}ud$ systems with four quarks on finite mass. We work in the framework of NRQCD. A first result that qualitatively confirms our results in the static-light approach is presented.

In Chapter 7 we summarize an investigation of the static-light $b\bar{b}u\bar{d}$ system. We present possible structures the system can exist in and collect related prospects and challenges. We perform a first attempt to identify a bound state in the experimentally interesting $I(J^{\mathcal{P}}) = 1(1^+)$ channel.

We conclude in Chapter 8 and give an overview on research questions to work on in the future.

This thesis essentially summarizes several publications to which I have contributed significantly. Chapter 4 and 5 are based on papers [5, 6] and proceedings contribution [7]. Results from Chapter 6 and 7 are presented in proceedings contributions [8, 9].

2. Lattice QCD

Quantum Chromodynamics (QCD) is the theory of quarks and gluons and the forces between them. The coupling parameter of the strong force which acts on quarks and gluons depends on the energy of the system. In the high energy regime, the coupling is small, while in the low energy regime it grows exceedingly. Therefore, it is not possible to study the low-energy regime of QCD and thus observables like a hadron mass perturbatively. Lattice QCD provides a numerical method to solve QCD. In this chapter Lattice QCD is introduced based on [10, 11]. For an introduction to QCD in general, we refer to e.g. [12, 13, 14]. Moreover, we introduce Heavy Quark Effective Field Theory and Nonrelativistic QCD, two approaches to treat heavy quarks on the lattice.

2.1. The path integral formalism

In Lattice QCD we work on a finite four-dimensional space-time volume V. The path integral formalism provides a convenient way to quantize QCD fields. For the numerical approach it is essential to change from the Minkowski space-time to the Euclidean space-time: The Minkowski action S is replaced by the Euclidean action S_{E} via $S \to iS_{\mathrm{E}}$. This way, a rapidly oscillating complex factor is replaced by a real weight factor, whose advantages we discuss in Section 2.4.1. The concept of the path integral is based on the principle of least action: In a classical theory there is only one physical path a particle can take, i.e. the one that corresponds to the minimal action. In case of quantum theory a particle can take all possible paths. In the framework of the path integral formalism an integration over all these paths weighted by the corresponding action is performed. One introduces a special integration measure $D\phi = \Pi_{n \in V} d\phi(n)$, which contains all field variables $\phi(n)$ at all space-time points n of the given lattice volume V. Using the path integral formalism, the so-called partition function Z can be expressed via:

$$Z = \int D\psi D\bar{\psi} DA e^{-S_{\mathrm{E}}[\psi,\bar{\psi},A]} \tag{2.1}$$

with $\psi, \bar{\psi}$ fermion fields and A the gluon field. S_{E} is the Euclidean action:

$$S_E = \sum_{f \in \{u,d,s,c,b,t\}} \int \mathrm{d}^4 x \left(\frac{1}{4} F_{\mu\nu}^a(x) F_{a,\mu\nu}(x) + \bar{\psi}_f(x) M_f \psi_f(x) \right) = S_{\mathrm{G}} + S_{\mathrm{F}}. \tag{2.2}$$

Here, $M_f = \gamma_\mu D_\mu + m_f$ is the Dirac operator for the flavor f. In the following, we suppress the sum over flavors for the sake of readability.

2.2. Gluons on the Lattice

To discretize the gluon field one has to keep in mind that gluon fields transport color charge from one space-time point to another. Consistently, on the lattice, gluons should "live" on

the links between neigbouring lattice sites while quark fields should "live" on the lattice sites. The lattice gluon field is taken to be a member of the $SU(3)$ gauge group, i.e. a unitary 3×3 matrix. It is referred to as $U_\mu^{ab}(x)$, where μ is the direction of the link, x is its starting point on the lattice and $U_\mu^{ab}(x)$ connects x with the neighboring point $x + \hat{\mu}$. Indices a, b denote the entry of the color $SU(3)$ matrix[1]. For small lattice spacings a the lattice gauge field is related to the continuum gauge field A_μ via $U_\mu \approx e^{iagA_\mu}$ with g the QCD bare coupling constant. To give a physically meaningful theory, gauge invariance must be preserved when moving from the continuum to the lattice theory. Let $G(x)$ be a $SU(3)$ gauge transformation matrix at space-time point x. Quark and gluon field transform under gauge transformation in the following way:

$$
\begin{aligned}
U_\mu^{(G)} &= G(x)U_\mu(x)G^\dagger(x + \hat{\mu}), \\
\psi^{(G)}(x) &= G(x)\psi(x), \\
\bar{\psi}^{(G)}(x) &= \bar{\psi}(x)G^\dagger(x).
\end{aligned}
\tag{2.3}
$$

With (2.3) one can immediately see that color traces of closed loops of gauge fields and products of gauge fields with a quark field at one end and an antiquark field at the other end give gauge invariant objects. Therefore these objects are the building blocks of most observables in Lattice QCD.

A naive discretization of the continuum gluon action

$$
S_G = \int d^4x \frac{1}{4} F_{\mu\nu}^a F_a^{\mu\nu}
\tag{2.4}
$$

is the Wilson plaquette action:

$$
S_{WP} = \beta \sum_p \left(1 - \frac{1}{3} \mathrm{Re}\{\mathrm{Tr}\, U_P\} \right)
\tag{2.5}
$$

with the inverse bare coupling $\beta = \frac{6}{g^2}$ and U_P a so-called plaquette

$$
U_P(x) = U_i(x)U_k(x + \hat{k})U_i^\dagger(x + \hat{k})U_k^\dagger(x)
\tag{2.6}
$$

with $U_\mu^\dagger(x)$ connecting the space-time point $x + \hat{\mu}$ with x. Notice, that the Wilson plaquette action has discretization errors of $\mathcal{O}(a^2)$ [10]. The coupling constants β which is equivalent to g is the only input parameter for a calculation which includes gluon fields only. In particular, the gauge action does not depend on the lattice spacing a explicitly. In fact, the lattice spacing is obtained in the following way: One performs a lattice computation of an experimentally precisely known observable. Then one identifies the computed value with the value provided by experiment. There are various ways to discretize the gauge action besides the one shown in (2.5). It is not meaningful to compare computations with different gauge actions with each other, unless the results are converted into physical units.

---

[1] For the sake of readability color indices are suppressed in this chapter.

2.3. Fermions on the lattice

A naive discretization of the continuum action for free fermions[2]

$$S_{\mathrm{F}}^{(\mathrm{free})} = \int \mathrm{d}^4 x \bar{\psi} \left(\gamma_\mu \partial_\mu + m_f \right) \psi \tag{2.7}$$

can be written down easily by essentially replacing the continuum derivative by a discretized derivative:

$$S_{\mathrm{F,naiv}}^{(\mathrm{free})} = a^4 \sum_x \left(\bar{\psi}_x \sum_{\mu=0}^3 \gamma_\mu \frac{\psi_{x+\hat{\mu}} - \psi_{x-\hat{\mu}}}{2a} + m_f \bar{\psi}_x \psi_x \right). \tag{2.8}$$

Generalizing the free fermion action to the naive fermion action in an external gauge field yields:

$$S_{\mathrm{F,naive}} = a^4 \sum_x \left(\bar{\psi}_x \sum_{\mu=0}^3 \gamma_\mu \frac{U_\mu(x)\psi_{x+\hat{\mu}} - U_{-\mu}(x)\psi_{x-\hat{\mu}}}{2a} + m_f \bar{\psi}_x \psi_x \right). \tag{2.9}$$

The lattice Dirac operator reads:

$$D_{\mathrm{lat}}(x,y) = \gamma_\mu \frac{U_\mu(x)\delta_{x+\hat{\mu},y} - U_{-\mu}(x)\delta_{x-\hat{\mu},y}}{2a} + m_f \delta_{x,y}. \tag{2.10}$$

In the following, we limit ourselves to dealing with the free theory by formally setting $U_\mu = 1$. Performing a Fourier transform of $D_{\mathrm{lat}}^{(\mathrm{free})}$ yields:

$$\tilde{D}_{\mathrm{lat}}^{(\mathrm{free})}(p) = m_f + \frac{i}{a} \sum_{\mu=0}^3 \gamma_\mu \sin(p_\mu a). \tag{2.11}$$

The inverse of the free lattice Dirac operator in momentum space reads:

$$\left(\tilde{D}_{\mathrm{lat}}^{\mathrm{free}} \right)^{-1}(p) = \frac{m_f - \frac{i}{a}\sum_\mu \gamma_\mu \sin(p_\mu a)}{m_f^2 + \frac{1}{a^2}\sum_\mu \sin^2(p_\mu a)}, \tag{2.12}$$

which is the lattice fermion propagator in momentum space. Taking the continuum limit $a \to 0$ of (2.12) for massless fermions one gets:

$$\left(\tilde{D}_{\mathrm{lat}}^{\mathrm{free}} \right)^{-1}(p) \Big|_{m_f=0} = \frac{-\frac{i}{a}\sum_\mu \gamma_\mu \sin(p_\mu a)}{\frac{1}{a^2}\sum_\mu \sin^2(p_\mu a)} \xrightarrow{a \to 0} \frac{-i\sum_\mu \gamma_\mu p_\mu}{p^2}. \tag{2.13}$$

In the continuum the propagator has a pole at $p = (0,0,0,0)$ which corresponds to one single massless fermion. The discretized version of the propagator (2.12) has, however, poles if the components of p are either $p_\mu = 0$ or $p_\mu = \frac{\pi}{a}$. On the lattice the momentum is limited by the boundaries of the Brillouin zone, $-\frac{\pi}{a} < p_\mu \leq \frac{\pi}{a}$. So there are 16 momenta p that give a pole: $(0,0,0,0)$ which is called the physical pole and 15 additional poles at $(\frac{\pi}{a},0,0,0), (0,\frac{\pi}{a},0,0), (0,0,\frac{\pi}{a},0), \ldots, (\frac{\pi}{a},\frac{\pi}{a},\frac{\pi}{a},\frac{\pi}{a})$. The 15 additional poles are called doublers and, since they are not in agreement with the physical reality, a severe drawback of the naive

---

[2]Fermions are spinors and therefore live in spin and color space. However, for the sake of readability, we will suppress spin and color indices in this chapter, since the spin and color structures we consider are fairly trivial.

discretzation and need to be removed. There are many possibilities to discretize the fermion field. Examples can be found in [15, 16, 17, 18]. Since in this thesis most of the computations are performed using a special kind of fermion discretization, the so-called Wilson twisted-mass discretization, we limit ourselves to a presentation of Wilson fermions and the Wilson twisted-mass formalism.

2.3.1. Wilson fermions

One way to deal with the problem of fermion doublers is to use the so-called Wilson action instead of the naive discretization of the fermion action. The idea is to introduce a term to the momentum space lattice Dirac operator (2.11) that distinguishes between the physical pole of the inverse of the Dirac operator and the 15 non physical doublers.

The momentum space Dirac operator reads in the free theory:

$$\tilde{D}_{\text{Wilson}}^{(\text{free})}(p) = m_f + \frac{i}{a} \sum_{\mu=0}^{3} \gamma_\mu \sin(p_\mu a) + \frac{1}{a} \sum_{\mu=0}^{3} (1 - \cos(p_\mu a)). \tag{2.14}$$

The newly introduced term is referred to as the Wilson term. In the physical case, i.e. for $p_\mu = 0$ it vanishes, but for $p_\mu = \frac{\pi}{a}$ it provides a term $\frac{2}{a}$ which acts as an extra mass term. Hence, the doublers carry more mass than the physical fermion. In the continuum limit $a \to 0$ the mass of the doublers diverges and they decouple from the theory. For later reference we state the full Wilson Dirac operator:

$$D_{\text{Wilson}}(x,y) = (m_f + \frac{4}{a})\delta_{x,y} - \frac{1}{2a} \sum_{\mu=\pm 0}^{\pm 3} (1 - \gamma_\mu) U_\mu \delta_{x+\hat{\mu},y} \tag{2.15}$$

with $\gamma_{-\mu} = -\gamma_\mu$.

2.3.2. Wilson twisted mass fermions

A special kind of Wilson fermions are Wilson twisted-mass fermions. An extensive introduction to Wilson twisted-mass QCD can be found in [19]. For details on their implementation on the lattice, cf. e.g. [20]. One of the main motivations to develop twisted mass QCD was to provide a way to deal with Dirac zero modes, i.e. small eigenvalues of the Dirac operator that cause numerical problems (cf. discussion in [10]). Moreover, the twisted mass discretization gives rise to automatic $\mathcal{O}(a)$ improvement of lattice calculations, cf. e.g. [21, 22].

In its simplest form, Wilson twisted mass Lattice QCD (tmLQCD) includes two quark flavors of the same mass[3]. The no longer present isospin degree of freedom gives rise to an additional mass term. For twisted mass quark and antiquark fields χ and $\bar{\chi}$ the tmLQCD action reads:

$$S_{\text{tm}} = a^4 \sum_{x,y} \bar{\chi}(x) \left(D_{\text{Wilson}}^{m_f=0}(x,y)\mathbb{1}_2 + m\mathbb{1}_2\delta_{x,y} + i\mu\gamma_5\sigma^3\delta_{x,y} \right) \chi(y) \tag{2.16}$$

with $D_{\text{Wilson}}^{m_f=0}(x,y)$ the massless Wilson Dirac operator (i.e. (2.15) with $m_f = 0$). m is the mass of the two mass degenerate flavors and μ is the so-called twisted mass. Note the special structure of the additional mass term $i\mu\gamma_5\sigma^3\delta_{x,y}$: In contrast to the conventional mass term,

---

[3]For twisted mass QCD with mass non degenerate quarks, cf. e.g. [23]

it acts non-trivially in Dirac and flavor space (via γ_5 and σ^3 respectively). Parity and isospin are no symmetries of tmLQCD. However, one can show that both symmetries are restored in the continuum limit. Therefore, e.g. isospin breaking effects in tmLQCD results can be used to provide a first estimate of discretization errors. For an example how to deal with isospin breaking effects, cf. Section 5.3.

In the following, it is convenient to introduce the so-called polar mass

$$M = \sqrt{m_R^2 + \mu_R^2} \tag{2.17}$$

and the twist angle

$$\alpha = \arctan\left(\frac{\mu_R}{m_R}\right) \tag{2.18}$$

with m_R and μ_R the renormalized untwisted and twisted mass. For $m_R = 0$, $\mu_R > 0$ and therefore $\alpha = \frac{\pi}{2}$ one speaks of the discretization being at maximal twist. The bare untwisted mass must be tuned accordingly. It can be shown that at maximal twist automatic $\mathcal{O}(a)$ improvement for physical quantities is implied. With the transformation

$$\psi = R(\alpha)\chi, \ \bar\psi = \bar\chi R(\alpha), \ R(\alpha) = e^{i\frac{\alpha}{2}\gamma_5\sigma^3} \tag{2.19}$$

the action (2.16) reads:

$$S_{\text{tm}} = a^4 \sum_{x,y} \bar\psi(x) \left(D_{\text{tm}}(x,y)\mathbb{1}_2 + M\mathbb{1}_2\delta_{x,y}\right)\psi(y) \tag{2.20}$$

with the twisted mass Dirac operator

$$D_{\text{tm}}(x,y) = \frac{4}{a}e^{-i\alpha\gamma_5\sigma^3}\delta_{x,y} - \frac{1}{2a}\sum_{\mu=\pm 0}^{\pm 3} e^{-i\alpha\gamma_5\sigma^3}U_\mu(x)\delta_{x+\hat\mu,y} - \frac{1}{2a}\sum_{\mu=\pm 0}^{\pm 3}\gamma_\mu U_\mu(x)\delta_{x+\hat\mu,y}. \tag{2.21}$$

By comparison with Equation (2.15) one can see that the naive parts of the operator (cf. the third term of (2.21)) are not affected by the twist. The parts that belong to the so-called Wilson term are rotated. Since in the $\psi, \bar\psi$ basis in (2.20), only the term which is responsible for removing the doublers is rotated while the mass term and the kinetic terms stay unaffected, this basis is called the physical basis. In the $\chi, \bar\chi$ basis in (2.16), also the mass term is rotated, therefore it is referred to as the twisted basis.

2.3.3. The quenched approximation

For the sake of completeness, we also mention that it is possible to omit the fermionic contribution in the action in the path integral (2.1) entirely, which is called the quenched approximation. This means that quarks are only allowed as valence quarks. In the early days of Lattice QCD the majority of calculations have been performed in the quenched approximation. Taking into account quarks requires a lot of numerical effort, as we discuss in Section 2.4. In the quenched approximation the quark pair production and annihilation from the vacuum is suppressed. Therefore it misses an important part of QCD dynamics. Instead of omitting all dynamical quark flavors in the simulation one can consider only a few of the flavors (e.g. only the light u and d) or give the dynamical sea quarks and the valence quarks different masses. Those approximations are called partial quenching. A discussion of the quality of quenched computations can be found in [24].

2. Lattice QCD

2.4. Computation of observables on the lattice

2.4.1. Generation of gauge link configurations

The expectation value of an observable O is obtained in the path integral formalism via:

$$\langle O \rangle = \frac{1}{Z} \int D\psi D\bar{\psi} DU O[\psi, \bar{\psi}, A] e^{-S_{\mathrm{E}}[\psi, \bar{\psi}, U]}. \tag{2.22}$$

By integrating out the fermion fields, the expression becomes

$$\langle O \rangle = \frac{1}{Z} \int DU \prod_f \det(D_f[U]) O[U] e^{-S_{\mathrm{G}}[U]}. \tag{2.23}$$

where $\det(D_f[U])$ is the determinant of the fermion Dirac operator of the flavor f. The observable is determined by integrating over all gauge fields weighted by the factor $\det(D_f[U]) e^{-S_{\mathrm{G}}[U]}$. Note that, due to γ_5-hermiticity, the fermion determinant is real

$$\det(D_f^\dagger) = \det(\gamma_5 D_f \gamma_5) = \det(D_f). \tag{2.24}$$

Moreover, in tmLQCD the fermion determinant is positive definite. So if one is able to generate N_{conf} gauge field configurations $\{U_i\}$ with the probability of $\det(D_f[U]) e^{-S_{\mathrm{G}}[U]}$, one can derive the expectation value $\langle O \rangle$ via:

$$\langle O \rangle \simeq \frac{1}{N_{\mathrm{conf}}} \sum_{i=1}^{N_{\mathrm{conf}}} O(U_i). \tag{2.25}$$

Usually, the gauge field configurations are generated using Hybrid Monte Carlo Algorithms [25]. Taking into account the fermion determinant represents the major challenge. One can work in the quenched approximation, where $\det(D_f) = 1$ but this introduces an unknown systematic error. If the fermion determinant is not omitted the generation of gauge field configurations is computationally very expensive due to the fact that the fermion operator has to be inverted at each computation step of the algorithm. Therefore high performance computers need to be used. To illustrate the computational expenditure, we give an example. In [26] the computational cost C in Tflops·year for a calculation performed by the CP-PACS collaboration with $n_{\mathrm{f}} = 2$ dynamical quark flavors is quantified:

$$C = 2.8 \frac{N_{\mathrm{conf}}}{1000} \cdot \left(\frac{0.6}{m_\pi/m_\rho} \right)^6 \cdot \left(\frac{L}{3\,\mathrm{fm}} \right)^5 \cdot \left(\frac{a^{-1}}{2\,\mathrm{GeV}} \right)^7. \tag{2.26}$$

So for a typical number of configurations $N_{\mathrm{conf}} = 1000$, a typical spatial lattice extent of $3\,\mathrm{fm}$, a lattice spacing of $0.05\,\mathrm{fm}$ and a relation of the pion mass to the ρ meson mass of $m_\pi/m_\rho = 0.6$ one expects the computational cost of about 2.8 Tflops·year. A today's common laptop has a capacity of about 100 Gflops [27]. The serial generation of 1000 gauge configurations in the above mentioned setup would take such a laptop about 28 years of non-stop operation.

2.4.2. Statistical data analysis

A sample of measurements from a Lattice QCD simulation can be seen as a set of N random variables $\{X_i\}$. The data must be analyzed statistically to obtain a meaningful value for

the observable and its error. First we consider the case of uncorrelated data, i.e. if for all measurements X_i holds:

$$\langle X_i X_j \rangle = \langle X_i \rangle \langle X_j \rangle = \langle X \rangle^2, \qquad i \neq j \tag{2.27}$$

with $\langle X \rangle$ the expectation value of the measurements. In this case the estimate for the observable and its statistical error are well-known:

$$\langle X \rangle = \hat{X} \pm \sigma, \qquad \sigma = \frac{\hat{\sigma}_X}{\sqrt{N}} \tag{2.28}$$

with

$$\hat{X} = \frac{1}{N} \sum_{i=1}^{N} X_i \tag{2.29}$$

and

$$\hat{\sigma}_X^2 = \frac{1}{N-1} \sum_{i=1}^{N} \left(X_i - \hat{X} \right)^2. \tag{2.30}$$

However, in most cases the measurements obtained from a lattice computation are correlated to some extent. Therefore one needs to make some effort to deal with the correlation of the measurements to find a meaningful result. One strategy to remove autocorrelation is *data blocking*. The data sample is divided into sub-samples of the size K. The mean values of the sub-samples are then considered as as new variables X_i. One repeats this step for various values of K. If the new variables are uncorrelated, the variance of the new variables for one value of K is constant with respect to the previous value of K. Once this behavior is observed, the sub-sample variables can be assumed to be statistically independent. To take into account correlations of fluctuations in the data, which is essential e.g. in the case of quantities based on the correlation function (cf. Section 3.1.1), a special error estimation procedure is necessary. One example is the so-called *jackknife method*. Consider a sample of N measurements $\{Y_i\}$. For the full sample we define

$$\hat{Y} = \frac{1}{N} \sum_{i=1}^{N} Y_i. \tag{2.31}$$

Now we construct N reduced samples by removing one at a time the nth value from the full sample. We obtain $N-1$ values $\hat{Y}_i$ via

$$\hat{Y}_i = \frac{1}{N-1} \sum_{i \neq j}^{N} Y_j. \tag{2.32}$$

The statistical error $\sigma_{\hat{Y}}$ of $\hat{Y}$ is calculated via

$$\sigma_{\hat{Y}}^2 = \frac{N-1}{N} \sum_{i=1}^{N} \left(\hat{Y}_i - \hat{Y} \right)^2. \tag{2.33}$$

So the final result is

$$\langle Y \rangle = \hat{Y} \pm \sigma_{\hat{Y}}. \tag{2.34}$$

Both, data blocking and the jackknife method are applied in the data analysis in Chapters 5 and 7.

2.5. Sources of systematic errors

Controlling the systematic errors of a lattice computation is essential to get a meaningful result. In this section we state common examples for sources of systematic error. One obvious source of systematic error is the error that arises due to the finite lattice spacing $a \neq 0$, the so-called *cutoff effects* or *discretization errors*. Lattice QCD results depend on a. For example in case of the Wilson twisted mass discretization (cf. Section 2.3.2) this error is of $\mathcal{O}(a^2)$. However, results obtained for a fixed quark mass but for different lattice spacings a should allow for a consistent continuum extrapolation $a \rightarrow 0$, which is a meaningful test of the obtained result. As we show in Section 5.3.4 it is also possible to use the breaking of isospin symmetry by Wilson twisted mass fermions to check for cutoff effects.

Another systematic error arises from the *finite volume* of the four-dimensional lattice. If the volume is too small, it cannot represent the infinite volume of the real world and computations are distorted. The lightest particle, the pion, defines the smallest acceptable lattice volume. However, the lattice volumes used in this thesis are reasonably large, therefore we expect negligible finite volume effects.

Quenching of dynamical quark flavors is another source of systematic error. Due to the absence of spontaneous quark pair production from the vacuum, which is not in accordance with physical reality, quenching effects yield some uncertainty to the results of a calculation. However, generally the error from quenching is expected to be small compared to the statistical error of the computation (cf. e.g. [28]). For this reason, this kind of systematic error is not further addressed throughout the thesis.

Finally we mention systematic errors due to the use of *unphysically heavy quark masses*. The heavier the the quark masses used in a simulation the lower the numerical effort which is required. Therefore many lattice computations are performed with non physically heavy quark masses. Similar to the treatment of cutoff effects one can perform several simulations with the same lattice spacing but with different values of the quark mass. Then one can perform an extrapolation to the physical point. Such an extrapolation is performed in Section 5.5.

2.6. Effective theories for heavy quarks

There are many reasons to study systems that involve heavy quarks, cf. eg. [29]: One prominent example is heavy quarkonium physics which is well understood both theoretically and experimentally. Observables can be determined with different methods which allows for precision tests of QCD. Moreover, decays of charm and bottom mesons provide information to determine elements of the CKM matrix. i.e. fundamental parameters of the standard model. It is also possible to use heavy quark physics in order to explore physics beyond the standard model. One example is to probe loop effects by means of processes that involve flavor changing neutral currents or rare B decays. In the standard model, these processes are suppressed by the Glashow-Iliopuolos-Maiani (GIM) mechanism. In this thesis we study heavy light four quark systems to understand the nature of experimentally observed states or predict possible four quark states, respectively.

Two of the six quark flavors are heavy compared to the hadronic energy scale: charm (~ 1000 MeV) and bottom (~ 4000 MeV). Actually, also the top quark is heavy, but due to its short lifetime, top physics can be treated perturbatively. The Compton wave length λ is inversely proportional to the quark mass m_Q, i.e. $\lambda \propto \frac{1}{m_Q}$. If the Compton wave length is

smaller than or comparable to the lattice spacing a, a lattice QCD computation will suffer from severe discretization effects. Hence, one of the main motivations to develop an effective theory for heavy quarks was the following: In the past it was not possible to choose the lattice spacing fine enough to resolve the Compton wave lengths of the heavy quarks. Note that the Compton wave lengths of charm and bottom quarks are $1/m_c \sim 0.13$ fm and $1/m_b \sim 0.04$ fm. In many cases, these lengths are still smaller than or comparable to lattice spacings nowadays used (i.e. 0.05-0.2 fm). However, recently there are also studies that involve Lattice QCD techniques to treat heavy quarks relativistically, cf. e.g. [30, 31].

One way to study heavy quarks is to use an Effective Field Theory (EFT), i.e. a theory to calculate observables like mass spectra, decay rates and hadronic matrix elements in a model independent manner. The idea is to separate low energy degrees of freedom $m_Q v \ll m_Q$ from high energy degrees of freedom $\sim m_Q$, where v is the heavy quark spatial velocity. Then one can treat the low energy degrees of freedom using conventional lattice QCD techniques. The high energy degrees of freedom that can subsumed in a heavy Lagrangian $\mathcal{L}_{\text{heavy}}$ are treated perturbatively. Theoretically, one needs an infinite number of renormalization conditions to remove all ultraviolet divergences from $\mathcal{L}_{\text{heavy}}$. What makes EFTs predictive anyway is, that in practice, one is only interested in a certain order of the perturbative expansion, which makes the number of necessary input parameters finite. The following sections are essentially based on [29, 32, 33].

2.6.1. The dynamics of heavy quark systems

To derive an effective theory for heavy quarks it is important to understand the dynamics of heavy quark systems. Systems that contain heavy and light quarks behave differently from systems that contain only quarks of equal masses. In case of heavy-light systems, such as B mesons, the dynamics of the light quarks is dominated by the QCD energy scale Λ_{QCD}, whereas the dynamic of the heavy quarks is dominated by their mass m_Q. The light quarks hardly influence the heavy quarks, since $\Lambda_{\text{QCD}} \ll m_Q$. The heavy quarks stay almost at rest compared to the light quarks and their motion is suppressed by Λ_{QCD}/m_Q. Therefore the expansion parameter for the perturbative treatment of the heavy quarks in a heavy-light system is Λ_{QCD}/m_Q. The related theory is known as Heavy Quark Effective Field Theory (HQET).

For a system with quarks of equal masses such as bottomonium states, the momentum of one quark cannot be neglected with respect to the other. Consequently, there are three relevant scales in the system: $m_Q \gg m_Q v \gg m_Q v^2$. Therefore, the expansion parameter for a perturbative treatment of the heavy-heavy system is v. The accuracy of a perturbative expansion can be estimated: One assumes that the kinetic energy $m_Q v^2$ is of order of the 2S-1S splitting in a meson. For charmonium $c\bar{c}$ with $\psi(2S) - \psi(1S) \sim 700\,\text{MeV}$ and $m_\psi \sim 3\,\text{GeV}$ one gets a spatial velocity $v^2 \sim 0.3$. For bottomonium one gets with $\Upsilon(2S) - \Upsilon(1S) \sim 600\,\text{MeV}$ and $m_\Upsilon \sim 9\,\text{GeV}$ a spatial velocity $v^2 \sim 0.1$. The related theory is referred to as Nonrelativistic QCD (NRQCD). Note that NRQCD is applicable to heavy-light systems as well, while conversely HQET obviously is not suited to treat heavy-heavy systems.

2.6.2. The Foldy-Wouthuysen-Tani transformation

One way to derive an effective Lagrangian for heavy quarks is the so-called Foldy-Wouthuysen-Tani (FWT) transformation. In this work, we limit ourselves to the derivation in the contin-

uum [33]. For details on effective field theories for heavy quarks on the lattice, cf. [34, 35]. As a motivation we remind the reader of the derivation of the Pauli equation: For small velocities $v \ll 1$, i.e. $e^{ip_\mu x^\mu} \approx e^{-im_Q t}$, one finds the Pauli equation as the nonrelativistic equivalent of the Dirac equation. The heavy quark spinor can be written as

$$\mathcal{Q} = e^{-im_Q t} \begin{pmatrix} Q \\ X \end{pmatrix} \tag{2.35}$$

with two two-component spinors Q and X. Consider the Dirac equation

$$(i\gamma^\mu D_\mu - m_Q)\mathcal{Q} = 0, \quad \text{with} \quad \gamma^0 = \begin{pmatrix} +1 & 0 \\ 0 & -1 \end{pmatrix}, \quad \gamma^i = \begin{pmatrix} 0 & +\sigma^i \\ -\sigma^i & 0 \end{pmatrix} \tag{2.36}$$

with the γ-matrices in the Dirac representation. Rewriting $(i\gamma^0 D_0 - i\gamma^i D_i - m_Q)\mathcal{Q} = 0$ in terms of Q and X yields:

$$\begin{aligned} &+ iD_0 e^{-im_Q t} Q - i\sigma^i D_i e^{-im_Q t} X - m_Q e^{-im_Q t} Q = 0, \\ &- iD_0 e^{-im_Q t} X + i\sigma^i D_i e^{-im_Q t} Q - m_Q e^{-im_Q t} X = 0. \end{aligned} \tag{2.37}$$

By performing the D_0 derivative explicitly

$$D_0 e^{-im_Q t} Q = -im_Q Q e^{-im_Q t} + e^{-im_Q t} D_0 Q \tag{2.38}$$

and rearranging Equations (2.37), one finds:

$$\begin{aligned} iD_0 Q &= i\vec{\sigma} \cdot \mathbf{D} X, \\ (iD_0 + 2m_Q)X &= i\vec{\sigma} \cdot \mathbf{D} Q. \end{aligned} \tag{2.39}$$

Notice that component X is the smaller than Q by a factor $2m_Q$. If we neglect $D_0 X$, we find $X = \frac{i}{2m_Q}\vec{\sigma} \cdot \mathbf{D} Q$. Hence, the two equations (2.39) can be combined into one:

$$iD_0 Q = \frac{-1}{2m_Q}\vec{\sigma} \cdot \mathbf{D}\vec{\sigma} \cdot \mathbf{D} Q. \tag{2.40}$$

Using the property of Pauli matrices

$$(\vec{\sigma} \cdot \mathbf{a})(\vec{\sigma} \cdot \mathbf{b}) = \mathbf{a} \cdot \mathbf{b} + i\vec{\sigma} \cdot (\mathbf{a} \times \mathbf{b}) \tag{2.41}$$

yields:

$$\vec{\sigma} \cdot \mathbf{D}\vec{\sigma} \cdot \mathbf{D} = \mathbf{D}^2 + i\vec{\sigma} \cdot (\mathbf{D} \times \mathbf{D}). \tag{2.42}$$

Taking into account the cross product of the spatial derivative $\mathbf{D}$

$$\mathbf{D} \times \mathbf{D} Q = (i\nabla - q\mathbf{A}) \times (i\nabla - q\mathbf{A})Q = -iq\nabla \times \mathbf{A} Q = -iq\mathbf{B} Q \tag{2.43}$$

we end up with

$$0 = \left(iD_0 + \frac{\mathbf{D}^2}{2m_Q} + \frac{q\vec{\sigma} \cdot \mathbf{B}}{2m_Q} \right) Q \tag{2.44}$$

which is the well-known Pauli equation we will recover below. Now the idea is to derive a continuum effective Dirac theory for heavy quarks in $\mathcal{O}\left(\left(\frac{1}{m_Q} \right)^n \right)$ by decoupling particle and

antiparticle components of the Dirac Lagrangian $\mathcal{L}$ up to a given order. Doing so, we get one-particle equations instead of an equation for particle and antiparticle. Since the Pauli equation (2.44) is a one-particle equation, this seems to be the right strategy. Notice that, as a consequence, heavy quark pair production will not be included in the effective theory. In the following calculations color indices are suppressed.

Consider the particle/antiparticle projector

$$P_{\pm} = \frac{1}{2}(1 \pm \gamma^0) \tag{2.45}$$

and the Dirac Lagrangian

$$\mathcal{L} = \bar{\Psi}(-m + i\gamma^0 D_0 + i\gamma^j D_j)\Psi. \tag{2.46}$$

A transformation to decouple particles and antiparticles must remove terms from (2.46) that do not commute with γ^0 in the particle/antiparticle projector, i.e. $i\gamma^j D_j$. With the redefinition of the spinor Ψ in (2.46)

$$\Psi = \exp\left(\frac{1}{2m_Q}i\gamma^j D_j\right)\Psi_{(1)}, \qquad \bar{\Psi} = \bar{\Psi}_{(1)}\exp\left(\frac{1}{2m_Q}i\gamma^j D_j\right) \tag{2.47}$$

one finds

$$\mathcal{L} = \bar{\Psi}_{(1)}(-m + i\gamma^0 D_0)\Psi_{(1)} + \sum_n \left(\frac{1}{m_Q}\right)^n \bar{\Psi}_{(1)} O_{(1)n} \Psi_{(1)}. \tag{2.48}$$

The redefinition introduces an infinite number of terms with higher powers in $\frac{1}{m_Q}$. Consider the $\frac{1}{m_Q}$ term

$$O_{(1)1} = -\frac{1}{2}D_j D^j - \frac{iq}{8}[\gamma^j, \gamma^k]F_{jk} - \underbrace{\frac{iq}{2}\gamma^j\gamma^0 F_{j0}}_{\text{anticommutes with } \gamma^0}. \tag{2.49}$$

The anticommuting term can be cancelled by a second redefinition of the spinor $\Psi_{(1)}$:

$$\Psi_{(1)} = \exp\left(\frac{1}{2m_Q^2}\left(-\frac{iq}{2}\gamma^j\gamma^0 F_{j0}\right)\right)\Psi_{(2)}, \qquad \bar{\Psi}_{(1)} = \bar{\Psi}_{(2)}\exp\left(\frac{1}{2m_Q^2}\left(-\frac{iq}{2}\gamma^j\gamma^0 F_{j0}\right)\right) \tag{2.50}$$

We observe that all anticommuting terms of order $\frac{1}{m_Q}$ canceled. However, anticommuting terms of order $\left(\frac{1}{m_Q}\right)^2$ are introduced. The new anticommuting terms can be canceled by a third redefinition. One can repeat this procedure until the desired order in $\frac{1}{m_Q}$ is reached. With the final spinor redefinition $\bar{\bar{\Psi}} = \begin{pmatrix} \psi \\ \xi \end{pmatrix}$ and after some algebraic reformulations, the resulting Lagrangian of order $\left(\frac{1}{m_Q}\right)^2$ reads

$$
\begin{aligned}
\mathcal{L}_{\text{heavy}} =& \psi^\dagger \left[iD_0 + \frac{\mathbf{D}^2}{2m_Q} + \frac{q\vec{\sigma}\mathbf{B}}{2m_Q} + \frac{q}{8m_Q^2}\left(\mathbf{D}^* \cdot \mathbf{E} + i\vec{\sigma} \cdot (\mathbf{D} \times \mathbf{E} - \mathbf{E} \times \mathbf{D})\right)\right]\psi \\
&+ \xi^\dagger \left[iD_0 - \frac{\mathbf{D}^2}{2m_Q} - \frac{q\vec{\sigma}\mathbf{B}}{2m_Q} - \frac{q}{8m_Q^2}\left(\mathbf{D}^* \cdot \mathbf{E} + i\vec{\sigma} \cdot (\mathbf{D} \times \mathbf{E} - \mathbf{E} \times \mathbf{D})\right)\right]\xi \\
&+ \mathcal{O}\left(\left(\frac{1}{m_Q}\right)^3\right)
\end{aligned} \tag{2.51}
$$

with $\mathbf{B}$ and $\mathbf{E}$ the chromomagnetic and chromoelectric fields. As desired, particle and antiparticle fields are separated. Because the action for ξ can be obtained from the action for ψ, only one of the terms is necessary. Moreover, as announced above, the Pauli equation (2.44) is recovered.

Note that at this stage the Lagrangian (2.51) looks the same for HQET and NRQCD. What makes the theories different is that the size of each term is different, i.e. to obtain the same order in $\Lambda_{\mathrm{QCD}}/m_Q$ or v, respectively, different terms have to be included to the Lagrangian. To determine which terms are needed in which order, one has to perform power counting, cf. [29, 33].

2.6.3. Power counting in Heavy Quark Effective Field Theory

As stated above, the energy scale of the light quarks in a hadron is Λ_{QCD}. Because the typical momentum transfer in a heavy-light system is of order of the energy of the light quarks, the temporal and spatial covariant derivatives D_0 and $\mathbf{D}$ are of order Λ_{QCD},

$$|D_0| \sim |\mathbf{D}| \sim \Lambda_{\mathrm{QCD}}. \tag{2.52}$$

Also the gluon potential A_μ is governed by the light degrees of freedom, therefore

$$|qA_0| \sim |q\mathbf{A}| \sim \Lambda_{\mathrm{QCD}} \tag{2.53}$$

and consequently

$$|q\mathbf{E}| \sim |q\mathbf{B}| \sim \Lambda_{\mathrm{QCD}}^2. \tag{2.54}$$

Hence, the order of $\left(\frac{1}{m_Q}\right)^n$ of the terms in the heavy Lagrangian (2.51) can be read off easily. In the static limit, i.e. for $m_Q \to \infty$, the HQET Lagrangian reduces to:

$$\mathcal{L}_{\mathrm{HQET}} = \psi^\dagger i D_0 \psi. \tag{2.55}$$

The Lagrangian does not depend on flavor nor on spin. One can show [36, 37], that in Euclidean space-time the heavy quark propagator $\mathcal{Q}^{-1}$ can be written as:

$$\mathcal{Q}_{BC}^{-1}(t, t') = U(\mathbf{x}, t; \mathbf{x}, t') \left[\theta(t - t') \left(\frac{1 + \gamma_0}{2} \right)_{BC} \mathrm{e}^{-M(t-t')} + \theta(t' - t) \left(\frac{1 - \gamma_0}{2} \right)_{BC} \mathrm{e}^{-M(t'-t)} \right]. \tag{2.56}$$

The heavy quark appears simply as a color source.

2.6.4. Power counting in nonrelativistic QCD

In heavy-heavy mesons, quark and antiquark orbit each other with the spatial velocity v. The quantities that appear in (2.51) have the following powers in v: The absolute value of the spatial momentum $|\mathbf{k}|$ is proportional to v:

$$|\mathbf{k}| \sim m_Q v. \tag{2.57}$$

The kinetic energy is $E_{\mathrm{kin}} \sim m_Q v^2$. For the absolute value of the spatial covariant derivative $|\mathbf{D}|$ one can estimate

$$|\mathbf{D}| \sim \sqrt{2m_Q E_{\mathrm{kin}}} \sim m_Q v. \tag{2.58}$$

At small distances the kinetic energy and the Coulomb potential energy have to be in equilibrium to form a stable system, therefore

$$E_{kin} \sim V_{\text{Coulomb}} \qquad \text{and} \qquad |qA_0| \sim E_{\text{kin}} \sim m_Q v^2. \tag{2.59}$$

With the free Schrödinger equation

$$(iD_0 + \frac{\mathbf{D}^2}{2m_Q})\psi = 0 \tag{2.60}$$

one finds

$$|D_0| \sim |\frac{\mathbf{D}^2}{2m_Q}| \sim m_Q v^2. \tag{2.61}$$

Finally, using Yang-Mills equations one can show that [34]:

$$|q\mathbf{E}| \sim m_Q^3 v^3 \qquad \text{and} \qquad |q\mathbf{B}| \sim m_Q^2 v^4. \tag{2.62}$$

Note that one $\mathcal{O}(v^4)$ term is missing in (2.51) which can be determined by means of the kinetic energy:

$$E_{\text{kin}} = \sqrt{\mathbf{k}^2 + m_Q^2} = \frac{\mathbf{k}^2}{2m_Q} - \frac{\mathbf{k}^4}{8m_Q^3} + \frac{\mathbf{k}^6}{16m_Q^5} - \mathcal{O}\left(\left(\frac{1}{m_Q}\right)^7\right). \tag{2.63}$$

Including the missing $\mathcal{O}(v^4)$ term in (2.51) we find the NRQCD Lagrangian of $\mathcal{O}(v^4)$:

$$\mathcal{L}_{\text{NRQCD}} = \psi^\dagger \left[\underbrace{iD_0}_{\sim v^2} + \underbrace{\frac{\mathbf{D}^2}{2m_Q}}_{\sim v^2} + \underbrace{\frac{q\vec{\sigma}\mathbf{B}}{2m_Q}}_{\sim v^4} + \underbrace{\frac{\mathbf{D}^4}{8m_Q^3}}_{\sim v^4} + \frac{q}{8m_Q^2}\left(\underbrace{\mathbf{D}^* \cdot \mathbf{E}}_{\sim v^4} + i\vec{\sigma} \cdot (\underbrace{\mathbf{D} \times \mathbf{E}}_{\sim v^4} - \underbrace{\mathbf{E} \times \mathbf{D}}_{\sim v^4}) \right) \right] \psi. \tag{2.64}$$

3. Hadron Spectroscopy

Lattice QCD is a nonperturbative approach to QCD. It allows for first-principle computation of low energy observables such as the masses of mesons and baryons. The reproduction of the hadronic mass spectrum in accordance with experimental measurements provides important tests for the theory of QCD. In this work, hadron spectroscopy is used to predict bound states that have not been measured experimentally yet, such as a possibly existing $\bar{b}\bar{b}ud$ four-quark state (cf. Chapter 5) or to investigate states whose nature is not sufficiently clear, such as the $Z_b^{\pm}$ meson (cf. Chapter 7). This chapter presents general aspects of hadron spectroscopy using examples of a static-light B meson and a pion. A more general introduction to hadron spectroscopy can be found e.g. in [10].

3.1. Basic concepts of hadron spectroscopy discussed in the context of the static-light B meson

The static light B meson is a very important quantity in this thesis. We chose it as an example system to introduce the correlation function as well as numerical techniques as the point source method and the timeslice source method.

3.1.1. The creation operator

To perform a spectroscopy calculation, as a first step we have to write down a suitable creation operator that excites the hadronic state we want to investigate. A hadron can be described by its flavor quantum number I, total angular momentum J, parity P and charge conjugation C. The creation operator has to generate field excitations with these quantum numbers from the vacuum. In case of a static-light B meson we have one static antiquark $\bar{Q}$ and one quark $q \in \{u, d, s, c\}$ of finite mass, i.e. $B = \bar{Q}q$. The operator reads:

$$O_B(x) = \overline{Q}_A^a(x)\Gamma_{AB}q_B^a(x) \tag{3.1}$$

with Γ a combination of Dirac γ-matrices which accounts for angular momentum and parity of the meson. Capital letters $A, B, ... = 0, 1, 2, 3$ denote spin indices, lower case letters $a, b, ... = 1, 2, 3$ denote color indices.

3.1.2. The correlation function

Once a suitable operator is found, we define the correlation function in time via

$$C(t' - t) = \langle\Omega| O_B(\mathbf{x}, t')^{\dagger}O_B(\mathbf{x}, t) |\Omega\rangle = \sum_n \langle\Omega| O_B^{\dagger}(\mathbf{x}) |n\rangle \langle n| O_B(\mathbf{x}) |\Omega\rangle \, e^{-(E_n - E_\Omega)\Delta t}$$

$$\tag{3.2}$$

3. Hadron Spectroscopy

with $\Delta t = t' - t$ and E_Ω the vacuum energy. $|n\rangle$ is the n-th energy eigenstate of the system and $O_B(\mathbf{x}, t) |\Omega\rangle$ is referred to as a trial state. At large time separations Δt, excited states are suppressed while the ground state dominates. The effective mass is defined via

$$am_{\text{eff}}(t) = \ln \left(\frac{C(t' - t)}{C((t' - t) + a)} \right) \tag{3.3}$$

with the lattice spacing a. For large time separations one finds the mass m_B of the B meson:

$$am_B(t) = a \left(E_0 - E_\Omega \right) = \lim_{t \to \infty} \ln \left(\frac{C(t)}{C(t + a)} \right). \tag{3.4}$$

With (3.1) the correlation function of the static light B meson can be worked out in detail:

$$
\begin{aligned}
C(t' - t) &= \langle \Omega | O_B^\dagger(\mathbf{x}, t') O_B(\mathbf{x}, t) |\Omega\rangle \\
&= \langle \Omega | \left(\overline{Q}_B^a(\mathbf{x}, t') \Gamma_{BA} \psi_A^a(\mathbf{x}, t') \right)^\dagger \overline{Q}_C^b(\mathbf{x}, t) \Gamma_{CD} \psi_D^b(\mathbf{x}, t) |\Omega\rangle \\
&= \langle \Omega | \psi_A^{a\,\dagger}(\mathbf{x}, t') \Gamma_{AB}^\dagger \gamma_0 Q_B^a(\mathbf{x}, t') \overline{Q}_C^b(\mathbf{x}, t) \Gamma_{CD} \psi_D^b(\mathbf{x}, t) |\Omega\rangle \\
&= \langle \Omega | \overline{\psi}_A^a(\mathbf{x}, t') \left(\gamma_0 \Gamma^\dagger \gamma_0 \right)_{AB} Q_B^a(\mathbf{x}, t') \overline{Q}_C^b(\mathbf{x}, t) \Gamma_{CD} \psi_D^b(\mathbf{x}, t) |\Omega\rangle \\
&= - \langle \Omega | \left(\gamma_0 \Gamma^\dagger \gamma_0 \right)_{AB} Q_B^a(\mathbf{x}, t') \overline{Q}_C^b(\mathbf{x}, t) \Gamma_{CD} \psi_D^b(\mathbf{x}, t) \overline{\psi}_A^a(\mathbf{x}, t') |\Omega\rangle
\end{aligned}
$$

We find the heavy and light quark propagator $\mathcal{Q}^{-1}$ and $\mathcal{D}^{-1}$ after integration over all fermion fields.

$$= - \left\langle \left(\gamma_0 \Gamma^\dagger \gamma_0 \right)_{AB} \left(\mathcal{Q}^{-1} \right)_{BC}^{ab} (\mathbf{x}, t; \mathbf{x}, t') \Gamma_{CD} \left(\mathcal{D}^{-1} \right)_{DA}^{ba} (\mathbf{x}, t'; \mathbf{x}, t) \right\rangle$$

$\langle \dots \rangle$ is a path integral over all gauge configurations.

$$= - \left\langle \left(\gamma_0 \Gamma^\dagger \gamma_0 \right)_{AB} U^{ab}(\mathbf{x}, t; \mathbf{x}, t') \left(\frac{1 - \gamma_0}{2} \right)_{BC} \Gamma_{CD} \left(\mathcal{D}^{-1} \right)_{DA}^{ba} (\mathbf{x}, t'; \mathbf{x}, t) \right\rangle e^{-M(t' - t)}$$

Due to the structure of color as well as spin indices the expression can be written as a trace.

$$= - \left\langle \text{Tr}_{\text{spin,color}} \left[\left(\gamma_0 \Gamma^\dagger \gamma_0 \right) U(\mathbf{x}, t; \mathbf{x}, t') \left(\frac{1 - \gamma_0}{2} \right) \Gamma \mathcal{D}^{-1}(\mathbf{x}, t'; \mathbf{x}, t) \right] \right\rangle e^{-M(t' - t)}. \tag{3.5}$$

In the first five lines of equation (3.5) the quark fields are actually operators. In all other lines due to the path integral formalism there are no operators anymore. Note that we used

$$\left(\mathcal{Q}^{-1} \right)_{BC}^{ab} (\mathbf{x}, t; \mathbf{x}, t') = U^{ab}(\mathbf{x}, t; \mathbf{x}, t') \left[\theta(t - t') \left(\frac{1 + \gamma_0}{2} \right)_{BC} e^{-M(t - t')} + \theta(t' - t) \left(\frac{1 - \gamma_0}{2} \right)_{BC} e^{-M(t' - t)} \right] \tag{3.6}$$

for the heavy quark propagator (cf. Section 2.6.3).

The correlation function contains the light quark propagator $\mathcal{D}^{-1}$. Being the inverse of the Dirac operator, each entry $\mathcal{D}^{-1}(x, y)_{AB}^{ab}$ of a quark propagator connects the points (x, a, A) and (y, b, B) in space-time, color and spin space. For lattice volumes nowadays in use, the quark propagator is a matrix with $\mathcal{O}(10^{13})$ entries. Since the propagator describes the propagation in one particular gauge field, the entries of this matrix are correlated and parts of the matrix are less important than others. Computing and storing the full propagator would be an impossible task and a waste of computing resources. Instead, one uses only parts of the full propagator that are needed for the computation. Examples for this strategy are presented in the following section.

3.2. Using sources to express the quark propagator

The general idea is to express the relevant part of the quark propagator, which is the inverse of a large matrix, the Dirac operator, by a quantity which is less demanding to compute [38, 39, 40, 41, 42]. For a start, one can write down the following system of equations:

$$\mathcal{D}_{AB}^{ab}(x;y)\phi_B^b(y) = \xi_A^a(x). \tag{3.7}$$

Assuming that the spinor field ξ is known, one can solve for the spinor field ϕ. In order to solve for ϕ, the inverse operator of $\mathcal{D}$ is applied to both sides of equation (3.7). If ξ has a very simple form, one can easily express the components of the inverse $\mathcal{D}^{-1}$ by the spinor ϕ.

3.2.1. The point source method

In order to compute the light quark propagator $\mathcal{D}^{-1}$ from one space-time point to all other points in a resource-saving way, one can make use of point sources. We start with an equation describing the Dirac operator $\mathcal{D}$:

$$\mathcal{D}_{AB}^{ab}(x,y)\phi_B^b[\tilde{a},\tilde{A},\tilde{x}](y) = \xi_A^a[\tilde{a},\tilde{A},\tilde{x}](x). \tag{3.8}$$

$\xi_A^a[\tilde{a},\tilde{A},\tilde{x}](x)$ is a so called point source located at a point $\tilde{x}$, which has the form of a spinor at $\tilde{x}$ with 12 entries which are all zero but one, which is 1, formally expressed by:

$$\xi_A^a[\tilde{a},\tilde{A},\tilde{x}](x) = \delta^{a,\tilde{a}}\delta_{A,\tilde{A}}\delta(x-\tilde{x}). \tag{3.9}$$

Now one can solve equation (3.8) for ϕ and express the inverse of the Dirac operator $\mathcal{D}^{-1}(z,\tilde{x})$, which is the quark propagator from $\tilde{x}$ to any other space-time point z:

$$\begin{aligned}
&\mathcal{D}_{AB}^{ab}(x,y)\phi_B^b[\tilde{a},\tilde{A},\tilde{x}](y) = \xi_A^a[\tilde{a},\tilde{A},\tilde{x}](x) \\
\Longleftrightarrow &(\mathcal{D}^{-1})_{CA}^{ca}(z,x)\mathcal{D}_{AB}^{ab}(x,y)\phi_B^b[\tilde{a},\tilde{A},\tilde{x}](y) = (\mathcal{D}^{-1})_{CA}^{ca}(z,x)\xi_A^a[\tilde{a},\tilde{A},\tilde{x}](x) \\
\Longleftrightarrow &\delta_{C,B}\delta_{c,b}\delta(z-y)\phi_B^b[\tilde{a},\tilde{A},\tilde{x}](y) = (\mathcal{D}^{-1})_{CA}^{ca}(z,x)\xi_A^a[\tilde{a},\tilde{A},\tilde{x}](x) \\
\Longleftrightarrow &\phi_C^c[\tilde{a},\tilde{A},\tilde{x}](z) = (\mathcal{D}^{-1})_{CA}^{ca}(z,x)\xi_A^a[\tilde{a},\tilde{A},\tilde{x}](x) \\
\Longleftrightarrow &\phi_C^c[\tilde{a},\tilde{A},\tilde{x}](z) = (\mathcal{D}^{-1})_{C\tilde{A}}^{c\tilde{a}}(z,\tilde{x}).
\end{aligned} \tag{3.10}$$

ϕ is called a sink. ϕ carries information about the propagation from a fixed space-time point $\tilde{x}$ to an arbitrary space-time point z. In order to get all relevant information of the propagator $\mathcal{D}^{-1}$, one needs to solve Equation (3.8) for each possible index pair $(\tilde{a},\tilde{A})$, i.e. 12 times[1].

Expression (3.5) then reads (cf. the second last step, since the trace cannot be performed in a distinct way anymore):

$$C(t'-t) = -\left\langle \left(\gamma_0\Gamma^\dagger\gamma_0\right)_{AB} U(\mathbf{x},t;\mathbf{x},t')^{ab} \left(\frac{1-\gamma_0}{2}\right)_{BC} \Gamma_{CD}\phi_D^b[a,A,\mathbf{x},t](\mathbf{x},t')\right\rangle e^{-M(t'-t)}. \tag{3.11}$$

Point sources provide so-called point-to-all propagators. The advantage of the use of point sources is that the technique is rather straight-forward to implement and it does not introduce any stochastic noise. The downside of using this technique, however, originates from

---

[1] (number of spin components)$\times$(number of color components)$= 4 \times 3 = 12$

the fact that the light quark propagator has a fixed starting point $\tilde{x}$. Due to this, translational invariance cannot be exploited, i.e. spacial averaging which would reduce the statistical error (gauge noise) cannot be applied. To take into account another starting point we would have to perform another 12 inversions of the system (3.8) which would be computationally expensive. Because we want to take into account various heavy quark separations the point source method is not the method of choice for the systems investigated in this thesis.

In practice the exact computation of a propagator from any space-time point to any other is not possible for reasons stated above. However, an unbiased stochastic estimation can be made. In the following, methods that employ stochastic sources are introduced.

3.2.2. The volume source method

The most obvious idea to compute propagators between arbitrary space-time points is the method of so-called stochastic all-to-all propagators. We start with N stochastic volume sources $\xi[n]_A^a(x) = \pm\frac{1}{\sqrt{2}} \pm i\frac{1}{\sqrt{2}}$ which have the property:

$$\frac{1}{N}\sum_{n=1}^{N} \xi_A^a[n](x) \left(\xi_B^b[n](y)\right)^* = \delta^{ab}\delta_{AB}\delta(x-y) + \mathcal{O}\left(\frac{1}{\sqrt{N}}\right) \quad \text{off-diagonal noise.} \qquad (3.12)$$

One finds for the propagator:

$$\frac{1}{N}\sum_{n=1}^{N} \phi_A^a[n](x) \left(\xi_B^b[n](y)\right)^* = \left(\mathcal{D}^{-1}\right)_{AB}^{ab}(x;y) + \sum_{c,C,z}\left(\mathcal{D}^{-1}\right)_{AC}^{ac}(x;z)\times\mathcal{O}\left(\frac{1}{\sqrt{N}}\right) \quad \text{off-diagonal noise.}$$
$$(3.13)$$

We do not go into detail here because the approach is not used throughout this thesis, but we briefly state advantages and disadvantages of the technique. Obviously, translational invariance can be exploited to reduce gauge noise. However, one can show that the stochastic sources introduce V^2 noise terms of $\mathcal{O}\left(\frac{1}{\sqrt{N}}\right)$ with $V = TL^3$ the space-time volume of the lattice. The volume source method is only advantageous if the size of the propagator is small compared to the signal evoked by the correlation function. This is only the case for small time separations $t' - t$. For larger time separations as we are interested in in this thesis the signal-to-noise ratio deteriorates. Volume sources are not used in this work.

3.2.3. The timeslice source method

Instead of using stochastic volume sources one can chose to locate stochastic sources on a specific timeslice, i.e. all space-time points x with one particular time component $x_0 = \tilde{t}$. We consider N such sources. Each of them takes the form:

$$\xi_A^a[n,\tilde{t}](x) = \delta(t-\tilde{t})\left(\pm\frac{1}{\sqrt{2}} \pm i\frac{1}{\sqrt{2}}\right). \qquad (3.14)$$

Note that a different distribution of random numbers than $\pm\frac{1}{\sqrt{2}}$ are possible, as long as the sources fulfill the constraint:

$$\frac{1}{N}\sum_{n} \xi_A^a[n,\tilde{t}](x) \left(\xi_B^b[n,\tilde{t}](y)\right)^* = \delta^{ab}\delta_{AB}\delta(x_0-\tilde{t})\delta(y_0-\tilde{t})\delta(\mathbf{x}-\mathbf{y}) + \mathcal{O}\left(\frac{1}{\sqrt{N}}\right) \quad \text{off-diagonal noise.}$$
$$(3.15)$$

In order to express the quark propagator $\mathcal{D}^{-1}$ by the spinors ξ and ϕ one has to solve N linear systems:

$$
\begin{aligned}
&\mathcal{D}_{AB}^{ab}(x,y)\phi_B^b[n,\tilde{t}](y) = \xi_A^a[n,\tilde{t}](x)\\
\Longleftrightarrow\;& \left(\mathcal{D}^{-a}\right)_{CA}^{ca}(z,x)\mathcal{D}_{AB}^{ab}(x,y)\phi_B^b[n,\tilde{t}](y) = \left(\mathcal{D}^{-a}\right)_{CA}^{ca}(z;x)\xi_A^a[n,\tilde{t}](x)\\
\Longleftrightarrow\;& \phi_C^c[n,\tilde{t}](z) = \left(\mathcal{D}^{-a}\right)_{CA}^{ca}(z,x)\xi_A^a[n,\tilde{t}](x)\\
\Longleftrightarrow\;& \sum_n \phi_C^c[n,\tilde{t}](z)\left(\xi_B^b[n,\tilde{t}](y)\right)^* = \left(\mathcal{D}^{-a}\right)_{CA}^{ca}(z;x)\sum_n \xi_A^a[n,\tilde{t}](x)\left(\xi_B^b[n,\tilde{t}](y)\right)^*\\
\Longleftrightarrow\;& \sum_n \phi_C^c[n,\tilde{t}](z)\left(\xi_B^b[n,\tilde{t}](y)\right)^* = \left(\mathcal{D}^{-1}\right)_{CB}^{cb}(z;y)\delta(y_0-\tilde{t})\\
&\qquad\qquad\qquad\qquad\qquad + \sum_{a,A,\mathbf{x}} \left(\mathcal{D}^{-1}\right)_{CA}^{ca}(z;\mathbf{x},\tilde{t})\times\mathcal{O}\left(\frac{1}{\sqrt{N}}\right)\;\text{off-diagonal noise.}
\end{aligned}
$$
(3.16)

Using timeslice sources the correlation function (3.5) becomes:

$$
\begin{aligned}
C(t-t') = &-\frac{1}{N}\sum_n \left\langle \left(\gamma_0\Gamma^\dagger\gamma_0\right)_{AB} U(t,t')^{ab}\left(\frac{1-\gamma_0}{2}\right)_{BC}\Gamma_{CD}\phi_D^b[n,t](t')\left(\xi_A^a[n,t](t)\right)^* \right\rangle \mathrm{e}^{-M(t'-t)}\\
&- \left\langle \left(\gamma_0\Gamma^\dagger\gamma_0\right)_{AB}U(t,t')^{ab}\left(\frac{1-\gamma_0}{2}\right)_{BC}\Gamma_{CD}\sum_{c,C,\mathbf{z}}\left(\mathcal{D}^{-1}\right)_{DC}^{bc}(\mathbf{x},t';\mathbf{x},t)\right.\\
&\left.\times\mathcal{O}\left(\frac{1}{\sqrt{N}}\right)\;\text{off-diagonal noise}\right\rangle,
\end{aligned}
$$
(3.17)

where t is fixed. Spacial translational invariance of the correlation function can be exploited. However, for each light propagator, V_s^2 stochastic noise terms of $\mathcal{O}\left(\frac{1}{\sqrt{N}}\right)$ are introduced with V_s the spacial lattice extent. However, timeslice sources turn out to be more efficient than volume sources for large separations $t'-t$. The reason is that all propagators $\mathcal{D}^{-1}$ connect timeslices at t and t'. So for large t their space-time separations are all in the same order of magnitude. Therefore, the stochastic noise cannot be bigger than the signal evoked by the correlation function. The meson correlation functions discussed in Chapters 4, 5 and 7 are computed using timeslice sources.

3.2.4. The one-end trick

In Section 7.2 correlation functions that contain a heavy quark-antiquark pair and a pion are computed. Therefore we present the pion correlation function to discuss a very efficient method of computation.

The charged pion operator reads:

$$
\mathcal{O}_\pi(x) = \sum_{\mathbf{x}} \bar{u}(x)\gamma_5 d(x) \quad\text{and}\quad \mathcal{O}_\pi^\dagger(x) = -\sum_{\mathbf{x}} \bar{d}(x)\gamma_5 u(x).
$$
(3.18)

3. Hadron Spectroscopy

We obtain the correlation function in time via

$$
\begin{aligned}
C(y_0 - x_0) &= \langle\Omega|\, \mathcal{O}_\pi^\dagger(x)\mathcal{O}_\pi(y)\, |\Omega\rangle \\
&= -\langle\Omega|\sum_{\mathbf{x}} \bar{d}(x)\gamma_5 u(x) \sum_{\mathbf{y}} \bar{u}(y)\gamma_5 d(y)\,|\Omega\rangle \\
&= -\langle\Omega|\sum_{\mathbf{x}} \bar{d}_A^a(x)\,(\gamma_5)_{AB}\,u_B^a(x) \sum_{\mathbf{y}} \bar{u}_C^b(y)\,(\gamma_5)_{CD}\,d_D^b(y)\,|\Omega\rangle \\
&= \sum_{\mathbf{x},\mathbf{y}} \langle\Omega|\,(\gamma_5)_{AB}\, \underbrace{u_B^a(x)\bar{u}_C^b(y)}_{\mathcal{D}^{-1(u)}(x;y)_{BC}^{ab}}\,(\gamma_5)_{CD}\, \underbrace{d_D^b(y)\bar{d}_A^a(x)}_{\mathcal{D}^{-1(d)}(y;x)_{DA}^{ba}}\,|\Omega\rangle
\end{aligned}
\tag{3.19}
$$

twisted-mass γ_5-hermiticity

$$
= \sum_{\mathbf{x},\mathbf{y}} \left\langle (\gamma_5)_{AB}\left(\mathcal{D}^{-1(u)}\right)_{BC}^{ab}(x;y)\,(\gamma_5)_{CD}\left(\gamma_5\left(\mathcal{D}^{-1(d)}\right)^\dagger(x;y)\gamma_5\right)_{DA}^{ba}\right\rangle
$$

rename indices

$$
= \sum_{\mathbf{x},\mathbf{y}} \left\langle \left(\mathcal{D}^{-1(u)}\right)_{AB}^{ab}(x;y)\left(\mathcal{D}^{-1(d)}\right)^{\dagger\,ba}_{\ BA}(x;y)\right\rangle.
$$

For this special kind of correlation function where exactly two propagators are connected at space-time point x but no additional propagators connect to this point, the use of the so-called one-end trick is advantageous. Note that in the case discussed here, the one-end trick could equivalently be applied to the space-time point y instead of x.

$$
\begin{aligned}
C(y_0 - x_0) &= \sum_{\mathbf{x},\mathbf{y}} \left\langle \left(\mathcal{D}^{-1(u)}\right)_{AB}^{ab}(x;y)\left(\mathcal{D}^{-1(d)}\right)^{\dagger\,ba}_{\ BA}(x;y)\right\rangle \\
&= \frac{1}{N}\sum_n \left\langle \sum_{\mathbf{x},\mathbf{z},\mathbf{y}} \left(\mathcal{D}^{-1(u)}\right)_{AC}^{ac}(x;\mathbf{y},v_0)\xi_C^c[n,y_0](\mathbf{y},v_0)\right. \\
&\qquad\qquad \left.\left(\xi_B^b[n,y_0](\mathbf{z},z_0)\right)^* \left(\mathcal{D}^{-1(d)}\right)^{\dagger\,ba}_{\ BA}(x;\mathbf{z},z_0)\right\rangle + \text{ noise} \\
&= \frac{1}{N}\sum_n \left\langle \sum_{\mathbf{x},\mathbf{z},\mathbf{y}} \left(\mathcal{D}^{-1(d)}(\vec{x};\mathbf{z},z_0)\xi[n,y_0](\mathbf{z},z_0)\right)^\dagger \right. \\
&\qquad\qquad \left. \mathcal{D}^{-1(u)}(x;\mathbf{y},v_0)\xi[n,y_0](\mathbf{y},v_0)\right\rangle + \text{ noise} \\
&= \frac{1}{N}\sum_n \left\langle \sum_{\mathbf{x}} \phi^{(d)\dagger}[n,y_0](x)\phi^{(u)}[n,y_0](x)\right\rangle + \text{ noise}
\end{aligned}
\tag{3.20}
$$

where in the second line a property of the source terms is used:

$$
\begin{aligned}
\frac{1}{N}\sum_n \xi[n,y_0]_B^b(\mathbf{y},v_0)\left(\xi[n,y_0]_c^c(\mathbf{z},z_0)\right)^* =\ & \delta^{bc}\delta_{BC}\delta(v_0-y_0)\delta(z_0-y_0)\delta(\mathbf{y}-\mathbf{z}) \\
& + \mathcal{O}\left(\frac{1}{\sqrt{N}}\right)\ \text{off-diagonal noise.}
\end{aligned}
\tag{3.21}
$$

In the last line the relation

$$\sum_{\mathbf{u}} \mathcal{D}^{ab}_{AB}(v;u)\phi[n,\tilde{t}]^b_B(u) = \xi[n,\tilde{t}]^a_A(v) \Longrightarrow \phi[n,\tilde{t}]^b_B(u) = \sum_{\mathbf{v}} \mathcal{D}^{-1}(u;v)^{ba}_{BA}\xi[n,\tilde{t}]^a_A(v) \quad (3.22)$$

is used in order to get rid of the source terms. Note that the source terms ξ are identical regardless of the flavor u or d. The stochastic noise in Equation (3.20) corresponds to V_s^3 noise terms of $\mathcal{O}\left(\frac{1}{\sqrt{N}}\right)$. Note that in case of standard timeslice sources one has to expect V_s^4 stochastic noise terms. The number of signal terms is V_s^2 in both cases. Therefore, using the one-end-trick to compute the pion correlation function is clearly favorable.

3.3. Lattice techniques to improve the signal quality

In this section we briefly introduce commonly used techniques to improve the signal quality that are also applied in this thesis.

The larger the overlap of a trial state with the ground state of a system the better excited states in a correlation function are suppressed. Performing the average over neighboring spatial loops of link variables improves the overlap. The method is called *APE smearing* [43]. Smearing is applied to the spatial links, according to

$$U^{(N_{\mathrm{APE}})}(x,x+\hat{k}) = P_{SU(3)}\left(U^{(N_{\mathrm{APE}}-1)}(x,x+\hat{k}) + \alpha_{\mathrm{APE}}\sum_{j=\pm1,\pm2,\pm3}^{j\neq\pm k} U^{(N_{\mathrm{APE}}-1)}(x,x+\hat{j})\right.$$
$$\left.U^{(N_{\mathrm{APE}}-1)}(x+\hat{j},x+\hat{j}+\hat{k})U^{(N_{\mathrm{APE}}-1)}(x+\hat{j}+\hat{k},x+\hat{k})\right),$$
$$(3.23)$$

which recursively relates the N_{APE}-th iteration with the previous one. $U^{(0)}$ are the original (unsmeared) links and α_{APE} is a weight parameter. $P_{SU(3)}$ denotes a projection back to $SU(3)$. The concrete number of smearing steps N_{APE} and of α_{APE} depends on the observable as well as on the parameters of the lattice setup and has to be adjusted for every computation. A smearing technique which is applied to the light quark fields is *Gaussian smearing* [44]. It is defined by

$$\chi^{(N_{\mathrm{Gauss}})}(x) = \frac{1}{1+6\kappa}\left(\chi^{(N_{\mathrm{Gauss}}-1)}(x)\right.$$
$$\left.+ \kappa_{\mathrm{Gauss}}\sum_{j=\pm1,\pm2,\pm3} U^{(N_{\mathrm{APE}})}(x,x+\hat{j})\chi^{(N_{\mathrm{Gauss}}-1)}(x+\hat{j})\right),$$
$$(3.24)$$

which again relates the N_{Gauss}-th iteration with the previous one. $\chi^{(0)}$ are the original unsmeared light quark fields, $U^{(N_{\mathrm{Gauss}})}$ denote Gaussian smeared spatial links. The parameter κ_{Gauss} has to be adjusted.

The signal quality of static quark propagators in temporal direction can be improved by applying *HYP smearing*. For each line of temporal links the HYP smearing algorithm performs smearing over all loops of links inside a hypercube of a certain width. Details of the smearing process depend on three parameters α_1, α_2 and α_3. For more information on HYP smearing, cf. [45].

4. Heavy-light four-quark systems

In this chapter, heavy-light four-quark systems $\bar{b}\bar{b}qq$ and $b\bar{b}q\bar{q}$ are introduced. The lighter quarks q can have different flavors: $q \in \{u, d, s, c\}$. One way to treat the heavy quarks is to assume them to have an infinite mass, i.e. to be in the static approximation. Since B mesons are possible building blocks of the static-light $\bar{b}\bar{b}qq/b\bar{b}q\bar{q}$ systems, we give a brief overview of B meson properties. In the static approximation, it is possible to obtain the potential between these mesons as a function of the separation of the heavy quarks. We state general properties of static-light BB and $B\bar{B}$ systems such as symmetries and quantum numbers. We describe differences between systems in continuum QCD and systems in twisted mass Lattice QCD. In order to investigate whether the binding between the four-quarks is sufficiently strong to form a bound state it is convenient to assume the so-called Born-Oppenheimer perspective.

4.1. B mesons: Terminology

B mesons are mesons containing a $\bar{b}$ antiquark and a lighter quark q. Equivalently, $\bar{B}$ mesons contain a b quark and a lighter quark $\bar{q}$. Their masses are around 5.3 GeV and are dominated by the contribution of the bottom quark/antiquark. The naming scheme of B mesons is the following [2]: The heavy (anti-)quark (here $b/\bar{b}$) determines the main symbol B. If the light quark q is s or c, this is indicated by a lower index. In the case of $q \in \{u, d\}$, no lower index is given. An upper index indicates the electric charge of the meson. If the heavy (anti-)quark has a positive charge, one speaks of a meson, otherwise of an antimeson. For antimesons that are electrically charged, no further labeling is needed, whereas electrically neutral antimesons are indicated with a bar. However, to improve readability in this thesis we label all antimesons with a bar. A star $*$ identifies mesons with an even angular momentum quantum number and positive parity $J^{\mathcal{P}} = 0^+, 2^+, \ldots$ as well as mesons with an odd angular momentum quantum number and negative parity $J^{\mathcal{P}} = 1^-, 3^-, \ldots$. If a meson has angular momentum and parity different from $J^{\mathcal{P}} = 0^-$ ("scalar") or 1^- ("vector") the angular momentum J is added as a subscript. In Table 4.1 some examples for experimentally established B mesons are listed.

4.2. B mesons in the static approximation

In this and the following section, we introduce properties of B mesons and $\bar{b}\bar{b}qq/b\bar{b}q\bar{q}$ systems in the static approximation. These sections are essentially based on [5]. To investigate B mesons using Lattice QCD, the lighter quarks (u, d, s, c) can be treated fully dynamically. This is, however, not possible when it comes to the bottom quark, whose mass is larger than the typical ultraviolet cut-off on the lattice, i.e. the inverse lattice spacing. One way to treat the b quark is to use Heavy Quark Effective Theory (HQET), which is introduced in Section 2.6. The leading order of HQET is the static approximation, which means that the bottom quark is treated as infinitely heavy and hence static, i.e. its spatial position is fixed. This approximation is used in all lattice computations in Chapters 5 and 7. Thus, B mesons can

4. Heavy-light four-quark systems

	flavor content	I	J	P	Q	mass in MeV
$B^+/\bar{B}^-$	$u\bar{b}/\bar{u}b$	$\frac{1}{2}$	0	-	+1/-1	5279.31 ± 0.15
B^0	$d\bar{b}$	$\frac{1}{2}$	0	-	0	5279.62 ± 0.15
B^0_s	$s\bar{b}$	0	0	-	0	5366.82 ± 0.22
$\bar{B}^-_c$	$\bar{c}b$	0	0	-	-1	6275.10 ± 1.00
B^{+*}	$u\bar{b}$	$\frac{1}{2}$	1	-	+1	5324.65 ± 0.25

Table 4.1.: Flavor content, isopin I, angular momentum J, parity P, electromagnetic charge Q and mass of various experimentally established B mesons included in the Particle Data Group review [2].

be approximated as static-light mesons made from a static antiquark $\bar{Q}$ and a light quark $q \in \{u, d\}$. Analogously static-light B_s and B_c mesons are made from a static antiquark $\bar{Q}$ and a light s or c quark, respectively.

Quantum numbers

We now discuss the quantum numbers that characterizes the static-light B meson.

Flavor quantum numbers: For B mesons, the isospin is $I = 1/2$ and $I_z \in \{-1/2, +1/2\}$.

Angular momentum: There are no interactions involving the static quark spin. As a consequence, B and B^* mesons are degenerate in the static approximation. Hence it is more appropriate to classify static-light mesons by the total angular momentum j of their lighter degrees of freedom. The total angular momentum is $j = |l \pm 1/2|$, where l is the orbital angular momentum which also includes the gluonic spin and $\pm 1/2$ is the spin of the light quark.

Parity and charge conjugation: Parity is also a quantum number, $\mathcal{P} \in \{+, -\}$. Charge conjugation is not a good quantum number, since the two quarks in a meson are non-identical.

Trial states

The trial states to investigate static-light mesons $\bar{Q}q$ are $\bar{Q}\Gamma\psi|\Omega\rangle$. Here, Q and ψ denote the static and light quark fields, respectively. A static quark has only two spinor components, so it can be written as $\bar{Q}(\mathbb{1} + \gamma_0)/2$. Accordingly, for the ground state (S meson), Γ can be chosen as $\gamma_5(\mathbb{1} - \gamma_0)/2$, or $\gamma_j(\mathbb{1} - \gamma_0)/2$, while for the first excited state (P_- meson), Γ can be $(\mathbb{1} + \gamma_0)/2$ or $\gamma_j\gamma_5(\mathbb{1} + \gamma_0)/2$. S denotes the state with orbital angular momentum $l = 0$, total angular momentum $|j| = |j_z| = \frac{1}{2}$ and parity $\mathcal{P} = -$. In the static approximation the heavy quark spin decouples from the system, so this corresponds to $J^{\mathcal{P}} = 0^-$ ($B^\pm$ or B^0 meson) or $J^{\mathcal{P}} = 1^-$ (B^* meson). P_- corresponds to $J^{\mathcal{P}} = 0^+$ (B^*_0 meson) or $J^{\mathcal{P}} = 1^+$ (B^*_1 meson). For a more detailed discussion of S and P_- states, cf. [5]. Note that this holds in QCD, while in twisted mass Lattice QCD S and P_- are from the same sector, since parity is not an exact symmetry, as we clarify below. For a more detailed discussion, cf. [5, 46, 47].

4.3. BB and $B\bar{B}$ systems in the static approximation

4.3.1. Continuum

Our aim is to to determine the potential of a pair of static-light B mesons respectively a static-light B meson and a static-light $\bar{B}$ meson as a function of their spatial separation r, taken to be along the z-axis. We will consider the B meson to be $\bar{Q}q$, i.e. the static quarks to be antiquarks and the $\bar{B}$ mesons to be $Q\bar{q}$. Let the positions of the static (anti-)quarks be $\mathbf{r}_1 = (0, 0, -r/2)$ and $\mathbf{r}_2 = (0, 0, +r/2)$, i.e. $r = |\mathbf{r}_1 - \mathbf{r}_2|$. These coordinates then define the position of each static-light meson.

Quantum numbers

The quantum numbers that characterize the BB and $B\bar{B}$ states are the following:

Flavor quantum numbers: The isospin is carried only by the $u/\bar{u}$ and $d/\bar{d}$ quarks. The BB system and the $B\bar{B}$ system can thus have isospin $I \in \{0\,,\,1\}$ and $I_z \in \{-1\,,\,0\,,\,+1\}$. In the case of BB systems we also consider symmetric flavor combinations ss and cc as well as antisymmetric flavor combinations $s^{(1)}s^{(2)} - s^{(2)}s^{(1)}$ and $c^{(1)}c^{(2)} - c^{(2)}c^{(1)}$ with $s^{(1)}s^{,(2)}$ and $c^{(1)}, c^{(2)}$ hypothetical degenerate flavors with the mass of the s and the c quark, respectively.

Angular momentum: Rotational symmetry is restricted to rotations around the axis of separation of static (anti-)quarks, hence the states can be classified by the z-component of the total angular momentum. Since the spin of the static (anti-)quark decouples from the system, it is more appropriate to label states by j_z of the relativistic quarks or antiquarks qq and $q\bar{q}$ i.e. $j_z \in \{-1\,,\,0\,,\,+1\}$.

Parity and charge conjugation: BB states can be labeled by the eigenvalue of the parity operator $\mathcal{P} \in \{+\,,\,-\}$. For $B\bar{B}$ states, however, parity is not a good quantum number, because here heavy quark and antiquark are separated by r and a parity transformation interchanges the positions of particle and antiparticle. Instead, parity in combination with charge conjugation $\mathcal{C}$ can be considered. For $B\bar{B}$, $\mathcal{P} \circ \mathcal{C}$ is an adequate quantum number.

Reflection along x-axis: For states BB and $B\bar{B}$ with $j_z = 0$ there exists another symmetry: reflection around one of the axes perpendicular to the axis of separation, chosen here to be the x-axis. We label the corresponding quantum number by $\mathcal{P}_x$, which can take values $\{+\,,\,-\}$. Note that when using $|j_z|$ instead of j_z, $\mathcal{P}_x$ is a quantum number for all states, i.e. also for $j_z \neq 0$.

Summarizing, BB states can be labeled by five quantum numbers $(I, I_z, |j_z|, \mathcal{P}, \mathcal{P}_x)$ while $B\bar{B}$ systems can be labeled by another five quantum numbers $(I, I_z, |j_z|, \mathcal{P} \circ \mathcal{C}, \mathcal{P}_x)$.

Trial states

In general, BB trial states take the form:

$$O_{BB,r}(t)|\Omega\rangle = (\mathcal{C}\Gamma)_{AB}(\mathcal{C}\tilde{\Gamma})_{CD}\Big(\bar{Q}_C^a(\mathbf{r}_1,t)\psi_A^{(f)a}(\mathbf{r}_1,t)\Big)\Big(\bar{Q}_D^b(\mathbf{r}_2,t)\psi_B^{(f')b}(\mathbf{r}_2,t)\Big)|\Omega\rangle, \quad (4.1)$$

where $\mathcal{C}$ is the charge conjugation matrix that can be chosen as $\mathcal{C} = \gamma_0\gamma_2$. Γ, $\tilde{\Gamma}$ are combinations of γ matrices and $r = |\mathbf{r}_1 - \mathbf{r}_2|$. Note that one has to couple the light degrees of freedom of both mesons in spinor space, because these degrees of freedom determine the angular momentum quantum number $|j_z|$. If one separately couples the heavy and light degrees of freedom in both mesons instead, the resulting angular momentum quantum number is not well-defined. For $\tilde{\Gamma}$, only $\tilde{\Gamma} \in \{(\mathbb{1} + \gamma_0), (\mathbb{1} + \gamma_0)\gamma_j\gamma_5\}$, $j = 1, 2, 3$, give non-zero correlation functions. The corresponding potential does not depend on the particular choice. Note that the coupling of the light degrees of freedom in spinor space via Γ determines the quantum numbers $|j_z|$, $\mathcal{P}$ and $\mathcal{P}_x$. We consider the following flavour combinations:

- $\psi^{(f)}\psi^{(f')} = ud - du$ with $I = 0$,

- $\psi^{(f)}\psi^{(f')} = uu$ with $I = 1$, $I_z = 1$,

- $\psi^{(f)}\psi^{(f')} = dd$ with $I = 1$, $I_z = -1$,

- $\psi^{(f)}\psi^{(f')} = ud + du$ with $I = 1$, $I_z = 0$.

We also consider, as mentioned above, symmetric flavor combinations ss and cc as well as antisymmetric flavor combinations $s^{(1)}s^{(2)} - s^{(2)}s^{(1)}$ and $c^{(1)}c^{(2)} - c^{(2)}c^{(1)}$ with $s^{(1)}s,^{(2)}$ and $c^{(1)}, c^{(2)}$. $B\bar{B}$ trial states take the form:

$$O_{B\bar{B},t}(t)|\Omega\rangle = \Gamma_{AB}\tilde{\Gamma}_{CD}\Big(\bar{Q}_C^a(\mathbf{r}_1,t)\psi_A^{(f)a}(\mathbf{r}_1,t)\Big)\Big(Q_D^b(\mathbf{r}_2,t)\bar{\psi}_B^{(f')b}(\mathbf{r}_2,t)\Big)|\Omega\rangle, \qquad (4.2)$$

where Γ and $\tilde{\Gamma}$ are given combinations of γ matrices. For $\tilde{\Gamma}$, only $\tilde{\Gamma} = \{(\mathbb{1}+\gamma_0)\gamma_5, (\mathbb{1}+\gamma_0)\gamma_j\}$, $j = 1, 2, 3$, give non-zero correlation functions. The obtained potential does not depend on the particular choice. Note that the coupling of the light degrees of freedom in spinor space via Γ determines the quantum numbers $|j_z|$, $\mathcal{P} \circ \mathcal{C}$ and $\mathcal{P}_x$. We consider the following flavour combinations:

- $\psi^{(f)}\bar{\psi}^{(f')} = u\bar{u} + d\bar{d}$ with $I = 0$,

- $\psi^{(f)}\bar{\psi}^{(f')} = u\bar{d}$ with $I = 1$, $I_z = 1$,

- $\psi^{(f)}\bar{\psi}^{(f')} = d\bar{u}$ with $I = 1$, $I_z = -1$,

- $\psi^{(f)}\bar{\psi}^{(f')} = u\bar{u} - d\bar{d}$ with $I = 1$, $I_z = 0$.

4.3.2. Twisted mass Lattice QCD

Trial states

Working with twisted mass fermions on the lattice, it is convenient to express the trial states in the twisted basis. For more details on twisted mass Lattice QCD, cf. Section 2.3.2. The trial states read:

$$O_{BB,r}(t)|\Omega\rangle = (\mathcal{C}\Gamma)_{AB}(\mathcal{C}\tilde{\Gamma})_{CD}\Big(\bar{Q}_C^a(\mathbf{r}_1,t)\chi_A^{(f)a}(\mathbf{r}_1,t)\Big)\Big(\bar{Q}_D^b(\mathbf{r}_2,t)\chi_B^{(f')b}(\mathbf{r}_2,t)\Big)|\Omega\rangle \qquad (4.3)$$

and

$$O_{B\bar{B},r}|\Omega\rangle = \Gamma_{AB}\tilde{\Gamma}_{CD}\Big(\bar{Q}_C^a(\mathbf{r}_1,t)\chi_A^{(f)a}(\mathbf{r}_1,t)\Big)\Big(Q_D^b(\mathbf{r}_2,t)\bar{\chi}_B^{(f')b}(\mathbf{r}_2,t)\Big)|\Omega\rangle, \qquad (4.4)$$

respectively. The lattice formulation of QCD breaks some continuum symmetries that are restored only in the continuum limit. Moreover, twisted mass fermions break two additional continuum symmetries (with respect to e.g. standard Wilson fermions): parity and isospin. This breaking is a discretization effect which is proportional to that lattice spacing a, i.e. in the continuum these symmetries are restored. However, a certain combination of parity and isospin yields a symmetry of twisted mass Lattice QCD.

Quantum numbers

Rotational symmetry: Continuum QCD is symmetric under spatial rotations described by the rotation group $SO(3)$. On the lattice, this group is broken to the cubic group $H(3)$, which implies that the symmetry constraints are less strict and hence mixing within different representations of the full $SO(3)$ group can occur. In our case, instead of an infinite number of representations labeled by $j_z = 0, \pm 1, \pm 2, \ldots$, there are only four different cubic representations, where the continuum representations are mixed, corresponding to $j_z \in \{0, \pm 4, \pm 8, \ldots\}$, to $j_z \in \{+1, -3, +5, \ldots\}$, to $j_z \in \{-1, +3, -5, \ldots\}$ and to $j_z \in \{\pm 2, \pm 6, \pm 10, \ldots\}$. We do not attempt to assign continuum j_z values to the extracted lattice states in a rigorous way. However, since large angular momentum is usually associated with high energy, it is plausible that we investigate the lowest lying states corresponding to $j_z = 0$ and $|j_z| = 1$, respectively.

Isospin: As we mentioned above, twisted mass Lattice QCD breaks isospin at finite lattice spacing. The most prominent example of this fact is the splitting between the neutral and charged pion masses. In our investigations, the consequence is that I is not a quantum number, only I_z is conserved. This leads to a mixing between the continuum sectors ($I = 0$, $I_z = 0$) and ($I = 1$, $I_z = 0$).[1] As we will mention in Section 5.3, isospin breaking can give some estimate about the size of cut-off effects.

Parity and charge conjugation: Parity $\mathcal{P}$ and consequently also $\mathcal{P} \circ \mathcal{C}$ is broken by twisted mass fermions. However, a particular combination of parity and isospin rotation is still a symmetry: $\mathcal{P}^{(\mathrm{tm})} \equiv \mathcal{P} \times [u \leftrightarrow d]$, i.e. parity combined with light flavor exchange. For BB systems the properties of trial states under $\mathcal{P}^{(\mathrm{tm})}$ depend on the considered flavor structure:

- $I_z = 0$ trial states (with light flavor structure $ud \pm du$) have definite properties under $\mathcal{P}^{(\mathrm{tm})}$.

- $I_z = \pm 1$ trial states (light flavor structure uu or dd) do not have definite properties under $\mathcal{P}^{(\mathrm{tm})}$.

- Trial states with light flavor structure $uu \pm dd$ have a definite $\mathcal{P}^{(\mathrm{tm})}$ quantum number, but I_z is not definite.

There is no conceptual advantage of using either uu/dd or $uu \pm dd$, since the spectrum of the two sectors (no matter whether they are split by I_z or by $\mathcal{P}^{(\mathrm{tm})}$) is degenerate. Due to simpler notation, we decide for uu/dd. For $B\bar{B}$ states $\mathcal{P}^{(\mathrm{tm})} \circ \mathcal{C}$ is a quantum number for each of the flavor structures $u\bar{u} \pm d\bar{d}$ and $u\bar{d}/d\bar{u}$.

---

[1]In principle, also mixing with $I = 2, 3, 4, \ldots$ occurs. In practice, however, this is not expected to be problem, as higher isospin states are related to multi-quark states that have by construction small overlap with our trial states. Therefore, any mixing with higher isospin states is strongly suppressed.

4. Heavy-light four-quark systems

Reflection along x-axis: As in the continuum, it is important to consider also reflections around one of the axes perpendicular to the axis of separation. Again, we choose the x-axis. $\mathcal{P}_x^{(\mathrm{tm})}$ is defined as $\mathcal{P}_x \times [u \leftrightarrow d]$. Note that for BB systems the properties of trial states with different flavor structures are:

- $I_z = 0$ trial states (light flavor structure $ud \pm du$) have definite $\mathcal{P}_x^{(\mathrm{tm})}$ properties.
- For states with $I_z = \pm 1$ (light flavor structure uu or dd), only $\mathcal{P}^{(\mathrm{tm})} \circ \mathcal{P}_x^{(\mathrm{tm})}$ is a quantum number.

For $B\bar{B}$ systems the properties of trial states with different flavour structures are:

- For $I_z = 0$ trial states (light flavour structure $u\bar{u} \pm d\bar{d}$) only $\mathcal{P}^{(\mathrm{tm})} \circ \mathcal{P}_x^{(\mathrm{tm})}$ is a quantum number.
- States with $I_z = \pm 1$ (light flavour structure $u\bar{d}$ or $d\bar{u}$) have definite $\mathcal{P}_x^{(\mathrm{tm})}$ properties.

We list all the trial states and quantum numbers for the twisted mass case in tables in the Appendix. For BB systems with $I_z = \pm 1$, i.e. $\chi^{(1)}\chi^{(2)} = uu$ or dd, see Table A.2 while for BB systems with $I_z = 0$, i.e. $\chi^{(1)}\chi^{(2)} = ud \pm du$, see Table A.3. For $B\bar{B}$ systems with $I_z = \pm 1$, i.e. $\chi^{(1)}\chi^{(2)} = u\bar{d}$ or $d\bar{u}$, see Table A.4 and for $B\bar{B}$ systems with $I_z = 0$, i.e. $\chi^{(1)}\chi^{(2)} = u\bar{u} \pm d\bar{d}$, see Table A.5.

4.3.3. Interpretation of trial states in terms of individual B mesons

In this Section we express for later reference the trial states of the BB system in terms of individual B mesons. This Section is essentially taken from [5]. An equivalent discussion for the $B\bar{B}$ system is presented in [48]. The creation operators in the trial states introduced in Equation (4.1) excite BB meson pairs. Due to coupling of heavy and light quarks, the individual B mesons inside these states are, however, not of definite parity and spin. The BB trial states are formed by linear combinations of different B mesons. To analyze this content, one can introduce parity and spin projectors. The parity projectors are:

$$P_{\mathcal{P}=\pm} = \frac{1 \pm \gamma_0}{2} \tag{4.5}$$

and spin projectors for the non-static quark fields are:

$$P_{j_z=\uparrow,\downarrow} = \frac{1 \pm i\gamma_0\gamma_3\gamma_5}{2}, \tag{4.6}$$

where the plus (minus) sign corresponds to $j_z = \uparrow$ ($j_z = \downarrow$).

We work explicitly in the Dirac representation of the γ-matrices with the following conventions:

$$\gamma_0 = \begin{pmatrix} \mathbb{1} & 0 \\ 0 & -\mathbb{1} \end{pmatrix} \quad , \quad \gamma_j = \begin{pmatrix} 0 & -i\sigma_j \\ +i\sigma_j & 0 \end{pmatrix}, \tag{4.7}$$

which is the most convenient, since it yields diagonal parity projectors. The four parity-spin projectors have then the following form:

$$P_{\mathcal{P}=+}P_{j_z=\uparrow} = \mathrm{diag}(1,0,0,0) = (1\,0\,0\,0)(1\,0\,0\,0)^T \equiv \mathbf{v}^\dagger_{\mathcal{P}=+,j_z=\uparrow}\mathbf{v}_{\mathcal{P}=+,j_z=\uparrow}, \tag{4.8}$$

$$P_{\mathcal{P}=+}P_{j_z=\downarrow} = \mathrm{diag}(0,1,0,0) = (0\,1\,0\,0)(0\,1\,0\,0)^T \equiv \mathbf{v}^\dagger_{\mathcal{P}=+,j_z=\downarrow}\mathbf{v}_{\mathcal{P}=+,j_z=\downarrow}, \tag{4.9}$$

$$P_{\mathcal{P}=-}P_{j_z=\downarrow} = \mathrm{diag}(0,0,1,0) = (0\,0\,1\,0)(0\,0\,1\,0)^T \equiv \mathbf{v}^\dagger_{\mathcal{P}=-,j_z=\downarrow}\mathbf{v}_{\mathcal{P}=-,j_z=\downarrow}, \tag{4.10}$$

$$P_{\mathcal{P}=-}P_{j_z=\uparrow} = \mathrm{diag}(0,0,0,1) = (0\,0\,0\,1)(0\,0\,0\,1)^T \equiv \mathbf{v}^\dagger_{\mathcal{P}=-,j_z=\uparrow}\mathbf{v}_{\mathcal{P}=-,j_z=\uparrow}. \tag{4.11}$$

The sum of the four above projectors is, of course, the identity operator

$$1 \;=\; P_{\mathcal{P}=+}P_{j_z=\uparrow} + P_{\mathcal{P}=+}P_{j_z=\downarrow} + P_{\mathcal{P}=-}P_{j_z=\uparrow} + P_{\mathcal{P}=-}P_{j_z=\downarrow}, \tag{4.12}$$

which can be inserted into the light spin coupling of a BB creation operator with a Dirac gamma structure Γ:

$$\psi^T \mathcal{C}\Gamma\psi = \sum_{\substack{\mathcal{P}_1=\pm \\ j_1=\uparrow,\downarrow}} \sum_{\substack{\mathcal{P}_2=\pm \\ j_2=\uparrow,\downarrow}} \psi^T \mathbf{v}^\dagger_{\mathcal{P}=\mathcal{P}_1,j_z=j_1} \underbrace{\mathbf{v}_{\mathcal{P}=\mathcal{P}_1,j_z=j_1}\mathcal{C}\Gamma\mathbf{v}^\dagger_{\mathcal{P}=\mathcal{P}_2,j_z=j_2}}_{=c_{\mathcal{P}_1 j_1;\mathcal{P}_2 j_2}} \mathbf{v}_{\mathcal{P}=\mathcal{P}_2,j_z=j_2}\psi. \tag{4.13}$$

The coefficients $c_{\mathcal{P}_1 j_1;\mathcal{P}_2 j_2}$ represent the static-light meson content, i.e. they can take a value of ±1 or $\pm i$ indicating that a given trial state excites the two B mesons with parity $\mathcal{P} = \mathcal{P}_1$, spin $j_z = j_1$ and parity $\mathcal{P} = \mathcal{P}_2$, spin $j_z = j_2$ or the value 0, if a given meson pair is not excited by the considered operator. We remind that $\mathcal{P} = +$ corresponds to the P_- meson and $\mathcal{P} = -$ to the S meson. Together with the light angular momentum j_1 and j_2, there are 16 possibilities for the meson content related to a given trial state, but only 4 coefficients $c_{\mathcal{P}_1 j_1;\mathcal{P}_2 j_2}$ are always non-zero. In Table 4.2 the meson contents for all possible Γ structures are listed for the BB system (left) and for the $B\bar{B}$ system (right).

As one can see from Table 4.2, a BB trial state with e.g. $\Gamma = \gamma_5 + \gamma_0\gamma_5$ only contains S meson contributions. Therefore this Γ structure corresponds to a ground state meson. For further details, cf. Section 5.3.4.

Γ physical	meson content	Γ physical	meson content
γ_5	$-S_\uparrow S_\downarrow + S_\downarrow S_\uparrow - P_\uparrow P_\downarrow + P_\downarrow P_\uparrow$	γ_5	$+S_\uparrow S_\uparrow + S_\downarrow S_\downarrow + P_\uparrow P_\uparrow + P_\downarrow P_\downarrow$
$\gamma_0\gamma_5$	$-S_\uparrow S_\downarrow + S_\downarrow S_\uparrow + P_\uparrow P_\downarrow - P_\downarrow P_\uparrow$	$\gamma_0\gamma_5$	$-S_\uparrow S_\uparrow - S_\downarrow S_\downarrow + P_\uparrow P_\uparrow + P_\downarrow P_\downarrow$
$\mathbb{1}$	$-S_\uparrow P_\downarrow + S_\downarrow P_\uparrow - P_\uparrow S_\downarrow + P_\downarrow S_\uparrow$	$\mathbb{1}$	$+S_\uparrow P_\uparrow + S_\downarrow P_\downarrow + P_\uparrow S_\uparrow + P_\downarrow S_\downarrow$
γ_0	$-S_\uparrow P_\downarrow + S_\downarrow P_\uparrow + P_\uparrow S_\downarrow - P_\downarrow S_\uparrow$	γ_0	$+S_\uparrow P_\uparrow + S_\downarrow P_\downarrow - P_\uparrow S_\uparrow - P_\downarrow S_\downarrow$
γ_3	$-iS_\uparrow S_\downarrow - iS_\downarrow S_\uparrow + iP_\uparrow P_\downarrow + iP_\downarrow P_\uparrow$	γ_3	$+iS_\uparrow S_\uparrow - iS_\downarrow S_\downarrow - iP_\uparrow P_\uparrow + iP_\downarrow P_\downarrow$
$\gamma_0\gamma_3$	$-iS_\uparrow S_\downarrow - iS_\downarrow S_\uparrow - iP_\uparrow P_\downarrow - iP_\downarrow P_\uparrow$	$\gamma_0\gamma_3$	$-iS_\uparrow S_\uparrow + iS_\downarrow S_\downarrow - iP_\uparrow P_\uparrow + iP_\downarrow P_\downarrow$
$\gamma_3\gamma_5$	$-iS_\uparrow P_\downarrow - iS_\downarrow P_\uparrow + iP_\uparrow S_\downarrow + iP_\downarrow S_\uparrow$	$\gamma_3\gamma_5$	$-iS_\uparrow P_\uparrow + iS_\downarrow P_\downarrow + iP_\uparrow S_\uparrow - iP_\downarrow S_\downarrow$
$\gamma_0\gamma_3\gamma_5$	$-iS_\uparrow P_\downarrow - iS_\downarrow P_\uparrow - iP_\uparrow S_\downarrow - iP_\downarrow S_\uparrow$	$\gamma_0\gamma_3\gamma_5$	$-iS_\uparrow P_\uparrow + iS_\downarrow P_\downarrow - iP_\uparrow S_\uparrow + iP_\downarrow S_\downarrow$
γ_1	$+iS_\uparrow S_\uparrow - iS_\downarrow S_\downarrow - iP_\uparrow P_\uparrow + iP_\downarrow P_\downarrow$	γ_1	$+iS_\uparrow S_\downarrow + iS_\downarrow S_\uparrow - iP_\uparrow P_\downarrow - iP_\downarrow P_\uparrow$
$\gamma_0\gamma_1$	$+iS_\uparrow S_\uparrow - iS_\downarrow S_\downarrow + iP_\uparrow P_\uparrow - iP_\downarrow P_\downarrow$	$\gamma_0\gamma_1$	$-iS_\uparrow S_\downarrow - iS_\downarrow S_\uparrow - iP_\uparrow P_\downarrow - iP_\downarrow P_\uparrow$
$\gamma_1\gamma_5$	$+iS_\uparrow P_\uparrow - iS_\downarrow P_\downarrow - iP_\uparrow S_\uparrow + iP_\downarrow S_\downarrow$	$\gamma_1\gamma_5$	$-iS_\uparrow P_\downarrow - iS_\downarrow P_\uparrow + iP_\uparrow S_\downarrow + iP_\downarrow S_\uparrow$
$\gamma_0\gamma_1\gamma_5$	$+iS_\uparrow P_\uparrow - iS_\downarrow P_\downarrow + iP_\uparrow S_\uparrow - iP_\downarrow S_\downarrow$	$\gamma_0\gamma_1\gamma_5$	$-iS_\uparrow P_\downarrow - iS_\downarrow P_\uparrow - iP_\uparrow S_\downarrow - iP_\downarrow S_\uparrow$
γ_2	$-S_\uparrow S_\uparrow - S_\downarrow S_\downarrow + P_\uparrow P_\uparrow + P_\downarrow P_\downarrow$	γ_2	$-S_\uparrow S_\downarrow + S_\downarrow S_\uparrow + P_\uparrow P_\downarrow - P_\downarrow P_\uparrow$
$\gamma_0\gamma_2$	$-S_\uparrow S_\uparrow - S_\downarrow S_\downarrow - P_\uparrow P_\uparrow - P_\downarrow P_\downarrow$	$\gamma_0\gamma_2$	$+S_\uparrow S_\downarrow - S_\downarrow S_\uparrow + P_\uparrow P_\downarrow - P_\downarrow P_\uparrow$
$\gamma_2\gamma_5$	$-S_\uparrow P_\uparrow - S_\downarrow P_\downarrow + P_\uparrow S_\uparrow + P_\downarrow S_\downarrow$	$\gamma_2\gamma_5$	$+S_\uparrow P_\downarrow - S_\downarrow P_\uparrow - P_\uparrow S_\downarrow + P_\downarrow S_\uparrow$
$\gamma_0\gamma_2\gamma_5$	$-S_\uparrow P_\uparrow - S_\downarrow P_\downarrow - P_\uparrow S_\uparrow - P_\downarrow S_\downarrow$	$\gamma_0\gamma_2\gamma_5$	$+S_\uparrow P_\downarrow - S_\downarrow P_\uparrow + P_\uparrow S_\downarrow - P_\downarrow S_\uparrow$

Table 4.2.: Relation between the physical basis γ structure and the static-light meson content. For brevity, $P_{-;\downarrow/\uparrow}$ is denoted as $P_{\downarrow/\uparrow}$. **(left):** BB system (table taken from [5]). **(right):** $B\bar{B}$ system (table taken from [48]).

4.4. Heavy-light four-quark systems from the Born-Oppenheimer perspective

In this thesis we study heavy-heavy-light-light four-quark systems $\bar{b}\bar{b}ud$ and $b\bar{b}u\bar{d}$. From basic principles of QCD we know that these systems form bound states if the b quarks are heavy enough, cf. e.g. [49]. One way to understand in more detail why binding should occur is to use the Born-Oppenheimer perspective [50], where the wave function of the two heavy b quarks is determined considering the effective potential of the b quarks in the presence of the light quarks. At very short separations of the b quarks, they interact with a perturbative one-gluon-exchange Coulomb potential, while at large separations, the interaction is screened by the light quarks and the four quarks form two rather weakly interacting B mesons, respectively a B and a $\bar{B}$ meson. In Figure 4.1 we illustrate the situation by means of a BB system. In this case, a screened Coulomb potential is expected. This potential clearly produces a bound state if the b quarks are heavy enough (cf. also Appendix A.4).
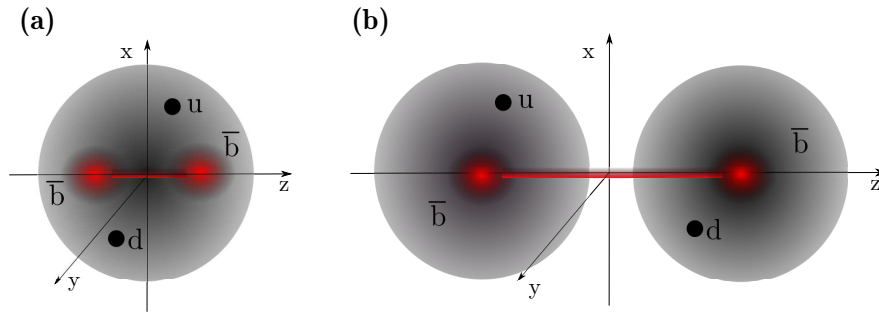

Figure 4.1.: The BB system for short and long $\bar{b}\bar{b}$ separations. (a) At very short $\bar{b}\bar{b}$ separations, the $\bar{b}$ quarks interact with a perturbative one-gluon-exchange Coulomb potential. (b) At large separations the light quarks, for instance ud, screen the interaction and the four quarks form two rather weakly interacting B mesons.

4.4.1. The Born-Oppenheimer approximation – derivation

Historically, the Born-Oppenheimer approximation was developed to allow for a separation of the molecular wavefunction into one part that accounts for the electrons and one part that accounts for the nuclei. This section follows [51].

The Born-Oppenheimer approximation was developed in 1927 by Max Born and J. Robert Oppenheimer. Assuming a large difference between the mass of the electrons and the nuclei in a molecule, the approximation can significantly reduce the complexity of the Schrödinger equation which one has to solve to obtain the wavefunction of the molecule. In the following, we assume a system of N electrons with mass m_e and charge $-e$ located at positions $\mathbf{r}_\mu$ and two nuclei located at $\mathbf{R}_{1,2}$ with mass M and charge Z. The wavefunction of the system Ψ is split into a part Ψ_e that accounts for the electrons and one part Ψ_n that accounts for the nuclei:

$$\Psi(\mathbf{r}_1, ..., \mathbf{r}_N, \mathbf{R}_1, \mathbf{R}_2) = \Psi_n(\mathbf{R}_1, \mathbf{R}_2) \otimes \Psi_e(\mathbf{r}_1, ..., \mathbf{r}_N). \tag{4.14}$$

The Hamiltonian for the full system reads

$$H = \sum_{k=1}^{2} \frac{-1}{2M} \Delta_k + \frac{Z^2 e^2}{|\mathbf{R}_1 - \mathbf{R}_2|} + H_{\mathrm{e}} \tag{4.15}$$

with

$$H_{\mathrm{e}} = \sum_{\nu=1}^{N} \frac{-1}{2m_e} \Delta_\nu + \sum_{\nu=2}^{N} \sum_{\mu=1}^{\nu-1} \frac{e^2}{|\mathbf{r}_\nu - \mathbf{r}_\mu|} - \sum_{\nu=1}^{N} \sum_{k=1}^{2} \frac{Ze^2}{|\mathbf{r}_\nu - \mathbf{R}_k|}. \tag{4.16}$$

Δ_i is the spatial derivative with respect to the coordinates of the i-th particle. In the following, we proceed in two steps:

1. The Schrödinger equation of the electrons is solved in order to obtain Ψ_{e}. Due to $M \gg m_{\mathrm{e}}$, the nuclei move much slower than the electrons. Therefore $\mathbf{R}_{1,2}$ can be considered to be constant. Only electrons are taken into account here.

2. Taking into account the solution for the electrons, the nuclear Schrödinger equation is solved in order to obtain Ψ_{n}. Here only the motion of the nuclei has to be considered.

The Schrödinger equation for the Hamiltonian of the electrons H_{e} reads:

$$H_{\mathrm{e}} \Psi_{\mathrm{e}}(\mathbf{r}_1, ..., \mathbf{r}_N) = E_{\mathrm{e}}(\mathbf{R}) \Psi_{\mathrm{e}}(\mathbf{r}_1, ..., \mathbf{r}_N). \tag{4.17}$$

The energy eigenvalue E_e is a function of $\mathbf{R} = \mathbf{R}_1 - \mathbf{R}_2$ due to translational symmetry of the full system. Taking into account the Hamiltonian H_{e} (4.16), we can apply the full Hamiltonian (4.15) to the full wavefunction Ψ and find:

$$H\Psi = H\Psi_{\mathrm{n}}\Psi_{\mathrm{e}} = \left(\sum_{k=1}^{2} \frac{-1}{2M} \Delta_k + \frac{Z^2 e^2}{|\mathbf{R}_1 - \mathbf{R}_2|} + E_{\mathrm{e}}(\mathbf{R}) \right) \Psi_{\mathrm{n}}\Psi_{\mathrm{e}}. \tag{4.18}$$

The full Hamiltonian reduces to a Hamiltonian that for the two nuclei takes the form:

$$H_{\mathrm{n}} = \sum_{k=1}^{2} \frac{-1}{2M} \Delta_k + \frac{Z^2 e^2}{|\mathbf{R}_1 - \mathbf{R}_2|} + E_{\mathrm{e}}(\mathbf{R}). \tag{4.19}$$

The equation that remains to be solved reads:

$$H_{\mathrm{n}} \Psi_{\mathrm{n}} = E \Psi_{\mathrm{n}}. \tag{4.20}$$

After a change of coordinates into the center-of-mass system of the nuclei

$$\mathbf{R} = \mathbf{R}_1 - \mathbf{R}_2 \quad , \quad \mathbf{R}_c = \frac{\mathbf{R}_1 + \mathbf{R}_2}{2} \tag{4.21}$$

the Hamiltonian of the nuclei H_{n} can be written:

$$H_{\mathrm{n}} = -\frac{1}{2M_c} \Delta_{\mathbf{R}_c} - \frac{1}{2\mu} \Delta_{\mathbf{R}} + \frac{Z^2 e^2}{R} + E_{\mathrm{e}}(\mathbf{R}) \text{ with } \mu = \frac{M}{2}, \, M_c = 2M. \tag{4.22}$$

We observe that H_n commutes with $\mathbf{P}_c = -i\nabla_c$, the center-of-mass momentum operator of the nuclei. Therefore, Ψ_{n} can be written in terms of relative momentum and center-of-mass momentum eigenfunctions, i.e.

$$\Psi_{\mathrm{n}} = \Psi_c \Psi_{\mathrm{rel}}. \tag{4.23}$$

So the center-of-mass contribution can be split off. Therefore $H_n \Psi_n = E \Psi_n$ becomes $H'_n \Psi_{\rm rel} = E' \Psi_{\rm rel}$ with

$$H'_n = -\frac{1}{2\mu} \nabla_{\mathbf{R}} + V(\mathbf{R}) \tag{4.24}$$

where $V(\mathbf{R})$ contains the electronic contribution of the energy and the Coulomb term

$$V(\mathbf{R}) = \frac{Z^2 e^2}{R} + E_e(\mathbf{R}). \tag{4.25}$$

Summarizing: Once the potential of the nuclei at constant positions in the presence of the electrons $V(\mathbf{R})$ is known, (4.24) describes the behavior of the full system, as long as $M \gg m_e$.

4.4.2. The Born-Oppenheimer approximation – application to heavy-light four quark systems

The Born-Oppenheimer approximation can be applied to B-mesonic systems if one considers light quarks ud instead of electrons and heavy quarks $\bar{b}\bar{b}$ instead of nuclei. For the two lighter quarks ud, the heavy antiquarks $\bar{b}\bar{b}$ can be approximated as static color charges, which allows to determine the light quark energy using Lattice QCD. On the other hand, once the energy of the light quarks ud is determined, it can be utilized as an effective potential for the heavy antiquarks $\bar{b}\bar{b}$. This potential can be inserted into Schrödinger's equation. The energy eigenvalue provides insight whether the potential is sufficiently attractive to host a bound state. If the energy eigenvalue is negative, the potential corresponds to a bound state. Otherwise there is no bound state, but essentially a two-meson state. For further details on this approach, cf. Section 5.4.4.

4.5. Using Lattice QCD to obtain static-light four-quark potentials

In this section we show how to get a potential from a correlation function of a static light four-quark system. All static-light four-quark potentials discussed in Chapters 5 and 7 are obtained following the approach outlined in this section. We consider the static-light four quark trial state, e g. for a BB system, cf. Equation (4.3):

$$O_{BB,r}(t)|\Omega\rangle = (\mathcal{C}\Gamma)_{AB}(\mathcal{C}\tilde{\Gamma})_{CD} \left(\bar{Q}^a_C(\mathbf{r}_1, t) \chi^{(f)a}_A(\mathbf{r}_1, t) \right) \left(\bar{Q}^b_D(\mathbf{r}_2, t) \chi^{(f')b}_B(\mathbf{r}_2, t) \right) |\Omega\rangle$$

with $r = |\mathbf{r}_1 - \mathbf{r}_2|$. One can obtain the correlation function in time $C(t, r)$ for each separation r of the static quarks:

$$C(t, r) = \langle \Omega | O^\dagger_{BB,r}(t) O_{BB,r}(0) | \Omega \rangle. \tag{4.26}$$

The effective mass is given by:

$$am_{\text{eff},r} = \ln \left(\frac{C(t, r)}{C(t + a, r)} \right) \tag{4.27}$$

with a the lattice spacing. By fitting a constant to the effective mass plateau at large temporal separations t, one finds the potential $V(r) = E_0(r) - E_\Omega$ of the BB state:

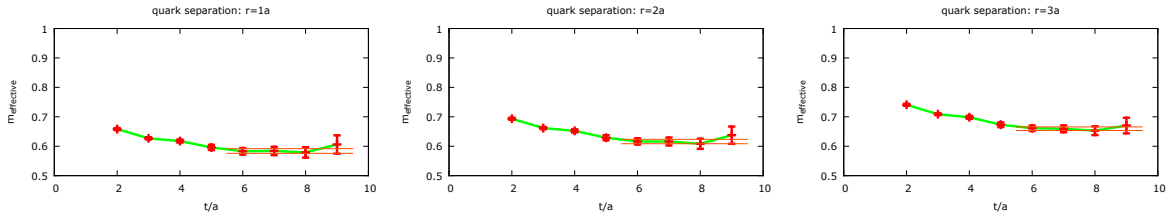$$aV(r) = \lim_{t \to \infty} \ln \left(\frac{C(t, r)}{C(t + a, r)} \right), \tag{4.28}$$

Figure 4.2.: Example plots for the effective mass $m_{\text{eff},r}$ for different static quark separations $r = 1a$, $2a$, $3a$. The horizontal red lines are the results of fitting a constant to the effective mass at large t, $6a \leq t \leq 9a$.

(cf. Section 3.1.2). In Figure 4.2 example plots of the effective mass are shown for static quark separations $r = 1a$, $2a$, $3a$. The horizontal red lines show the results of the fits to the effective mass. By combining the fit results, the full BB potential depending on the separation r can be found, cf. Figure 4.3. For each gauge configuration used in the lattice computation and
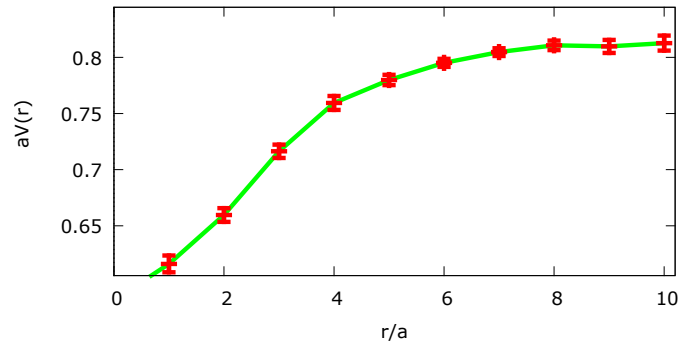

Figure 4.3.: The full BB potential $V(r)$ obtained by combining fit results to the effective mass for different static quark separations r.

for each separation r one effective mass can be obtained. Thus, one can perform fits to the respective effective mass plateaus for each gauge configuration and obtain the full potential. The jackknife error (cf. Section 2.4.2) can be calculated for each potential point $V(r)$. Note the following: Although each potential point $V(r)$ slightly depends on the quality of the fit, the error from the fit procedure is not taken into account at this stage. In Figure 4.3 the error bars on the potential points are only jackknife errors.

5. $\bar{b}\bar{b}qq$ systems in the Born-Oppenheimer approximation

Heavy-light tetraquark systems are expected to be studied in more and more detail by experimental collaborations in the near future. The theoretical investigation of possibly existing four-quark states can provide orientation for future experimental research. In this chapter we study possibly existing four quark states with two heavy antiquarks $\bar{b}\bar{b}$ and two light quarks qq. To this end we compute the potential of the two heavy antiquarks in the presence of two lighter quarks using Lattice QCD. We work in the Born-Oppenheimer approximation and consider the limit of infinitely heavy $\bar{b}$ quarks, i.e. the static limit. For large $\bar{b}\bar{b}$ separations, the potential can be interpreted as the potential between two static-light B mesons. We show various BB potentials that correspond to different combinations of B mesons. We investigate attractive ground state potentials using light quark combinations $qq \in \{u, d\}$ as well as strange and charm quarks, i.e. $qq \in \{s, c\}$. For the quark combination $qq \in \{u, d\}$ we perform an extrapolation to the physical pion mass and confirm that binding increases when the mass of the lighter quarks qq decreases. This chapter essentially summarizes [5, 6].

5.1. The $\bar{b}\bar{b}qq$ system – Expectations

It is possible to build various BB systems according to different combinations of $B_{(s,c)}^{(*)}$ mesons (B, B^*, B_0^* and B_1^*, etc.). These systems are listed in detail in Section 5.3. In this section we state qualitative expectations for such BB systems with special focus on candidates for bound states. The behavior of the system can be characterized by the $\bar{b}\bar{b}$ interaction which depends on the heavy quark separation r. This Section closely follows [6].

Expectations for the $\bar{b}\bar{b}$ interaction at small separations r

- The spin interaction of the $\bar{b}$ quarks is quite small and can possibly be neglected, since it is proportional to $1/m_b{}^2$. This can be seen in the framework of HQET, cf. [52] and references therein as well as Sections 2.6.2 and 2.6.3.

- In case of a bound $\bar{b}\bar{b}qq$ state, i.e. a tetraquark, the antiquarks $\bar{b}\bar{b}$ are expected to be in a color triplet 3, which is attractive, and not in a color sextet 6, which is repulsive. In other words, at small separations r, the antiquarks $\bar{b}\bar{b}$ form an antidiquark.

  The complete four-quark system $\bar{b}\bar{b}qq$ necessarily forms a color singlet. Therefore light quarks qq must be in a color antitriplet $\bar{3}$.

- This color antitriplet is antisymmetric. Moreover, the light quarks qq are assumed to be in a spatially symmetric s-wave. Therefore, the Pauli principle implies a symmetric spin-flavor structure. This can either be a spin singlet with an antisymmetric flavor combination or a spin triplet with a symmetric flavor combination.

Ensemble	β	lattice	$a\mu$	m_π[MeV]	a [fm]	confs
E17.32	4.35	$32^3 \times 64$	0.00175	340	0.0420(17)	100
B40.24	3.90	$24^3 \times 48$	0.0040	340	0.0790(26)	480
B85.24	3.90	$24^3 \times 48$	0.0085	480	0.0790(26)	400
B150.24	3.90	$24^3 \times 48$	0.0150	650	0.0790(26)	260

Table 5.1.: Parameters of $n_f = 2$ gauge ensembles generated by ETMC [53, 54, 55, 56]. Shown are the inverse bare coupling β, lattice size $(L/a)^3 \times (T/a)$, bare twisted light sea quark mass in lattice units $a\mu$, pion mass m_π, lattice spacing a and the number of configurations used.

Expectations for the $\bar{b}\bar{b}$ interaction at large separations r

- At large separations r, screening of the $\bar{b}\bar{b}$ interaction is expected due to the light quarks qq. When the $\bar{b}\bar{b}$ separation is larger than around two times the radius of a $B_{(s,c)}^{(*)}$ meson, there is essentially no overlap between the wave functions of the light quarks and, consequently, the $\bar{b}\bar{b}$ interaction practically vanishes.

- The more massive the light quarks are, the more compact their wave functions in the $B_{(s,c)}^{(*)}$ mesons and, thus, the stronger the screening. In other words, the corresponding $\bar{b}\bar{b}$ potential becomes more and more narrow and will at some point not anymore be able to host a bound state. Consequently, for a sufficiently heavy pair of light quarks qq the screening should prevent the formation of $\bar{b}\bar{b}qq$ tetraquarks.

In the following sections, we perform a Lattice QCD study to check whether the qualitative expectations are fulfilled. Among other things, we conduct calculations to investigate the mass dependence of the four-quark binding.

5.2. Lattice QCD setup

The central quantity of this chapter is the potential of two static antiquarks $\bar{b}$ in the presence of two quarks of finite mass which we compute by means of Lattice QCD. Computations are performed using four ensembles of gauge link configurations with two dynamical quark flavors generated by the European Twisted Mass Collaboration (ETMC). The quark action is Wilson twisted mass tuned to maximal twist (cf. Section 2.3.2), while the gluon action is tree-level Symanzik improved. This guarantees automatic $\mathcal{O}(a)$ improvement of spectral quantities, i.e. discretization errors in the resulting $\bar{b}\bar{b}$ potentials appear only quadratically in the lattice spacing a. Information about these ensembles is collected in Table 5.1. Further details, in particular regarding their generation, can be found in [53, 54]. To improve the signal quality of the correlation functions we compute, spatial links are APE smeared (parameters $N_{\text{APE}} = 30, \alpha_{\text{APE}} = 0.5$) and Gaussian smearing (parameters $N_{\text{Gauß}} = 50, \kappa_{\text{Gauß}} = 0.5$) is applied to the light quark fields, cf. Section 3.3. Light quark propagators are computed using stochastic timeslice sources with 12 inversions per timeslice, cf. Section 3.2.3.

For $\bar{b}\bar{b}$ potentials in the presence of two light quarks qq with $q \in \{u, d\}$, we use Lattice QCD results from [57, 58], which were obtained using ensemble B40.24. We extend these computations to pairs of quarks that we interpret as a and c quarks, i.e. $qq = ss$ and $qq = cc$. We

introduce hypothetical degenerate flavors with the mass of the strange or the charm quark to be able to study the antisymmetric flavor combinations $qq = (s^{(1)}s^{(2)} - s^{(2)}s^{(1)})/\sqrt{2}$ and $qq = (c^{(1)}c^{(2)} - c^{(2)}c^{(1)})/\sqrt{2}$. We will comment on these flavor combinations in more detail in Section 5.4. For $q \in \{s, c\}$, the $\bar{b}\bar{b}$ interaction is screened at significantly smaller $\bar{b}\bar{b}$ separations (cf. the discussion in Section 5.1). To be able to resolve the corresponding potentials properly, we decided to use ensemble E17.32 which has a finer lattice spacing $a \approx 0.042\,\mathrm{fm}$ for flavor combinations $qq \in \{(s^{(1)}s^{(2)} - s^{(2)}s^{(1)})/\sqrt{2}\ ,\ ss\ ,\ (c^{(1)}c^{(2)} - c^{(2)}c^{(1)})/\sqrt{2}\ ,\ cc\}$. The physical lattice extent for E17.32 is much smaller than for B40.24. However, this should not introduce significant finite volume effects compared to the statistical errors at the rather small separations we are interested in.

The u/d quarks are non-physically heavy for the ensembles we use. Moreover, since there are no s and c sea quarks, the Lattice QCD results we get are in a partially quenched approximation (cf. Section 2.3.3). For the computation of $\bar{b}\bar{b}$ potentials in the presence of light s and c quarks, we also use a much smaller number of gauge link configurations, because the propagators of the heavier s and c quarks introduce less statistical noise than the propagators of the lighter u/d quarks.

5.3. BB potentials in all channels

5.3.1. Computation of correlation functions of BB systems

For a given operator O_{BB}, a trial state with static quarks Q and Wilson twisted mass quarks χ reads

$$O_{BB,r}(t)|\Omega\rangle = (\mathcal{C}\Gamma)_{AB}(\mathcal{C}\tilde{\Gamma})_{CD}\Big(\bar{Q}_C^a(\mathbf{r}_1, t)\chi_A^{(f)a}(\mathbf{r}_1, t)\Big)\Big(\bar{Q}_D^b(\mathbf{r}_2, t)\chi_B^{(f')b}(\mathbf{r}_2, t)\Big)|\Omega\rangle$$

(cf. Equation (4.3)). We define the correlation function

$$C(t, r) = \langle\Omega|O_{BB,r}^\dagger(t)O_{BB,r}(0)|\Omega\rangle, \tag{5.1}$$

where the argument of O_{BB} is Euclidean time. For each correlation function we perform symmetry transformations. This has two advantages: On the one hand, one can verify the obtained results by identifying pairs of correlation functions that are connected via the transformations according to certain rules. On the other hand averaging over these pairs of correlation functions decreases the statistical error. Verification and averaging according to the symmetry transformations is performed for all correlation functions used in this chapter. Details on how symmetry transformations are performed and rules are deduced are presented in Section 7.2.3 using the example of a $B\bar{B}$ system.

5.3.2. HYP smearing

In this section which is based on [5], we use lattice data from the B40.24 ensemble. We start by comparing results with and without HYP smearing (cf. Section 3.3) with parameters $\alpha_1 = \alpha_2 = 1$ and $\alpha_3 = 0.5$ of world lines of static quarks, cf. Fig. 5.1. We show only attractive potentials with the asymptotic value twice the mass of the B meson in the ground state $2m(S)$. This value which comes from multiplets A, E and K of Tables A.2 and A.3 is subtracted from each potential. For more information on S state B mesons, cf. Section 4.2. In general,

for separations $r \approx 2a$, the results from HYP and non-HYP cases are compatible, but with visibly reduced statistical errors for the former. In the small-separation region, however, HYP smearing significantly distorts the potential by filtering out UV fluctuations. We, therefore, restrict the remaining discussion to separations $r \geq 2a$ and use the HYP results, which exhibit significantly smaller errors.
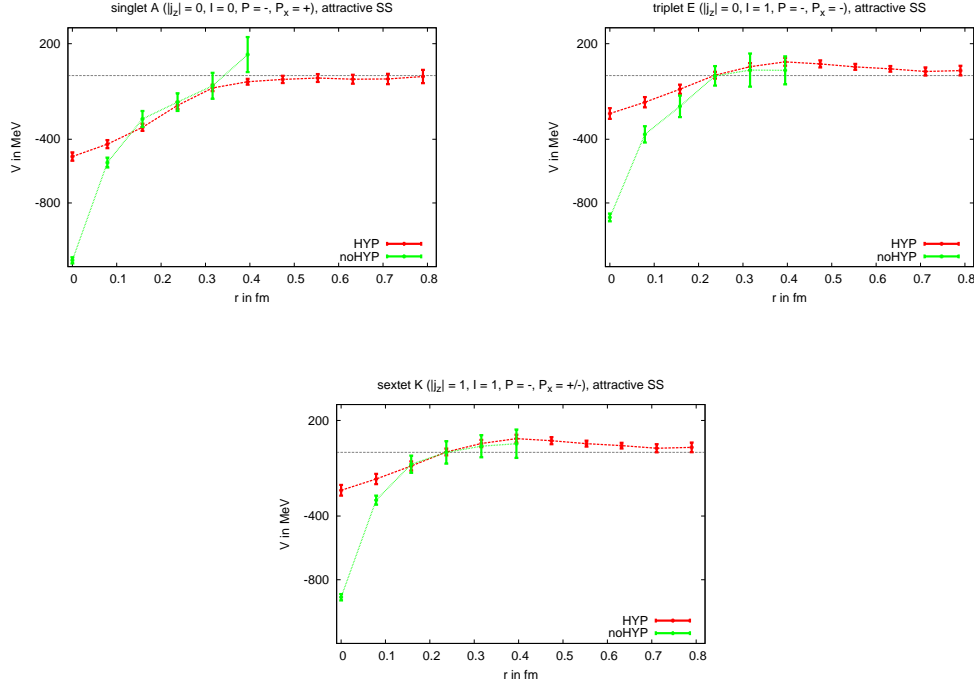

Figure 5.1.: Comparison of attractive SS potentials obtained with HYP2 smearing (red dashed lines) and without HYP2 smearing (green solid lines). Shown are only attractive potentials with $2m(S)$ as the asymptotic value (subtracted from the potential), from multiplets A, E and K of Tables A.3 and A.2.

5.3.3. Increasing the number of sources per timeslice

The correlation functions in this chapter are computed using timeslice sources with $N = 12$ inversions per timeslice (cf. Section 3.2.3). In the following we discuss, how increasing N reduces the statistical error and how inversion and contractions scale with increasing N.

If the number of inversions per configuration N is increased, one expects a reduction of the statistical error. The static-light BB system contains four light quarks, i.e. two light quark propagators have to be computed (cf. Section 3.2.3). So if N is increased from 4 to 6, ideally the error decreases by a factor $\frac{4}{6} \sim 0.7$. The computation of the correlation functions (cf. (4.3)) has been performed using the B85.24 ensemble with $N = 4$ respectively $N = 6$ sources per timeslice. We chose $\Gamma = \gamma_5 + \gamma_0\gamma_5$. However, the result might depend significantly on the choice for Γ. The correlation function is shown in Figure 5.2. As expected, the ratio of the

errors on each value is

$$\frac{\text{error}_{N=6}}{\text{error}_{N=4}} \simeq 0.7. \tag{5.2}$$

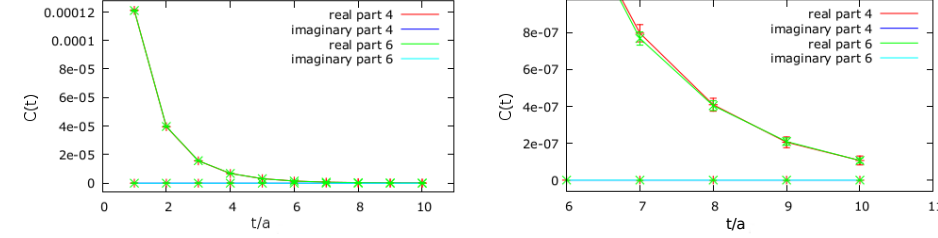As the comparison of different numbers of inversions per configuration shows, the statistical

Figure 5.2.: The real and imaginary part of the correlation function of the static-light BB four-quark system computed using $N = 4$ respectively $N = 6$ sources per timeslice. Left side: The entire correlation function, right side: an enlarged section of the correlation function.

precision of the potential can be improved by increasing N. So one wants to perform as many inversions per configuration as possible in order to get a precise result. In the following, we estimate the computational costs: It takes a constant amount of time to perform one inversion or contraction, independent of how many inversions are performed in total. One has to perform $N(N-1)$ contractions because each propagator is comprised in a combination of a source $\xi[n]$ and a different sink $\phi[n']$, $n \neq n'$ (cf. Section 3.2.3). Furthermore $2 \times N$ sources are needed per timeslice, N for up quarks and N for down quarks. So to move from $N = 4$ to $N = 6$ the time requirement increases by a factor of $\left(\frac{3}{2}\right)^2$ if the contractions are performed serially. Note that the inversion and contraction procedures can be parallelized. In Table 5.2 the computational costs per gauge configuration are listed. Computations have been performed on the FUCHS-CSC high performance computer in Frankfurt am Main. For the inversions the code tmLQCD [20] was used.

N	inversions/time	contractions/time
4	8/8 hours	$8 \times 7 = 56$ / 2.5 days
6	12 / 12 hours	$12 \times 11 = 132$ / 5.5 days

Table 5.2.: Computational costs per gauge configuration (not parallelized).

5.3.4. Potentials

The discussion and plots from this section are based on [5]. The BB system consists of two B mesons and each of these mesons corresponds to the quantum numbers $I_z = \pm 1/2$, $j_z = \pm 1/2$, $\mathcal{P} = \pm$, i.e. 8 possibilities in total. This gives $8 \times 8 = 64$ different correlation functions for the BB system. Equivalently, one can consider the spin coupling of the dynamical quarks (the 4×4 matrix Γ, i.e. 16 possibilities) and their flavor content (4 possibilities), which again gives $16 \times 4 = 64$ different correlation functions.

5. $\bar{b}\bar{b}qq$ systems in the Born-Oppenheimer approximation

Note that, although some of the potentials have different quantum numbers, they are related in the continuum by isospin symmetry or by rotational symmetry around the z-axis. The former symmetry yields $I = 0$ singlets and degenerate $I = 1$ triplets while the latter yields $|j_z| = 1$ doublets. Moreover, there are qualitatively 6 different potentials: attractive potentials with the asymptotic value of $2m(S)$, $m(S) + m(P_-)$ or $2m(P_-)$ and repulsive potentials with the same asymptotic values. For a discussion of S and $P_\pm$ states, cf. [5]. The number of potentials for each case, together with their degeneracies is:

SS potentials,	attractive:	$1(A) \oplus 3(E) \oplus 6(K)$	(10 channels),
	repulsive:	$1(B) \oplus 3(F) \oplus 2(I)$	(6 channels),
SP_- potentials,	attractive:	$1(B) \oplus 1(C) \oplus 3(E) \oplus 3(G) \oplus 2(I) \oplus 6(L)$	(16 channels),
	repulsive:	$1(A) \oplus 1(D) \oplus 3(F) \oplus 3(H) \oplus 2(J) \oplus 6(K)$	(16 channels),
P_-P_- potentials,	attractive:	$1(A) \oplus 3(E) \oplus 6(K)$	(10 channels).
	repulsive:	$1(B) \oplus 3(F) \oplus 2(I)$	(6 channels),

where we use the labeling by $A, B, C, \ldots$ of the multiplets according to Tables A.2 and A.3 in the Appendix where we list all multiplets with their corresponding quantum numbers. Thus, the 64 trial states (4.1) correspond to 24 different potentials in the continuum. However, due to isospin symmetry breaking in twisted mass Lattice QCD, the $I = 1$ potentials with $I_z = 0$ and $I_z = \pm 1$ and otherwise identical quantum numbers are only degenerate in the continuum limit.

We present results for all $(I, I_z, |j_z|, \mathcal{P}, \mathcal{P}_x)$ channels in Figures 5.3 and 5.4. The potentials were normalized by a single additive constant, such that the lowest asymptotic value corresponds to $2m(S)$. The horizontal lines correspond to $2m(S)$, $m(S) + m(P_-)$ and $2m(P_-)$.

Figure 5.3 shows 12 potentials corresponding to $I = 0$, with flavor structure $ud \pm du$, quantum numbers contained in the label of each plot and Γ-structures given in Table A.3. There are four singlet channels ($I = 0$, $j_z = 0$) with different combinations of $\mathcal{P}/\mathcal{P}_x$ and two spin doublet channels ($I = 0$, $j_z = \pm 1$) with either $\mathcal{P} = +$ or $\mathcal{P} = -$. One of the main physical motivations of this thesis is to investigate whether two B mesons can form a bound tetraquark state. From this point of view, attractive potentials with an asymptotic value of $2m(S)$ are most interesting. The reason is, that for bound state formation an attractive potential is mandatory, while restriction to the ground state allows to obtain the best quality of data. Moreover, excited states would require a very strongly bound state, otherwise the decay to a ground state SS pair is possible and a statement about binding by solving the Schrödinger equation (cf. Section 5.4.4) is questionable. Hence, the spin/isospin singlet A (scalar isosinglet) with $\Gamma = \gamma_5 + \gamma_0\gamma_5$ and flavor structure $ud - du$ is clearly the best candidate for further investigations. We will discuss this case in detail in Section 5.4.

Figure 5.4 shows 24 potentials with $I = 1$ and flavor structure uu, dd or $ud + du$. In the plots, solid lines correspond to $I_z = 0$, while dashed lines correspond to $I_z = \pm 1$. There are four isospin triplet channels ($I = 1$, $j_z = 0$) with different combinations of $\mathcal{P}/\mathcal{P}_x$ and two spin/isospin sextet channels ($I = 1$, $j_z = \pm 1$) with either $\mathcal{P} = +$ or $\mathcal{P} = -$. As mentioned above, the difference between $I_z = 0$ and $I_z = \pm 1$ is due to the breaking of isospin symmetry by Wilson twisted mass fermions. As such, it is only a discretization effect that vanishes in the continuum limit. Therefore the differences in the results for these two I_z channels can be used to estimate the size of cut-off effects in the computations. This is quite useful, since we only have one lattice spacing available. As can be seen in Figure 5.4, the above
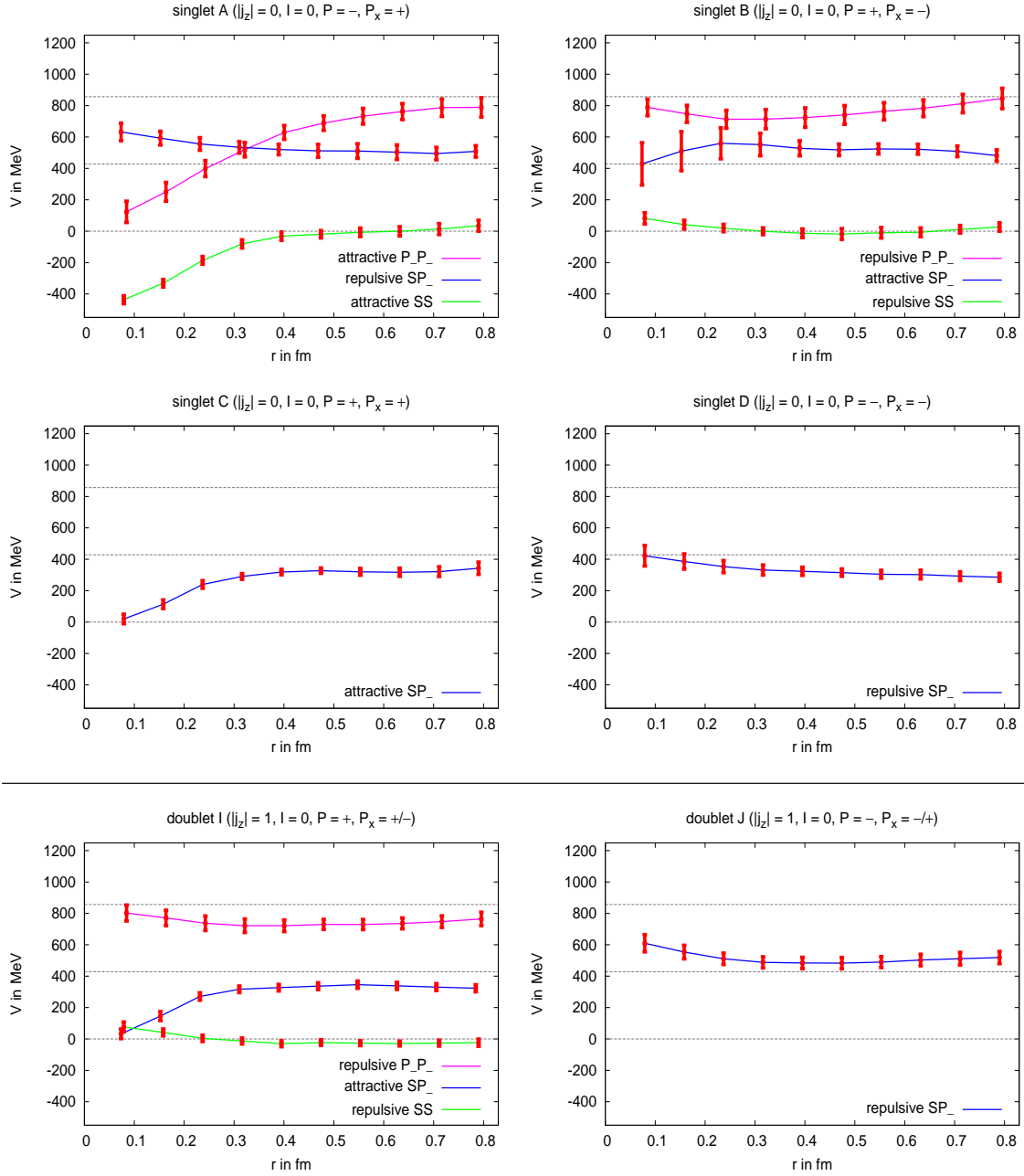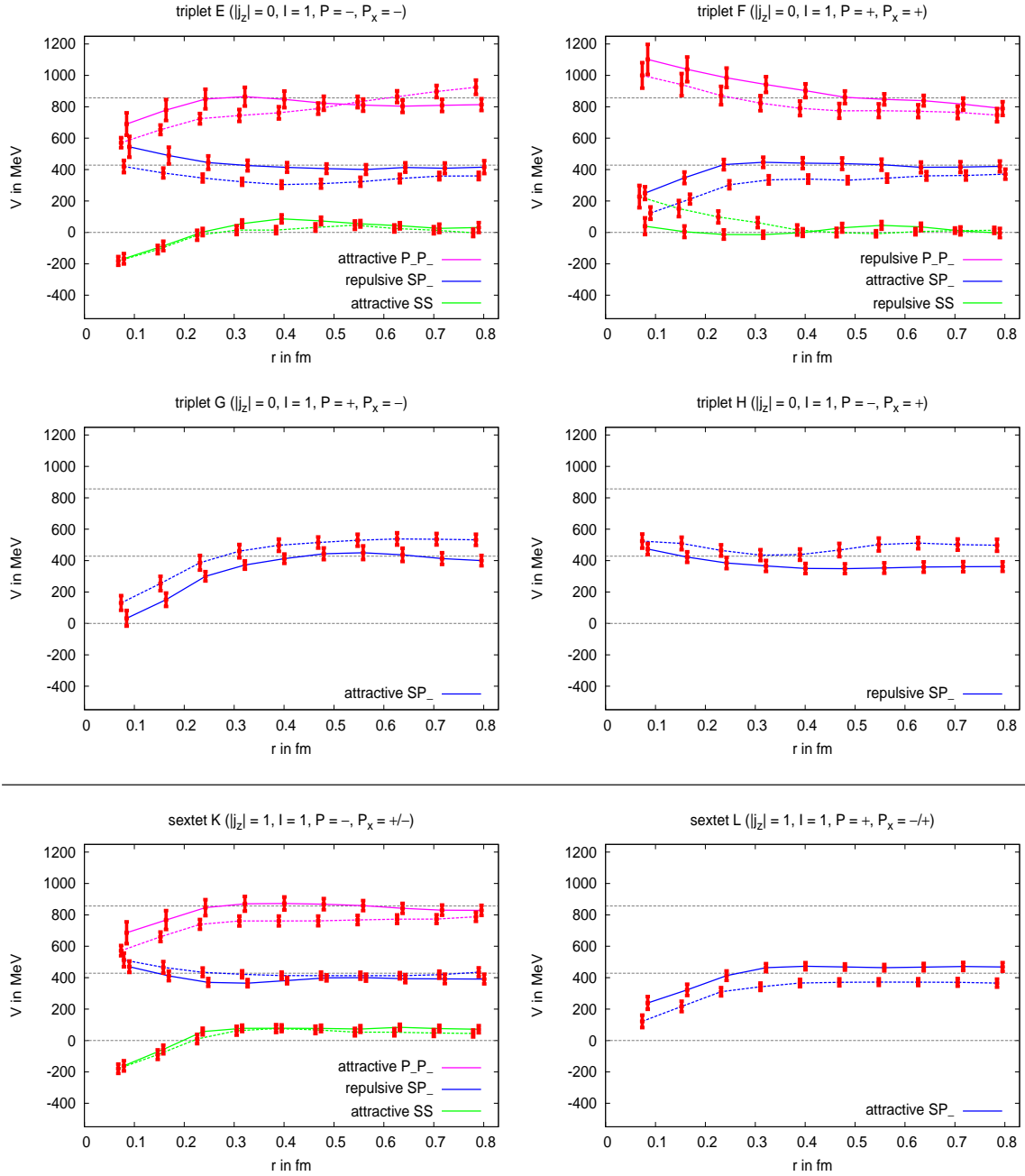
Figure 5.3.: All 12 extracted potentials in the $I = 0$ channel. From all potentials the asymptotic value of $2m(S)$ is subtracted. The three horizontal lines correspond to the asymptotic values of $2m(S)$, $m(S) + m(P_-)$ and $2m(P_-)$.

mentioned differences between I_z channels give consistent results in most of the cases (i.e. within statistical error of each other). Only in few cases the differences exceed the 1σ-level, but they are never larger than approximately 2σ. This indicates that the discretization effects are rather small in our setup and leads to the conclusion that lattice discretization errors are

Figure 5.4.: All 24 extracted potentials in the $I = 1$ channel. From all potentials the asymptotic value of $2m(S)$ is subtracted. The three horizontal lines correspond to the asymptotic values of $2m(S)$, $m(S) + m(P_-)$ and $2m(P_-)$.

smaller than statistical errors. As mentioned above, we are especially interested in attractive potentials with the asymptotic value of $2m(S)$.

5.4. Investigation of attractive ground state potentials

In this section which is based on [6] we study attractive $\bar{b}\bar{b}$ potentials in the presence of two light quarks qq with the asymptotic value of $2m(S)$ in more detail. We investigate whether the potentials are sufficiently attractive to host a bound state.

In case of light quarks $q \in \{u, d\}$, the scalar isosinglet with isospin $I = 0$, antisymmetric light quark spin $j = 0$ and flavor $qq = (ud - du)/\sqrt{2}$ (in the following denoted as the scalar u/d channel), as well as the vector isotriplet with isospin $I = 1$, symmetric spin $j = 1$ and flavor $qq \in \{uu, (ud + du)/\sqrt{2}, dd\}$ (in the following denoted as the vector u/d channel) are the two attractive channels between ground state mesons (B and B^*) (cf. Section 5.3).

For symmetric flavor combinations of light quarks $qq = ss, cc$, the only attractive channel for two ground state mesons $B_{s,c}^{(*)}$ is the vector channel, i.e. with light quark spin $j = 1$. It corresponds to $\Gamma = (1 + \gamma_0)\gamma_k$, $k = 1, 2, 3$, in the creation operator (4.3). Using hypothetical degenerate flavors with the mass of the s or the c quark we are able to study also the scalar channel, i.e. $j = 0$, with strange and charm quarks. Those flavors allow us to form antisymmetric flavor combinations $qq = (s^{(1)}s^{(2)} - s^{(2)}s^{(1)})/\sqrt{2}$ and $qq = (c^{(1)}c^{(2)} - c^{(2)}c^{(1)})/\sqrt{2}$. The scalar channel corresponds to $\Gamma = (1 + \gamma_0)\gamma_5$ in the creation operator (4.3).

5.4.1. Quantum numbers of possibly existing $\bar{b}\bar{b}qq$ tetraquarks

We study exclusively states which for large $\bar{b}\bar{b}$ separations correspond to pairs of ground state mesons $B_{(s,c)}^{(*)}$ in a spatially symmetric s-wave. The parity of these states is the product of the parity quantum numbers of the two mesons, which are both negative. Therefore the parity is positive, i.e. $\mathcal{P} = +$.

As argued above, the two antiquarks $\bar{b}\bar{b}$ are expected to be in an antisymmetric color triplet. Since their flavor is symmetric, their spin j_b must also be symmetric due to the Pauli principle, i.e. $j_b = 1$. Similarly, for an antisymmetric qq flavor combination, i.e. $qq = (ud - du)/\sqrt{2}$, $j = 0$, while for symmetric flavor combinations, i.e. $qq \in \{uu, (ud + du)/\sqrt{2}, dd, ss, cc\}$, $j = 1$. The total spin J of the $\bar{b}\bar{b}qq$ system is the combination of j and j_b.

Altogether, the possibly existing $\bar{b}\bar{b}qq$ tetraquarks we are going to investigate have the following quantum numbers:

- $qq = (ud - du)/\sqrt{2}$:
  $I(J^{\mathcal{P}}) = 0(1^+)$.

- $qq \in \{uu, (ud + du)/\sqrt{2}, dd\}$:
  $I(J^{\mathcal{P}}) \in \{1(0^+), 1(1^+), 1(2^+)\}$.

- $qq \in \{ss, cc\}$:
  $I(J^{\mathcal{P}}) \in \{0(0^+), 0(1^+), 0(2^+)\}$.

Additionally, as mentioned above, we study the hypothetical flavor combinations $qq = (s^{(1)}s^{(2)} - s^{(2)}s^{(1)})/\sqrt{2}$ and $qq = (c^{(1)}c^{(2)} - c^{(2)}c^{(1)})/\sqrt{2}$.

5.4.2. Fit function for Lattice QCD $\bar{b}\bar{b}$ potential results

Using Lattice QCD $\bar{b}\bar{b}$ potentials can be computed only for a limited number of discrete separations. Therefore, a suitable fit function is required to interpolate between the Lattice QCD

results and also to extrapolate beyond them. This fit function is based on the qualitative expectations discussed in Section 5.1 and will be used in the Schrödinger equation in Section 5.4.4, where we determine whether and in which channels bound four-quark states exist. The following considerations are taken from [6].

For two heavy antiquarks $\bar{b}\bar{b}$ inside a cloud of two light quarks qq, i.e. at small $\bar{b}\bar{b}$ separations, we expect a Coulomb-like potential of order $-\alpha_s/3r \approx -\pi/24r$ corresponding to a color triplet. At larger separations r, the potential will be screened by the light quarks qq. This is due to the decrease of the wave function ψ of each of the light quarks with respect to their separations from the heavy antiquarks. One expects this decrease to follow an exponential of a power of r, i.e. $\psi \propto \exp(-(r/d)^p)$, where d roughly describes the size of each of the $\bar{b}q$ systems, i.e. the size of a $B_{(s,c)}^{(*)}$ meson $\lesssim 0.5\,\mathrm{fm}$. The parameter p characterizes the radial profile of the light quark wave function inside the $B_{(s,c)}^{(*)}$ meson. Assuming the $q\bar{b}$ interaction inside the $B_{(s,c)}^{(*)}$ meson is dominated by a linear confining potential, one can estimate the parameter p. In the case, where the quark q is rather heavy, e.g. $q = c$, the corresponding non-relativistic Schrödinger equation is solved by Airy functions, resulting in $p = 3/2$. A similar but relativistic treatment for a lighter quark yields $p = 2$ instead.

For very large separations, the $\bar{b}\bar{b}$ interaction will be be screened entirely by the light quarks, so the system will basically consist of two independent static-light B mesons. The potential will take a value of $\approx 2m_B$. One way to account for this would be to subtract twice the static-light meson mass from the $\bar{b}\bar{b}$ potentials to bring the potential to zero for very large $\bar{b}\bar{b}$ separations. We refer to this procedure as method A. The static light meson mass can be computed via the meson correlation function (cf. Equation (3.2)). The statistical errors of the potential as well as the statistical error on the meson mass added in quadrature have to be taken into account. These considerations suggest the fit function $V(r) = -\frac{\alpha}{r}\exp\left(-\left(\frac{r}{d}\right)^p\right)$ for the $\bar{b}\bar{b}$ potentials. It turns out that subtracting twice the B meson mass from the potentials before performing the fit does not result in a potential sufficiently close to zero at very large $\bar{b}\bar{b}$ separations. The most likely reason is stronger contamination with higher excited states in case of BB correlation functions compared to B correlation functions. As a consequence, the fit function does not describe the data properly, so the quality of the fit is bad.

To improve the situation, we try a more elaborate method to bring the potential to zero at large separations. In order to satisfy the asymptotic behavior one can subtract an offset, which is the value of the potential corresponding to the largest available $\bar{b}\bar{b}$ separation $\tilde{r}$. One can not only take into account the value corresponding to $\tilde{r}$, but to the n points $\tilde{r}, \tilde{r} - a \ldots$, $\tilde{r} - (n-1)a$.

The offset $\tilde{V}$ is then determined by the fit function:

$$\tilde{V} = \sum_{j=0}^{n} w_j V(\tilde{r} - ja) \quad \text{with} \qquad w_j = \frac{1/\sigma_j{}^2}{\sum_{k=0}^{n} 1/\sigma_k{}^2} \tag{5.3}$$

with σ_i the error of the potential point $V(\tilde{r} - ja)$. The new observable, now denoted as potential difference $\delta V(r)$, is

$$\delta V(r) = V(r) - \tilde{V}. \tag{5.4}$$

We refer to this method as method B. The error of the potential can be calculated via a jackknife analysis (cf. Section 2.4.2) of the potential differences.

In Figure 5.5 a potential obtained using the different methods is shown. Compared to method A (red), method B (green, blue, yellow) has by construction a slightly better signal
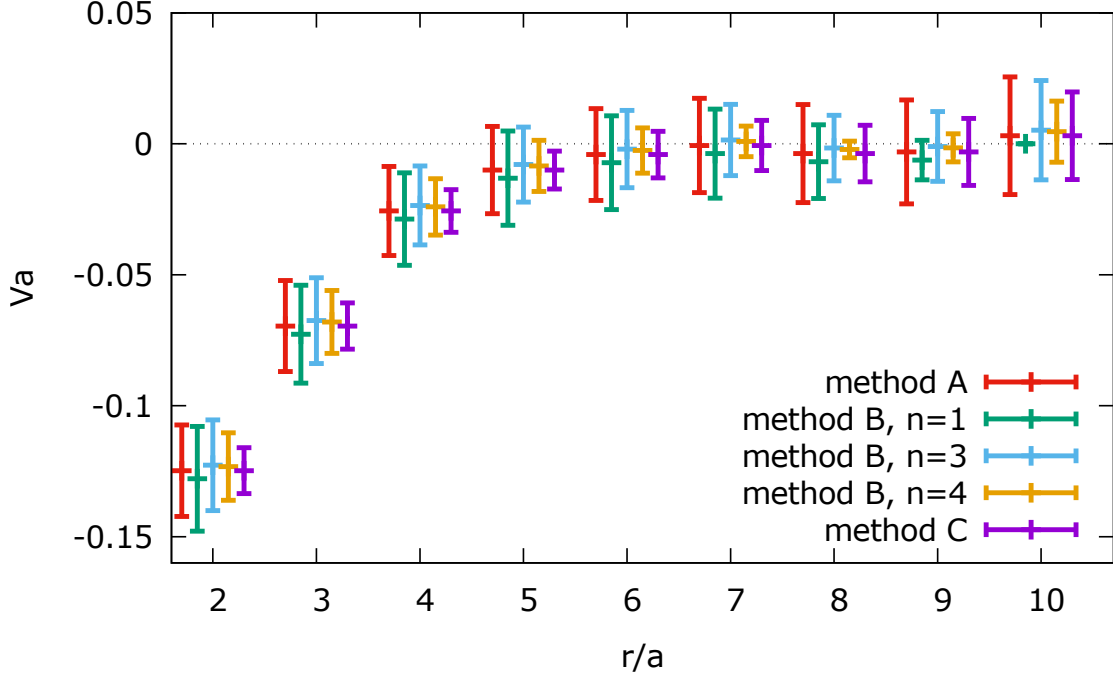
Figure 5.5.: The $\bar{b}\bar{b}ud$ potential obtained with different methods (points slightly shifted horizontally to improve visibility): The meson mass method referred to as method A (red), the potential difference method referred to as method B for $n = 1, 2, 3$ points (green, blue, yellow) and the plain potential without subtraction of an offset, referred to as method C (purple, points shifted vertically to allow for comparison).

for large r. Nevertheless the impact is small. The purple points in Figure 5.5 correspond to a third method which we refer to as method C: The potential and its statistical error are used without subtracting any offset. For comparison in the plot the points are normalized by a single additive constant to be at the same level as the other points at large separations. The signal is more stable than in the other cases. So it is advantageous to consider this quantity instead of differences. To this end, we introduce a fourth fit parameter V_0 to the fit function. V_0 accounts for twice the mass of the static-light B meson. It turns out that the quality of the fits performed using method C is indeed better than method A or B.

These considerations suggest the following fit function for Lattice QCD $\bar{b}\bar{b}$ potential results:

$$V(r) \;=\; -\frac{\alpha}{r}\exp\left(-\left(\frac{r}{d}\right)^p\right) + V_0, \tag{5.5}$$

where it is expected that $\alpha \approx 2\alpha_s/3 \approx \pi/24 \approx 0.13$, $d \lesssim 0.5\,\mathrm{fm}$ and $p \approx 1.5\ldots 2.0$. The constant V_0 is necessary to account for twice the mass of the static-light meson. As will be demonstrated below, this fit function is consistent with Lattice QCD results and the crude quantitative expectations for α, d and p are fulfilled.

5. $\bar{b}\bar{b}qq$ systems in the Born-Oppenheimer approximation

5.4.3. Determination of fit parameters

To describe the Lattice QCD $\bar{b}\bar{b}$ potential results $V^{\mathrm{lat}}(r)$ by continuous functions, we perform uncorrelated χ^2 minimizing fits of eq. (5.5), i.e. we minimize

$$\chi^2 \;=\; \sum_{r=r_{\min},\dots,r_{\max}} \left(\frac{V(r) - V^{\mathrm{lat}}(r)}{\Delta V^{\mathrm{lat}}(r)} \right)^2 \tag{5.6}$$

with respect to the parameters α, d and V_0, while keeping $p = 2$ fixed (cf. the discussion in Section 5.4.2). In principle, one could also use p as a fit parameter. Our Lattice QCD results are, however, not sufficiently precise to extract a stable and precise value also for p. Therefore, we set $p = 2$ as motivated in Section 5.4.2. With this choice, the Lattice QCD results are well described by the fit function (5.5), i.e. the resulting $\chi^2/\mathrm{dof} < 1$ (Equation (5.6)). ΔV^{lat} denote the corresponding statistical errors.

We perform these fits for the scalar u/d, the vector u/d, the scalar s, the vector s and the scalar c channel. The Lattice QCD $\bar{b}\bar{b}$ potential of the remaining vector c channel is, however, strongly screened and consistent with $V^{\mathrm{lat}}(r) = 0$ for $r > 2a$. Such results are not sufficient to perform a stable fit.

To investigate and quantify systematic errors, we perform a large number of fits for each of the mentioned five channels where we vary the following parameters:

- The range of temporal separations $t_{\min} \leq t \leq t_{\max}$ of the correlation function $C(t,r)$ (Equation (5.1)) at which $V^{\mathrm{lat}}(r)$ is read off, according to:

    - $t_{\max} - t_{\min} \geq a$;
    - for u/d channels:
      $4a \leq t_{\min},\, t_{\max} \leq 9a$;
    - for s and c channels:
      $10a \leq t_{\min} \leq 14a,\, t_{\max} \leq 19a$

    (Note that the lattice spacing is smaller in case of the s and c channels compared to the u/d channels, cf. Table 5.1.) Small $t_{\min}$ might lead to a contamination by excited states; large $t_{\min}$ and $t_{\max}$ drastically increase statistical errors.

- The range of spatial $\bar{b}\bar{b}$ separations $r_{\min} \leq r \leq r_{\max}$ considered in the χ^2 minimizing fit (5.6), according to:

    - for the vector u/d channel:
      $r_{\min} = 2a$;
    - for all other channels:
      $r_{\min} \in \{2a, 3a\}$;
    - for u/d channels:
      $r_{\max} \in \{8a, 9a, 10a\}$;
    - for s and c channels:
      $r_{\max} \in \{7a, 8a\}$

    The Lattice QCD results are not sufficiently precise to allow for stable fits with $r_{\min} = 3a$ for the vector u/d channel. Furthermore, $V^{\mathrm{lat}}(r)$ at small $r < 2a$ are expected to suffer from sizable lattice discretization errors, while $V^{\mathrm{lat}}(r)$ at large r is essentially a constant, i.e. has little effect on the relevant fit parameters α and d.

For each of the fitting parameters α, d and V_0, we construct a distribution by considering the results of all the above listed fits weighted by $\exp(-\chi^2/\mathrm{dof})$ with χ^2 from Equation (5.6). The central values of α, d and V_0 are then defined as the medians of the corresponding distributions and the lower/upper systematic uncertainties are given by the difference of the 16th/84th percentiles to the medians (in the case of a Gaussian distribution, an uncertainty defined in this way would correspond to its width, i.e. 1σ). Since in general the distributions are asymmetric, the systematic uncertainties are asymmetric as well. For more details regarding this method of estimating systematic errors we refer to [59].

Finally, to include statistical errors, we compute the jackknife errors of the medians of α, d and V_0 and add them in quadrature to the corresponding systematic uncertainties.

To illustrate this error estimation procedure, we show in Figure 5.6 example histograms representing the distribution of α and d for the scalar u/d channel. The green, red and blue bars correspond to the systematic, statistical and combined errors, respectively. In the following, we will always use and quote the combined errors represented by the blue bars.
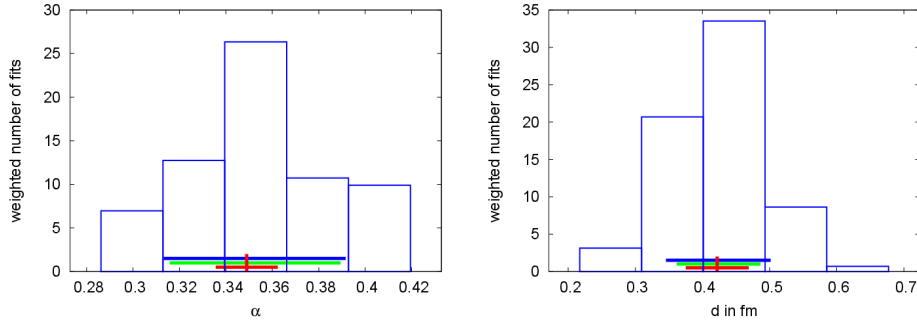

Figure 5.6.: Histograms used to estimate systematic errors for α and d for the scalar u/d channel (green, red and blue bars represent systematic, statistical and combined errors, respectively).

The final results for α and d are collected in Table 5.3. We do not list results for V_0, since it is an irrelevant constant corresponding to twice the mass of a static-light meson. The fit function (5.5) with the parameter sets from Table 5.3 and the corresponding error bands are shown in Figure 5.7. Clearly, these results confirm the qualitative expectation discussed above:

- The screening of the $\bar{b}\bar{b}$ interaction is stronger for heavier light quarks qq.

Moreover, the following statement about scalar and vector channels can be made:

- The scalar channels are more attractive than the corresponding vector channels.

5.4.4. Numerical solution of the Schrödinger equation

We define $U(r) = V(r)|_{V_0=0,p=2}$ with $V(r)$ from of Equation (5.5). $U(r)$ with a set of fit parameters α and d from Table 5.3 corresponds to the ground state energy of a $qq\bar{b}\bar{b}$ four-quark system in a specific channel minus the energy of a pair of far separated $B^{(*)}_{(s,c)}$ mesons.

qq	spin	α	d in fm
$(ud - du)/\sqrt{2}$	scalar	$0.35^{+0.04}_{-0.04}$	$0.42^{+0.08}_{-0.08}$
$uu,\ (ud + du)/\sqrt{2},\ dd$	vector	$0.29^{+0.04}_{-0.06}$	$0.16^{+0.02}_{-0.01}$
$(s^{(1)}s^{(2)} - s^{(2)}s^{(1)})/\sqrt{2}$	scalar	$0.27^{+0.08}_{-0.05}$	$0.20^{+0.10}_{-0.10}$
ss	vector	$0.18^{+0.09}_{-0.02}$	$0.18^{+0.11}_{-0.05}$
$(c^{(1)}c^{(2)} - c^{(2)}c^{(1)})/\sqrt{2}$	scalar	$0.19^{+0.12}_{-0.07}$	$0.12^{+0.03}_{-0.02}$

Table 5.3.: Parameters α and d obtained from χ^2 minimizing fits of (5.5) to Lattice QCD $\bar{b}\bar{b}$ potential results.

Thus, the corresponding Hamiltonian for the relative coordinate of the $\bar{b}\bar{b}$ quarks is

$$H \ = \ \frac{\mathbf{p}^2}{2\mu} + 2m_H + U(r), \tag{5.7}$$

where $\mu = m_H/2$ is the reduced mass. At large separations, each $\bar{b}$ quark carries the mass of a $B^{(*)}_{(s,c)}$ meson because of screening, and thus $m_H = m_{B^{(*)}_{(s,c)}}$. At small separations, $m_H = m_b$ could be more appropriate. Throughout this section, we always consider two choices, $m_H = m_{B_{(s,c)}}$ and $m_H = m_b$, which yield qualitatively identical results. Any dependence on the heavy $\bar{b}$ spins is neglected, because $V(r)$ has been computed in the static limit $m_b \to \infty$. Since the $\bar{b}$ quarks are quite heavy, we expect the static limit to be a reasonable approximation. Note, however, that a similar study [60] with infinitely heavy $\bar{b}$ quarks that takes into account the heavy quark spin finds the same bound state as we report on here with a slightly reduced binding energy.

To investigate the existence of a bound state, we solve the Schrödinger equation with the Hamiltonian (5.7) numerically. The strongest binding is expected in an s-wave, for which the radial equation is

$$\left(-\frac{1}{2\mu}\frac{d^2}{dr^2} + U(r) \right) R(r) \ = \ \underbrace{\left(E - 2m_H \right)}_{=E_B} R(r) \tag{5.8}$$

with the wave function $\psi = \psi(r) = R(r)/r$. If $E_B = E - 2m_H < 0$, $-E_B$ can be interpreted as the binding energy. We proceed as explained in [61] and solve this equation by imposing Dirichlet boundary conditions $R(r = \infty) = 0$ and using 4th order Runge-Kutta shooting.

For the scalar u/d channel, the lowest eigenvalue $E_B < 0$, which implies the existence of a bound four-quark state. For all other channels, i.e. the vector u/d and the s and c channels, $E_B > 0$, i.e. the corresponding $qq\bar{b}\bar{b}$ tetraquarks will most likely not exist in these channels [1].

The central value and the combined systematic and statistical error for the binding energy E_B of the tetraquark state in the scalar u/d channel is obtained by the method discussed in

---

[1]As mentioned previously in Section 5.4.3, the Lattice QCD results for the vector c channel are not sufficient to perform a quantitative analysis. The $\bar{b}\bar{b}$ potential in this channel is, however, much less attractive than in the other channels, e.g. the scalar c channel. Therefore, a bound four-quark state in the vector c channel can be excluded.
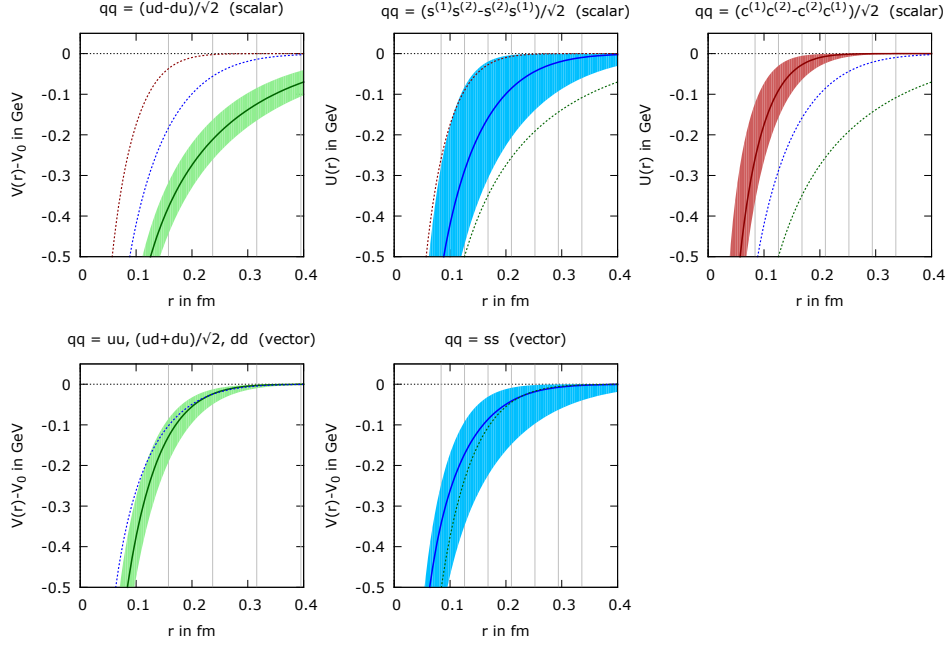
Figure 5.7.: $\bar{b}\bar{b}$ potentials in the presence of two lighter quarks qq (qq flavor: up/down in green, strange in blue, charm in red; qq spin: $j_z = 0$, i.e. scalar, in the upper line, $j = 1$, i.e. vector, in the lower line). The plotted curves with the error bands correspond to eq. (5.5) with the parameter sets from Table 5.3. Vertical lines indicate lattice separations $r = 2a, 3a, \ldots$ of Lattice QCD potential results $V^{\text{lat}}(r)$ used to generate the parameter sets from Table 5.3 via χ^2 minimizing fits.

Section 5.4.3 (generating a distribution for E_B from the fits listed in the same section):

$$E_B = -90^{+46}_{-42}\,\text{MeV} \quad (\text{for } m_H = m_B), \tag{5.9}$$

$$E_B = -93^{+47}_{-43}\,\text{MeV} \quad (\text{for } m_H = m_b). \tag{5.10}$$

These binding energies are roughly twice as large as their combined systematic and statistical errors. In other words, the confidence level for this $ud\bar{b}\bar{b}$ tetraquark state is around 2σ. The corresponding histogram for $m_H = m_B$ representing the determination of the errors as explained above is shown in Figure 5.8.

To quantify also the non-existence of bound four-quark states in the remaining channels, we determine numerically by which factors the heavy masses m_H in the Schrödinger equation (5.8) have to be increased to obtain bound states, i.e. tiny but negative energies E_B (the potentials $U(r)$ are kept unchanged, i.e. we stick to the medians for α and d from Table 5.3). The resulting factors are collected in Table 5.4. While the scalar s channel is quite close to be able to host a bound state, the scalar c channel and the vector channels are rather far away, since they would require $\bar{b}$ quarks approximately $1.6 \ldots 3.3$ times as heavy as they are in nature. Note that the factors listed in Table 5.4 could also be relevant for quark models aiming at studying the binding of tetraquarks quantitatively.

In Figure 5.9, we present our results in an alternative graphical way. Binding energy isolines $E_B(\alpha, d) = $ constant are plotted in the α-d-plane starting at a tiny energy $E_B = -0.1\,\text{MeV}$ up to rather strong binding, $E_B = -100\,\text{MeV}$ (gray dashed lines have been computed with
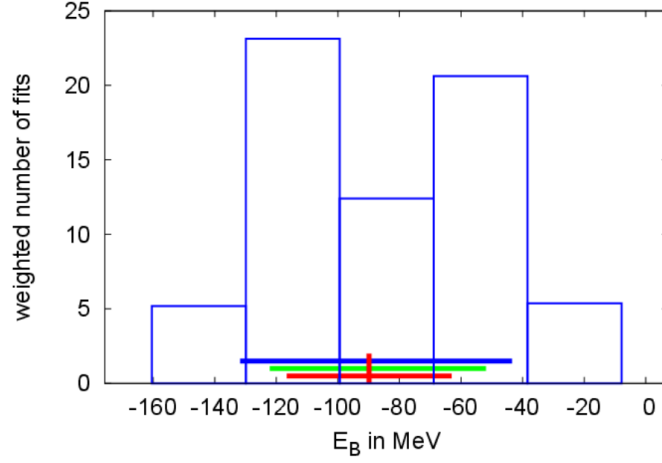
Figure 5.8.: Histogram used to estimate the systematic error for the binding energy E_B for the scalar u/d channel and $m_H = m_B$ (green, red and blue bars represent systematic, statistical and combined errors, respectively).

qq	spin	$m_H = m_{B_{(s,c)}}$	$m_H = m_b$
$(ud - du)/\sqrt{2}$	scalar	0.46	0.49
uu, $(ud + du)/\sqrt{2}$, dd	vector	1.49	1.57
$(s^{(1)}s^{(2)} - s^{(2)}s^{(1)})/\sqrt{2}$	scalar	1.20	1.29
ss	vector	2.01	2.18
$(c^{(1)}c^{(2)} - c^{(2)}c^{(1)})/\sqrt{2}$	scalar	2.57	3.24

Table 5.4.: Factors by which the mass m_H has to be multiplied to obtain a tiny but negative energy E_B. The factor $\ll 1$ indicates a strongly bound state, while for values $\gg 1$ bound states are essentially excluded.

$m_H = m_{B_{(s,c)}}$, gray solid lines with $m_H = m_b$). The three plots correspond to u/d, s and c light quarks qq, respectively. For the detailed discussion about systematic error estimation for α and d, cf. Section 5.4.3. The extensions of the point clouds represent the systematic uncertainties with respect to α and d. If a point cloud is localized above or left of the isoline with $E_B = -0.1\,\text{MeV}$ (approximately the binding threshold), the corresponding four quarks $\bar{b}\bar{b}qq$ will not form a bound state. A localization below or right of that isoline is a strong indication for the existence of a tetraquark. In case the point cloud is intersected by that isoline, the estimated systematic error is too large to make a definite statement regarding the existence or non-existence of a bound four-quark state. The big red and green bars in horizontal and vertical direction represent the combined systematic and statistical errors of α and d, as quoted in Table 5.3. One can observe and conclude the following from Figure 5.9:

- There is clear evidence for a tetraquark state in the scalar u/d channel.

- The scalar s channel is close to binding/unbinding. For a further investigation of this channel, cf. [62] where a corresponding resonance treatment using techniques from

scattering theory can be found.

- The scalar c and all vector channels do not host a bound four-quark state.

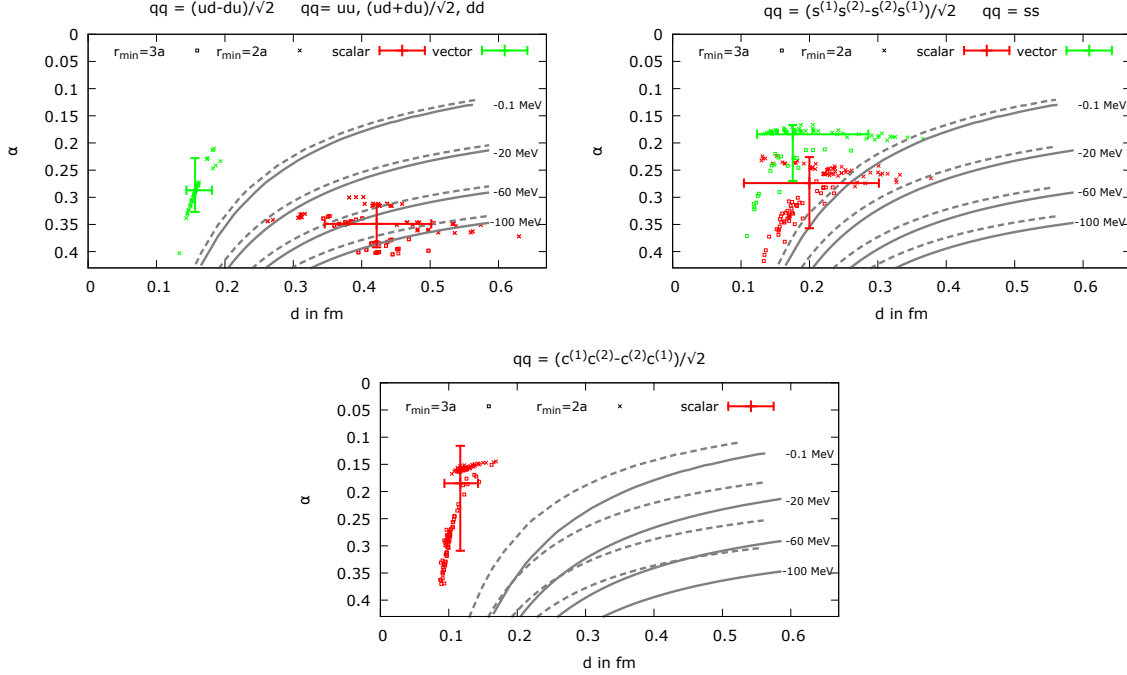These findings are consistent with the results presented above in Table 5.4.

Figure 5.9.: Binding energy isolines $E_B(\alpha, d) = $ constant in the α-d-plane for u/d, s and c light quarks qq, respectively (gray dashed lines: $m_H = m_{B_{(s,c)}}$; gray solid lines: $m_H = m_b$). Each fit of Equation (5.5) to Lattice QCD $\bar{b}\bar{b}$ potential results is represented by a dot: red: scalar channels; green: vector channels; crosses: $r_{\min} = 2a$; boxes: $r_{\min} = 3a$. The red and green bars are the corresponding combined systematic and statistical errors.

5.5. BB potentials at the physical pion mass

All the results for light quarks qq, $q \in \{u, d\}$ that we have shown so far correspond to one ensemble of gauge field configurations B40.24, at a lattice spacing $a \approx 0.079\,\mathrm{fm}$ and at a pion mass of around $340\,\mathrm{MeV}$. Now we are interested in the results at the physical pion mass. We have argued in Section 5.3 that cut-off effects are comparatively small in our setup by comparing lattice results corresponding to the same continuum channel, but affected by different discretization effects. We have found that the results from these different lattice channels are compatible within statistical uncertainties.

In the following we quantify to what extent the unphysically heavy u/d quark mass affects our conclusion – in particular how much stronger the binding is at physically light u/d quark masses for the scalar isosinglet and whether binding occurs for the vector isotriplet case.

5. $\bar{b}\bar{b}qq$ systems in the Born-Oppenheimer approximation

The investigation is essentially taken form [5]. We perform computations for two additional ensembles corresponding to the same lattice spacing, B85.24 and B150.24, with pion masses of around $480\,\mathrm{MeV}$ and $650\,\mathrm{MeV}$, respectively. We use the same strategy as in Section 5.4.3, i.e. to quantify systematic errors we perform several fits of the potentials in different ranges $t_{\min} \leq t \leq t_{\max}$ of temporal separations of the correlation function $C(t,r)$ at which the potential $V(r)$ is read off and different ranges of the static quark separation $r_{\min} \leq r \leq r_{\max}$ of the potential $V(r)$. The fitting ansatz is Equation (5.5).
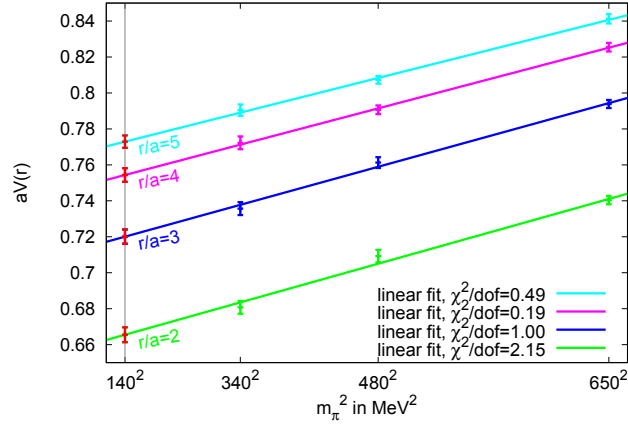

Figure 5.10.: Examples of fits of Eq. (5.11) for the t-interval $t/a \in [4,9]$ and for $r/a = 2, 3, 4, 5$ in the scalar isosinglet case. Three pion masses are used to extrapolate to the physical pion mass.

For each t-range and each r, we extrapolate the potentials to the physical pion mass. The extrapolation procedure is motivated by chiral perturbation theory: Since the leading order of chiral perturbation theory is typically proportional to m_π^2, we use an ansatz linear in m_π^2, i.e

$$V(r, m_\pi) = V(r, m_\pi^{\mathrm{phys}}) + c\left[m_\pi^2 - (m_\pi^{\mathrm{phys}})^2\right], \tag{5.11}$$

where $V(r, m_\pi^{\mathrm{phys}})$ and c are fitting parameters and m_π^{phys} is the physical pion mass. Note also that this approach led to consistent extrapolations both for static-light mesons [46, 47], and static-light baryons [63]. Both systems are quite similar to static-static-light-light tetraquarks studied in this work.

Examples of such fits are shown in Figure 5.10 for the t-interval $t/a \in [4,9]$ and for $r/a = 2, 3, 4, 5$. In all cases, the linear fitting ansatz gives a good description of the lattice data. The extrapolated potential $V(r)$ at the physical point can then be used in the same way as potentials at non-physical pion masses, i.e. for fits of Equation (5.5), using various t- and r-intervals to determine systematic uncertainties.

The results of this procedure for our different ensembles are shown in Table 5.5, together with the outcome for the extrapolated potential. We essentially get the same results with the tendency that binding in the scalar isosinglet case ($I = 0$, $j = 0$) becomes stronger towards

Table 5.5.: Extracted values of the fitting parameters α and d (in fm) and of the binding energy E (in MeV) in the scalar isosinglet channel ($I = 0$, $j = 0$). We show results for three ensembles differing in the pion mass and for the potentials extrapolated to the physical pion mass.

Ensemble	m_π [MeV]	α	d [fm]	E_B [MeV]
B150.24	650	$0.31^{+0.03}_{-0.03}$	$0.34^{+0.03}_{-0.03}$	-30^{+10}_{-12}
B85.24	480	$0.28^{+0.02}_{-0.02}$	$0.37^{+0.04}_{-0.04}$	-27^{+9}_{-8}
B40.24	340	$0.35^{+0.04}_{-0.04}$	$0.42^{+0.08}_{-0.08}$	-90^{+46}_{-42}
extrapolation	140	$0.34^{+0.03}_{-0.03}$	$0.45^{+0.12}_{-0.10}$	-90^{+43}_{-36}

Table 5.6.: Extracted values of the fitting parameters α and d (in fm) in the vector isotriplet channel ($I = 1$, $j = 1$). No binding is observed. We show results for three ensembles differing in the pion mass and for the potentials extrapolated to the physical pion mass.

Ensemble	m_π [MeV]	α	d [fm]
B150.24	650	$0.28^{+0.04}_{-0.04}$	$0.15^{+0.02}_{-0.01}$
B85.24	480	$0.30^{+0.06}_{-0.05}$	$0.14^{+0.04}_{-0.02}$
B40.24	340	$0.29^{+0.04}_{-0.06}$	$0.16^{+0.03}_{-0.02}$
extrapolation	140	$0.29^{+0.05}_{-0.06}$	$0.16^{+0.05}_{-0.02}$

the physical pion mass. For the physical pion mass, we observe binding of:

$$E_B = -90^{+43}_{-36} \text{ MeV}. \tag{5.12}$$

We conclude that the attraction between two B mesons (a static antiquark and a physically light up/down quark) in the I = 0 channel is strong enough to form a tetraquark state. Although they were obtained with only a single lattice spacing, we have strong hints that cut-off effects are under control and should not affect the final conclusion. An analogous procedure for the vector isotriplet channel ($I = 1$, $j = 1$) yields the results in Table 5.6. Regardless of the pion mass, we observe no binding and the results are essentially independent on m_π within our precision. One can observe that the parameter α is the same for $I = 0$ and $I = 1$ potentials within uncertainties. We can conclude that it is the much smaller value of the potential range d that is responsible for the absence of binding in the vector isotriplet channel, as compared to the scalar isosinglet case.

Finally, we summarize our results for both channels in Figure 5.11. For each pion mass, we show the results of individual fits of Equation (5.5) for different t- and r-fitting intervals, as well as the final error bar reflecting the combined statistical and systematic uncertainties. Values above or left of the binding threshold (the isoline $0 \, \text{MeV}$) correspond to no binding, while ones below or right of this threshold indicate that a bound state exists. The central values of the error bars correspond to the respective entries in Tables 5.5 and 5.6.
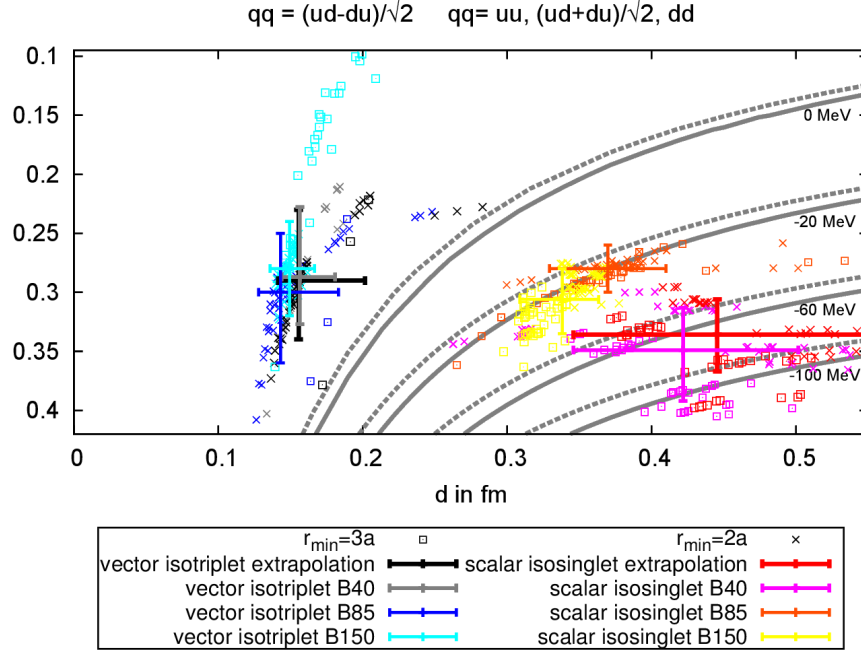
Figure 5.11.: Binding energy isolines $E_B(\alpha, d) = \mathrm{const}$ in the $\alpha - d$ plane for the scalar isosinglet ($I = 0$, $j = 0$) and vector isotriplet ($I = 1$, $j = 1$) channels and four pion masses: $140\,\mathrm{MeV}$ (extrapolated), $340\,\mathrm{MeV}$, $480\,\mathrm{MeV}$ and $650\,\mathrm{MeV}$. The dashed and solid lines correspond to $m_H = m_B$ or $m_H = m_b$ in the Schrödinger equation, respectively. The crosses and squares are the fits of Equation 5.5 for $r_{min}/a = 2, 3$, respectively, and different r_{max}/a and t-intervals. The error bars represent combined systematic and statistical errors.

5.6. Summary

In this chapter, we presented an investigation of $\bar{b}\bar{b}qq$ potentials for infinitely heavy b quarks and lighter quark flavors $q \in \{u, d, s, c\}$ for different isospin channels $I = 0$ and $I = 1$. For s and c quarks with finite mass or isospin $I = 1$ we found no evidence for a bound state. We found strong evidence for a $\bar{b}\bar{b}ud$ bound state in the $I = 0$ channel with quantum numbers $I(J^{\mathcal{P}}) = 0(1^+)$. An extrapolation to the physical pion mass yielded a binding energy of $E_B = -90^{+43}_{-36}$ MeV. With this result we predict a new tetraquark state that has not been measured experimentally, yet.

6. $\bar{b}\bar{b}ud$ systems in Nonrelativistic QCD

In this chapter we investigate $\bar{b}\bar{b}ud$ systems with b quarks of finite mass. We treat the b quarks in the framework of Nonrelativistic QCD (NRQCD). In Chapter 5 we studied $\bar{b}\bar{b}ud$ four-quark systems with static b quarks. In the $I(J^{\mathcal{P}}) = 0(1^+)$ channel we found evidence for a bound four-quark state. The binding energy of this state was found to be $E_{\text{binding}} = 90^{+36}_{-43}\text{MeV}$. Furthermore, in another study [64] using bottom quarks of finite mass similar results were obtained. Such a tetraquark candidate can be a very important prediction to give directions for future experimental research. However, it is crucial to investigate the candidate system under conditions that are as realistic as possible. Therefore using b quarks of finite mass instead of infinitely heavy b quarks and taking into account the spin of the heavy quarks in addition to the spin of the dynamical quarks is the next logical step. However, as we state below, both the static-light as well as finite-mass approach have advantages and disadvantages. We investigate the $\bar{b}\bar{b}ud$ system by taking into account various structures of the four-quark state. We present techniques to explore the bound state predicted in the previous section. Furthermore, we discuss not yet resolved discrepancies of results computed with NRQCD from results computed in the static approximation. Results of this chapter have been published in [9].

6.1. $\bar{b}\bar{b}ud$ systems with b quarks of finite mass – Expectations

6.1.1. Properties of the $\bar{b}\bar{b}ud$ system

Using heavy quarks of finite mass instead of static quarks has a particular advantage: In the former case, relativistic effects and the spin of the heavy quarks contributes to the energy of the system (cf. Section 5.1). Therefore, B and B^* mesons are not any more degenerate in mass. A bound $\bar{b}\bar{b}ud$ system with the quantum numbers $I(J^{\mathcal{P}}) = 0(1^+)$ can be realized either by a mesonic BB^* or B^*B^* molecule or by a diquark-antidiquark structure.

Possible structures

The $\bar{b}\bar{b}ud$ state with four quarks of finite mass in the $I(J^{\mathcal{P}}) = 0(1^+)$ channel can exist in different structures. In the following, we present a selection of these structures, which we take into account in the further analysis by means of their creation operators. Note that we suppress the space-time argument of the operators.

Mesonic molecule BB^*:
The BB^* operator reads:

$$O_{BB^*} = \bar{b}_A^a \Gamma_{AB}^1 u_B^a \bar{b}_C^b \Gamma_{CD}^2 d_D^b - \bar{b}_A^a \Gamma_{AB}^1 d_B^a \bar{b}_C^b \Gamma_{CD}^2 u_D^b \tag{6.1}$$

where the antisymmetric flavor combination $ud - du$ results in isospin $I = 0$. To realize quantum numbers $J^{\mathcal{P}} = 1^+$, we choose $\Gamma^1 = \gamma_5$ and $\Gamma^2 = \gamma_i$.

Mesonic molecule $B^* B^*$:

The $B^* B^*$ operator reads:

$$O_{B^* B^*} = \bar{b}_A^a \Gamma_{AB}^1 u_B^a \bar{b}_C^b \Gamma_{CD}^2 d_D^b - \bar{b}_A^a \Gamma_{AB}^1 d_B^a \bar{b}_C^b \Gamma_{CD}^2 u_D^b. \tag{6.2}$$

To realize quantum numbers $J^{\mathcal{P}} = 1^+$, we choose $\varepsilon_{ilm} \left(\Gamma^1 = \gamma_l, \, \Gamma^2 = \gamma_m \right)$, where ε_{ilm} is the Levi-Civita tensor.

Diquark-antidiquark Dd:
The Dd operator reads:

$$O_{Dd} = \varepsilon^{abc} \bar{b}_A^b \Gamma_{AB}^1 \bar{b}_B^c \epsilon^{ab'c'} \left(u_C^{b'} \Gamma_{CD}^2 d_D^{c'} - d_C^{b'} \Gamma_{CD}^2 u_D^{c'} \right). \tag{6.3}$$

To realize quantum numbers $J^{\mathcal{P}} = 1^+$, we choose the gamma matrix combinations $\Gamma^1 = \mathcal{C}\gamma_i$ and $\Gamma^2 = \mathcal{C}\gamma_5$ with the charge conjugation matrix $\mathcal{C}$.

Momentum projections

In addition to different four-quark structures, we take into account different possible momentum projections. On the one hand, we consider the system to have total momentum zero. On the other hand we consider the individual B mesons to have zero momentum each. To illustrate how the different projections are realized, we start with the creation operator of a B meson with constituent quarks of finite mass on the lattice:

$$O_{B(\mathbf{p})}(t) = \frac{1}{\sqrt{V_s}} \sum_{\mathbf{x} \in V_s} \bar{b}(\mathbf{x}, t) \Gamma u(\mathbf{x}, t) \, \mathrm{e}^{-i\mathbf{x} \cdot \mathbf{p}} \tag{6.4}$$

with $\mathbf{p} = \frac{2\pi}{L}\mathbf{n}$ and $n_i = 0, 1, ..., L/a - 1$ (with L the spatial lattice extent and a the lattice spacing). For simplicity, we suppress color and spin indices. $V_s = L^3$ is the spacial lattice volume. To realize zero momentum, we set $\mathbf{p} = 0$ and expression (6.4) reads:

$$O_{B(0)}(t) = \frac{1}{\sqrt{V_s}} \sum_{\mathbf{x} \in V_s} \bar{b}(\mathbf{x}, t) \Gamma u(\mathbf{x}, t). \tag{6.5}$$

Note that in contrast to the case of static light B mesons (cf. Chapters 5 and 7) the sum over the spatial lattice volume is mandatory because the position of the b quarks is not fixed. Now we consider the creation operator of a mesonic molecule of B mesons where each meson carries a specified arbitrary momentum:

$$O_{B(\mathbf{p})B(\mathbf{q})}(t) = \frac{1}{\sqrt{V_s}} \sum_{\mathbf{x} \in V_s} \bar{b}(\mathbf{x}, t) \Gamma u(\mathbf{x}, t) \, \mathrm{e}^{-i\mathbf{x} \cdot \mathbf{p}} \frac{1}{\sqrt{V_s}} \sum_{\mathbf{y} \in V_s} \bar{b}(\mathbf{y}, t) \Gamma u(\mathbf{y}, t) \, \mathrm{e}^{-i\mathbf{y} \cdot \mathbf{q}}. \tag{6.6}$$

To realize a momentum projection where the full system has overall zero momentum, we have to constrain the individual momenta according to $\mathbf{p} + \mathbf{q} = 0$. Expression (6.6) then reads:

$$O_{[BB](0)}(t) = \frac{1}{\sqrt{V_s}} \sum_{\mathbf{x} \in V_s} \bar{b}(\mathbf{x}, t) \Gamma u(\mathbf{x}, t) \frac{1}{\sqrt{V_s}} \sum_{\mathbf{y} \in V_s} \bar{b}(\mathbf{y}, t) \Gamma u(\mathbf{y}, t) \, \mathrm{e}^{-i(\mathbf{x} - \mathbf{y}) \cdot \mathbf{p}}. \tag{6.7}$$

In order to find a mesonic molecule, both B mesons have to be located at the same spatial position, i.e. we demand $\mathbf{x} = \mathbf{y}$. Thus we find

$$O_{[BB](0)}(t) = \frac{1}{\sqrt{V_s}} \sum_{\mathbf{x} \in V_s} \bar{b}(\mathbf{x}, t)\Gamma u(\mathbf{x}, t)\bar{b}(\mathbf{x}, t)\Gamma u(\mathbf{x}, t). \tag{6.8}$$

In case of individual B mesons projected to zero momentum each, we set $\mathbf{p} = \mathbf{q} = 0$ and (6.6) reads:

$$O_{B(0)B(0)}(t) = \frac{1}{\sqrt{V_s}} \sum_{\mathbf{x} \in V_s} \bar{b}(\mathbf{x}, t)\Gamma u(\mathbf{x}, t) \frac{1}{\sqrt{V_s}} \sum_{\mathbf{y} \in V_s} \bar{b}(\mathbf{y}, t)\Gamma u(\mathbf{y}, t). \tag{6.9}$$

Note that the summation over spatial points $\mathbf{x}$ and $\mathbf{y}$ has to be performed before the individual mesons are multiplied. Therefore we cannot set $\mathbf{x} = \mathbf{y}$ here. The operator corresponds to a meson scattering state.

All operators considered in this thesis

In case of the BB^* structure (cf. Equation (6.1)) we take into account the two different momentum projections:

- $B(0)B^*(0)$ – Each meson is separately projected to zero momentum. For reasons described below we will only use this operator at the sink.

- $[BB^*](0)$ – The whole four-quark system is projected to zero momentum.

The different momentum projections give two different operators. We call them $O_{B(0)B^*(0)}$ and $O_{[BB^*](0)}$.

As in the previous case, there are two different momentum projections to be taken into account for the B^*B^* structure (cf. (6.2)):

- $B^*(0)B^*(0)$ – Each meson is separately projected to zero momentum. For reasons described below we will only use this operator at the sink.

- $[B^*B^*](0)$ – The whole four-quark system is projected to zero momentum.

The different momentum projections give the two different operators $O_{B^*(0)B^*(0)}$ and $O_{[B^*B^*](0)}$.

For the diquark-antidiquark structure (cf. (6.3)) there is only one reasonable momentum projection. Diquark and antidiquark are jointly projected to zero momentum: $[Dd](0)$. We refer to the corresponding operator as $O_{[Dd](0)}$.

6.1.2. The correlation matrix for all different structures

We can build a correlation matrix (C_{ij}) using the operators we defined in Section 6.1.1. The matrix elements read:

$$C_{ij}(t_{\text{sink}} - t_{\text{source}}) = \langle \Omega | O_i(t_{\text{sink}})O_j^\dagger(t_{\text{source}}) | \Omega \rangle \tag{6.10}$$

with $O_i, O_j \in \{O_{B(0)B^*(0)}, O_{[BB^*](0)}, O_{B^*(0)B^*(0)}, O_{[B^*B^*](0)}, O_{[Dd](0)}\}$. Due to the fact that we use point sources to compute the light quark propagators it is not possible to project the mesons separately to zero momentum at the source. The reason is that one needs to sum

over all positions of the individual mesons to project each of them to zero momentum, cf. Equation (6.9). However, the point source is fixed at position $\mathbf{x}_{\text{source}}$. This leads to some restrictions to the correlation matrix as we will point out below. We give an overview of the correlation matrix in Table 6.1. Most of the matrix elements can be exactly computed

source sink	$O^\dagger_{[BB^*](0)}$	$O^\dagger_{[B^*B^*](0)}$	$O^\dagger_{[Dd](0)}$	$O^\dagger_{B(0)B^*(0)}$	$O^\dagger_{B^*(0)B^*(0)}$
$O_{[BB^*](0)}$	d.c.	d.c.	d.c.	n.d.c.	n.d.c.
$O_{[B^*B^*](0)}$	d.c.	d.c.	d.c.	n.d.c.	n.d.c.
$O_{[Dd](0)}$	d.c.	d.c.	d.c.	n.d.c.	n.d.c.
$O_{B(0)B^*(0)}$	d.c.	d.c.	d.c.	n.c.	n.c.
$O_{B^*(0)B^*(0)}$	d.c.	d.c.	d.c.	n.c.	n.c.

Table 6.1.: Schematic representation of the correlation matrix. The meaning of the abbreviations is the following: d.c.: exactly directly computable, n.d.c.: not directly computable but can be obtained indirectly, n.c.: neither exactly computable directly nor indirectly.

directly. These elements are tagged by the label d.c. (directly computable). Elements that take into account separately projected mesons at the source cannot be computed directly. In case they have off-diagonal counterparts that can be obtained by complex conjugation of their off-diagonal counterparts. The label of these elements is n.d.c. (not directly computable). All other elements cannot be computed using point sources directly nor indirectly. We refer to them as n.c.-elements (not computable). From Table 6.1 we can see that there are four elements of this type. Using the GEP, one can only obtain the overlap factors and energies for the 2×2 and 3×3 submatrices of the 5×5 correlation matrix represented by Table 6.1 which do not contain n.c.-elements. In the following section, we present a way to approximately compute the missing overlaps and energies.

Computing the missing overlaps and energies

In the following we consider a matrix built of only two operators for simplicity. Extending the method to a larger matrix is straightforward. Consider the operators

$$O_1 = \sum_{\mathbf{x}} B(x) \sum_{\mathbf{y}} B(y) \tag{6.11}$$

and

$$O_2 = \sum_{\mathbf{x}} B(x)B(x). \tag{6.12}$$

with $B(x) = \bar{b}(x)\Gamma u(x)$. Operator O_1 represents a mesonic molecule where each meson is separately projected to zero momentum. Operator O_2 describes a mesonic molecule with both mesons jointly projected to zero momentum. The correlation matrix reads:

$$C_{ij}(t_{\text{sink}} - t_{\text{source}}) = \langle\Omega| O_i(t_{\text{sink}})O^\dagger_j(t_{\text{source}}) |\Omega\rangle. \tag{6.13}$$

In this example we can only exactly compute C_{12} and C_{22} directly. We cannot take into account $O^\dagger_1$ at the source because we only have light-quark propagators with the fixed starting

point $\mathbf{x} = \mathbf{x}_{\text{source}}$. However, we can exactly reconstruct C_{21} using

$$C_{21}(t_{\text{sink}} - t_{\text{source}}) = C_{12}^{\dagger}(t_{\text{sink}} - t_{\text{source}}). \tag{6.14}$$

The element C_{11} can only be computed approximately. Consider the spectral decomposition of the correlation matrix element C_{ij}:

$$C_{ij}(t_{\text{sink}} - t_{\text{source}}) = \sum_{n=1}^{\infty} Z_i^{(n)} Z_j^{*(n)} \mathrm{e}^{-E_n(t_{\text{sink}} - t_{\text{source}})} \tag{6.15}$$

with overlap factors $Z_k^{(n)}$ and energies E_n. After multiplying O_1 and O_2 by appropriate phases the overlap factors will be real. Thus,

$$C_{ij}(t_{\text{sink}} - t_{\text{source}}) = \sum_{n=1}^{\infty} Z_i^{(n)} Z_j^{(n)} \mathrm{e}^{-E_n(t_{\text{sink}} - t_{\text{source}})}. \tag{6.16}$$

Once C_{12} and C_{22} are computed, one can perform a coupled fit to the data of the form

$$C_{12} = \sum_{n=1}^{N} Z_1^{(n)} Z_2^{(n)} \mathrm{e}^{-E_n(t_{\text{sink}} - t_{\text{source}})}, \tag{6.17}$$

$$C_{22}(t_{\text{sink}} - t_{\text{source}}) = \sum_{n=1}^{N} Z_2^{(n)} Z_2^{(n)} \mathrm{e}^{-E_n(t_{\text{sink}} - t_{\text{source}})} \tag{6.18}$$

with parameters $Z_1^{(n)}$, $Z_2^{(n)}$ and E_n for $n = 1...N$ (here $N = 2$).

6.2. Investigation of the BB^* molecule by means of NRQCD

As a first step we only use molecule-like operators projected to zero momentum $[B^*B](0)$ and $[B^*B^*](0)$. A recent study on static-light $\bar{b}\bar{b}ud$ four-quark states that takes into account heavy spin effects [60] shows, that the $\bar{b}\bar{b}ud$ bound state is not just a composite of a B and a B^* meson. The bound state is rather a $50\%/50\%$ mixture of a BB^* and a B^*B^* molecule. For this reason, besides the BB^* operator, we also consider the B^*B^* operator in our study.

6.2.1. Lattice QCD setup

Computations have been performed using 200 configurations of the ensemble C54 of gauge link configurations generated by the RBC and UKQCD collaborations. The ensemble is produced using the Iwasaki gauge action and domain-wall fermions with $n_f = 2 + 1$ dynamical quark flavors. Information on these configurations can be found in Table 6.2 or in [65]. Light propagators are computed using point sources starting at multiple source locations. This way, in total 1676 measurements are available. The bottom quark is treated in the framework of NRQCD and the action is tadpole-improved (cf. [65] for further details). We use Gaussian smearing for all quark fields, cf. Section 3.3.

Ens.	β	lattice	$am_{u,d}$	am_s	m_π[MeV]	a [fm]	measurements
C54	2.13	$24^3 \times 64$	0.005	0.04	336	0.1119(17)	1676

Table 6.2.: Ensemble C54 of gauge link configurations. β: inverse gauge coupling, lattice size $(L/a)^3 \times (T/a)$, $m_{u,d}$: u/d light sea and valence quark mass, m_s: strange sea and valence quark mass, m_π: pion mass, a: lattice spacing, measurements: number of samples taken on different gauge link configurations or different source locations.

6.2.2. Correlation functions

As already emphasized, the positions of bottom quarks of finite mass are not fixed. Therefore, the computation of a $\bar{b}\bar{b}$ potential in the presence of two light quarks ud is not as easy as in our study in Chapter 5. This is a disadvantage of the approach. However, one can directly compute the energy $E_{\bar{b}\bar{b}ud}$ of the lowest $\bar{b}\bar{b}ud$ state in the $I(J^{\mathcal{P}}) = 0(1^+)$ channel. If $E_{\bar{b}\bar{b}ud}$ lies below the BB^* threshold in the limit lattice volume $V \to \infty$, i.e. $E_{\bar{b}\bar{b}ud} < E_B + E_{B^*}$, this indicates the existence of a $\bar{b}\bar{b}ud$ bound state.

We compute the effective energy of a BB^* and B^*B^* molecule-like operators as well as the effective energies of B and the B^* meson operators and choose the overall momentum of all meson-like systems to be zero. The correlation function of the BB^* mesonic molecule reads:

$$
\begin{aligned}
\mathcal{C}_{BB^*\text{-mol}}(t) =& \left\langle O_{[B_1 B_1^*](0)}(0) O^\dagger_{[B_1 B_1^*](0)}(t) \right\rangle \\
& \sum_{\mathbf{x}'} \left\langle \left(\bar{b}(\mathbf{x},0)\Gamma_1 d(\mathbf{x},0)\bar{b}(\mathbf{x},0)\Gamma_2 u(\mathbf{x},0) - \bar{b}(\mathbf{x},0)\Gamma_1 u(\mathbf{x},0)\bar{b}(\mathbf{x},0)\Gamma_2 d(\mathbf{x},0) \right) \right. \\
& \left. \left(\bar{d}(\mathbf{x}',t)\Gamma_1' b(\mathbf{x}',t)\bar{u}(\mathbf{x}',t)\Gamma_2' b(\mathbf{x}',t) - \bar{u}(\mathbf{x}',t)\Gamma_1' b(\mathbf{x}',t)\bar{d}(\mathbf{x}',t)\Gamma_2' b(\mathbf{x}',t) \right) \right\rangle.
\end{aligned}
\tag{6.19}
$$

The correlation function of the B^*B^* mesonic molecule takes the form:

$$
\begin{aligned}
\mathcal{C}_{B^*B^*\text{-mol}}(t) =& \left\langle O_{[B_1^* B_1^*](0)}(0) O^\dagger_{[B_1^* B_1^*](0)}(t) \right\rangle \\
& \sum_{\mathbf{x}'} \left\langle \left(\bar{b}(\mathbf{x},0)\Gamma_1 d(\mathbf{x},0)\bar{b}(\mathbf{x},0)\Gamma_2 u(\mathbf{x},0) - \bar{b}(\mathbf{x},0)\Gamma_1 u(\mathbf{x},0)\bar{b}(\mathbf{x},0)\Gamma_2 d(\mathbf{x},0) \right) \right. \\
& \left. \left(\bar{d}(\mathbf{x}',t)\Gamma_1' b(\mathbf{x}',t)\bar{u}(\mathbf{x}',t)\Gamma_2' b(\mathbf{x}',t) - \bar{u}(\mathbf{x}',t)\Gamma_1' b(\mathbf{x}',t)\bar{d}(\mathbf{x}',t)\Gamma_2' b(\mathbf{x}',t) \right) \right\rangle
\end{aligned}
\tag{6.20}
$$

with ε_{ilm} ($\Gamma_1 = \gamma_l$, $\Gamma_2 = \gamma_m$) and ε_{ijk} $\left(\Gamma_1' = \gamma_0 \gamma_j^\dagger \gamma_0, \Gamma_2' = \gamma_0 \gamma_k^\dagger \gamma_0 \right)$. To decrease the statistical error, in each case we average over the three spin polarizations. Furthermore, the correlation functions of the B and of the B^* meson read:

$$
\mathcal{C}_B(t) = \sum_{\mathbf{x}'} \left\langle \bar{b}(\mathbf{x},0)\Gamma_1 d(\mathbf{x},0)\bar{d}(\mathbf{x}',t)\Gamma_1' b(\mathbf{x}',t) \right\rangle
\tag{6.21}
$$

and

$$
\mathcal{C}_{B^*}(t) = \sum_{\mathbf{x}'} \left\langle \bar{b}(\mathbf{x},0)\Gamma_2 d(\mathbf{x},0)\bar{d}(\mathbf{x}',t)\Gamma_2' b(\mathbf{x}',t) \right\rangle
\tag{6.22}
$$

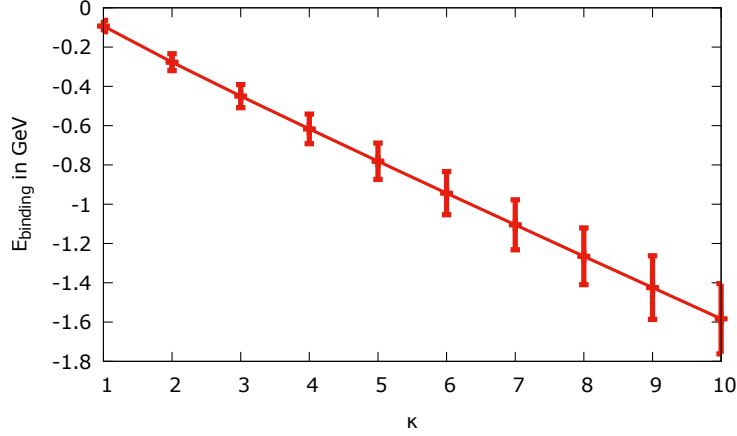with $\Gamma_1 = \gamma_5$, $\Gamma_2 = \gamma_i$, $\Gamma_1' = -\gamma_5$ and $\Gamma_2' = -\gamma_i^\dagger$.

Figure 6.1.: The binding energy E_{binding} of a four-quark state from static-light potential cal-culations as a function of the factor κ by which the physical b quark mass is increased. The line based on a linear fit is drawn to guide the eye.

In order to verify the expectation that taking into account the B^*B^* operator improves the signal of the $\bar{b}\bar{b}ud$ ground state of interest, we perform calculations with and without this very operator. To do so, we first compute the effective masses from the correlation functions build of the operators corresponding to the BB^* molecule, the B and B^* mesons, respectively, via

$$aE_i^{(\text{eff})}(t) = \ln\left(\mathcal{C}_i(t)/\mathcal{C}_i(t+a)\right) \quad , \quad i = BB^*\text{-mol}, B, B^*. \tag{6.23}$$

Next we build a 2×2 correlation matrix taking into account both the BB^* and the B^*B^* operator and extract the ground state by solving the Generalized Eigenvalue Problem [66]. We have performed computations with a bottom quark mass m_Q corresponding to the values m_b and $5m_b$ with m_b the physical b quark mass. We decided to also study such unphysically heavy bottom quarks, because we expect from our previous static-light computations, cf. Chapter 5 and [5, 6, 61], that the binding energy of a four-quark state increases with an increased heavy quark mass. We therefore expect a clearer result also for this computation. In Figure 6.1 we show, that indeed the binding energy increases when m_Q is increased. To produce the plot we consider the potential (5.5) and parameters α and d determined in Section 5.4.3: $\alpha = 0.34$ and $d = 0.42\,\text{fm}$. We insert the potential into the Schrödinger equation. The reduced mass $\mu = \frac{m_Q}{2}$ used in the Schrödinger equation is replaced by $\kappa\mu$. We solve the Schrödinger equation and compute the binding energy E_{binding} for various values of κ. One can see that the binding energy changes from $\approx -100\,\text{MeV}$ to $\approx -800\,\text{MeV}$ as the value κ is increased from 1 to 5. For details, cf. Appendix A.4, where we consider the spectrum of the hydrogen atom to estimate the binding energy.

6.2.3. Numerical results

The effective energies $E_{BB^*\text{-mol}}^{(\text{eff})}$ corresponding to the BB^* molecule-like operator are shown in Figure 6.2 both for $m_Q = m_b$ and $m_Q = 5m_b$. The horizontal grey lines and error bands correspond to the sum of the energies of the mesons $E_B + E_{B^*}$. These can be obtained rather

precisely by fitting constants to the corresponding effective energies (cf. Equation (6.23)) at large temporal separations t. We show plots of the effective B and B^* energies in Figure 6.3. For $m_Q = 5m_b$ and large temporal separations t the effective energy in Figure 6.2 seems to
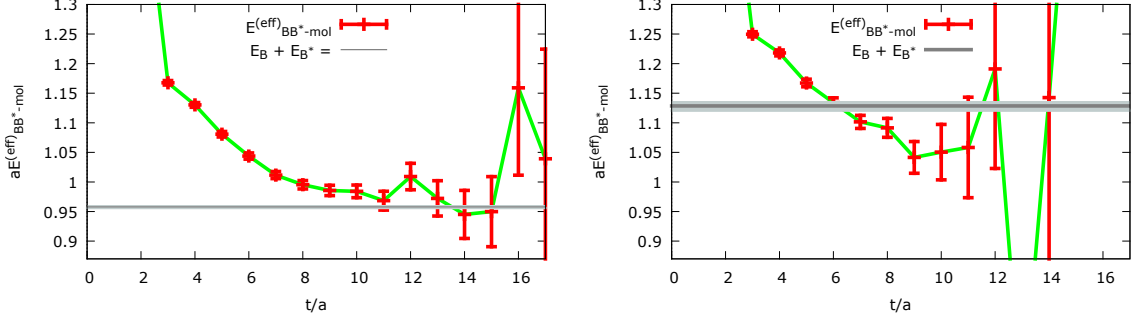

Figure 6.2.: The effective energy corresponding to the BB^* molecule-like operator in units of the lattice spacing as a function of the temporal separation t/a (red points) in comparison to $E_B + E_{B^*}$ (horizontal grey line). **(left)**: $m_Q = m_b$. **(right)**: $m_Q = 5m_b$.

be below $E_B + E_{B^*}$, which might be an indication for a bound four-quark state. However, the plateau quality is not sufficient to make solid statements. Extracting the ground state of a 2×2 correlation matrix considering the BB^* as well as the B^*B^* operator, both for $m_Q = m_b$ and $m_Q = 5m_b$ yields the effective energy shown in Figure 6.4. One can see that the effective energy lies below the $E_B + E_{B^*}$ threshold. This supports the expectation from [60] that the $\bar{b}\bar{b}ud$ state is a superposition of a BB^* and a B^*B^* system rather than just a combination of a B and a B^* meson.

The results shown in Figure 6.4 clearly indicate that the $\bar{b}\bar{b}ud$ four-quark state is smaller than the sum of the masses of the B and the B^* meson. This qualitatively confirms the result found in the static-light case (cf. Chapter 5), a bound $\bar{b}\bar{b}ud$ four-quark state in the $I(J^{\mathcal{P}}) = 0(1^+)$ channel.

6.2.4. Discussion: The binding energy of the $\bar{b}\bar{b}ud$ system

In Chapter 5 we present calculations of the binding energy of the $\bar{b}\bar{b}ud$ state by solving the Schrödinger equation with a static-light potential. In Figure 6.1 we show that this method yields a binding energy of $\approx -100\,\text{MeV}$ for a physically heavy b quark mass m_b and a binding energy of $\approx -800\,\text{MeV}$ for an increased b quark mass of $5m_b$. In Section 6.2.3 we derive the binding energy by means of NRQCD. It can be estimated by reading off the difference between the $E_B + E_{B^*}$ threshold and the effective energy plateau in Figure 6.4. Taking into account the lattice spacing $a = 0.1119\,\text{fm}$ the corresponding binding energy for the physical b quark mass m_b is $-20\ldots-90\,\text{MeV}$ and the binding energy for the increased b quark mass $5m_b$ is $-140\ldots-230\,\text{MeV}$.

This discrepancy compared to the static-light potential results could be due to a possibly underestimated systematic uncertainty of the parameters α and d of the static-light potential. A different choice of parameters yields a different binding energy. We show the impact of changing the parameters by considering the Coulomb-like part of the static-light potential
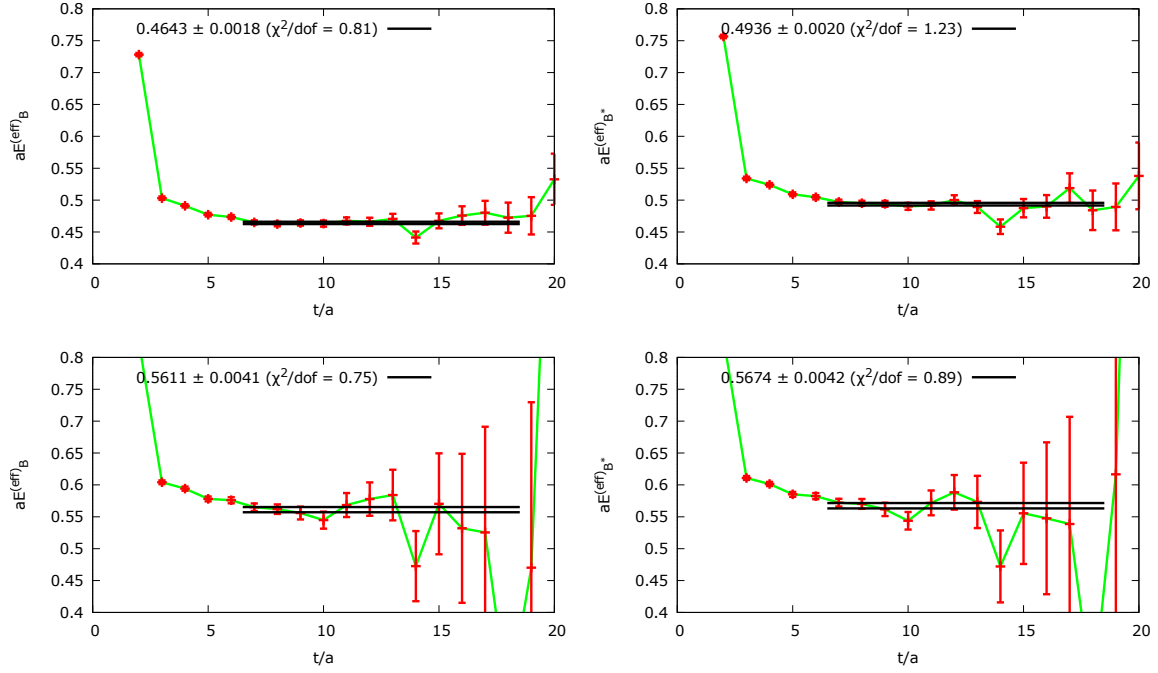
Figure 6.3.: Effective masses of the B and the B^* meson. **(top)**: $m_Q = m_b$. **(bottom)**: $m_Q = 5m_b$. Results of a linear fit in the range $7 \leq t/a \leq 18$ as well as the values $\chi^2/\text{d.o.f}$ are given in each panel.
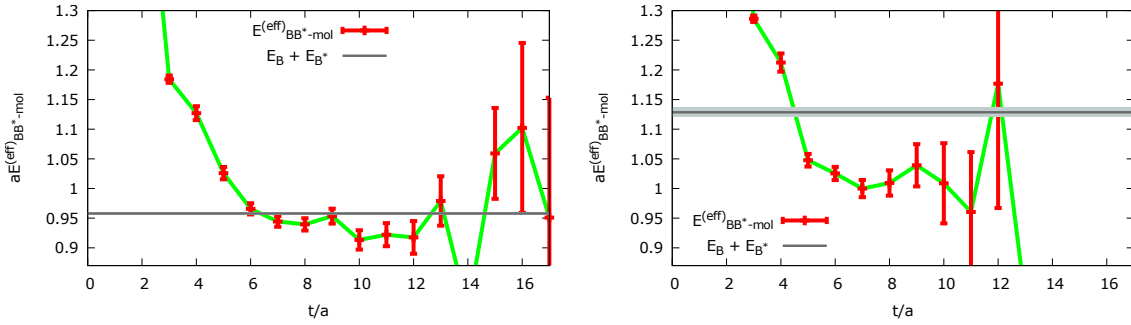

Figure 6.4.: The effective energy of the ground state of the 2×2 correlation matrix taking into account the BB^* as well as the B^*B^* molecule-like operators in units of the lattice spacing as a function of the temporal separation t/a (red points) in comparison to $E_B + E_{B^*}$ (horizontal grey line). **(left)**: $m_Q = m_b$. **(right)**: $m_Q = 5m_b$.

(5.5) for different values of α. The results are presented in Figure 6.5: One can estimate which values of α are required to get a certain binding energy indicated by the horizontal line if the mass of the b-quark is increased by different factors κ. The respective values for α correspond to the intersection points of the horizontal lines with the different curves. For example in case of a b-quark mass κm_b with $\kappa = 5$ the binding energy is $-140 \ldots -230\,\text{MeV}$ so corresponding value is $\alpha \approx 0.15 \ldots 0.19$. At the same time we can estimate from the figure that the value $\alpha = 0.35$ we derived in Chapter 5 yields a much larger value for the binding energy. This provides a possible explanation of the binding energy of $\approx 800\,\text{MeV}$ which is expected according to the static-light results, cf. Figure 6.1, compared to $-140 \ldots -230\,\text{MeV}$ from NRQCD. In the future it would be interesting and important to review both results and find the reason for the discrepancy.
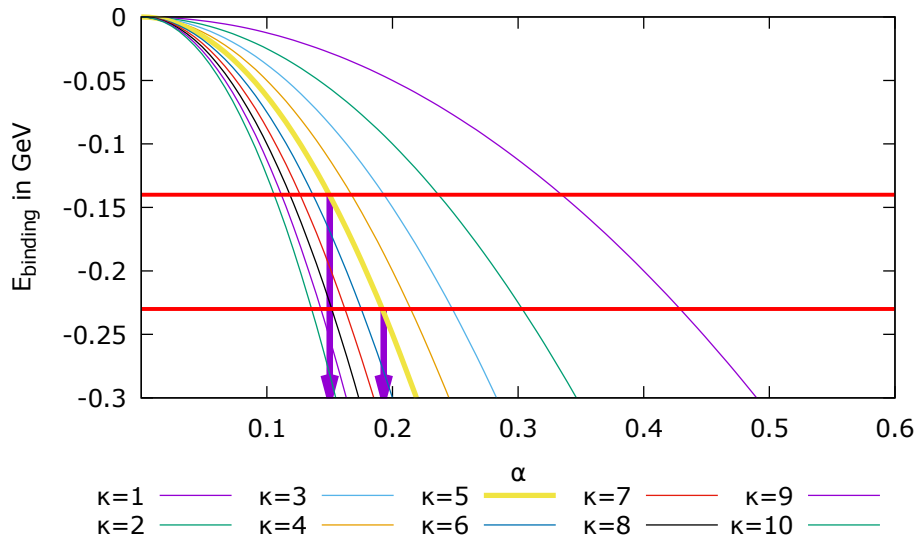

Figure 6.5.: From this figure the requested values of α to get a binding energy of $-140 \ldots -230\,\text{MeV}$ can be estimated for different factors κ with which m_b is multiplied. The arrows indicate, that in case of a b-quark mass that is multiplied by $\kappa = 5$ the corresponding value is $\alpha \approx 0.15 \ldots 0.19$.

6.3. Summary

In this chapter we investigated the $\bar{b}\bar{b}ud$ state in the $I(J^{\mathcal{P}}) = 0(1^+)$ channel by taking into account heavy quark spin effects. We described various possible four-quark structures. As a first step we took into account mesonic molecule-like four-quark operators. We qualitatively confirmed findings of a $\bar{b}\bar{b}ud$ bound state in the static approximation in this channel and pointed out possibly necessary refining work.

7. $b\bar{b}u\bar{d}$ systems in the Born-Oppenheimer approximation

A number of mesons observed in experiment, e.g. at the LHCb or at Belle, lack a satisfactory theoretical description. Examples are the so-called XYZ mesons (cf. e.g. [67]). According to their properties they cannot be $q\bar{q}$ mesons but must contain additional constituents. They are candidates for exotic hadrons like hybrids or tetraquarks. The charged $Z_b(10610)$ and $Z_b(10650)$ states (cf. e.g. [4]) are well-known tetraquark candidates. These states are bottomonium-like, which can be concluded from their mass and decay products. However, they also carry electric charge, which means they must include additional quarks. It is most likely that these additional quarks are a light quark-antiquark pair. So the quark content of the $Z_b^{\pm}$ states is assumed to be $b\bar{b}u\bar{d}/b\bar{b}d\bar{u}$. In this chapter we study heavy-light four quark systems with one heavy and one light quark-antiquark pair, $b\bar{b}u\bar{d}$. As in Chapter 5 we consider the heavy quarks to have infinite mass and we use the Born-Oppenheimer approximation. We take into account various structures of the four-quark system.

7.1. The $b\bar{b}u\bar{d}$ four-quark system – Expectations

The recently measured states $Z_b(10610)$ and $Z_b(10650)$ are experimentally very interesting examples for a $b\bar{b}q\bar{q}$ four-quark candidate. They have the quantum numbers $I(J^{\mathcal{P}}) = 1(1^+)$. In the following we consider the positively charged state Z_b^+ (cf. e.g. [4, 68, 69, 70, 71]). However, all results also hold for Z_b^-. Isospin $I = 1$ and positive electromagnetic charge is realized by light quark flavours $u\bar{d}$. Parity $\mathcal{P} = +$ is consistent with a possible loosely bound $B^{(*)}\bar{B}^*$ structure, since both $B^{(*)}$ and $\bar{B}^*$ have $\mathcal{P} = -$ and hence in combination result in $P = +$. Note, however, that in the static approximation B and B^* mesons are degenerate in mass. Therefore we will not distinguish them in the following. Numerically we find most evidence for a four-quark bound state with the light total angular momentum $j = 0$ (cf. Section 7.2.1). In the static approximation the different spin alignments of the static quarks are degenerate, i.e. we cannot distinguish $j_b = 0$ or $j_b = 1$. This means, the total angular momentum can either be $J = 0$ or $J = 1$, i.e. all our statements apply to $b\bar{b}u\bar{d}$ four-quark system not only with $I(J^{\mathcal{P}}) = 1(1^+)$, but also with $I(J^{\mathcal{P}}) = 1(0^+)$. Up to now, only the $I(J^{\mathcal{P}}) = 1(1^+)$ channel can be measured experimentally. To measure the $I(J^{\mathcal{P}}) = 1(0^+)$ channel a different experimental setup than realized in current experiments would be necessary.

$b\bar{b}u\bar{d}$ states in the $I(J^{\mathcal{P}}) = 1(1^+)$ channel may have different structures. We distinguish between four-quark structures such as the mesonic molecule $B\bar{B}$ and two-particle states such as a bottomonium state and a pion, $Q\bar{Q} + \pi$. Examples of the different possible structures and their descriptions can be found in Table 7.1.

A theoretical description of the $b\bar{b}u\bar{d}$ system is necessary for an understanding of QCD. Furthermore, the same methods applied in case of the Z_b states described here could be
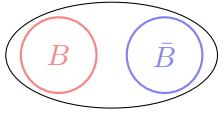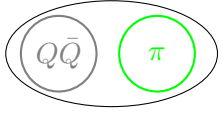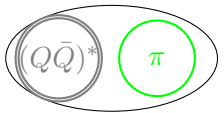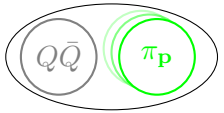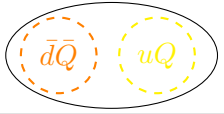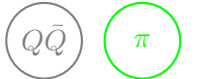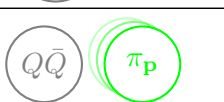
label	description	sketch
$B\bar{B}$	A bound four-quark state made of a loosely bound $B\bar{B}$ meson pair (a so-called mesonic molecule)	
$Q\bar{Q}\pi$	A bound four-quark state made of a bottomonium state and a loosely bound pion π^+ with zero momentum (a so-called mesonic molecule). In the static approximation, a bottomonium state is realized by the static quark Q and the static antiquark $\bar{Q}$ connected by a gluonic string.	
$(Q\bar{Q})^*\pi$	A bound four-quark state made of an excited bottomonium state and a loosely bound pion π^+ with zero momentum.	
$Q\bar{Q}\pi_{\mathbf{p}}$	A bound four-quark state made of a bottomonium state and a loosely bound pion π^+ with nonzero momentum.	
-	A bound four-quark state made of a diquark (color antitriplett) and an anti-diquark (color triplett).	
$B + \bar{B}$	A two-particle state made of a B meson and a far separated $\bar{B}$ meson.	
$Q\bar{Q} + \pi$	A two-particle state made of a bottomonium state and a far separated pion π^+ with zero momentum.	
$(Q\bar{Q})^* + \pi$	A two-particle state made of an excited bottomonium state and a far separated pion π^+ with zero momentum.	
$Q\bar{Q} + \pi_{\mathbf{p}}$	A two-particle state made of a bottomonium state and a far separated pion π^+ with nonzero momentum.	

Table 7.1.: Examples for possible structures of a $b\bar{b}u\bar{d}$ state in the $I(J^{\mathcal{P}}) = 1(1^+)$ channel. In the text, the structures are referred to by their labels. For discussion in the text it is convenient to distinguish $Q\bar{Q}\pi$ and $Q\bar{Q}\pi_{\mathbf{p}}$ as well as $Q\bar{Q} + \pi$ and $Q\bar{Q} + \pi_{\mathbf{p}}$, even though $Q\bar{Q}\pi$ is a special case of $Q\bar{Q}\pi_{\mathbf{p}}$ and $Q\bar{Q} + \pi$ is a special case of $Q\bar{Q} + \pi_{\mathbf{p}}$.

applied to less well understood states, e.g. the X(3872) [3], or used to predict new states.

Ground state and higher excitations: possible scenarios

In the following, we present different structures the $b\bar{b}u\bar{d}$ ground state and higher excited states in the $I(J^{\mathcal{P}}) = 1(1^+)$ channel can correspond to. We list the potentials that belong to the states.

- Ground state (denoted as $V_0(r)$):
    - As numerical results indicate (cf. Section 7.2), one can identify V_0 with the ground state of a bottomonium state and a pion at zero momentum, $Q\bar{Q} + \pi$. The bottomonium state is represented by two static quarks connected by a gluonic string.

- First excited state (denoted as $V_1(r)$):
    - For small separations r of b and $\bar{b}$ one can distinguish different cases:
        * A two-particle state $B + \bar{B}$ or a four-quark state $B\bar{B}$,
        * a diquark-antidiquark state,
        * an excited bottomonium state and a pion, realized as a two-particle state $(Q\bar{Q})^* + \pi$ or a four-quark state $(Q\bar{Q})^*\pi$ or
        * a two-particle state corresponding to a bottomonium state and a pion with nonzero momentum $Q\bar{Q} + \pi_{\mathbf{p}}$ or a four-quark state $Q\bar{Q}\pi_{\mathbf{p}}$.

      Note that in QCD the state can also correspond to a mixture of the above mentioned structures or a coexistence of four quarks without any manifest structure.
    - For large separations r of b and $\bar{b}$ the first excited state and the ground state swap places (cf. Figure 7.1). The first excited state corresponds to a bottomonium state and a pion at zero momentum. The ground state corresponds to a two-particle state of a B meson and a $\bar{B}$ meson, $B + \bar{B}$. This can be understood as follows: The gluonic string between the two heavy quarks will not persist for large separations, because its energy increases exceedingly. Therefore all other structures except $B + \bar{B}$ are excluded.

One possible scenario is sketched in Figure 7.1. The blue curve is the ground state potential V_0 which is clearly attractive. This can be estimated from the well-known behavior of the static $Q\bar{Q}$ potential. V_0 is expected to have the same shape as the static quark-antiquark potential shifted by the mass of the pion. The ordering of the lowest excited states is, however, less clear. In particular in case of non-vanishing pion momentum, it depends on the light quark mass as well as on the spatial lattice extent L: Momentum values are quantized on the lattice, $\mathbf{p} = \frac{2\pi}{L}\mathbf{n}$ with $n_i = 0, 1, ..., L/a - 1$ (with a the lattice spacing). So for larger lattice extents, the potentials that correspond to non-zero momentum states will move closer and closer together and more states will lie below a possible four-quark potential. This behavior is indicated by the fading green curves in the figure. The red curve accounts for a possible $b\bar{b}u\bar{d}$ four-quark potential which one would like to identify in order to investigate a possibly existing tetraquark state. The yellow curve is the potential of the first excitation of a bottomonium state and a pion at rest which might lie above the four-quark potential or not.

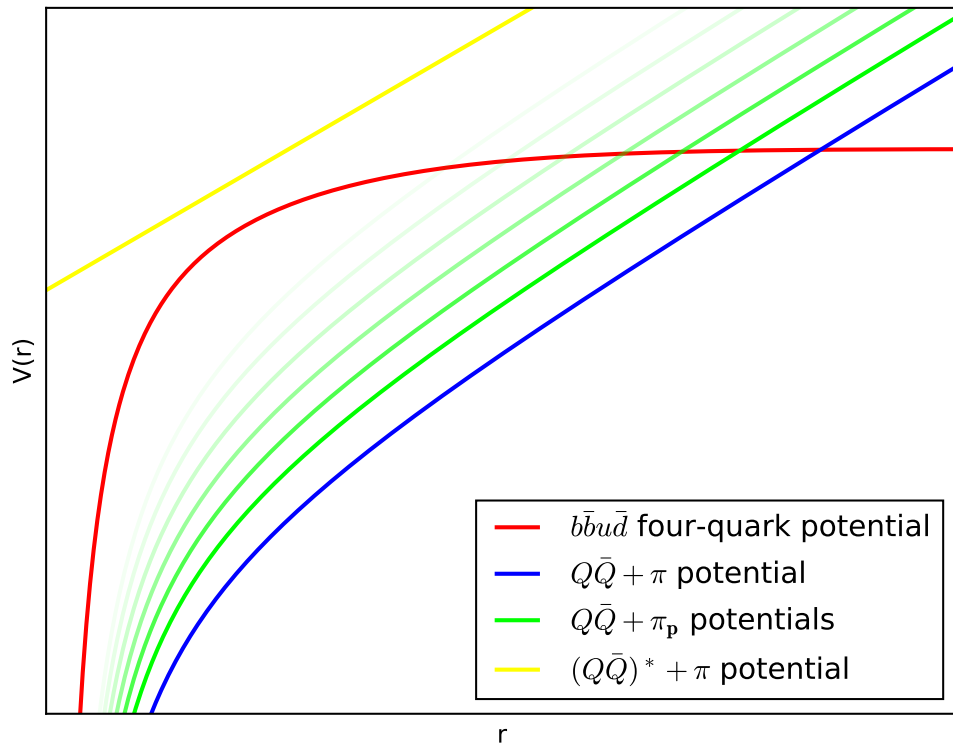Figure 7.1.: Cartoon-like illustration of one possible scenario for the $b\bar{b}u\bar{d}$ spectrum. blue: Potential of the bottomonium ground state and a pion at rest, $Q\bar{Q} + \pi$. green: Green curves indicate $Q\bar{Q} + \pi_{\mathbf{p}}$ potentials for different momenta $\mathbf{p}$. red: $b\bar{b}u\bar{d}$ four-quark potential. yellow: Potential of the excited bottomonium state and a pion at rest, $(Q\bar{Q})^* + \pi$.

7.2. Ground state and first excited state in a two-operator basis

For a start we investigate the first excited $b\bar{b}u\bar{d}$ state by considering two operators representing the structures $Q\bar{Q} + \pi$ and $B\bar{B}$ (respectively $B + \bar{B}$). The aim is to check, whether the $B\bar{B}$ potential is still attractive enough to host a bound state if contributions from the $Q\bar{Q}+\pi$ state have been removed. The results presented in this section are summarized in [8].

Important for the computation are suitable creation operators O_j that generate field excitations which are similar to the four-quark states of interest. The correlation functions of these operators evaluated at large temporal separations provide the low lying masses which can be interpreted as potentials $V_0(r)$, $V_1(r)$, ..., because the operator and thus also the masses depend on the heavy quark separation r. The correlation functions read:

$$C_{jk}(t,r) = \langle\Omega| O_j^\dagger(t)O_k(0) |\Omega\rangle \underset{t\to\infty}{=} A_{jk}^0 \exp\left(-V_0(r)t\right) + A_{jk}^1 \exp\left(-V_1(r)t\right) + ... \qquad (7.1)$$

The creation operators we consider are one that excites a $B\bar{B}$ state and the one that excites a $Q\bar{Q} + \pi$ state:

$$O_1(t) = O_{B\bar{B},r} = \Gamma_{AB}\tilde{\Gamma}_{CD}\bar{Q}_C^a(\mathbf{x},t)u_A^a(\mathbf{x},t)\bar{d}_B^b(\mathbf{y},t)Q_D^b(\mathbf{y},t) \qquad (7.2)$$

$$O_2(t) = O_{Q\bar{Q}+\pi,r} = \bar{Q}_A^a(\mathbf{x},t)U^{ab}(\mathbf{x},t;\mathbf{y},t)\tilde{\Gamma}_{AB}Q_B^b(\mathbf{y})\sum_{\mathbf{z}}\bar{d}_C^c(\mathbf{z},t)\left(\gamma_5\right)_{CD}u_D^c(\mathbf{z},t) \qquad (7.3)$$

with $\tilde{\Gamma}, \Gamma$ combinations of Dirac matrices (One can show that $\tilde{\Gamma}$ drops out during the calculation of the correlation matrix elements. It has no influence on the result.). r is the separation of the static quarks, $r = |\mathbf{x} - \mathbf{y}|$. We refer to the four elements of the correlation matrix which can be build from these operators in the following way:

$$\langle\Omega| O_{B\bar{B}}^\dagger(t)O_{B\bar{B}}(0) |\Omega\rangle \equiv C_{11}(t,r), \qquad (7.4)$$

$$\langle\Omega| O_{B\bar{B}}^\dagger(t)O_{Q\bar{Q}+\pi}(0) |\Omega\rangle \equiv C_{12}(t,r), \qquad (7.5)$$

$$\langle\Omega| O_{Q\bar{Q}+\pi}^\dagger(t)O_{B\bar{B}}(0) |\Omega\rangle \equiv C_{21}(t,r), \qquad (7.6)$$

$$\langle\Omega| O_{Q\bar{Q}+\pi}^\dagger(t)O_{Q\bar{Q}+\pi}(0) |\Omega\rangle \equiv C_{22}(t,r). \qquad (7.7)$$

7.2.1. Correlation functions

In the following we present the correlation matrix elements explicitly. We denote Γ^0 as the combination of Dirac matrices appearing in the operator $O(0)$ in the correlation function and Γ^t as the combination appearing in the operator $O(t)$. In the correlation matrix elements C_{12} and C_{21} we suppress this label since only one of the matrices appears. The correlation matrix element C_{11} reads:

$$\begin{aligned}
C_{11}(t,r) &= \langle\Omega| O_{B\bar{B}}^\dagger(t_1)O_{B\bar{B}}(t_0) |\Omega\rangle \\
&= - 2e^{-2Mt} \left(\gamma_0\Gamma^{t*}\gamma_0\right)_{AB} \left(\Gamma^{0T}\right)_{DC} \\
&\qquad \left\langle \mathrm{Tr}_{\mathrm{col}}\left\{U(\mathbf{x},t;\mathbf{x},0)\mathcal{D}^{-1(u)}(\mathbf{x},0;\mathbf{x},t)_{CA}\right\}\mathrm{Tr}_{\mathrm{col}}\left\{U(\mathbf{y},0;\mathbf{y},t)\mathcal{D}^{-1(d)}(\mathbf{y},t;\mathbf{y},0)_{BD}\right\}\right\rangle.
\end{aligned}$$
$$(7.8)$$

where $\mathcal{D}^{-1}$ is the light quark propagator. More details on the correlation function C_{11}, especially on its implementation in terms of timeslice sources can be found in [48]. Matrix

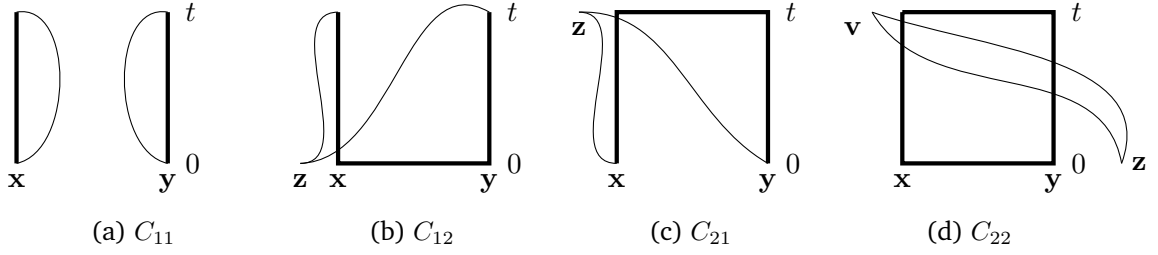(a) C_{11} (b) C_{12} (c) C_{21} (d) C_{22}

Figure 7.2.: The diagrams corresponding to the correlation matrix elements C_{11}, C_{12}, C_{21} and C_{22}. Bold lines correspond to heavy quark propagators, thin lines correspond to light quark propagators. The spatial points $\mathbf{z}$ and $\mathbf{v}$ represent the arbitrary positions of the spacial point on the timeslice.

elements C_{12}, C_{21} and C_{22} are rewritten using timeslice sources. In case of C_{22} the one-end trick is used, cf. Section 3.2. Matrix element C_{12} reads:

$$
\begin{aligned}
C_{12}(t,r) &= \langle\Omega| O^{\dagger}_{B\bar{B}}(t) O_{Q\bar{Q}+\pi}(0) |\Omega\rangle \\
&= + 2e^{-2Mt} \left(\gamma_5\gamma_0\Gamma\gamma_0\right)_{KV} \\
&\quad \frac{1}{N}\sum_n \left\langle \mathrm{Tr_{col}}\left\{ \phi^{(d)\dagger}[n,0]_K(\mathbf{x},t)U(\mathbf{x},t;\mathbf{x},0)U(\mathbf{x},0;\mathbf{y},0)U(\mathbf{y},0;\mathbf{y},t)\phi^{(d)}[n,0]_V(\mathbf{y},t) \right\}\right\rangle.
\end{aligned}
$$

Matrix element C_{21} reads:

$$
\begin{aligned}
C_{21}(t,r) &= \langle\Omega| O^{\dagger}_{Q\bar{Q}+\pi}(t) O_{B\bar{B}}(0) |\Omega\rangle \\
&= -2e^{-2Mt} \left(\left(\Gamma\gamma_5\right)^T\right)_{KU} \\
&\quad \frac{1}{N}\sum_n \left\langle \mathrm{Tr_{col}}\left\{ \phi^{(u)\dagger}[n,t]_K(\mathbf{y},0)U(\mathbf{y},0;\mathbf{y},t)U(\mathbf{y},t;\mathbf{x},t)U(\mathbf{x},t;\mathbf{x},0)\phi^{(u)}[n,t]_U(\mathbf{x},0) \right\}\right\rangle
\end{aligned}
$$

$$(7.9)$$

and finally, matrix element C_{22} reads:

$$
\begin{aligned}
C_{22}(t,r) &= \langle\Omega| O^{\dagger}_{Q\bar{Q}+\pi}(t) O_{Q\bar{Q}+\pi}(t) |\Omega\rangle \\
&= +2e^{-2M(t_1-t_0)} \\
&\quad \frac{1}{N}\sum_n \left\langle \sum_{\mathbf{v}} \mathrm{Tr_{col}}\left\{ U(\mathbf{y},0;\mathbf{y},t)U(\mathbf{y},t;\mathbf{x},t)U(\mathbf{x},t;\mathbf{x},0)U(\mathbf{x},0;\mathbf{y},0) \right\} \right. \\
&\quad\quad \left. \mathrm{Tr_{col}}\left\{ \phi^{(u)\dagger}[n,t](\mathbf{v},t)\phi^{(u)}[n,t](\mathbf{v},0) \right\}\right\rangle.
\end{aligned}
$$

$$(7.10)$$

Figure 7.2 shows the correlation matrix elements C_{11}, C_{12}, C_{21} and C_{22} in a diagrammatic form.

The matrix Γ in (7.2) has to be chosen such that the operators O_1 and O_2 generate the same quantum numbers. Only taking into account $O_{B\bar{B}}$ we find the strongest attraction for

$\Gamma = \gamma_5 - \gamma_0\gamma_5$. This combination reads in the twisted-mass basis $\Gamma^{\left(\begin{smallmatrix} u\bar{d} \\ d\bar{u} \end{smallmatrix}\right)} = \gamma_5 \pm i\gamma_0$ (cf. Table A.4 in the Appendix). The numerical analysis in this section has been performed using this choice of Γ.

7.2.2. Correlation functions in the code

The majority of the following considerations has never been presented before for a $b\bar{b}u\bar{d}$ system. Therefore we show them here in great detail.

It turned out to be convenient to use a more general form of the correlation matrix elements for the numerical implementation. We refer to this version of the correlation matrix by (C_{jk}^{code}). (C_{jk}^{code}) can be transformed to correlation matrix (C_{jk}) (cf. Equation (7.1)) according to several simple replacement rules. For the matrix elements we find:

$$C_{11}^{\text{code}} = \Gamma_{AB}^0 \Gamma_{CD}^t \left\langle \left[\phi_C^{a(\alpha)\dagger}(0,t) U^{ab}(0,t;0,0) \xi_A^{b(\alpha)}(0,0) \right] \left[\xi_B^{c(\beta)\dagger}(r,0) U^{cd}(r,0;r,t) \phi_D^{d(\beta)}(r,t) \right] \right\rangle \tag{7.11}$$

(The implementation of C_{11} is taken from [48].),

$$C_{12/21}^{\text{code}} = \Gamma_{AB} \left\langle \text{Tr}_{\text{col}} \left\{ \phi_A^{(\alpha)\dagger}(r,t) U^\dagger(r,0;r,t) U^\dagger(0,0;r,0) U(0,0;0,t) \phi_B^{(\alpha)}(0,t) \right\} \right\rangle \tag{7.12}$$

and

$$C_{22}^{\text{code}} = \left\langle \text{Tr}_{\text{col}} \left\{ U(r,0;r,t) U^\dagger(0,t;r,t) U^\dagger(0,0;0,t) U(0,0;r,0) \right\} \sum_{\mathbf{z}} \text{Tr}_{\text{col}} \left\{ \phi_A^{(\alpha)\dagger}(\mathbf{z},t) \phi_A^{(\alpha)}(\mathbf{z},t) \right\} \right\rangle \tag{7.13}$$

with $\alpha = u/d$. Without loss of generality we assume the heavy quarks to be separated along the z-axis. Note that we compute the correlation functions once considering temporal separations in positive time direction and once considering temporal separations in negative time direction. These computations are physically equivalent and we use them to reduce the statistical error. The notation $C_{12/21}^{\text{code}}$ is used because C_{12}^{code} can be found via $C_{12}^{\text{code}} = \left(C_{21}^{\text{code}} \right)^*$. Due to the γ_5-hermiticity, the flavor of the second light propagator in the correlation functions changes, i.e.

- $u\bar{d}$ in $C_{ij} \leftrightarrow u\bar{u}$ in C_{ij}^{code}

- $d\bar{u}$ in $C_{ij} \leftrightarrow d\bar{d}$ in C_{ij}^{code}

for $C_{ij} \in \{C_{11}, C_{12}, C_{21}, C_{22}\}$. The replacement rules for the matrices $\Gamma_{\text{code}}^0, \Gamma_{\text{code}}^t$ in C_{11}^{code} and $\Gamma_{\text{physical}}^0, \Gamma_{\text{physical}}^t$ in $C_{11}(t)$ read (cf. [48]):

- $\Gamma^0, \Gamma^t \hat{=} \left(\gamma_0 \Gamma_{\text{physical}}^t \gamma_0 \gamma_5 \right), \left({\Gamma_{\text{physical}}^0}^* \gamma_5 \right)$

- One has to use the negative time direction.

- One has to complex conjugate each correlation function.

- There is an overall factor -2. The relative sign is important while the factor 2 can be omitted, since it appears in every matrix element.

7. $b\bar{b}u\bar{d}$ systems in the Born-Oppenheimer approximation

The replacement rules for the gamma matrix Γ_{code} in $C_{12/21}^{\text{code}}$ and Γ_{physical} in $C_{12/21}(t)$ read:

- One has to use the negative time direction.

- $\Gamma_{\text{code}} \hat{=} \left(\Gamma_{\text{physical}}\gamma_5\right)^T$

- There is an overall factor -2. The relative sign is important while the factor 2 can be omitted, since it appears in every matrix element.

The rules for C_{22} read:

- One has to use the negative time direction.

- There is an overall factor +2. The relative sign is important while the factor 2 can be omitted, since it appears in every matrix element.

C_{22}^{code} is independent of Γ matrices, so Equation (7.13) and the above mentioned replacement rules provides everything one needs to know for implementing C_{22}^{code} and translating the result to the physical C_{22}. In the case of C_{11}^{code} there are two different matrices Γ^0 and Γ^t while in case of $C_{12/21}^{\text{code}}$ there is only one Γ. Now we compose the correlation matrix. According to the rules for C_{11} and $C_{12/21}$ we find for the Γ matrix combination of choice $\Gamma^{\left(\begin{smallmatrix}u\bar{d}\\d\bar{u}\end{smallmatrix}\right)} = \gamma_5 \pm i\gamma_0$:

- $\Gamma^{\left(\begin{smallmatrix}u\bar{d}\\d\bar{u}\end{smallmatrix}\right)} = \gamma_5 + i\gamma_0$ ($u\bar{d}$, i.e. we have to use $u\bar{u}$ because of γ_5-hermiticity):

$$
\begin{aligned}
C_{11}(\Gamma^0, \Gamma^t) &= -(C_{11}^{\text{code}}(\gamma_0\Gamma^t\gamma_0\gamma_5, \Gamma^{0*}\gamma_5))^* \\
&= -(C_{11}^{\text{code}}(\gamma_0(\gamma_5 + i\gamma_0)\gamma_0\gamma_5, (\gamma_5 + i\gamma_0)^*\gamma_5))^* \\
&= -(C_{11}^{\text{code}}(-1 + i\gamma_0\gamma_5, 1 - i\gamma_0\gamma_5))^* \\
&= -(-C_{11}^{\text{code}}(1, 1) + iC_{11}^{\text{code}}(\gamma_0\gamma_5, 1) + iC_{11}^{\text{code}}(1, \gamma_0\gamma_5) + C_{11}^{\text{code}}(\gamma_0\gamma_5, \gamma_0\gamma_5))^* \\
&= (C_{11}^{\text{code}}(1, 1))^* + i(C_{11}^{\text{code}}(\gamma_0\gamma_5, 1))^* + i(C_{11}^{\text{code}}(1, \gamma_0\gamma_5))^* - (C_{11}^{\text{code}}(\gamma_0\gamma_5, \gamma_0\gamma_5))^*
\end{aligned}
$$

and

$$
\begin{aligned}
C_{12/21}(\Gamma) &= -C_{12/21}^{\text{code}}\left((\Gamma\gamma_5)^T\right) \\
&= -C_{12/21}^{\text{code}}\left(((\gamma_5 + i\gamma_0)\gamma_5)^T\right) \\
&= -C_{12/21}^{\text{code}}\left((1 + i\gamma_0\gamma_5)^T\right) \\
&= -C_{12/21}^{\text{code}}(1 - i\gamma_0\gamma_5) \\
&= -C_{12/21}^{\text{code}}(1) + iC_{12/21}^{\text{code}}(\gamma_0\gamma_5).
\end{aligned}
$$

- $\Gamma^{\left(\begin{smallmatrix}u\bar{d}\\d\bar{u}\end{smallmatrix}\right)} = \gamma_5 - i\gamma_0$ ($d\bar{u}$, i.e. we have to $d\bar{d}$ because of γ_5-hermiticity):

$$
C_{11}(\Gamma^0, \Gamma^t) = (C_{11}^{\text{code}}(1, 1))^* - i(C_{11}^{\text{code}}(\gamma_0\gamma_5, 1))^* - i(C_{11}^{\text{code}}(1, \gamma_0\gamma_5))^* - (C_{11}^{\text{code}}(\gamma_0\gamma_5, \gamma_0\gamma_5))^*
$$

(7.14)

and

$$
C_{12/21}(\Gamma) = -C_{12/21}^{\text{code}}(1) - iC_{12/21}^{\text{code}}(\gamma_0\gamma_5). \tag{7.15}
$$

7.2.3. Symmetries

Symmetry checks are useful to support the correctness of the implemented correlation matrix elements. Furthermore, one can average over correlation matrix elements that are connected via a symmetry transformation to reduce the statistical error. According to the structure of the four-quark state, the six available symmetries are:

- twisted mass parity,

- charge conjugation,

- twisted mass γ_5-hermiticity,

- twisted mass time reversal,

- π cubic rotations,

- $\pi/2$ cubic rotations.

All correlation matrix elements have been checked for all symmetries according to the symmetry rules that are determined in Appendix A.3. Furthermore, all correlation matrix elements have been averaged according to their symmetries.

7.2.4. Performing the Lattice QCD computations

A $b\bar{b}u\bar{d}$ bound state would be excluded in case that taking into account operator $O_2 = O_{Q\bar{Q}+\pi}$, cf. Equation (7.3), would yield a first excited state which was not attractive enough to have negative energy eigenvalues. For a start we are interested in the qualitative result whether the first excited state is attractive or not. Therefore, it is sufficient to perform Lattice QCD computations using only a part of the available gauge configurations. However, in the future calculations using a larger amount of gauge configurations will be necessary to be able to make statements about the structure of the $b\bar{b}u\bar{d}$ state.

We perform computations using 100 gauge link configurations of the B85.24 ensemble. Details on the configurations can be found in Table 5.1. We apply the same smearing techniques and use the same methods to compute the light quark propagators as described in Section 5.2. The extraction of the first excited state is a numerically challenging task, because the fit tends to be very unstable. One popular method is to create the matrix $C(t) = C_{ij}(t)$, $i, j = 1, 2$ and compute ground state and first excited state with the Generalized Eigenvalue Problem (GEP) [66].

In Figure 7.3 one finds an example plot of the potentials computed by means of the GEP as well as the pure $Q\bar{Q}$ potential for comparison. The blue curve is the ground state $V_0(r)$ that the GEP yields for the 2×2 matrix $(C_{jk}(t))$ given in Equation (7.1). By comparison with the pure $Q\bar{Q}$ potential one can see, that it is the $Q\bar{Q} + \pi$ potential (the quark mass in lattice units is $am_\pi \simeq 0.2$). The red curve is the potential $V_1(r)$. It is the first excited state that the GEP yields for the 2×2 matrix $(C_{jk}(t))$. One can see that it is attractive. This attractive potential is a candidate to host a four-quark bound state. It is analyzed further in the following section.
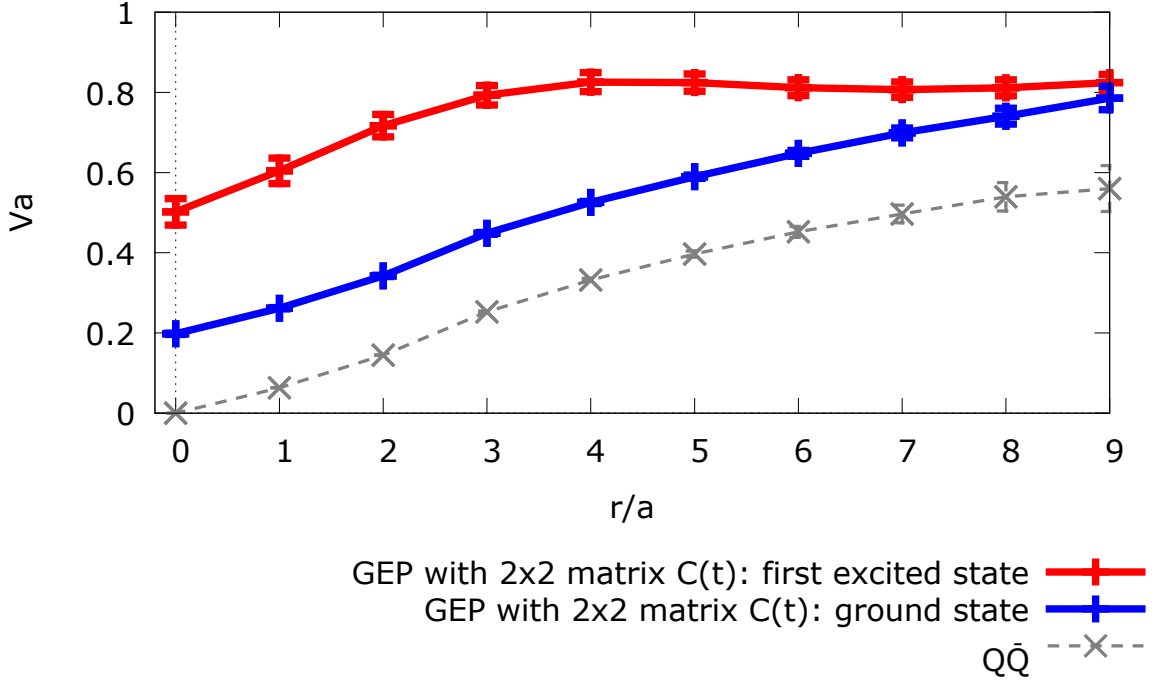
Figure 7.3.: The potential computed by means of the GEP.

7.2.5. Solving the Schrödinger equation to check for a bound state

To determine the binding energy of the four-quark state, we fit the ansatz (cf. Equation (5.5))

$$V(r) \;=\; -\frac{\alpha}{r}\exp\left(-\left(\frac{r}{d}\right)^p\right) + V_0,$$

to the extracted lattice potential $V_1(r)$ with respect to V_0, α and d. As in Chapter 5, we fix the parameter $p = 2$. We determine an analytical expression for the potential. The expression is applied to the s-wave Schrödinger equation (cf. Equation (5.8))

$$\left(-\frac{1}{2\mu}\frac{d^2}{dr^2} + U(r)\right)R(r) \;=\; E_B R(r) \qquad \text{with } U(r) = V(r)|_{V_0=0,p=2} \text{ and } \mu = m_b/2$$

to compute the binding energy E_B. For more details on the extraction of the binding energy in the Born-Oppenheimer approximation, cf. [7] and Section 5.4.4. A number of ~ 30 fits is performed for different ranges $t_{\min}/a...t_{\max}/a$ at which the potential is read off (cf. Equation (7.1)) and for different ranges $r_{\min}/a...r_{\max}/a$ at which the fit (5.5) is conducted:

- $t_{\min}/a \in \{6,7,8\}$,

- $t_{\max}/a \in \{7,8,9\}$,

- $r_{\min}/a = 2$,

- $r_{\max}/a \in \{6,7,8,9\}$.

The mean value and standard deviation of the computed values is an estimate for the binding energy. The analysis yields for quantum numbers $I(J^P) = 1(1^+)$ and equivalently $I(J^P) = 1(0^+)$ (cf. Section 7.1):

$$E_B = (-58 \pm 71) \text{ MeV}. \tag{7.16}$$

The negative binding energy shows that a $b\bar{b}u\bar{d}$ bound state is not excluded.

7.3. The first excited state - further considerations

As stated in Section 7.1, it is possible that the first excited $b\bar{b}u\bar{d}$ state corresponds to different structures in addition to the bound $B\bar{B}$ state we have taken into account in Section 7.2. To identify a possible $b\bar{b}u\bar{d}$ bound state it is important to distinguish between potentials corresponding to a four-quark state (e.g. $B\bar{B}$) and potentials corresponding to a two-particle state (e.g. $Q\bar{Q} + \pi_{\mathbf{p}}$) state. In the following we present a possible strategy to further investigate the structure of the first excited state.

7.3.1. The first excited state: four-quark or two-particle state

We consider the the $b\bar{b}u\bar{d}$ system in the static approximation. The heavy quarks $b, \bar{b}$ are approximated by the static quarks $Q, \bar{Q}$. The static quarks are located at the fixed positions $\mathbf{x}_0$ and $\mathbf{y}_0$ respectively. Their wavefunctions are Dirac delta functions $\delta(\mathbf{x} - \mathbf{x}_0)$ and $\delta(\mathbf{x} - \mathbf{y}_0)$. The light quarks u and $\bar{d}$ have no fixed location, their positions are referred to as $\mathbf{u}$ and $\mathbf{v}$ respectively. The quantum mechanical wavefunctions of the four-quark state Ψ_{4q} and the wavefunction of the two-particle state Ψ_{2p} each are composed of the wavefunctions of the heavy quarks $\delta(\mathbf{x} - \mathbf{x}_0)$ and $\delta(\mathbf{x} - \mathbf{y}_0)$ as well as of the wavefunction of the light quarks $\psi_{4q/2p}(\mathbf{x})$. The wavefunctions of the heavy quarks decouple from the system because the heavy quark positions are fixed. In the following, we only consider the wavefunctions of the light quarks ψ_{4q} and ψ_{2p}. In case of a four-quark state, the light antiquarks/quarks must be located in the vicinity of the respective static quarks/antiquarks. Let $d_{\text{hadron}} \simeq 1 \,\text{fm}$ denote the typical extent of a hadron. We introduce the function $f(\mathbf{x})$. $f(\mathbf{x})$ is 0, if $|\mathbf{x}| > d_{\text{hadron}}$, else a complicated nonzero function. The four-quark state $\psi_{4q}(\mathbf{u}, \mathbf{v})$ can be modeled as:

$$\psi_{4q}(\mathbf{u}, \mathbf{v}) = f(\mathbf{x}_0 - \mathbf{v})f(\mathbf{y}_0 - \mathbf{u}). \tag{7.17}$$

We will see below that the setup also accounts for the case of a mesonic molecule built of a bottomonium state and a pion. In case of a two-particle state, it is convenient to use center of mass coordinates $\mathbf{r} = \mathbf{u} - \mathbf{v}$ and $\mathbf{R} = \frac{\mathbf{u}+\mathbf{v}}{2}$. $\mathbf{p}$ is the momentum of the pion. The center of mass of the pion system is equally distributed over the volume V, which can be modeled as a plane wave. We introduce the function $g(\mathbf{r})$ which is 0, if $|\mathbf{r}| > d_{\text{hadron}}$, else a complicated nonzero function. The two-particle state $\psi_{2p}(\mathbf{R}, \mathbf{r})$ can be modeled as:

$$\psi_{2p}(\mathbf{R}, \mathbf{r}) = \frac{1}{\sqrt{V}}e^{i\mathbf{p}\cdot\mathbf{R}}g(\mathbf{r}) \tag{7.18}$$

The two-particle wavefunction is essentially independent of the positions of the heavy quarks. ψ_{4q} and ψ_{2p} serve as trial states in the following investigation of the overlap of four-quark and two-particle states with the first excited $b\bar{b}u\bar{d}$ state.

7. $b\bar{b}u\bar{d}$ systems in the Born-Oppenheimer approximation

7.3.2. Volume dependence

Consider the overlap of the trial states introduced in Section 7.3.1 with the first excited $b\bar{b}u\bar{d}$ state. We refer to this state as $|1\rangle$. It is necessary to distinguish between two cases.

Case 1: $|1\rangle$ is a two-particle state.

$$\psi_1 = \frac{1}{\sqrt{V_s}} e^{i\mathbf{p}\cdot\mathbf{R}} g'(\mathbf{r}) \tag{7.19}$$

with $g'(\mathbf{r})$ a function which is 0, if $|\mathbf{r}| > d_{\text{hadron}}$, else a complicated nonzero function. For a large lattice volume, one can make the following statements: The overlap of $|1\rangle$ with a two-particle trial state is constant with respect to V_s:

$$\langle 1|\psi_{2p}\rangle = \frac{1}{V_s} \int d^3R \int d^3r\, e^{-i\mathbf{p}\cdot\mathbf{R}} g^{*\prime}(\mathbf{r}) e^{i\mathbf{p}\cdot\mathbf{R}} g(\mathbf{r}) = \text{const.} \tag{7.20}$$

Conversely, the overlap of $|1\rangle$ with a four-quark trial state shrinks with an increasing lattice volume:

$$\langle 1|\psi_{4q}\rangle = \frac{1}{\sqrt{V_s}} \int d^3u \int d^3v\, e^{-i\mathbf{p}\cdot\mathbf{R}} g^{*\prime}(\mathbf{r}) f(\mathbf{x}_0 - \mathbf{v}) f(\mathbf{y}_0 - \mathbf{u})$$
$$\sim \begin{cases} \frac{1}{\sqrt{V_s}} & \text{if } |\mathbf{x}_0 - \mathbf{y}_0| < d_{\text{hadron}} \\ 0 & \text{otherwise} \end{cases} \tag{7.21}$$

since $\int d^3u \int d^3v\, e^{-i\mathbf{p}\cdot\mathbf{R}}$ yields a constant contribution. Note that for any trial state where two light quarks are generated in the vicinity of the heavy quarks the calculation and result is the same.

Case 2: $|1\rangle$ is a bound four-quark state

$$\psi_1 = f'(\mathbf{x}_0 - \mathbf{v}) f'(\mathbf{y}_0 - \mathbf{u}) \tag{7.22}$$

with $f'(\mathbf{r})$ a function which is 0, if $|\mathbf{r}| > d_{\text{hadron}}$, else a complicated nonzero function. We find that for a large lattice volume the overlap with a two-particle state shrinks with an increasing lattice volume:

$$\langle 1|\psi_{2p}\rangle = \frac{1}{\sqrt{V}} \int d^3u \int d^3v\, f^{*\prime}(\mathbf{x}_0 - \mathbf{v}) f^{*\prime}(\mathbf{y}_0 - \mathbf{u}) e^{-i\mathbf{p}\cdot\mathbf{R}} g(\mathbf{r})$$
$$\sim \begin{cases} \frac{1}{\sqrt{V}} & \text{if } |\mathbf{x}_0 - \mathbf{y}_0| < d_{\text{hadron}} \\ 0 & \text{otherwise} \end{cases}. \tag{7.23}$$

The overlap with a four-quark state is independent of the lattice volume:

$$\langle 1|\psi_{4q}\rangle = \int d^3u \int d^3v\, f^{*\prime}(\mathbf{x}_0 - \mathbf{v}) f^{*\prime}(\mathbf{y}_0 - \mathbf{u}) f(\mathbf{x}_0 - \mathbf{v}) f(\mathbf{y}_0 - \mathbf{u}) = \text{const.} \tag{7.24}$$

One way to study the overlap on the lattice is building a correlation matrix by means of four-quark and two-particle operators. Examples for such operators are shown in Equations (7.2) and (7.3), respectively. The correlation matrix (cf. Equation (7.1)) reads:

$$C_{jk}(t,r) = \langle \Omega | O_j^\dagger(t) O_k(0) | \Omega \rangle \underset{t\to\infty}{=} A_{jk}^0 \exp\left(-V_0(r)t\right) + A_{jk}^1 \exp\left(-V_1(r)t\right) + \ldots$$

$O_1 = O_{B\bar{B},r}$ is a four-quark operator and $O_2 = O_{Q\bar{Q}+\pi,r}$ is a two-particle operator. By performing a coupled multi-exponential fit to the correlation matrix elements C_{jk}, the overlap coefficients A^0_{jk} and A^1_{jk} can be obtained. For example, A^0_{22} corresponds to the overlap of a two-particle state with the ground $b\bar{b}u\bar{d}$ state. We know that the ground state corresponds to $Q\bar{Q} + \pi$, so due to our previous considerations A^0_{22} should be constant with respect to a change of the lattice volume. This case can serve as a check of the implementation of the fitting procedure. A^0_{11}, however, is the overlap of the first excited $b\bar{b}u\bar{d}$ state with a four-quark state. If the first excited state is a four-quark state, A^0_{11} will not change with respect to the lattice volume. Conversely, if A^0_{11} changes with respect to the lattice volume, this indicates that the first excited state is a two-particle state. At the same time, A^1_{22} will show the following behavior: In case the first excited state is a four-quark state, A^1_{22} will depend on the lattice volume. If the first excited state is a two-particle state, A^1_{22} will be independent of a change of the lattice volume.

Note that the volume dependence can only be observed if the lattice volume is large enough in every case. If $V \sim d^3_{\text{hadron}}$, the four quarks will be located close to each other in any case, because a possible pion cannot separate from the heavy quarks. One has to make sure, that $V_s \gtrsim (2d_{\text{hadron}})^3$. The investigation only works for a sufficiently large volume.

7.4. Summary

In this chapter we investigate the $b\bar{b}u\bar{d}$ four-quark state in the $I(J^{\mathcal{P}}) = 1(1^+)$ channel. A $b\bar{b}u\bar{d}$ bound state must have two properties: The light quarks must be close to the heavy quarks and the corresponding potential must be sufficiently attractive to host a bound state. We take into account different possible structures of the $b\bar{b}u\bar{d}$ state and identify a candidate for an attractive $b\bar{b}u\bar{d}$ potential. By calculating the corresponding binding energy we find signatures consistent with a $b\bar{b}u\bar{d}$ tetraquark. This result supports that the charged $Z_b(10610)$ and $Z_b(10650)$ states are indeed tetraquark states.

8. Conclusion

In this thesis we investigate heavy-light four-quark states using Lattice QCD. We show examples for theoretical investigations that can be interesting for experimental research and vice versa.

On the one hand we show that theory can make predictions on worthwhile objects of search in experiment. We investigate the existence or non-existence of $\bar{b}\bar{b}qq$ four-quark states, $qq \in \{u, d, s, c\}$. Using the Born-Oppenheimer approximation and considering the b quarks to be infinitely heavy, these systems can be seen e.g. as bound states of two static-light B mesons, namely BB. We find evidence that bound states with $qq \in \{s, c\}$ or with isospin $I = 1$ do not exist. Furthermore, we find strong evidence for the existence a $\bar{b}\bar{b}ud$ bound state in the $I(J^{\mathcal{P}}) = 0(1^+)$ channel. Performing an extrapolation to the physical pion mass, we find the binding energy of this state to be $E_B = -90^{+43}_{-36}$ MeV, which is an indication for strong binding. In a follow-up study, we use four quarks of finite mass by means of NRQCD instead of static b quarks. We succeed in qualitatively confirming the static-light result. This way, we predict a tetraquark state that has not yet been measured experimentally but that might be searched for in the future.

On the other hand we aim at finding an interpretation of a state that recently has been measured experimentally but up to now lack a satisfactory theoretical description in particular from Lattice QCD. We investigate a $b\bar{b}u\bar{d}$ four-quark state with the same quantum numbers as the experimentally interesting $Z_b(10610)$ and $Z_b(10650)$ states. In the Born-Oppenheimer approximation we make a first step in supporting the widespread conviction that the state is a tetraquark candidate.

The results of this thesis show that Lattice QCD in combination with the Born-Oppenheimer approximation is a powerful tool to investigate heavy-light four-quark states. Certainly, the use of the static approximation of the heavy quarks is an effective approach that requires to make additional assumptions beyond pure QCD. However, the approach yields useful results. We can see this from the fact that results obtained in the Born-Oppenheimer approximation (cf. Chapter 5) can be reproduced in case the static approximation of the heavy quarks is set aside (cf. Chapter 6). Moreover, we are able to obtain results rather easily which could not be obtained in case of four fully dynamical quarks without excessive investment of computational resources and development of special numerical techniques.

In the following, we name suggestions how to continue the presented projects further. Future work regarding the investigation of static-light BB systems could include for instance the following topics: The dependence of the binding energy of short spatial lattice separations needs to be explored. By now, the very short separations $< 2a$ with a the lattice spacing have been omitted in the study. One way to include them is to perform calculations by means of a smaller lattice spacing that yields more precise data at smaller separations. Moreover,

one could take into account values of the BB potential also for off-diagonal separations of the heavy quarks. This would yield more data at small separations. The next step regarding the NRQCD investigation of the BB state involves the need for computations of additional correlation functions: The four-quark state can be computed in more detail using the operator basis which is presented in Chapter 6. This way the signal quality of the effective energy of the four-quark state is expected to improve. Regarding the static-light $b\bar{b}u\bar{d}$ four-quark state, a possible task becomes clear throughout Chapter 7: The first excited state should be studied in more detail, e.g. by investigating the volume dependence of the state with sufficiently large statistics. This way one can find out whether the first excited state is a four-quark or a two-particle state. This is important for the interpretation of the resulting potential and thus for any statement about the $b\bar{b}u\bar{d}$ tetraquark.

A. Appendix

A.1. Notation and conventions

Three-dimensional vectors are printed in bold type $\mathbf{x} = (x_1, x_2, x_3)$. Four-dimensional vectors are written as $x \equiv (\mathbf{x}, t)$.

Throughout this thesis we work in natural units $\hbar = c = 1$. If not otherwise stated, we use the chiral representation of the Dirac matrices

$$\gamma^0 = \begin{pmatrix} 0 & -\mathbb{1}_2 \\ -\mathbb{1}_2 & 0 \end{pmatrix}, \quad \gamma^j = \begin{pmatrix} 0 & \sigma^j \\ -\sigma^j & 0 \end{pmatrix}, \tag{A.1}$$

with the Pauli matrices

$$\sigma^1 = \begin{pmatrix} 0 & 1 \\ 1 & 0 \end{pmatrix}, \quad \sigma^2 = \begin{pmatrix} 0 & -i \\ +i & 0 \end{pmatrix}, \quad \sigma^3 = \begin{pmatrix} +1 & 0 \\ 0 & -1 \end{pmatrix} \tag{A.2}$$

and

$$\gamma^5 = \gamma^0 \gamma^1 \gamma^2 \gamma^3 = \begin{pmatrix} \mathbb{1}_2 & 0 \\ 0 & -\mathbb{1}_2 \end{pmatrix}. \tag{A.3}$$

In Table A.1 we give an overview on frequently used symbols.

symbol	explanation
a	lattice spacing, usually given in fm
u, d, s, c, b, t	*up, down, strange, charm, bottom/beauty* and *top* quark in terms of valence quarks
$u(x), d(x), s(x), c(x), b(x), t(x)$	quark fields in a correlation function
q	quark of finite mass
$\psi(x)$	field of a quark of finite mass in a correlation function
Q	static quark
$Q(x)$	field of a static quark in a correlation function

Table A.1.: Collection of symbols frequently used throughout this thesis.

A.2. Quantum numbers of the BB system and the $B\bar{B}$ system

$\Gamma^{\left(\substack{uu\\dd}\right)}$ tb	$\mathcal{P}^{\text{(tm)}}\mathcal{P}_x^{\text{(tm)}}$, sec.	$\Gamma^{\left(\substack{uu\\dd}\right)}$ pb	$\mathcal{P}, \mathcal{P}_x$	type	mult.
$j_z = 0, I = 1, I_z = \pm$					
$\gamma_3 \pm i\gamma_0\gamma_3\gamma_5$	$+,\quad i$	$+\gamma_3 + \gamma_0\gamma_3$	$-, -$	att SS	E
γ_5	$+,\quad i$	$\mp i\mathbb{1}$	$-, -$	rep SP_-	E
$\gamma_3 \mp i\gamma_0\gamma_3\gamma_5$	$+,\quad i$	$+\gamma_3 - \gamma_0\gamma_3$	$-, -$	att P_-P_-	E
$\gamma_0\gamma_5 \pm i\mathbb{1}$	$+,\quad i$	$+\gamma_0\gamma_5 + \gamma_5$	$+, +$	rep SS	F
$\gamma_0\gamma_3$	$+,\quad i$	$\mp i\gamma_0\gamma_3\gamma_5$	$+, +$	att SP_-	F
$\gamma_0\gamma_5 \mp i\mathbb{1}$	$+,\quad i$	$+\gamma_0\gamma_5 - \gamma_5$	$+, +$	rep P_-P_-	F
γ_0	$-,\quad j$	$+\gamma_0$	$+, -$	att SP_-	G
$\gamma_3\gamma_5$	$-,\quad j$	$+\gamma_3\gamma_5$	$-, +$	rep SP_-	H
$j_z = 1, I = 1, I_z = \pm$					
$\gamma_{1/2} \pm i\gamma_0\gamma_{1/2}\gamma_5$	$-/+,\quad k/l$	$+\gamma_{1/2} + \gamma_0\gamma_{1/2}$	$-, +/-$	att SS	K
$\gamma_{2/1}\gamma_5$	$-/+,\quad k/l$	$+\gamma_{2/1}\gamma_5$	$-, +/-$	rep SP_-	K
$\gamma_{1/2} \mp i\gamma_0\gamma_{1/2}\gamma_5$	$-/+,\quad k/l$	$+\gamma_{1/2} - \gamma_0\gamma_{1/2}$	$-, +/-$	att P_-P_-	K
$\gamma_0\gamma_{1/2}$	$-/+,\quad k/l$	$\mp i\gamma_0\gamma_{1/2}\gamma_5$	$+, -/+$	att SP_-	L

Table A.2.: Quantum numbers of the BB system: Twisted basis (tb) and physical basis (pb) quantum numbers for uu and dd. Different physical basis multiplets are assigned capital letters, while different twisted mass sectors are assigned small letters. (Table taken from [5].)

$\Gamma^{(ud\pm du)}$ tb	$\mathcal{P}^{(\text{tm})}, \mathcal{P}_x^{(\text{tm})}$, sec.	$\Gamma^{(ud\pm du)}$ pb	$\mathcal{P}, \mathcal{P}_x$	type	mult.
$j_z = 0, I = 0$					
$\gamma_5^{(-)} - i\gamma_0^{(+)}$	$+, -, \quad a$	$(+\gamma_5 + \gamma_0\gamma_5)^{(-)}$	$-, +$	att SS	A
$\gamma_0\gamma_3\gamma_5^{(-)}$	$+, -, \quad a$	$+\gamma_0\gamma_3\gamma_5^{(-)}$	$-, +$	rep SP_-	A
$\gamma_5^{(-)} + i\gamma_0^{(+)}$	$+, -, \quad a$	$(+\gamma_5 - \gamma_0\gamma_5)^{(-)}$	$-, +$	att P_-P_-	A
$\gamma_0\gamma_3^{(-)} - i\gamma_3\gamma_5^{(+)}$	$-, +, \quad b$	$(+\gamma_0\gamma_3 + \gamma_3)^{(-)}$	$+, -$	rep SS	B
$\mathbb{1}^{(-)}$	$-, +, \quad b$	$+\mathbb{1}^{(-)}$	$+, -$	att SP_-	B
$\gamma_0\gamma_3^{(-)} + i\gamma_3\gamma_5^{(+)}$	$-, +, \quad b$	$(+\gamma_0\gamma_3 - \gamma_3)^{(-)}$	$+, -$	rep P_-P_-	B
$\gamma_3^{(+)}$	$-, -, \quad c$	$+i\gamma_3\gamma_5^{(-)}$	$+, +$	att SP_-	C
$\gamma_0\gamma_5^{(+)}$	$+, +, \quad d$	$+i\gamma_0^{(-)}$	$-, -$	rep SP_-	D
$j_z = 0, I = 1, I_z = 0$					
$\gamma_0\gamma_3^{(+)} - i\gamma_3\gamma_5^{(-)}$	$-, -, \quad c$	$(+\gamma_0\gamma_3 + \gamma_3)^{(+)}$	$-, -$	att SS	E
$\mathbb{1}^{(+)}$	$-, -, \quad c$	$+\mathbb{1}^{(+)}$	$-, -$	rep SP_-	E
$\gamma_0\gamma_3^{(+)} + i\gamma_3\gamma_5^{(-)}$	$-, -, \quad c$	$(+\gamma_0\gamma_3 - \gamma_3)^{(+)}$	$-, -$	att P_-P_-	E
$\gamma_5^{(+)} - i\gamma_0^{(-)}$	$+, +, \quad d$	$(+\gamma_5 + \gamma_0\gamma_5)^{(+)}$	$+, +$	rep SS	F
$\gamma_0\gamma_3\gamma_5^{(+)}$	$+, +, \quad d$	$+\gamma_0\gamma_3\gamma_5^{(+)}$	$+, +$	att SP_-	F
$\gamma_5^{(+)} + i\gamma_0^{(-)}$	$+, +, \quad d$	$(+\gamma_5 - \gamma_0\gamma_5)^{(+)}$	$+, +$	rep P_-P_-	F
$\gamma_0\gamma_5^{(-)}$	$+, -, \quad a$	$+i\gamma_0^{(+)}$	$+, -$	att SP_-	G
$\gamma_3^{(-)}$	$-, +, \quad b$	$+i\gamma_3\gamma_5^{(+)}$	$-, +$	rep SP_-	H
$j_z = 1, I = 0$					
$\gamma_0\gamma_{1/2}^{(-)} - i\gamma_{1/2}\gamma_5^{(+)}$	$-, -/+, \quad e/f$	$(+\gamma_0\gamma_{1/2} + \gamma_{1/2})^{(-)}$	$+, +/-$	rep SS	I
$\gamma_{2/1}^{(+)}$	$-, -/+, \quad e/f$	$+i\gamma_{2/1}\gamma_5^{(-)}$	$+, +/-$	att SP_-	I
$\gamma_0\gamma_{1/2}^{(-)} + i\gamma_{1/2}\gamma_5^{(+)}$	$-, -/+, \quad e/f$	$(+\gamma_0\gamma_{1/2} - \gamma_{1/2})^{(-)}$	$+, +/-$	rep P_-P_-	I
$\gamma_0\gamma_{1/2}\gamma_5^{(-)}$	$+, +/-, \quad g/h$	$\gamma_0\gamma_{1/2}\gamma_5^{(-)}$	$-, -/+$	rep SP_-	J
$j_z = 1, I = 1, I_z = 0$					
$\gamma_0\gamma_{1/2}^{(+)} - i\gamma_{1/2}\gamma_5^{(-)}$	$-, +/-, \quad f/e$	$(+\gamma_0\gamma_{1/2} + \gamma_{1/2})^{(+)}$	$-, +/-$	att SS	K
$\gamma_{2/1}^{(-)}$	$-, +/-, \quad f/e$	$+i\gamma_{2/1}\gamma_5^{(+)}$	$-, +/-$	rep SP_-	K
$\gamma_0\gamma_{1/2}^{(+)} + i\gamma_{1/2}\gamma_5^{(-)}$	$-, +/-, \quad f/e$	$(+\gamma_0\gamma_{1/2} - \gamma_{1/2})^{(+)}$	$-, +/-$	att P_-P_-	K
$\gamma_0\gamma_{1/2}\gamma_5^{(+)}$	$+, -/+, \quad h/g$	$\gamma_0\gamma_{1/2}\gamma_5^{(+)}$	$+, -/+$	att SP_-	L

Table A.3.: Quantum numbers of the BB system: Twisted basis (tb) and physical basis (pb) quantum numbers for $ud\pm du$. Different physical basis multiplets are assigned capital letters, while different twisted mass sectors are assigned small letters. (Table taken from [5].)

$\Gamma^{\binom{u\bar{d}}{d\bar{u}}}$ tb	$\mathcal{P}^{\text{(tm)}}\circ C$, sec.	$\Gamma^{\binom{u\bar{d}}{d\bar{u}}}$ ppb	$\mathcal{P}_x$	type	mult.
$j_z = 0,\ I = 1,\ I_z = \pm 1$					
$\gamma_5 \pm i\gamma_0$	$-,\quad i$	$+\gamma_5 - \gamma_0\gamma_5$	$-$	SS	E
$\gamma_0\gamma_3\gamma_5$	$-,\quad i$	$+\gamma_0\gamma_3\gamma_5$	$-$	SP_-	E
$\gamma_5 \mp i\gamma_0$	$-,\quad i$	$+\gamma_5 + \gamma_0\gamma_5$	$-$	P_-P_-	E
$\gamma_0\gamma_3 \pm i\gamma_3\gamma_5$	$+,\quad j$	$+\gamma_0\gamma_3 - \gamma_3$	$+$	SS	F
$\mathbb{1}$	$+,\quad j$	$+\mathbb{1}$	$+$	SP_-	F
$\gamma_0\gamma_3 \mp i\gamma_3\gamma_5$	$+,\quad j$	$+\gamma_0\gamma_3 + \gamma_3$	$+$	P_-P_-	F
γ_3	$+,\quad j$	$\pm i\gamma_3\gamma_5$	$-$	SP_-	G
$\gamma_0\gamma_5$	$-,\quad i$	$\pm i\gamma_0$	$+$	SP_-	H
$j_z = 1,\ I = 1,\ I_z = \pm 1$					
$\gamma_0\gamma_{1/2} \pm i\gamma_{1/2}\gamma_5$	$+/+,\quad k$	$+\gamma_0\gamma_{1/2} - \gamma_{1/2}$	$-/+$	SS	I
$\gamma_{2/1}$	$+/+,\quad k$	$\pm i\gamma_{2/1}\gamma_5$	$-/+$	SP_-	I
$\gamma_0\gamma_{1/2} \mp i\gamma_{1/2}\gamma_5$	$+/+,\quad k$	$+\gamma_0\gamma_{1/2} + \gamma_{1/2}$	$-/+$	P_-P_-	I
$\gamma_0\gamma_{1/2}\gamma_5$	$-/-,\quad l$	$+\gamma_0\gamma_{1/2}\gamma_5$	$+/-$	SP_-	J

Table A.4.: Quantum numbers of the $B\bar{B}$ system: Twisted basis (tb) and physical basis (pb) quantum numbers for $u\bar{d}$ and $d\bar{u}$. Different physical basis multiplets are assigned capital letters, while different twisted mass sectors are assigned small letters. (Table taken from [48].)

$\Gamma^{(u\bar{u}\pm d\bar{d})}$ tb	$\mathcal{P}^{(tm)}\circ C, \mathcal{P}_x^{(tm)}$, sec.	$\Gamma^{(u\bar{u}\pm d\bar{d})}$ ppb	$\mathcal{P}\circ C, \mathcal{P}_x$	type	mult.
$j_z = 0, I = 0$					
$i\mathbb{1}^{(-)} - \gamma_0\gamma_5^{(+)}$	$-,-,\quad a$	$(+\gamma_5 - \gamma_0\gamma_5)^{(+)}$	$-,-$	SS	A
$\gamma_0\gamma_3^{(-)}$	$-,-,\quad a$	$-i\gamma_0\gamma_3\gamma_5^{(+)}$	$-,-$	SP_-	A
$i^{(-)} + \gamma_0\gamma_5^{(+)}$	$-,-,\quad a$	$(+\gamma_5 + \gamma_0\gamma_5)^{(+)}$	$-,-$	P_-P_-	A
$\gamma_3^{(+)} - i\gamma_0\gamma_3\gamma_5^{(-)}$	$+,+,\quad b$	$(+\gamma_3 - \gamma_0\gamma_3)^{(+)}$	$+,+$	SS	B
$\gamma_5^{(-)}$	$+,+,\quad b$	$-i^{(+)}$	$+,+$	SP_-	B
$\gamma_3^{(+)} + i\gamma_0\gamma_3\gamma_5^{(-)}$	$+,+,\quad b$	$(+\gamma_3 + \gamma_0\gamma_3)^{(+)}$	$+,+$	P_-P_-	B
$\gamma_3\gamma_5^{(+)}$	$+,-,\quad c$	$+\gamma_3\gamma_5^{(+)}$	$+,-$	SP_-	C
$\gamma_0^{(+)}$	$-,+,\quad d$	$+\gamma_0^{(+)}$	$-,+$	SP_-	D
$j_z = 0, I = 1, I_z = 0$					
$i\mathbb{1}^{(+)} - \gamma_0\gamma_5^{(-)}$	$+,+,\quad b$	$(+\gamma_5 - \gamma_0\gamma_5)^{(-)}$	$-,-$	SS	E
$\gamma_0\gamma_3^{(+)}$	$+,+,\quad b$	$-i\gamma_0\gamma_3\gamma_5^{(-)}$	$-,-$	SP_-	E
$i\mathbb{1}^{(+)} + \gamma_0\gamma_5^{(-)}$	$+,+,\quad b$	$(+\gamma_5 + \gamma_0\gamma_5)^{(-)}$	$-,-$	P_-P_-	E
$\gamma_3^{(-)} - i\gamma_0\gamma_3\gamma_5^{(+)}$	$-,-,\quad a$	$(+\gamma_3 - \gamma_0\gamma_3)^{(-)}$	$+,+$	SS	F
$\gamma_5^{(+)}$	$-,-,\quad a$	$-i\mathbb{1}^{(-)}$	$+,+$	SP_-	F
$\gamma_3^{(-)} + i\gamma_0\gamma_3\gamma_5^{(+)}$	$-,-,\quad a$	$(+\gamma_3 + \gamma_0\gamma_3)^{(-)}$	$+,+$	P_-P_-	F
$\gamma_3\gamma_5^{(-)}$	$-,+,\quad d$	$+\gamma_3\gamma_5^{(-)}$	$+,-$	SP_-	G
$\gamma_0^{(-)}$	$+,-,\quad c$	$+\gamma_0^{(-)}$	$-,+$	SP_-	H
$j_z = 1, I = 0$					
$\gamma_{1/2}^{(+)} - i\gamma_0\gamma_{1/2}\gamma_5^{(-)}$	$+,-/+,\quad e/f$	$(+\gamma_{1/2} - \gamma_0\gamma_{1/2})^{(+)}$	$+,-/+$	SS	I
$\gamma_{2/1}\gamma_5^{(+)}$	$+,-/+,\quad e/f$	$+\gamma_{2/1}\gamma_5^{(+)}$	$+,-/+$	SP_-	I
$\gamma_{1/2}^{(+)} + i\gamma_0\gamma_{1/2}\gamma_5^{(-)}$	$+,-/+,\quad e/f$	$(+\gamma_{1/2} + \gamma_0\gamma_{1/2})^{(+)}$	$+,-/+$	P_-P_-	I
$\gamma_0\gamma_{1/2}^{(-)}$	$-,-/+,\quad g/h$	$-i\gamma_0\gamma_{1/2}\gamma_5^{(+)}$	$-,+/-$	SP_-	J
$j_z = 1, I = 1, I_z = 0$					
$\gamma_{1/2}^{(-)} - i\gamma_0\gamma_{1/2}\gamma_5^{(+)}$	$-,+/-,\quad h/g$	$(+\gamma_{1/2} - \gamma_0\gamma_{1/2})^{(-)}$	$+,-/+$	SS	K
$\gamma_{2/1}\gamma_5^{(-)}$	$-,+/-,\quad h/g$	$+\gamma_{2/1}\gamma_5^{(-)}$	$+,-/+$	SP_-	K
$\gamma_{1/2}^{(-)} + i\gamma_0\gamma_{1/2}\gamma_5^{(+)}$	$-,+/-,\quad h/g$	$(+\gamma_{1/2} + \gamma_0\gamma_{1/2})^{(-)}$	$+,-/+$	P_-P_-	K
$\gamma_0\gamma_{1/2}^{(+)}$	$+,+/-,\quad f/e$	$-i\gamma_0\gamma_{1/2}\gamma_5^{(-)}$	$-,+/-$	SP_-	L

Table A.5.: Quantum numbers of the $B\bar{B}$ system: Twisted basis (tb) and physical basis (pb) quantum numbers for $u\bar{u}\pm d\bar{d}$. Different physical basis multiplets are assigned capital letters, while different twisted mass sectors are assigned small letters. (Table taken from [48].)

A. Appendix

A.3. Symmetries of the $b\bar{b}u\bar{d}$ system

A.3.1. Symmetry checks of C_{11}

Without loss of generality, the static quarks are separated along the z-axis (here denoted as 3-axis). Their positions are $(0,0,0)$ and $(0,0,+r)$. The spin-dependent (dynamical quark) part of the correlation function C_{11} reads:

$$C_{11}^{\text{light}}(r,t) = \left(\Gamma^0\gamma_5\right)^*_{AB}\left(\gamma_5\Gamma^{tT}\right)^*_{DC}\mathcal{D}_{CA}^{-1(\alpha)}(0,t;0,0)\mathcal{D}_{BD}^{-1(\beta)}(r,0;r,t) \tag{A.4}$$

Twisted mass parity

$$\boxed{\mathcal{D}_{AB}^{-1(\alpha)}(x_1,t_1;x_2,t_2) \longrightarrow \left(\gamma_0\mathcal{D}^{-1(\tilde{\alpha})}(-x_1,t_1;-x_2,t_2)\gamma_0\right)_{AB}} \tag{A.5}$$

$$\left(\Gamma^0\gamma_5\right)^*_{AB}\left(\gamma_5\Gamma^{tT}\right)^*_{DC}\mathcal{D}_{CA}^{-1(\alpha)}(0,t;0,0)\mathcal{D}_{BD}^{-1(\beta)}(r,0;r,t)$$

$$\longrightarrow \left(\Gamma^0\gamma_5\right)^*_{AB}\left(\gamma_5\Gamma^{tT}\right)^*_{DC}\left(\gamma_0\mathcal{D}^{-1(\tilde{\alpha})}(0,t;0,0)\gamma_0\right)_{CA}\left(\gamma_0\mathcal{D}^{-1(\tilde{\beta})}(-r,0;-r,t)\gamma_0\right)_{BD}$$

$$= \left(\Gamma^0\gamma_5\right)^*_{AB}\left(\gamma_5\Gamma^{tT}\right)^*_{DC}(\gamma_0)_{CU}\,\mathcal{D}_{UV}^{-1(\tilde{\alpha})}(0,t;0,0)\,(\gamma_0)_{VA}\,(\gamma_0)_{BX}\,\mathcal{D}_{XY}^{-1(\tilde{\beta})}(-r,0;-r,t)\,(\gamma_0)_{YD}$$

$$= \left(\gamma_0\left(\Gamma^0\gamma_5\right)^*\gamma_0\right)_{VX}\left(\gamma_0\left(\gamma_5\Gamma^{tT}\right)^*\gamma_0\right)_{YU}\mathcal{D}_{UV}^{-1(\tilde{\alpha})}(0,t;0,0)\mathcal{D}_{XY}^{-1(\tilde{\beta})}(-r,0;-r,t)$$

shift $-r \to 0$

$$= \left(\gamma_0\left(\Gamma^0\gamma_5\right)^*\gamma_0\right)_{VX}\left(\gamma_0\left(\gamma_5\Gamma^{tT}\right)^*\gamma_0\right)_{YU}\mathcal{D}_{UV}^{-1(\tilde{\alpha})}(r,t;r,0)\mathcal{D}_{XY}^{-1(\tilde{\beta})}(0,0;0,t)$$

$$= \left(\gamma_0\left(\Gamma^0\gamma_5\right)^*\gamma_0\right)_{VX}\left(\gamma_0\left(\gamma_5\Gamma^{tT}\right)^*\gamma_0\right)_{YU}\mathcal{D}_{XY}^{-1(\tilde{\beta})}(0,0;0,t)\mathcal{D}_{UV}^{-1(\tilde{\alpha})}(r,t;r,0)$$

shift $t \to -t$

$$= \left(\gamma_0\left(\Gamma^0\gamma_5\right)^*\gamma_0\right)_{VX}\left(\gamma_0\left(\gamma_5\Gamma^{tT}\right)^*\gamma_0\right)_{YU}\mathcal{D}_{XY}^{-1(\tilde{\beta})}(0,-t;0,0)\mathcal{D}_{UV}^{-1(\tilde{\alpha})}(r,0;r,-t)$$

$$= \left(\gamma_0\left(\Gamma^0\gamma_5\right)^*\gamma_0\right)_{DC}\left(\gamma_0\left(\gamma_5\Gamma^{tT}\right)^*\gamma_0\right)_{AB}\mathcal{D}_{CA}^{-1(\tilde{\beta})}(0,-t;0,0)\mathcal{D}_{BD}^{-1(\tilde{\alpha})}(r,0;r,-t) \tag{A.6}$$

Symmetry transformation rules:

- $t \to -t$

- $\alpha \to \tilde{\beta}$, $\beta \to \tilde{\alpha}$, i.e. $u\bar{u} \leftrightarrow d\bar{d}$, $u\bar{d}, d\bar{u}$: no change

- $\left(\Gamma^0\gamma_5\right)^* \longrightarrow \left(\gamma_0\gamma_5\Gamma^{tT}\gamma_0\right)^*$

- $\left(\gamma_5\Gamma^{tT}\right)^* \longrightarrow \left(\gamma_0\Gamma^0\gamma_5\gamma_0\right)^*$

Charge conjugation

$$\boxed{\mathcal{D}_{AB}^{-1(\alpha)}(x_1,t_1;x_2,t_2) \longrightarrow \left(\gamma_0\gamma_2\left(\mathcal{D}^{-1(\alpha)}(x_2,t_2;x_1,t_1)\right)^T\gamma_2\gamma_0\right)_{AB}} \tag{A.7}$$

$$\left(\Gamma^0\gamma_5\right)^*_{AB}\left(\gamma_5\Gamma^{tT}\right)^*_{DC}\mathcal{D}^{-1(\alpha)}_{CA}(0,t;0,0)\mathcal{D}^{-1(\beta)}_{BD}(r,0;r,t)$$

$$\longrightarrow\left(\Gamma^0\gamma_5\right)^*_{AB}\left(\gamma_5\Gamma^{tT}\right)^*_{DC}\left(\gamma_0\gamma_2\left(\mathcal{D}^{-1(\alpha)}(0,0;0,t)\right)^T\gamma_2\gamma_0\right)_{CA}\left(\gamma_0\gamma_2\left(\mathcal{D}^{-1(\beta)}(r,t;r,0)\right)^T\gamma_2\gamma_0\right)_{BD}$$

$$=\left(\Gamma^0\gamma_5\right)^*_{AB}\left(\gamma_5\Gamma^{tT}\right)^*_{DC}\left(\gamma_0\gamma_2\right)_{CU}\left(\mathcal{D}^{-1(\alpha)}(0,0;0,t)\right)^T_{UV}\left(\gamma_2\gamma_0\right)_{VA}$$

$$\left(\gamma_0\gamma_2\right)_{BX}\left(\mathcal{D}^{-1(\beta)}(r,t;r,0)\right)^T_{XY}\left(\gamma_2\gamma_0\right)_{YD}$$

$$=\left(\gamma_2\gamma_0\left(\Gamma^0\gamma_5\right)^*\gamma_0\gamma_2\right)_{VX}\left(\gamma_2\gamma_0\left(\gamma_5\Gamma^{tT}\right)^*\gamma_0\gamma_2\right)_{YU}\mathcal{D}^{-1(\alpha)}_{VU}(0,0;0,t)\mathcal{D}^{-1(\beta)}_{YX}(r,t;r,0)$$

shift $t\rightarrow-t$

$$=\left(\gamma_2\gamma_0\left(\Gamma^0\gamma_5\right)^*\gamma_0\gamma_2\right)_{VX}\left(\gamma_2\gamma_0\left(\gamma_5\Gamma^{tT}\right)^*\gamma_0\gamma_2\right)_{YU}\mathcal{D}^{-1(\alpha)}_{VU}(0,-t;0,0)\mathcal{D}^{-1(\beta)}_{YX}(r,0;r,-t)$$

$$=\left(\gamma_2\gamma_0\Gamma^0\gamma_5\gamma_0\gamma_2\right)^*_{CD}\left(\gamma_2\gamma_0\gamma_5\Gamma^{tT}\gamma_0\gamma_2\right)^*_{BA}\mathcal{D}^{-1(\alpha)}_{CA}(0,-t;0,0)\mathcal{D}^{-1(\beta)}_{BD}(r,0;r,-t)$$

$$\text{(A.8)}$$

with

$$\left(\gamma_2\gamma_0\Gamma^0\gamma_5\gamma_0\gamma_2\right)^*_{CD}=\left(\left(\gamma_2\gamma_0\Gamma^0\gamma_5\gamma_0\gamma_2\right)^*\right)^T_{DC}=\left(\gamma_2\gamma_0\gamma_5\Gamma^{0T}\gamma_0\gamma_2\right)^*_{DC}\text{ and}\qquad\text{(A.9)}$$

$$\left(\gamma_2\gamma_0\gamma_5\Gamma^{tT}\gamma_0\gamma_2\right)^*_{BA}=\left(\left(\gamma_2\gamma_0\gamma_5\Gamma^{tT}\gamma_0\gamma_2\right)^*\right)^T_{AB}=\left(\gamma_2\gamma_0\Gamma^t\gamma_5\gamma_0\gamma_2\right)^*_{AB}\qquad\text{(A.10)}$$

Symmetry transformation rules:

- $t\rightarrow-t$

- flavor: no change

- $\left(\Gamma^0\gamma_5\right)^*\longrightarrow\left(\gamma_2\gamma_0\Gamma^t\gamma_5\gamma_0\gamma_2\right)^*$

- $\left(\gamma_5\Gamma^{tT}\right)^*\longrightarrow\left(\gamma_2\gamma_0\gamma_5\Gamma^{0T}\gamma_0\gamma_2\right)^*$

Twisted mass γ_5-hermiticity

$$\boxed{\mathcal{D}^{-1(\alpha)}_{AB}(x_1,t_1;x_2,t_2)\longrightarrow\left(\gamma_5\left(\mathcal{D}^{-1(\tilde{\alpha})}(x_2,t_2;x_1,t_1)\right)^\dagger\gamma_5\right)_{AB}}\qquad\text{(A.11)}$$

A. Appendix

$$\left(\Gamma^0\gamma_5\right)^*_{AB}\left(\gamma_5\Gamma^{tT}\right)^*_{DC}\mathcal{D}^{-1(\alpha)}_{CA}(0,t;0,0)\mathcal{D}^{-1(\beta)}_{BD}(r,0;r,t)$$

$$\longrightarrow \left(\Gamma^0\gamma_5\right)^*_{AB}\left(\gamma_5\Gamma^{tT}\right)^*_{DC}\left(\gamma_5\left(\mathcal{D}^{-1(\tilde{\alpha})}(0,0;0,t)\right)^\dagger\gamma_5\right)_{CA}\left(\gamma_5\left(\mathcal{D}^{-1(\tilde{\beta})}(r,t;r,0)\right)^\dagger\gamma_5\right)_{BD}$$

$$= \left(\Gamma^0\gamma_5\right)^*_{AB}\left(\gamma_5\Gamma^{tT}\right)^*_{DC}(\gamma_5)_{CU}\left(\mathcal{D}^{-1(\tilde{\alpha})}_{VU}(0,0;0,t)\right)^*(\gamma_5)_{VA}(\gamma_5)_{BX}\left(\mathcal{D}^{-1(\tilde{\beta})}_{YX}(r,t;r,0)\right)^*(\gamma_5)_{YD}$$

$$= \left(\gamma_5\left(\Gamma^0\gamma_5\right)^*\gamma_5\right)_{VX}\left(\gamma_5\left(\gamma_5\Gamma^{tT}\right)^*\gamma_5\right)_{YU}\left(\mathcal{D}^{-1(\tilde{\alpha})}_{VU}(0,0;0,t)\right)^*\left(\mathcal{D}^{-1(\tilde{\beta})}_{YX}(r,t;r,0)\right)^*$$

$$= \left(\left(\gamma_5\Gamma^0\right)_{CD}\left(\Gamma^{tT}\gamma_5\right)_{BA}\mathcal{D}^{-1(\tilde{\alpha})}_{CA}(0,0;0,t)\mathcal{D}^{-1(\tilde{\beta})}_{BD}(r,t;r,0)\right)^*$$

shift $t \to -t$

$$= \left(\left(\Gamma^{tT}\gamma_5\right)^T_{AB}\left(\gamma_5\Gamma^0\right)^T_{DC}\mathcal{D}^{-1(\tilde{\alpha})}_{CA}(0,-t;0,0)\mathcal{D}^{-1(\tilde{\beta})}_{BD}(r,0;r,t)\right)^* \tag{A.12}$$

Symmetry transformation rules:

- complex conjugation of the expression

- $t \to -t$

- $\alpha \to \tilde{\alpha}$, $\beta \to \tilde{\beta}$, i.e. $u\bar{u} \leftrightarrow d\bar{d}$, $u\bar{d} \leftrightarrow d\bar{u}$

- $\left(\Gamma^0\gamma_5\right)^* \longrightarrow \gamma_5\Gamma^t$

- $\left(\gamma_5\Gamma^{tT}\right)^* \longrightarrow \Gamma^{0T}\gamma_5$

Twisted mass time reversal

$$\boxed{\mathcal{D}^{-1(\alpha)}_{AB}(x_1,t_1;x_2,t_2) \longrightarrow \left(\gamma_0\gamma_5\mathcal{D}^{-1(\tilde{\alpha})}(x_1,-t_1;x_2,-t_2)\gamma_5\gamma_0\right)_{AB}} \tag{A.13}$$

$$\left(\Gamma^0\gamma_5\right)^*_{AB}\left(\gamma_5\Gamma^{tT}\right)^*_{DC}\mathcal{D}^{-1(\alpha)}_{CA}(0,t;0,0)\mathcal{D}^{-1(\beta)}_{BD}(r,0;r,t)$$

$$\longrightarrow \left(\Gamma^0\gamma_5\right)^*_{AB}\left(\gamma_5\Gamma^{tT}\right)^*_{DC}(\gamma_0\gamma_5)_{CU}\mathcal{D}^{-1(\tilde{\alpha})}_{UV}(0,-t;0,0)(\gamma_5\gamma_0)_{VA}(\gamma_0\gamma_5)_{BX}\mathcal{D}^{-1(\tilde{\beta})}_{XY}(r,0;r,-t)(\gamma_5\gamma_0)_{YD}$$

$$= \left(\gamma_5\gamma_0\left(\Gamma^0\gamma_5\right)^*\gamma_0\gamma_5\right)_{VX}\left(\gamma_5\gamma_0\left(\gamma_5\Gamma^{tT}\right)^*\gamma_0\gamma_5\right)_{YU}\mathcal{D}^{-1(\tilde{\alpha})}_{UV}(0,-t;0,0)\mathcal{D}^{-1(\tilde{\beta})}_{XY}(r,0;r,-t)$$

$$= \left(\gamma_5\gamma_0\left(\Gamma^0\gamma_5\right)^*\gamma_0\gamma_5\right)_{AB}\left(\gamma_5\gamma_0\left(\gamma_5\Gamma^{tT}\right)^*\gamma_0\gamma_5\right)_{DC}\mathcal{D}^{-1(\tilde{\alpha})}_{CA}(0,-t;0,0)\mathcal{D}^{-1(\tilde{\beta})}_{BD}(r,0;r,-t) \tag{A.14}$$

Symmetry transformation rules:

- $t \to -t$

- $\alpha \to \tilde{\alpha}$, $\beta \to \tilde{\beta}$, i.e. $u\bar{u} \leftrightarrow d\bar{d}$, $u\bar{d} \leftrightarrow d\bar{u}$

- $\left(\Gamma^0\gamma_5\right)^* \longrightarrow \gamma_5\gamma_0\left(\Gamma^0\gamma_5\right)^*\gamma_0\gamma_5 = \left(\gamma_5\gamma_0\Gamma^0\gamma_0\right)^*$

- $\left(\gamma_5\Gamma^{tT}\right)^* \longrightarrow \gamma_5\gamma_0\left(\gamma_5\Gamma^{tT}\right)^*\gamma_0\gamma_5 = \left(\gamma_0\Gamma^{tT}\gamma_0\gamma_5\right)^*$

π cubic rotation in $j-k$ plane

$$\boxed{\mathcal{D}_{AB}^{-1(\alpha)}(x_1,t_1;x_2,t_2) \longrightarrow \left(\gamma_j\gamma_k\mathcal{D}^{-1(\alpha)}(-x_1,t_1;-x_2,t_2)\gamma_k\gamma_j\right)_{AB}} \tag{A.15}$$

2-3 plane

$$\left(\Gamma^0\gamma_5\right)_{AB}^* \left(\gamma_5\Gamma^{tT}\right)_{DC}^* \mathcal{D}_{CA}^{-1(\alpha)}(0,t;0,0)\mathcal{D}_{BD}^{-1(\beta)}(r,0;r,t)$$

$$\longrightarrow \left(\Gamma^0\gamma_5\right)_{AB}^* \left(\gamma_5\Gamma^{tT}\right)_{DC}^* (\gamma_2\gamma_3)_{CU}\mathcal{D}_{UV}^{-1(\alpha)}(0,t;0,0)(\gamma_3\gamma_2)_{VA}(\gamma_2\gamma_3)_{BX}\mathcal{D}_{XY}^{-1(\beta)}(-r,0;-r,t)(\gamma_3\gamma_2)_{YD}$$

$$= \left(\gamma_3\gamma_2\left(\Gamma^0\gamma_5\right)^*\gamma_2\gamma_3\right)_{VX}\left(\gamma_3\gamma_2\left(\gamma_5\Gamma^{tT}\right)^*\gamma_2\gamma_3\right)_{XU}\mathcal{D}_{UV}^{-1(\alpha)}(0,t;0,0)\mathcal{D}_{XY}^{-1(\beta)}(-r,0;-r,t)$$

  shift $-r \to 0$

$$= \left(\gamma_3\gamma_2\left(\Gamma^0\gamma_5\right)^*\gamma_2\gamma_3\right)_{VX}\left(\gamma_3\gamma_2\left(\gamma_5\Gamma^{tT}\right)^*\gamma_2\gamma_3\right)_{XU}\mathcal{D}_{UV}^{-1(\alpha)}(r,t;r,0)\mathcal{D}_{XY}^{-1(\beta)}(0,0;0,t)$$

  shift $t \to -t$

$$= \left(\gamma_3\gamma_2\left(\Gamma^0\gamma_5\right)^*\gamma_2\gamma_3\right)_{DC}\left(\gamma_3\gamma_2\left(\gamma_5\Gamma^{tT}\right)^*\gamma_2\gamma_3\right)_{AB}\mathcal{D}_{BD}^{-1(\alpha)}(r,0;r,-t)\mathcal{D}_{CA}^{-1(\beta)}(0,-t;0,0)$$
$$\tag{A.16}$$

Symmetry transformation rules:

- $t \to -t$

- $\alpha \to \beta$, $\beta \to \alpha$, i.e. $u\bar{d} \leftrightarrow d\bar{u}$, $u\bar{u}, d\bar{d}$: no change

- $\left(\Gamma^0\gamma_5\right)^* \longrightarrow \left(\gamma_3\gamma_2\left(\gamma_5\Gamma^{tT}\right)^*\gamma_2\gamma_3\right) = \left(\gamma_3\gamma_2\gamma_5\Gamma^{tT}\gamma_2\gamma_3\right)^*$

- $\left(\gamma_5\Gamma^{tT}\right)^* \longrightarrow \left(\gamma_3\gamma_2\left(\Gamma^0\gamma_5\right)^*\gamma_2\gamma_3\right) = \left(\gamma_3\gamma_2\Gamma^0\gamma_5\gamma_2\gamma_3\right)^*$

1-3 plane

$$\left(\Gamma^0\gamma_5\right)_{AB}^* \left(\gamma_5\Gamma^{tT}\right)_{DC}^* \mathcal{D}_{CA}^{-1(\alpha)}(0,t;0,0)\mathcal{D}_{BD}^{-1(\beta)}(r,0;r,t)$$

$$\longrightarrow \left(\Gamma^0\gamma_5\right)_{AB}^* \left(\gamma_5\Gamma^{tT}\right)_{DC}^* (\gamma_1\gamma_3)_{CU}\mathcal{D}_{UV}^{-1(\alpha)}(0,t;0,0)(\gamma_3\gamma_1)_{VA}(\gamma_1\gamma_3)_{BX}\mathcal{D}_{XY}^{-1(\beta)}(-r,0;-r,t)(\gamma_3\gamma_1)_{YD}$$

$$= \left(\gamma_3\gamma_1\left(\Gamma^0\gamma_5\right)^*\gamma_1\gamma_3\right)_{VX}\left(\gamma_3\gamma_1\left(\gamma_5\Gamma^{tT}\right)^*\gamma_1\gamma_3\right)_{XU}\mathcal{D}_{UV}^{-1(\alpha)}(0,t;0,0)\mathcal{D}_{XY}^{-1(\beta)}(-r,0;-r,t)$$

  shift $-r \to 0$

$$= \left(\gamma_3\gamma_1\left(\Gamma^0\gamma_5\right)^*\gamma_1\gamma_3\right)_{VX}\left(\gamma_3\gamma_1\left(\gamma_5\Gamma^{tT}\right)^*\gamma_1\gamma_3\right)_{XU}\mathcal{D}_{UV}^{-1(\alpha)}(r,t;r,0)\mathcal{D}_{XY}^{-1(\beta)}(0,0;0,t)$$

  shift $t \to -t$

$$= \left(\gamma_3\gamma_1\left(\Gamma^0\gamma_5\right)^*\gamma_1\gamma_3\right)_{DC}\left(\gamma_3\gamma_1\left(\gamma_5\Gamma^{tT}\right)^*\gamma_1\gamma_3\right)_{AB}\mathcal{D}_{BD}^{-1(\alpha)}(r,0;r,-t)\mathcal{D}_{CA}^{-1(\beta)}(0,-t;0,0)$$
$$\tag{A.17}$$

Symmetry transformation rules:

- $t \to -t$

- $\alpha \to \beta$, $\beta \to \alpha$, i.e. $u\bar{d} \leftrightarrow d\bar{u}$, $u\bar{u}, d\bar{d}$: no change

- $\left(\Gamma^0\gamma_5\right)^* \longrightarrow \left(\gamma_3\gamma_1\left(\gamma_5\Gamma^{tT}\right)^*\gamma_1\gamma_3\right) = \left(\gamma_3\gamma_1\gamma_5\Gamma^{tT}\gamma_1\gamma_3\right)^*$

- $\left(\gamma_5\Gamma^{tT}\right)^* \longrightarrow \left(\gamma_3\gamma_1\left(\Gamma^0\gamma_5\right)^*\gamma_1\gamma_3\right) = \left(\gamma_3\gamma_1\Gamma^0\gamma_5\gamma_1\gamma_3\right)^*$

A. Appendix

$\pi/2$ cubic rotation around 1-axis ($\mathcal{R}_1(-\frac{\pi}{2})$)

$$\mathcal{D}_{AB}^{-1(\alpha)}(x_1, t_1; x_2, t_2) \longrightarrow \left((\frac{1}{\sqrt{2}}\mathbb{1} - \frac{1}{\sqrt{2}}\gamma_2\gamma_3)\mathcal{D}^{-1(\alpha)}(\tilde{x}_1, t_1; \tilde{x}_2, t_2)(\frac{1}{\sqrt{2}}\mathbb{1} + \frac{1}{\sqrt{2}}\gamma_2\gamma_3) \right)_{AB}$$

with $x = \begin{pmatrix} 0 \\ 0 \\ x \end{pmatrix}$ and $\tilde{x} = \begin{pmatrix} 0 \\ x \\ 0 \end{pmatrix}$

$$\tag{A.18}$$

$$\left(\Gamma^0\gamma_5 \right)_{AB}^* \left(\gamma_5\Gamma^{tT} \right)_{DC}^* \mathcal{D}_{CA}^{-1(\alpha)}(0, t; 0, 0)\mathcal{D}_{BD}^{-1(\beta)}(r, 0; r, t)$$

$$\longrightarrow \left(\Gamma^0\gamma_5 \right)_{AB}^* \left(\gamma_5\Gamma^{tT} \right)_{DC}^*$$

$$\left((\frac{1}{\sqrt{2}}\mathbb{1} - \frac{1}{\sqrt{2}}\gamma_2\gamma_3)\mathcal{D}^{-1(\alpha)}(0, t; 0, 0)(\frac{1}{\sqrt{2}}\mathbb{1} + \frac{1}{\sqrt{2}}\gamma_2\gamma_3) \right)_{CA}$$

$$\left((\frac{1}{\sqrt{2}}\mathbb{1} - \frac{1}{\sqrt{2}}\gamma_2\gamma_3)\mathcal{D}^{-1(\beta)}(\tilde{r}, 0; \tilde{r}, t)(\frac{1}{\sqrt{2}}\mathbb{1} + \frac{1}{\sqrt{2}}\gamma_2\gamma_3) \right)_{BD}$$

$$= \left((\frac{1}{\sqrt{2}}\mathbb{1} + \frac{1}{\sqrt{2}}\gamma_2\gamma_3) \left(\Gamma^0\gamma_5 \right)^* (\frac{1}{\sqrt{2}}\mathbb{1} - \frac{1}{\sqrt{2}}\gamma_2\gamma_3) \right)_{VX} \left((\frac{1}{\sqrt{2}}\mathbb{1} + \frac{1}{\sqrt{2}}\gamma_2\gamma_3) \left(\gamma_5\Gamma^{tT} \right)^* (\frac{1}{\sqrt{2}}\mathbb{1} - \frac{1}{\sqrt{2}}\gamma_2\gamma_3) \right)_{YU}$$

$$\mathcal{D}_{UV}^{-1(\alpha)}(0, t; 0, 0)\mathcal{D}_{XY}^{-1(\beta)}(\tilde{r}, 0; \tilde{r}, t)$$

$$= \frac{1}{2} \left((\mathbb{1} + \gamma_2\gamma_3) \left(\Gamma^0\gamma_5 \right)^* (\mathbb{1} - \gamma_2\gamma_3) \right)_{AB} \frac{1}{2} \left((\mathbb{1} + \gamma_2\gamma_3) \left(\gamma_5\Gamma^{tT} \right)^* (\mathbb{1} - \gamma_2\gamma_3) \right)_{DC}$$

$$\mathcal{D}_{CA}^{-1(\alpha)}(0, t; 0, 0)\mathcal{D}_{BD}^{-1(\beta)}(\tilde{r}, 0; \tilde{r}, t)$$

$$\tag{A.19}$$

Symmetry transformation rules:

- $\left(\Gamma^0\gamma_5 \right)^* \longrightarrow \frac{1}{2} \left((\mathbb{1} + \gamma_2\gamma_3) \left(\Gamma^0\gamma_5 \right)^* (\mathbb{1} - \gamma_2\gamma_3) \right) = \frac{1}{2} \left((\mathbb{1} - \gamma_2\gamma_3)\Gamma^0\gamma_5(\mathbb{1} + \gamma_2\gamma_3) \right)^*$

- $\left(\gamma_5\Gamma^{tT} \right)^* \longrightarrow \frac{1}{2} \left((1 + \gamma_2\gamma_3) \left(\gamma_5\Gamma^{tT} \right)^* (\mathbb{1} - \gamma_2\gamma_3) \right) = \frac{1}{2} \left((\mathbb{1} - \gamma_2\gamma_3)\gamma_5\Gamma^{tT}(\mathbb{1} + \gamma_2\gamma_3) \right)^*$

$\pi/2$ cubic rotation around 2-axis ($\mathcal{R}_2(\frac{\pi}{2})$)

$$\mathcal{D}_{AB}^{-1(\alpha)}(x_1, t_1; x_2, t_2) \longrightarrow \left((\frac{1}{\sqrt{2}}\mathbb{1} - \frac{1}{\sqrt{2}}\gamma_1\gamma_3)\mathcal{D}^{-1(\alpha)}(\tilde{x}_1, t_1; \tilde{x}_2, t_2)(\frac{1}{\sqrt{2}}\mathbb{1} + \frac{1}{\sqrt{2}}\gamma_1\gamma_3) \right)_{AB}$$

with $x = \begin{pmatrix} 0 \\ 0 \\ x \end{pmatrix}$ and $\tilde{x} = \begin{pmatrix} x \\ 0 \\ 0 \end{pmatrix}$

$$\tag{A.20}$$

$$\left(\Gamma^0\gamma_5\right)^*_{AB}\left(\gamma_5\Gamma^{tT}\right)^*_{DC}\mathcal{D}^{-1(\alpha)}_{CA}(0,t;0,0)\mathcal{D}^{-1(\beta)}_{BD}(r,0;r,t)$$

$$\longrightarrow \left(\Gamma^0\gamma_5\right)^*_{AB}\left(\gamma_5\Gamma^{tT}\right)^*_{DC}$$

$$\left(\left((\frac{1}{\sqrt{2}}\mathbb{1}-\frac{1}{\sqrt{2}}\gamma_1\gamma_3)\mathcal{D}^{-1(\alpha)}(0,t;0,0)(\frac{1}{\sqrt{2}}\mathbb{1}+\frac{1}{\sqrt{2}}\gamma_1\gamma_3)\right)\right)_{CA}$$

$$\left(\left((\frac{1}{\sqrt{2}}\mathbb{1}-\frac{1}{\sqrt{2}}\gamma_1\gamma_3)\mathcal{D}^{-1(\beta)}(\tilde{r},0;\tilde{r},t)(\frac{1}{\sqrt{2}}\mathbb{1}+\frac{1}{\sqrt{2}}\gamma_1\gamma_3)\right)\right)_{BD}$$

$$=\left(\left((\frac{1}{\sqrt{2}}\mathbb{1}+\frac{1}{\sqrt{2}}\gamma_1\gamma_3\right)\left(\Gamma^0\gamma_5\right)^*(\frac{1}{\sqrt{2}}\mathbb{1}-\frac{1}{\sqrt{2}}\gamma_1\gamma_3)\right)_{VX}\left(\left((\frac{1}{\sqrt{2}}\mathbb{1}+\frac{1}{\sqrt{2}}\gamma_1\gamma_3\right)\left(\gamma_5\Gamma^{tT}\right)^*(\frac{1}{\sqrt{2}}\mathbb{1}-\frac{1}{\sqrt{2}}\gamma_1\gamma_3)\right)_{YU}$$

$$\mathcal{D}^{-1(\alpha)}_{UV}(0,t;0,0)\mathcal{D}^{-1(\beta)}_{XY}(\tilde{r},0;\tilde{r},t)$$

$$=\frac{1}{2}\left((\mathbb{1}+\gamma_1\gamma_3)\left(\Gamma^0\gamma_5\right)^*(\mathbb{1}-\gamma_1\gamma_3)\right)_{AB}\frac{1}{2}\left((\mathbb{1}+\gamma_1\gamma_3)\left(\gamma_5\Gamma^{tT}\right)^*(\mathbb{1}-\gamma_1\gamma_3)\right)_{DC}$$

$$\mathcal{D}^{-1(\alpha)}_{CA}(0,t;0,0)\mathcal{D}^{-1(\beta)}_{BD}(\tilde{r},0;\tilde{r},t)$$

$$(A.21)$$

Symmetry transformation rules:

- $\left(\Gamma^0\gamma_5\right)^* \longrightarrow \frac{1}{2}\left((\mathbb{1}+\gamma_1\gamma_3)\left(\Gamma^0\gamma_5\right)^*(\mathbb{1}-\gamma_1\gamma_3)\right)=\frac{1}{2}\left((\mathbb{1}+\gamma_1\gamma_3)\Gamma^0\gamma_5(\mathbb{1}-\gamma_1\gamma_3)\right)^*$

- $\left(\gamma_5\Gamma^{tT}\right)^* \longrightarrow \frac{1}{2}\left((\mathbb{1}+\gamma_1\gamma_3)\left(\gamma_5\Gamma^{tT}\right)^*(\mathbb{1}-\gamma_1\gamma_3)\right)=\frac{1}{2}\left((\mathbb{1}+\gamma_1\gamma_3)\gamma_5\Gamma^{tT}(\mathbb{1}-\gamma_1\gamma_3)\right)^*$

$\pi/2$ cubic rotation around 3-axis $\left(\mathcal{R}_3(\frac{\pi}{2})\right)$

$$\boxed{\begin{aligned}&\mathcal{D}^{-1(\alpha)}_{AB}(x_1,t_1;x_2,t_2) \longrightarrow \left(\left((\frac{1}{\sqrt{2}}\mathbb{1}+\frac{1}{\sqrt{2}}\gamma_1\gamma_2)\mathcal{D}^{-1(\alpha)}(\tilde{x}_1,t_1;\tilde{x}_2,t_2)(\frac{1}{\sqrt{2}}\mathbb{1}-\frac{1}{\sqrt{2}}\gamma_1\gamma_2)\right)\right)_{AB}\\&\text{with }x=\begin{pmatrix}0\\0\\x\end{pmatrix}=\tilde{x}\end{aligned}}$$

$$(A.22)$$

$$\left(\Gamma^0\gamma_5\right)^*_{AB}\left(\gamma_5\Gamma^{tT}\right)^*_{DC}\mathcal{D}^{-1(\alpha)}_{CA}(0,t;0,0)\mathcal{D}^{-1(\beta)}_{BD}(r,0;r,t)$$

$$\longrightarrow \left(\Gamma^0\gamma_5\right)^*_{AB}\left(\gamma_5\Gamma^{tT}\right)^*_{DC}$$

$$\left(\left((\frac{1}{\sqrt{2}}\mathbb{1}+\frac{1}{\sqrt{2}}\gamma_1\gamma_2)\mathcal{D}^{-1(\alpha)}(0,t;0,0)(\frac{1}{\sqrt{2}}\mathbb{1}-\frac{1}{\sqrt{2}}\gamma_1\gamma_2)\right)\right)_{CA}$$

$$\left(\left((\frac{1}{\sqrt{2}}\mathbb{1}+\frac{1}{\sqrt{2}}\gamma_1\gamma_2)\mathcal{D}^{-1(\beta)}(\tilde{r},0;\tilde{r},t)(\frac{1}{\sqrt{2}}\mathbb{1}-\frac{1}{\sqrt{2}}\gamma_1\gamma_2)\right)\right)_{BD}$$

$$=\left(\left((\frac{1}{\sqrt{2}}\mathbb{1}-\frac{1}{\sqrt{2}}\gamma_1\gamma_2\right)\left(\Gamma^0\gamma_5\right)^*(\frac{1}{\sqrt{2}}\mathbb{1}+\frac{1}{\sqrt{2}}\gamma_1\gamma_2)\right)_{VX}\left(\left((\frac{1}{\sqrt{2}}\mathbb{1}-\frac{1}{\sqrt{2}}\gamma_1\gamma_2\right)\left(\gamma_5\Gamma^{tT}\right)^*(\frac{1}{\sqrt{2}}\mathbb{1}+\frac{1}{\sqrt{2}}\gamma_1\gamma_2)\right)_{YU}$$

$$\mathcal{D}^{-1(\alpha)}_{UV}(0,t;0,0)\mathcal{D}^{-1(\beta)}_{XY}(\tilde{r},0;\tilde{r},t)$$

$$=\frac{1}{2}\left((\mathbb{1}-\gamma_1\gamma_2)\left(\Gamma^0\gamma_5\right)^*(\mathbb{1}+\gamma_1\gamma_2)\right)_{AB}\frac{1}{2}\left((\mathbb{1}-\gamma_1\gamma_2)\left(\gamma_5\Gamma^{tT}\right)^*(\mathbb{1}+\gamma_1\gamma_2)\right)_{DC}$$

$$\mathcal{D}^{-1(\alpha)}_{CA}(0,t;0,0)\mathcal{D}^{-1(\beta)}_{BD}(\tilde{r},0;\tilde{r},t)$$

$$(A.23)$$

A. Appendix

Symmetry transformation rules:

- $\left(\Gamma^0\gamma_5\right)^* \longrightarrow \frac{1}{2}\left(\left(\mathbb{1}-\gamma_1\gamma_2\right)\left(\Gamma^0\gamma_5\right)^*\left(\mathbb{1}+\gamma_1\gamma_2\right)\right) = \frac{1}{2}\left(\left(\mathbb{1}+\gamma_1\gamma_2\right)\Gamma^0\gamma_5(\mathbb{1}-\gamma_1\gamma_2)\right)^*$

- $\left(\gamma_5\Gamma^{tT}\right)^* \longrightarrow \frac{1}{2}\left(\left(\mathbb{1}-\gamma_1\gamma_2\right)\left(\gamma_5\Gamma^{tT}\right)^*\left(\mathbb{1}+\gamma_1\gamma_2\right)\right) = \frac{1}{2}\left(\left(\mathbb{1}+\gamma_1\gamma_2\right)\gamma_5\Gamma^{tT}(\mathbb{1}-\gamma_1\gamma_2)\right)^*$

A.3.2. Symmetry checks of C_{12} and C_{21}

We limit ourselves to consider the correlation function C_{21} (C_{12} can be reconstructed according to $C_{12} = C_{21}^*$). The spin-dependent (dynamical quark) part of C_{21} reads (the sum over z is implicit):

$$C_{21}^{\text{light}}(r,t) = (\gamma_5)_{DC}\,(\Gamma)_{VU}\,\mathcal{D}_{UD}^{-1(\alpha)}(0,0;z,t)\mathcal{D}_{CV}^{-1(\beta)}(z,t;r,0) \tag{A.24}$$

$\mathcal{D}^{-1}$ is the dynamical quark propagator. Without loss of generality the static quarks are separated along the 3-axis.

Twisted mass parity

$$\boxed{\mathcal{D}_{AB}^{-1(\alpha)}(x_1,t_1;x_2,t_2) \longrightarrow \left(\gamma_0\mathcal{D}^{-1(\tilde{\alpha})}(-x_1,t_1;-x_2,t_2)\gamma_0\right)_{AB}} \tag{A.25}$$

$(\gamma_5)_{DC}\,(\Gamma)_{VU}\,\mathcal{D}_{UD}^{-1(\alpha)}(0,0;z,t)\mathcal{D}_{CV}^{-1(\beta)}(z,t;r,0)$

$\rightarrow (\gamma_5)_{DC}\,(\Gamma)_{VU}\left(\gamma_0\mathcal{D}^{-1(\tilde{\alpha})}(0,0;z,t)\gamma_0\right)_{UD}\left(\gamma_0\mathcal{D}^{-1(\tilde{\beta})}(z,t;-r,0)\gamma_0\right)_{CV}$

$\quad = (\gamma_0\gamma_5\gamma_0)_{KS}\,(\gamma_0\Gamma\gamma_0)_{PL}\,\mathcal{D}^{-1(\tilde{\alpha})}(0,0;z,t)_{LK}\mathcal{D}^{-1(\tilde{\beta})}(z,t;-r,0)_{SP}$

$\quad$ shift $-r \rightarrow 0$

$\quad = -(\gamma_5)_{KS}\,(\gamma_5\gamma_0\Gamma\gamma_0\gamma_5)_{PL}\,\mathcal{D}^{-1(\tilde{\alpha})}(r,0;z,t)_{LK}\mathcal{D}^{-1(\tilde{\beta})}(z,t;0,0)_{SP}$

$\quad \gamma_5$-hermiticity

$\quad = -(\gamma_5)_{KS}\,(\gamma_5\gamma_0\Gamma\gamma_0\gamma_5)_{PL}\left(\gamma_5\left(\mathcal{D}^{-1(\alpha)}(z,t;r,0)\right)^\dagger\gamma_5\right)_{LK}\left(\gamma_5\left(\mathcal{D}^{-1(\beta)}(0,0;z,t)\right)^\dagger\gamma_5\right)_{SP}$

$\quad = -(\gamma_5)_{VM}\,(\gamma_5)_{NU}\,\mathcal{D}^{-1(\alpha)}(z,t;r,0)_{VU}^*\mathcal{D}^{-1(\beta)}(0,0;z,t)_{NM}^*$

$\quad = -\left((\gamma_5)_{CD}\,(\gamma_5\gamma_0\Gamma\gamma_0\gamma_5)_{UV}^*\,\mathcal{D}^{-1(\beta)}(0,0;z,t)_{UD}\mathcal{D}^{-1(\alpha)}(z,t;r,0)_{CV}\right)^*$

$$\tag{A.26}$$

Symmetry transformation rules:

- complex conjugate

- $\alpha \leftrightarrow \beta$, i.e. $u\bar{u}, d\bar{d}$: no change, $u\bar{d} \leftrightarrow d\bar{u}$

- $\Gamma \rightarrow -\left(\gamma_5\gamma_0\Gamma\gamma_0\gamma_5\right)^*$, (no change, if $\Gamma = \gamma_0$ or $\Gamma = \gamma_5$)

Charge conjugation

$$\boxed{\mathcal{D}_{AB}^{-1(\alpha)}(x_1,t_1;x_2,t_2) \longrightarrow \left(\gamma_0\gamma_2\left(\mathcal{D}^{-1(\alpha)}(x_2,t_2;x_1,t_1)\right)^T\gamma_2\gamma_0\right)_{AB}} \tag{A.27}$$

$$(\gamma_5)_{DC}\,(\Gamma)_{VU}\,\mathcal{D}_{UD}^{-1(\alpha)}(0,0;z,t)\mathcal{D}_{CV}^{-1(\beta)}(z,t;r,0)$$

$$\rightarrow (\gamma_5)_{DC}\,(\Gamma)_{VU}\left(\gamma_0\gamma_2\left(\mathcal{D}^{-1(\alpha)}(z,t;0,0)\right)^T\gamma_2\gamma_0\right)_{UD}\left(\gamma_0\gamma_2\left(\mathcal{D}^{-1(\beta)}(r,0;z,t)\right)^T\gamma_2\gamma_0\right)_{CV}$$

$$= (\gamma_2\gamma_0\gamma_5\gamma_0\gamma_2)_{PL}\,(\gamma_2\gamma_0\Gamma\gamma_0\gamma_2)_{KS}\,\mathcal{D}^{-1(\alpha)}(z,t;0,0)_{PS}\mathcal{D}^{-1(\beta)}(r,0;z,t)_{KL}$$

γ_5-hermiticity

$$= (\gamma_5)_{PL}\,(\gamma_2\gamma_0\Gamma\gamma_0\gamma_2)_{KS}\left(\gamma_5\left(\mathcal{D}^{-1(\tilde{\alpha})}(0,0;z,t)\right)^\dagger\gamma_5\right)_{PS}\left(\gamma_5\left(\mathcal{D}^{-1(\tilde{\beta})}(z,t;r,0)\right)^\dagger\gamma_5\right)_{KL}$$

$$= \left((\gamma_5)_{DC}\,(\gamma_5\gamma_2\gamma_0\Gamma\gamma_0\gamma_2\gamma_5)_{VU}^*\,\mathcal{D}^{-1(\tilde{\alpha})}(0,0;z,t)_{UD}\mathcal{D}^{-1(\tilde{\beta})}(z,t;r,0)_{CV}\right)^* \tag{A.28}$$

Symmetry transformation rules:

- complex conjugate

- $\alpha \rightarrow \tilde{\alpha}$, $\beta \rightarrow \tilde{\beta}$, i.e. $u\bar{u} \leftrightarrow d\bar{d}$, $u\bar{d} \leftrightarrow d\bar{u}$

- $\Gamma \rightarrow (\gamma_5\gamma_2\gamma_0\Gamma\gamma_0\gamma_2\gamma_5)^*$, (no change, if $\Gamma = \gamma_0$ or $\Gamma = \gamma_5$)

Twisted mass time reversal

$$\boxed{\mathcal{D}_{AB}^{-1(\alpha)}(x_1,t_1;x_2,t_2) \longrightarrow \left(\gamma_0\gamma_5\mathcal{D}^{-1(\tilde{\alpha})}(x_1,-t_1;x_2,-t_2)\gamma_5\gamma_0\right)_{AB}} \tag{A.29}$$

$$(\gamma_5)_{DC}\,(\Gamma)_{VU}\,\mathcal{D}_{UD}^{-1(\alpha)}(0,0;z,t)\mathcal{D}_{CV}^{-1(\beta)}(z,t;r,0)$$

$$\rightarrow (\gamma_5)_{DC}\,(\Gamma)_{VU}\left(\gamma_0\gamma_5\mathcal{D}^{-1(\tilde{\alpha})}(0,0;z,-t)\gamma_5\gamma_0\right)_{UD}\left(\gamma_0\gamma_5\mathcal{D}^{-1(\tilde{\beta})}(z,-t;r,0)\gamma_5\gamma_0\right)_{CV}$$

$$= -(\gamma_5)_{KS}\,(\gamma_5\gamma_0\Gamma\gamma_0\gamma_5)_{PL}\,\mathcal{D}^{-1(\tilde{\alpha})}(0,0;z,-t)_{LK}\mathcal{D}^{-1(\tilde{\beta})}(z,-t;r,0)_{SP}$$

$$= -(\gamma_5)_{DC}\,(\gamma_5\gamma_0\Gamma\gamma_0\gamma_5)_{VU}\,\mathcal{D}^{-1(\tilde{\alpha})}(0,0;z,-t)_{UD}\mathcal{D}^{-1(\tilde{\beta})}(z,-t;r,0)_{CV} \tag{A.30}$$

Symmetry transformation rules:

- $t \rightarrow -t$

- $\alpha \rightarrow \tilde{\alpha}$, $\beta \rightarrow \tilde{\beta}$, i.e. $u\bar{u} \leftrightarrow d\bar{d}$, $u\bar{d} \leftrightarrow d\bar{u}$

- $\Gamma \rightarrow -(\gamma_5\gamma_0\Gamma\gamma_0\gamma_5)$, (no change, if $\Gamma = \gamma_0$ or $\Gamma = \gamma_5$)

π cubic rotation in $j-k$ plane

$$\boxed{\mathcal{D}_{AB}^{-1(\alpha)}(x_1,t_1;x_2,t_2) \longrightarrow \left(\gamma_j\gamma_k\mathcal{D}^{-1(\alpha)}(-x_1,t_1;-x_2,t_2)\gamma_k\gamma_j\right)_{AB}} \tag{A.31}$$

A. Appendix

2-3 plane

$$(\gamma_5)_{DC} \, (\Gamma)_{VU} \, \mathcal{D}_{UD}^{-1(\alpha)}(0,0;z,t)\mathcal{D}_{CV}^{-1(\beta)}(z,t;r,0)$$
$$\rightarrow (\gamma_5)_{DC} \, (\Gamma)_{VU} \left(\gamma_2\gamma_3\mathcal{D}^{-1(\alpha)}(0,0;z,t)\gamma_3\gamma_2 \right)_{UD} \left(\gamma_2\gamma_3\mathcal{D}^{-1(\beta)}(z,t;-r,0)\gamma_3\gamma_2 \right)_{CV}$$
$$\rightarrow (\gamma_3\gamma_2\gamma_5\gamma_2\gamma_3)_{KS} \, (\gamma_3\gamma_2\Gamma\gamma_2\gamma_3)_{PL} \, \mathcal{D}^{-1(\alpha)}(0,0;z,t)_{LK}\mathcal{D}^{-1(\beta)}(z,t;-r,0)_{SP}$$

shift $-r \rightarrow 0$

$$\rightarrow (\gamma_5)_{KS} \, (\gamma_3\gamma_2\Gamma\gamma_2\gamma_3)_{PL} \, \mathcal{D}^{-1(\alpha)}(r,0;z,t)_{LK}\mathcal{D}^{-1(\beta)}(z,t;0,0)_{SP}$$

γ_5-hermiticity

$$= (\gamma_5)_{KS} \, (\gamma_5\gamma_3\gamma_2\Gamma\gamma_2\gamma_3\gamma_5)_{PL} \left(\gamma_5 \left(\mathcal{D}^{-1(\tilde{\alpha})}(z,t;r,0) \right)^\dagger \gamma_5 \right)_{LK} \left(\gamma_5 \left(\mathcal{D}^{-1(\tilde{\beta})}(0,0;z,t) \right)^\dagger \gamma_5 \right)_{SP}$$

$$= \left((\gamma_5)_{CD} \, (\gamma_5\gamma_3\gamma_2\Gamma\gamma_2\gamma_3\gamma_5)_{UV}^* \, \mathcal{D}^{-1(\tilde{\beta})}(0,0;z,t)_{UD}\mathcal{D}^{-1(\tilde{\alpha})}(z,t;r,0)_{CV} \right)^*$$

$$\tag{A.32}$$

Symmetry transformation rules:

- complex conjugate

- $\alpha \rightarrow \tilde{\beta}$, $\beta \rightarrow \tilde{\alpha}$, i.e. $u\bar{u} \leftrightarrow d\bar{d}$, $u\bar{d}, d\bar{u}$: no change

- $\Gamma \rightarrow (\gamma_5\gamma_3\gamma_2\Gamma\gamma_2\gamma_3\gamma_5)^*$, (no change, if $\Gamma = \gamma_0$ or $\Gamma = \gamma_5$)

1-3 plane (analogous to 2-3-plane)

Symmetry transformation rules:

- complex conjugate

- $\alpha \rightarrow \tilde{\beta}$, $\beta \rightarrow \tilde{\alpha}$, i.e. $u\bar{u} \leftrightarrow d\bar{d}$, $u\bar{d}, d\bar{u}$: no change

$\pi/2$ cubic rotation around 1-axis $\left(\mathcal{R}_1(-\frac{\pi}{2}) \right)$

$$\boxed{ \begin{aligned} &\mathcal{D}_{AB}^{-1(\alpha)}(x_1,t_1;x_2,t_2) \longrightarrow \left((\frac{1}{\sqrt{2}}\mathbb{1} - \frac{1}{\sqrt{2}}\gamma_2\gamma_3)\mathcal{D}^{-1(\alpha)}(\tilde{x}_1,t_1;\tilde{x}_2,t_2)(\frac{1}{\sqrt{2}}\mathbb{1} + \frac{1}{\sqrt{2}}\gamma_2\gamma_3) \right)_{AB} \\ &\text{with } x = \begin{pmatrix} 0 \\ 0 \\ x \end{pmatrix} \text{ and } \tilde{x} = \begin{pmatrix} 0 \\ x \\ 0 \end{pmatrix} \end{aligned} }$$

$$\tag{A.33}$$

Symmetry transformation rules:

- relates 2 and 3 direction

$\pi/2$ cubic rotation around 2-axis ($\mathcal{R}_2(\frac{\pi}{2})$)

$$\boxed{\begin{aligned} &\mathcal{D}_{AB}^{-1(\alpha)}(x_1,t_1;x_2,t_2) \longrightarrow \left((\frac{1}{\sqrt{2}}\mathbb{1}-\frac{1}{\sqrt{2}}\gamma_1\gamma_3)\mathcal{D}^{-1(\alpha)}(\tilde{x}_1,t_1;\tilde{x}_2,t_2)(\frac{1}{\sqrt{2}}\mathbb{1}+\frac{1}{\sqrt{2}}\gamma_1\gamma_3)\right)_{AB} \\ &\text{with } x=\begin{pmatrix}0\\0\\x\end{pmatrix} \text{ and } \tilde{x}=\begin{pmatrix}x\\0\\0\end{pmatrix} \end{aligned}}$$

(A.34)

Symmetry transformation rules:

- relates 1 and 3 direction

$\pi/2$ cubic rotation around 3-axis ($\mathcal{R}_3(\frac{\pi}{2})$)

$$\boxed{\begin{aligned} &\mathcal{D}_{AB}^{-1(\alpha)}(x_1,t_1;x_2,t_2) \longrightarrow \left((\frac{1}{\sqrt{2}}\mathbb{1}+\frac{1}{\sqrt{2}}\gamma_1\gamma_2)\mathcal{D}^{-1(\alpha)}(\tilde{x}_1,t_1;\tilde{x}_2,t_2)(\frac{1}{\sqrt{2}}\mathbb{1}-\frac{1}{\sqrt{2}}\gamma_1\gamma_2)\right)_{AB} \\ &\text{with } x=\begin{pmatrix}0\\0\\x\end{pmatrix}=\tilde{x} \end{aligned}}$$

(A.35)

Symmetry transformation rules:

- Not important since $|j_z|=0$.

Twisted mass γ_5-hermiticity

$$\boxed{\mathcal{D}_{AB}^{-1(\alpha)}(x_1,t_1;x_2,t_2) \longrightarrow \left(\gamma_5\left(\mathcal{D}^{-1(\tilde{\alpha})}(x_2,t_2;x_1,t_1)\right)^{\dagger}\gamma_5\right)_{AB}}$$

(A.36)

$$\begin{aligned} &(\gamma_5)_{DC}\,(\Gamma)_{VU}\,\mathcal{D}_{UD}^{-1(\alpha)}(0,0;z,t)\mathcal{D}_{CV}^{-1(\beta)}(z,t;r,0) \\ &\to (\gamma_5)_{DC}\,(\Gamma)_{VU}\left(\gamma_5\left(\mathcal{D}^{-1(\tilde{\alpha})}(z,t;0,0)\right)^{\dagger}\gamma_5\right)_{UD}\left(\gamma_5\left(\mathcal{D}^{-1(\tilde{\beta})}(r,0;z,t)\right)^{\dagger}\gamma_5\right)_{CV} \\ &= (\gamma_5\gamma_5\gamma_5)_{MI}\,(\gamma_5\Gamma\gamma_5)_{HL}\left(\mathcal{D}^{-1(\tilde{\alpha})}(z,t;0,0)\right)^{\dagger}_{LM}\left(\mathcal{D}^{-1(\tilde{\beta})}(r,0;z,t)\right)^{\dagger}_{IH} \\ &= \left((\gamma_5)_{MI}\,(\gamma_5\Gamma\gamma_5)^*_{HL}\,\mathcal{D}^{-1(\tilde{\alpha})}(z,t;0,0)_{ML}\mathcal{D}^{-1(\tilde{\beta})}(r,0;z,t)_{HI}\right)^* \\ &\text{twisted-mass parity} \\ &= \left((\gamma_5)_{MI}\,(\gamma_5\Gamma\gamma_5)^*_{HL}\left(\gamma_0\mathcal{D}^{-1(\alpha)}(z,t;0,0)\gamma_0\right)_{ML}\left(\gamma_0\mathcal{D}^{-1(\beta)}(-r,0;z,t)\gamma_0\right)_{HI}\right)^* \\ &= \left((\gamma_0\gamma_5\gamma_0)_{ST}\,(\gamma_0\gamma_5\Gamma\gamma_5\gamma_0)^*_{RP}\,\mathcal{D}_{SP}^{-1(\alpha)}(z,t;0,0)\mathcal{D}_{RT}^{-1(\beta)}(-r,0;z,t)\right)^* \\ &\text{shift } -r\to 0 \\ &= -\left((\gamma_5)_{ST}\,(\gamma_0\gamma_5\Gamma\gamma_5\gamma_0)^*_{RP}\,\mathcal{D}_{SP}^{-1(\alpha)}(z,t;r,0)\mathcal{D}_{RT}^{-1(\beta)}(0,0;z,t)\right)^* \\ &= -\left((\gamma_5)_{DC}\,(\Gamma)_{VU}\,\mathcal{D}_{UD}^{-1(\beta)}(0,0;z,t)\mathcal{D}_{CV}^{-1(\alpha)}(z,t;r,0)\right)^* \end{aligned}$$

(A.37)

Symmetry transformation rules:

A. Appendix

- complex conjugate
- $\alpha \leftrightarrow \beta$, i.e. $u\bar{u}, d\bar{d}$: no change, $u\bar{d} \leftrightarrow d\bar{u}$
- $\Gamma \rightarrow -(\gamma_0\gamma_5\Gamma\gamma_5\gamma_0)^*$, (no change, if $\Gamma = \gamma_0$ or $\Gamma = \gamma_5$)

A.3.3. Symmetry checks of C_{22}

The spin-dependent (dynamical quark) part of C_{22} reads (the sum over z and v is implicit):

$$C_{22}^{\text{light}}(r,t) = (\gamma_5)_{DC}\,(\gamma_5)_{XY}\,\mathcal{D}_{YD}^{-1(\alpha)}(v,0;z,t)\mathcal{D}_{CX}^{-1(\beta)}(z,t;v,0) \tag{A.38}$$

Twisted mass parity

$$\boxed{\mathcal{D}_{AB}^{-1(\alpha)}(x_1,t_1;x_2,t_2) \longrightarrow \left(\gamma_0\mathcal{D}^{-1(\tilde{\alpha})}(-x_1,t_1;-x_2,t_2)\gamma_0\right)_{AB}} \tag{A.39}$$

$$
\begin{aligned}
&(\gamma_5)_{DC}\,(\gamma_5)_{XY}\,\mathcal{D}_{YD}^{-1(\alpha)}(v,0;z,t)\mathcal{D}_{CX}^{-1(\beta)}(z,t;v,0) \\
&\longrightarrow (\gamma_5)_{DC}\,(\gamma_5)_{XY}\left(\gamma_0\mathcal{D}^{-1(\tilde{\alpha})}(v,0;z,t)\gamma_0\right)_{YD}\left(\gamma_0\mathcal{D}^{-1(\tilde{\beta})}(z,t;v,0)\gamma_0\right)_{CX} \\
&= (\gamma_5)_{DC}\,(\gamma_5)_{XY}\,\mathcal{D}_{YD}^{-1(\tilde{\alpha})}(v,0;z,t)\mathcal{D}_{CX}^{-1(\tilde{\beta})}(z,t;v,0)
\end{aligned} \tag{A.40}
$$

Symmetry transformation rules:

- $\alpha \rightarrow \tilde{\alpha}, \beta \rightarrow \tilde{\beta}$, i.e. $u\bar{u} \leftrightarrow d\bar{d}, u\bar{d} \leftrightarrow d\bar{u}$

Charge conjugation

$$\boxed{\mathcal{D}_{AB}^{-1(\alpha)}(x_1,t_1;x_2,t_2) \longrightarrow \left(\gamma_0\gamma_2\left(\mathcal{D}^{-1(\alpha)}(x_2,t_2;x_1,t_1)\right)^T\gamma_2\gamma_0\right)_{AB}} \tag{A.41}$$

$$
\begin{aligned}
&(\gamma_5)_{DC}\,(\gamma_5)_{XY}\,\mathcal{D}_{YD}^{-1(\alpha)}(v,0;z,t)\mathcal{D}_{CX}^{-1(\beta)}(z,t;v,0) \\
&\longrightarrow (\gamma_5)_{DC}\,(\gamma_5)_{XY}\left(\gamma_0\gamma_2\mathcal{D}^{-1(\tilde{\alpha})}(z,t;v,0)\gamma_2\gamma_0\right)_{YD}\left(\gamma_0\gamma_2\mathcal{D}^{-1(\tilde{\beta})}(v,0;z,t)\gamma_2\gamma_0\right)_{CX} \\
&= (\gamma_5)_{DC}\,(\gamma_5)_{XY}\,\mathcal{D}_{YD}^{-1(\beta)}(v,0;z,t)\mathcal{D}_{CX}^{-1(\alpha)}(z,t;v,0)
\end{aligned} \tag{A.42}
$$

Symmetry transformation rules:

- $\alpha \leftrightarrow \beta$, i.e. $u\bar{u}, d\bar{d}$: no change, $u\bar{d} \leftrightarrow d\bar{u}$

Time reversal

$$\boxed{\mathcal{D}_{AB}^{-1(\alpha)}(x_1,t_1;x_2,t_2) \longrightarrow \left(\gamma_0\gamma_5\mathcal{D}^{-1(\tilde{\alpha})}(x_1,-t_1;x_2,-t_2)\gamma_5\gamma_0\right)_{AB}} \tag{A.43}$$

$$
\begin{aligned}
&(\gamma_5)_{DC}\,(\gamma_5)_{XY}\,\mathcal{D}_{YD}^{-1(\alpha)}(v,0;z,t)\mathcal{D}_{CX}^{-1(\beta)}(z,t;v,0) \\
&\longrightarrow (\gamma_5)_{DC}\,(\gamma_0\gamma_5)_{XY}\left(\gamma_0\mathcal{D}^{-1(\tilde{\alpha})}(v,0;z,-t)\gamma_5\gamma_0\right)_{YD}\left(\gamma_0\gamma_5\mathcal{D}^{-1(\tilde{\beta})}(z,-t;v,0)\gamma_5\gamma_0\right)_{CX} \\
&= (\gamma_5)_{DC}\,(\gamma_5)_{XY}\,\mathcal{D}_{YD}^{-1(\tilde{\alpha})}(v,0;z,-t)\mathcal{D}_{CX}^{-1(\tilde{\beta})}(z,-t;v,0)
\end{aligned}
$$

$$\tag{A.44}$$

Symmetry transformation rules:

- $t \to -t$

- $\alpha \to \tilde{\alpha}$, $\beta \to \tilde{\beta}$, i.e. $u\bar{u} \leftrightarrow d\bar{d}$, $u\bar{d} \leftrightarrow d\bar{u}$

Twisted mass γ_5-hermiticity

$$\boxed{\mathcal{D}_{AB}^{-1(\alpha)}(x_1, t_1; x_2, t_2) \longrightarrow \left(\gamma_5 \left(\mathcal{D}^{-1(\tilde{\alpha})}(x_2, t_2; x_1, t_1)\right)^\dagger \gamma_5\right)_{AB}}$$
(A.45)

$$
\begin{aligned}
(\gamma_5)_{DC} \, (\gamma_5)_{XY} \, &\mathcal{D}_{YD}^{-1(\alpha)}(v, 0; z, t) \mathcal{D}_{CX}^{-1(\beta)}(z, t; v, 0) \\
\longrightarrow (\gamma_5)_{DC} \, (\gamma_5)_{XY} &\left(\gamma_5 \left(\mathcal{D}^{-1(\tilde{\alpha})}(z, t; v, 0)\right)^\dagger \gamma_5\right)_{YD} \left(\gamma_5 \left(\mathcal{D}^{-1(\tilde{\beta})}(v, 0; z, t)\right)^\dagger \gamma_5\right)_{CX} \\
= (\gamma_5)_{DC} \, (\gamma_5)_{XY} &\left(\mathcal{D}^{-1(\tilde{\alpha})}(z, t; v, 0)\right)_{YD}^\dagger \left(\mathcal{D}^{-1(\tilde{\beta})}(v, 0; z, t)\right)_{CX}^\dagger \\
= \Big((\gamma_5)_{DC} \, (\gamma_5)_{XY} &\mathcal{D}^{-1(\tilde{\alpha})}(z, t; v, 0)_{DY} \mathcal{D}^{-1(\tilde{\beta})}(v, 0; z, t)_{XC}\Big)^* \\
= \Big((\gamma_5)_{DC} \, (\gamma_5)_{XY} &\mathcal{D}^{-1(\tilde{\beta})}(v, 0; z, t)_{CX} \mathcal{D}^{-1(\tilde{\alpha})}(z, t; v, 0)_{YD}\Big)^*
\end{aligned}
$$
(A.46)

Symmetry transformation rules:

- complex conjugate

- $\alpha \to \tilde{\beta}$, $\beta \to \tilde{\alpha}$, i.e. $u\bar{u} \leftrightarrow d\bar{d}$, $u\bar{d}, d\bar{u}$: no change

π and $\pi/2$ cubic rotations

- no change

A.4. Comparison of the BB system with the hydrogen atom

In Chapter 5 we state an analytical expression for the BB four-quark potential (cf. Equation (5.5)):

$$V(r) = -\frac{\alpha}{r} \mathrm{e}^{-\left(\frac{r}{d}\right)^2}.$$
(A.47)

Compared to (5.5) we omit the constant V_0, since it represents energy shift which is irrelevant here. If the mass of the b-quark m_b is large, the wave function of the system is highly located. Therefore it will feel essentially the short distance part of the potential, i.e. the Coulomb-like part

$$V_C(r) = -\frac{\alpha}{r}.$$
(A.48)

The radial part of the Schrödinger equation of the hydrogen atom in an s-wave (where the strongest binding is expected) reads:

$$\left(-\frac{1}{2\mu}\frac{d^2}{dr^2} - \frac{Ze^2}{4\pi\epsilon_0 r}\right)\psi = E\psi$$
(A.49)

with $\mu = \frac{m_b}{2}$. Comparison to Equation (A.48) yields $\frac{Ze^2}{4\pi\epsilon_0 r} \equiv \alpha$. The theoretical description of the hydrogen atom is well-known, cf. e.g. [72]. The binding energy of the n-th state is given by

$$E^{(n)} = -\left(\frac{Ze^2}{4\pi\epsilon_0}\right)^2 \frac{m_e}{2n^2}. \tag{A.50}$$

In case of a BB ground state potential $Z = 1$, $n = 1$ and $m_e = \mu$, therefore

$$E^{(1)} = -\frac{\alpha^2}{4} m_b. \tag{A.51}$$

We use results from Section 5.4.3 where we obtained parameters of the expression (A.47) $\alpha = 0.36$ and $d/a = 6.10$ [$a = 0.079\,\mathrm{fm}$]. In the following, we keep these parameters α and d fixed and solve the Schrödinger equation several times, replacing the reduced mass μ by $\kappa\mu$:

$$\left(-\frac{1}{2\kappa\mu}\frac{d^2}{dr^2} - \frac{Ze^2}{4\pi\epsilon_0 r}\right)\psi = E_{\mathrm{num}}^{(1)}\psi \tag{A.52}$$

with $\kappa \in [1, 10]$. This means, we formally increase the b quark mass. For a larger b quark mass one expects a better agreement of the theoretically calculated binding energy $E^{(1)}$ (cf. (A.51)) and the value $E_{\mathrm{num}}^{(1)}$ numerically obtained from the Schrödinger equation (A.52). The reason is that the heavier the b quark, the better Equation (A.48) describes the BB potential and therefore Equation (A.51) describes the binding energy. In Figure A.1 one can see that the numerically obtained binding energy $E_{\mathrm{num}}^{(1)}$ is is in agreement with the theory value $E^{(1)}$ (A.51) for various values of κ. As expected, the agreement improves for larger κ.
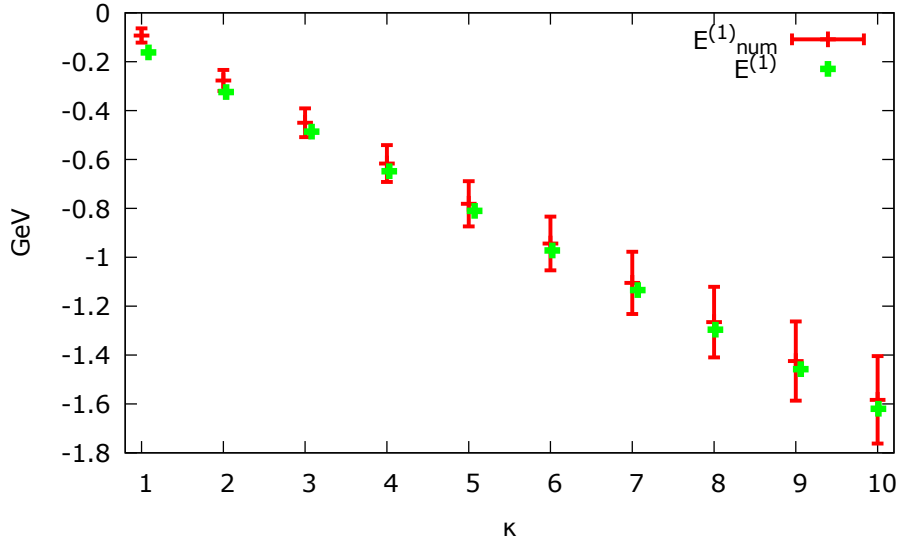

Figure A.1.: Comparison of $E^{(1)}$ from Equation (A.51) (green points) with binding energies $E_{\mathrm{num}}^{(1)}$ obtained by solving (A.52) (red points) for various values of κ.

Bibliography

[1] P. Bicudo, M. Cardoso, A. Peters, M. Pflaumer, and M. Wagner, "$ud\bar{b}\bar{b}$ tetraquark resonances with lattice QCD potentials and the Born-Oppenheimer approximation," `arXiv:1704.02383 [hep-lat]`.

[2] **Particle Data Group** Collaboration, C. Patrignani *et al.*, "Review of Particle Physics," *Chin. Phys.* **C40** no. 10, (2016) 100001.

[3] **Belle** Collaboration, K. Abe *et al.*, "Observation of a new narrow charmonium state in exclusive $B\pm \to K \pm \pi + \pi - J/\psi$ decays," in *Proceedings, 21st International Symposium on Lepton and Photon Interactions at High Energies (LP 03): Batavia, ILL, August 11-16, 2003*. 2003. `arXiv:hep-ex/0308029 [hep-ex]`.

[4] **Belle** Collaboration, A. Bondar *et al.*, "Observation of two charged bottomonium-like resonances in Y(5S) decays," *Phys. Rev. Lett.* **108** (2012) 122001, `arXiv:1110.2251 [hep-ex]`.

[5] P. Bicudo, K. Cichy, A. Peters, and M. Wagner, "BB interactions with static bottom quarks from Lattice QCD," *Phys. Rev.* **D93** no. 3, (2016) 034501, `arXiv:1510.03441 [hep-lat]`.

[6] P. Bicudo, K. Cichy, A. Peters, B. Wagenbach, and M. Wagner, "Evidence for the existence of $ud\bar{b}\bar{b}$ and the non-existence of $ss\bar{b}\bar{b}$ and $cc\bar{b}\bar{b}$ tetraquarks from lattice QCD," *Phys. Rev.* **D92** no. 1, (2015) 014507, `arXiv:1505.00613 [hep-lat]`.

[7] A. Peters, P. Bicudo, K. Cichy, B. Wagenbach, and M. Wagner, "Exploring possibly existing $qq\bar{b}\bar{b}$ tetraquark states with $qq = ud, ss, cc$," *PoS* **LATTICE2015** (2016) 095, `arXiv:1508.00343 [hep-lat]`.

[8] A. Peters, P. Bicudo, K. Cichy, and M. Wagner, "Investigation of $B\bar{B}$ four-quark systems using lattice QCD," *J. Phys. Conf. Ser.* **742** no. 1, (2016) 012006, `arXiv:1602.07621 [hep-lat]`.

[9] A. Peters, P. Bicudo, L. Leskovec, S. Meinel, and M. Wagner, "Lattice QCD study of heavy-heavy-light-light tetraquark candidates," *PoS* **LATTICE2016** (2016) 104, `arXiv:1609.00181 [hep-lat]`.

[10] C. Gattringer and C. B. Lang, "Quantum chromodynamics on the lattice," *Lect. Notes Phys.* **788** (2010) 1–343.

[11] C. Davies, "Lattice QCD," in *Heavy flavor physics: Theory and experimental results in heavy quark physics and CP violation. Proceedings, 55th Scottish Universities Summer School in Physics, SUSSP 2001, St. Andrews, UK, August 7-23, 2001*, pp. 105–146. 2002. `arXiv:hep-ph/0205181 [hep-ph]`.

Bibliography

[12] L. Ryder, *Quantum Field Theory*. Cambridge University Press, 1996.

[13] M. E. Peskin and D. V. Schroeder, *An Introduction to Quantum Field Theory; 1995 ed.*
Westview, Boulder, CO, 1995. `https://cds.cern.ch/record/257493`.

[14] A. Zee, *Quantum Field Theory in a Nutshell*. Nutshell handbook. Princeton Univ. Press,
Princeton, NJ, 2003. `https://cds.cern.ch/record/706825`.

[15] T. Misumi, "New fermion discretizations and their applications," *PoS* **LATTICE2012**
(2012) 005, `arXiv:1211.6999 [hep-lat]`.

[16] A. S. Kronfeld, "Lattice Gauge Theory with Staggered Fermions: How, Where, and Why
(Not)," *PoS* **LAT2007** (2007) 016, `arXiv:0711.0699 [hep-lat]`.

[17] K. Jansen, "Domain wall fermions and chiral gauge theories," *Phys. Rept.* **273** (1996)
1–54, `arXiv:hep-lat/9410018 [hep-lat]`.

[18] R. Narayanan, "Tata lectures on overlap fermions," `arXiv:1103.4588 [hep-lat]`.

[19] A. Shindler, "Twisted mass lattice QCD," *Phys. Rept.* **461** (2008) 37–110,
`arXiv:0707.4093 [hep-lat]`.

[20] K. Jansen and C. Urbach, "tmLQCD: A Program suite to simulate Wilson Twisted mass
Lattice QCD," *Comput. Phys. Commun.* **180** (2009) 2717–2738, `arXiv:0905.3331`
`[hep-lat]`.

[21] R. Frezzotti and G. C. Rossi, "Chirally improving Wilson fermions. 1. O(a)
improvement," *JHEP* **08** (2004) 007, `arXiv:hep-lat/0306014 [hep-lat]`.

[22] S. Aoki and O. Bar, "Twisted-mass QCD, O(a) improvement and Wilson chiral
perturbation theory," *Phys. Rev.* **D70** (2004) 116011, `arXiv:hep-lat/0409006`
`[hep-lat]`.

[23] R. Frezzotti and G. C. Rossi, "Twisted mass lattice QCD with mass nondegenerate
quarks," *Nucl. Phys. Proc. Suppl.* **128** (2004) 193–202, `arXiv:hep-lat/0311008`
`[hep-lat]`.

[24] M. F. L. Golterman, "How good is the quenched approximation of QCD?," *Pramana* **45**
(1995) S141–S154, `arXiv:hep-lat/9405002 [hep-lat]`.

[25] S. Duane, A. Kennedy, B. J. Pendleton, and D. Roweth, "Hybrid monte carlo," *Physics
Letters B* **195** no. 2, (1987) 216 – 222.

[26] **JLQCD, CP-PACS** Collaboration, A. Ukawa, "Computational cost of full QCD
simulations experienced by CP-PACS and JLQCD Collaborations," *Nucl. Phys. Proc.
Suppl.* **106** (2002) 195–196.

[27] "Floating point operations per second."
`https://de.wikipedia.org/wiki/Floating_Point_Operations_Per_Second`.
Accessed: 2017-05-08.

[28] F. Knechtli *et al.*, "Physical and cut-off effects of heavy sea quarks," *PoS* **LATTICE2014**
(2014) 288, `arXiv:1411.1239 [hep-lat]`.

[29] S. Hashimoto and T. Onogi, "Heavy quarks on the lattice," *Ann. Rev. Nucl. Part. Sci.* **54** (2004) 451–486, `arXiv:hep-ph/0407221 [hep-ph]`.

[30] C. McNeile, C. T. H. Davies, E. Follana, K. Hornbostel, and G. P. Lepage, "Heavy meson masses and decay constants from relativistic heavy quarks in full lattice QCD," *Phys. Rev.* **D86** (2012) 074503, `arXiv:1207.0994 [hep-lat]`.

[31] J. M. Flynn *et al.*, "The $B^*B\pi$ coupling with relativistic heavy quarks," *PoS* **LATTICE2013** (2014) 408, `arXiv:1311.2251 [hep-lat]`.

[32] A. V. Manohar, *Heavy Quark Physics*. Cambridge University Press, 2000.

[33] S. Meinel, *Heavy quark physics on the lattice with improved nonrelativistic actions*. PhD thesis, University of Cambridge, 2009.

[34] G. P. Lepage, L. Magnea, C. Nakhleh, U. Magnea, and K. Hornbostel, "Improved nonrelativistic QCD for heavy quark physics," *Phys. Rev.* **D46** (1992) 4052–4067, `arXiv:hep-lat/9205007 [hep-lat]`.

[35] B. A. Thacker and G. P. Lepage, "Heavy quark bound states in lattice QCD," *Phys. Rev.* **D43** (1991) 196–208.

[36] E. Eichten, "Heavy quarks on the lattice," *Nuclear Physics B - Proceedings Supplements* **4** (1988) 170 – 177.

[37] E. Eichten and B. Hill, "An effective field theory for the calculation of matrix elements involving heavy quarks," *Physics Letters B* **234** no. 4, (1990) 511 – 516.

[38] A. Abdel-Rehim, C. Alexandrou, J. Berlin, M. Dalla Brida, J. Finkenrath, and M. Wagner, "Investigating efficient methods for computing four-quark correlation functions," `arXiv:1701.07228 [hep-lat]`.

[39] S. Bernardson, P. McCarty, and C. Thron, "Monte Carlo methods for estimating linear combinations of inverse matrix entries in lattice QCD," *Comput. Phys. Commun.* **78** (1993) 256–264.

[40] S.-J. Dong and K.-F. Liu, "Stochastic estimation with Z(2) noise," *Phys. Lett.* **B328** (1994) 130–136, `arXiv:hep-lat/9308015 [hep-lat]`.

[41] **UKQCD** Collaboration, M. Foster and C. Michael, "Quark mass dependence of hadron masses from lattice QCD," *Phys. Rev.* **D59** (1999) 074503, `arXiv:hep-lat/9810021 [hep-lat]`.

[42] **UKQCD** Collaboration, C. McNeile and C. Michael, "Decay width of light quark hybrid meson from the lattice," *Phys. Rev.* **D73** (2006) 074506, `arXiv:hep-lat/0603007 [hep-lat]`.

[43] M. Albanese *et al.*, "Glueball masses and string tension in lattice qcd," *Physics Letters B* **192** no. 1, (1987) 163 – 169.

[44] S. Güsken, "A study of smearing techniques for hadron correlation functions," *Nuclear Physics B - Proceedings Supplements* **17** (1990) 361 – 364.

Bibliography

[45] A. Hasenfratz and F. Knechtli, "Simulation of dynamical fermions with smeared links," *Comput. Phys. Commun.* **148** (2002) 81–86, arXiv:hep-lat/0203010 [hep-lat].

[46] **ETM** Collaboration, K. Jansen, C. Michael, A. Shindler, and M. Wagner, "The Static-light meson spectrum from twisted mass lattice QCD," *JHEP* **12** (2008) 058, arXiv:0810.1843 [hep-lat].

[47] **ETM** Collaboration, C. Michael, A. Shindler, and M. Wagner, "The continuum limit of the static-light meson spectrum," *JHEP* **08** (2010) 009, arXiv:1004.4235 [hep-lat].

[48] B. Wagenbach, "Lattice investigation of heavy meson interactions," Master's thesis, Goethe-Universität Frankfurt am Main, 2014.

[49] B. A. Gelman and S. Nussinov, "Does a narrow tetraquark cc anti-u anti-d state exist?," *Phys. Lett.* **B551** (2003) 296–304, arXiv:hep-ph/0209095 [hep-ph].

[50] M. Born and R. Oppenheimer, "Zur quantentheorie der molekeln," *Annalen der Physik* **389** no. 20, (1927) 457–484. http://dx.doi.org/10.1002/andp.19273892002.

[51] T. Fließbach, *Lehrbuch zur Theoretischen Physik 3. Quantenmechanik*. Spektrum Akademischer Verlag, 1999.

[52] Y. Koma and M. Koma, "Spin-dependent potentials from lattice QCD," *Nucl. Phys.* **B769** (2007) 79–107, arXiv:hep-lat/0609078 [hep-lat].

[53] **ETM** Collaboration, R. Baron *et al.*, "Light Meson Physics from Maximally Twisted Mass Lattice QCD," *JHEP* **08** (2010) 097, arXiv:0911.5061 [hep-lat].

[54] **ETM** Collaboration, P. Boucaud *et al.*, "Dynamical Twisted Mass Fermions with Light Quarks: Simulation and Analysis Details," *Comput. Phys. Commun.* **179** (2008) 695–715, arXiv:0803.0224 [hep-lat].

[55] **ETM** Collaboration, P. Boucaud *et al.*, "Dynamical twisted mass fermions with light quarks," *Phys. Lett.* **B650** (2007) 304–311, arXiv:hep-lat/0701012 [hep-lat].

[56] **ETM** Collaboration, K. Jansen, F. Karbstein, A. Nagy, and M. Wagner, "$\Lambda_{\overline{MS}}$ from the static potential for QCD with $n_f = 2$ dynamical quark flavors," *JHEP* **01** (2012) 025, arXiv:1110.6859 [hep-ph].

[57] **ETM** Collaboration, M. Wagner, "Forces between static-light mesons," *PoS* **LATTICE2010** (2010) 162, arXiv:1008.1538 [hep-lat].

[58] **ETM** Collaboration, M. Wagner, "Static-static-light-light tetraquarks in lattice QCD," *Acta Phys. Polon. Supp.* **4** (2011) 747–752, arXiv:1103.5147 [hep-lat].

[59] K. Cichy, V. Drach, E. Garcia-Ramos, G. Herdoiza, and K. Jansen, "Overlap valence quarks on a twisted mass sea: a case study for mixed action Lattice QCD," *Nucl. Phys.* **B869** (2013) 131–163, arXiv:1211.1605 [hep-lat].

[60] P. Bicudo, J. Scheunert, and M. Wagner, "Including heavy spin effects in the prediction of a $\bar{b}\bar{b}ud$ tetraquark with lattice QCD potentials," *Phys. Rev.* **D95** no. 3, (2017) 034502, arXiv:1612.02758 [hep-lat].

[61] **ETM** Collaboration, P. Bicudo and M. Wagner, "Lattice QCD signal for a bottom-bottom tetraquark," *Phys. Rev.* **D87** no. 11, (2013) 114511, `arXiv:1209.6274 [hep-ph]`.

[62] M. Pflaumer, "Resonanzen in $\bar{b}\bar{b}ud$-Tetraquark-Systemen basierend auf statisch-leichten Gitter-QCD-Vier-Quark-Potentialen," Bachelor's thesis, Goethe-Universität Frankfurt am Main, 2016.

[63] **ETM** Collaboration, M. Wagner and C. Wiese, "The static-light baryon spectrum from twisted mass lattice QCD," *JHEP* **07** (2011) 016, `arXiv:1104.4921 [hep-lat]`.

[64] A. Francis, R. J. Hudspith, R. Lewis, and K. Maltman, "Lattice Prediction for Deeply Bound Doubly Heavy Tetraquarks," *Phys. Rev. Lett.* **118** no. 14, (2017) 142001, `arXiv:1607.05214 [hep-lat]`.

[65] Z. S. Brown, W. Detmold, S. Meinel, and K. Orginos, "Charmed bottom baryon spectroscopy from lattice QCD," *Phys. Rev.* **D90** no. 9, (2014) 094507, `arXiv:1409.0497 [hep-lat]`.

[66] B. Blossier, M. Della Morte, G. von Hippel, T. Mendes, and R. Sommer, "On the generalized eigenvalue method for energies and matrix elements in lattice field theory," *JHEP* **04** (2009) 094, `arXiv:0902.1265 [hep-lat]`.

[67] E. Braaten, "Towards a Theoretical Understanding of the XYZ Mesons from QCD," *EPJ Web Conf.* **113** (2016) 01015, `arXiv:1512.04497 [hep-ph]`.

[68] A. E. Bondar, A. Garmash, A. I. Milstein, R. Mizuk, and M. B. Voloshin, "Heavy quark spin structure in z_b resonances," *Phys. Rev. D* **84** (2011) 054010.

[69] **Belle Collaboration** Collaboration, A. Garmash *et al.*, "Observation of $Z_b(10610)$ and $Z_b(10650)$ decaying to b mesons," *Phys. Rev. Lett.* **116** (2016) 212001.

[70] **Belle** Collaboration, I. Adachi, "Observation of two charged bottomonium-like resonances," in *Flavor physics and CP violation. Proceedings, 9th International Conference, FPCP 2011, Maale HaChamisha, Israel, May 23-27, 2011*. 2011. `arXiv:1105.4583 [hep-ex]`.

[71] S. Ohkoda, Y. Yamaguchi, S. Yasui, and A. Hosaka, "Decays and productions via bottomonium for Z_b resonances and other B anti-B molecules," *Phys. Rev.* **D86** (2012) 117502, `arXiv:1210.3170 [hep-ph]`.

[72] F. Schwabl, *Quantenmechanik (QM I):*. Springer-Lehrbuch. Springer, 2002.

[73] **CP-PACS** Collaboration, S. Aoki *et al.*, "Lattice QCD Calculation of the rho Meson Decay Width," *Phys. Rev.* **D76** (2007) 094506, `arXiv:0708.3705 [hep-lat]`.

[74] **QCDSF** Collaboration, G. Bali and M. Hetzenegger, "Static-light meson-meson potentials," *PoS* **LATTICE2010** (2010) 142, `arXiv:1011.0571 [hep-lat]`.

[75] J. l. Ballot and J. M. Richard, "FOUR QUARK STATES IN ADDITIVE POTENTIALS," *Phys. Lett.* **B123** (1983) 449–451.

[76] M. Born and R. Oppenheimer, "Zur quantentheorie der molekeln," *Annalen der Physik* **389** no. 20, (1927) 457–484.

[77] N. Brambilla, X. Garcia i Tormo, J. Soto, and A. Vairo, "Erratum: Precision determination of $r_0\Lambda_{\overline{ms}}$ from the qcd static energy," *Phys. Rev. Lett.* **108** (2012) 269903.

[78] Z. S. Brown and K. Orginos, "Tetraquark bound states in the heavy-light heavy-light system," *Phys. Rev.* **D86** (2012) 114506, `arXiv:1210.1953 [hep-lat]`.

[79] M. S. Cook and H. R. Fiebig, "A Lattice study of interaction mechanisms in a heavy light meson meson system," `arXiv:hep-lat/0210054 [hep-lat]`.

[80] A. De Rújula, H. Georgi, and S. L. Glashow, "Hadron masses in a gauge theory," *Phys. Rev. D* **12** (Jul, 1975) 147–162.

[81] **ALPHA** Collaboration, M. Della Morte *et al.*, "Lattice HQET with exponentially improved statistical precision," *Phys. Lett.* **B581** (2004) 93–98, `arXiv:hep-lat/0307021 [hep-lat]`. [Erratum: Phys. Lett.B612,313(2005)].

[82] M. Della Morte, A. Shindler, and R. Sommer, "On lattice actions for static quarks," *JHEP* **08** (2005) 051, `arXiv:hep-lat/0506008 [hep-lat]`.

[83] W. Detmold, K. Orginos, and M. J. Savage, "BB Potentials in Quenched Lattice QCD," *Phys. Rev.* **D76** (2007) 114503, `arXiv:hep-lat/0703009 [HEP-LAT]`.

[84] T. Doi, T. T. Takahashi, and H. Suganuma, "Meson-meson and meson-baryon interactions in lattice QCD," *AIP Conf. Proc.* **842** (2006) 246–248, `arXiv:hep-lat/0601008 [hep-lat]`.

[85] C. E. Dreyer, A. Janotti, C. G. Van de Walle, and D. Vanderbilt, "Correct implementation of polarization constants in wurtzite materials and impact on iii-nitrides," *Phys. Rev. X* **6** (2016) 021038.

[86] S. Godfrey and N. Isgur, "Mesons in a relativized quark model with chromodynamics," *Phys. Rev. D* **32** (Jul, 1985) 189–231.

[87] A. Hasenfratz and F. Knechtli, "Flavor symmetry and the static potential with hypercubic blocking," *Phys. Rev.* **D64** (2001) 034504, `arXiv:hep-lat/0103029 [hep-lat]`.

[88] **ETM** Collaboration, K. Jansen, C. Michael, A. Shindler, and M. Wagner, "The Static-light meson spectrum from twisted mass lattice QCD," *JHEP* **12** (2008) 058, `arXiv:0810.1843 [hep-lat]`.

[89] M. Lüscher, "Volume dependence of the energy spectrum in massive quantum field theories," *Communications in Mathematical Physics* **105** no. 2, (1986) 153–188.

[90] C. B. Lang, D. Mohler, S. Prelovsek, and M. Vidmar, "Coupled channel analysis of the rho meson decay in lattice QCD," *Phys. Rev.* **D84** no. 5, (2011) 054503, `arXiv:1105.5636 [hep-lat]`. [Erratum: Phys. Rev.D89,no.5,059903(2014)].

[91] M. Lüscher and P. Weisz, "Quark confinement and the bosonic string," *JHEP* **07** (2002) 049, `arXiv:hep-lat/0207003 [hep-lat]`.

[92] **UKQCD** Collaboration, C. Michael and P. Pennanen, "Two heavy - light mesons on a lattice," *Phys. Rev.* **D60** (1999) 054012, `arXiv:hep-lat/9901007 [hep-lat]`.

[93] **ETM** Collaboration, C. Michael, A. Shindler, and M. Wagner, "The continuum limit of the static-light meson spectrum," *JHEP* **08** (2010) 009, arXiv:1004.4235 [hep-lat].

[94] C. Stewart and R. Koniuk, "Hadronic molecules in lattice QCD," *Phys. Rev.* **D57** (1998) 5581–5585, arXiv:hep-lat/9803003 [hep-lat].

[95] K. Symanzik, *Some topics in quantum field theory*, pp. 47–58. Springer Berlin Heidelberg, Berlin, Heidelberg, 1982.

[96] K. Symanzik, "Continuum Limit and Improved Action in Lattice Theories. 1. Principles and phi**4 Theory," *Nucl. Phys.* **B226** (1983) 187–204.

[97] B. Wagenbach, P. Bicudo, and M. Wagner, "Lattice investigation of heavy meson interactions," *J. Phys. Conf. Ser.* **599** no. 1, (2015) 012006, arXiv:1411.2453 [hep-lat].

[98] P. Weisz, "Continuum Limit Improved Lattice Action for Pure Yang-Mills Theory. 1.," *Nucl. Phys.* **B212** (1983) 1–17.

Acknowledgment

Curriculum Vitae

Personal information

Name: Antje Katharine Peters

E-Mail: peters@th.physik.uni- frankfurt.de

Date of birth: November 11, 1990

Place of birth: Westerland (Sylt)

Web page: `http://th.physik.uni-frankfurt.de/~peters/`

Education

April 2016 Research stay at the University of Arizona with Prof. Stefan Meinel

March 2016 Research stay at the Massachusetts Institute of Technology with Prof. William Detmold

since April 2014 PhD studies, Institut für Theoretische Physik, Goethe-Universität Frankfurt am Main, Supervisor: Prof. M. Wagner

September 2014 Bachelor's thesis (computer science),Title: *Das Aufzählungsproblem fur Anfragen erster Stufe auf Strukturen von beschränktem Grad*, Supervisor: Prof. N. Schweikardt

March 2014 Master's thesis, Title: *Determination of from the static quark-antiquark potential in momentum space*, Supervisor: Prof. M. Wagner

April 2013 − September 2014 Study of computer science, Goethe-Universität Frankfurt am Main

September 2012 Bachelor's thesis, Title: *Baryonische Zweikörperzerfälle im erweiterten linearen Sigma-Modell*, Supervisor: Prof. D. H. Rischke

October 2011 − January 2012 Study of physics, Università degli Studi di Catania, Catania/Italy

October 2010 − March 2014 Study of physics, Goethe-Universität Frankfurt am Main

September 2009 − September 2010 Study of physics, Rheinisch-Westfälische Technische Hochschule Aachen

June 2009 Abitur

July 2001 − July 2009 Gymnasium Sylt, Westerland (skipped year 9)

Publications and Conference proceedings

- P. Bicudo, M. Cardoso, A. Peters, M. Pflaumer and M. Wagner, "$ud\bar{b}\bar{b}$ tetraquark resonances with lattice QCD potentials and the Born-Oppenheimer approximation," [arXiv:1704.02383 [hep-lat]].

- A. Peters, P. Bicudo, L. Leskovec, S. Meinel and M. Wagner, "Lattice QCD study of heavy-heavy-light-light tetraquark candidates," PoS(LATTICE2016) 104 [arXiv:1609.00181 [hep-lat]].

- A. Peters, P. Bicudo, K. Cichy and M. Wagner, "Investigation of $B\bar{B}$ four-quark systems using lattice QCD," J. Phys. Conf. Ser. 742 (2016) no.1, 012006 [arXiv:1602.07621 [hep-lat]].

- P. Bicudo, K. Cichy, A. Peters and M. Wagner, "BB interactions with static bottom quarks from Lattice QCD," Phys. Rev. D **93** (2016) no.3, 034501 [arXiv:1510.03441 [hep-lat]].

- A. Peters, P. Bicudo, K. Cichy, B. Wagenbach and M. Wagner, "Exploring possibly existing $qq\bar{b}\bar{b}$ tetraquark states with $qq = ud, ss, cc$," PoS LATTICE **2015** (2016) 095 [arXiv:1508.00343 [hep-lat]].

- P. Bicudo, K. Cichy, A. Peters, B. Wagenbach and M. Wagner, "Evidence for the existence of $ud\bar{b}\bar{b}$ and the non-existence of $ss\bar{b}\bar{b}$ and $cc\bar{b}\bar{b}$ tetraquarks from lattice QCD,' Phys. Rev. D **92** (2015) no.1, 014507 [arXiv:1505.00613 [hep-lat]].

- F. Karbstein, A. Peters and M. Wagner, "$\Lambda_{\overline{\text{MS}}}^{(n_f=2)}$ from a momentum space analysis of the quark-antiquark static potential," JHEP **1409** (2014) 114 [arXiv:1407.7503 [hep-ph]].

- W. I. Eshraim, S. Janowski, A. Peters, K. Neuschwander and F. Giacosa, "Interaction of the pseudoscalar glueball with (pseudo)scalar mesons and nucleons," Acta Phys. Polon. Supp. **5** (2012) 1101 [arXiv:1209.3976 [hep-ph]].

Presentations

- *Lattice studies of heavy-light four-quark systems*, invited talk, Bergische Universität Wuppertal (Germany), May 2017

- *Lattice studies of tetraquark systems*, invited talk at the Effective Field Theory Seminar, Technische Universität München, Garching (Germany), January 2017,

- *Effective theories for heavy quarks: nonrelativistic QCD (NRQCD)*, Lattice Seminar, Goethe-Universität Frankfurt am Main (Germany), January 2017

- *Tetraquarks on the lattice*, Seminar on Theoretical Hadron Physics, Justus-Liebig-Universität Gießen (Germany), November 2016,

- *Lattice QCD study of heavy-heavy-light-light tetraquark candidates*, 34th International Symposium on Lattice Field Theory, Southampton (UK), July 2016

- *Lattice QCD investigation of BB and $B\bar{B}$ four-quark systems*, invited talk at the 11th International Workshop on Heavy Quarkonium, The Pacific Northwest National Laboratory, Richland (USA), June 2016

- *Investigation of BB and $B\bar{B}$ four-quark systems by means of lattice QCD*, Particle and Nuclear Theory seminar, University of Arizona, Tucson (USA), March 2016

- *Investigation of BB and $B\bar{B}$ four-quark systems by means of lattice QCD*, Lattice Club, Massachusetts Institute of Technology, Cambridge (USA), March 2016

- *BB and $B\bar{B}$ four-quark systems from lattice QCD*, Workshop for young scientists with research interests focused on physics at FAIR (FAIRNESS 2016), Garmisch-Partenkirchen (Germany), February 2016

- *Exploring possibly existing BB and $B\bar{B}$ tetraquark states by means of lattice QCD*, 8th Odense Winter School on Theoretical Physics, Odense (Denmark), November 2015

- *Exploring possibly existing $qq\bar{b}\bar{b}$ states with $qq = ud, ss, cc$*, 33rd International Symposium on Lattice Field Theory, Kobe (Japan), July 2015

- *Determination of $\Lambda_{\overline{MS}}$ from the static potential in momentum space*, 574. Wilhelm and Else Heraeus-Seminar "Strong Interactions in the LHC Era", Bad Honnef (Germany), November 2014

- *Determination of $\Lambda_{\overline{MS}}$ from the static potential for $n_f = 2$ quark flavors in momentum space*, DPG Spring Meeting, Mainz (Germany), March 2014

- *Determination of $\Lambda_{\overline{MS}}$ from the static potential in momentum space*, invited talk, Rheinische Friedrich-Wilhelms-Universität Bonn(Germany), January 2014

Teaching Experience

- SS 2017: Teaching Assistant, Höhere Quantenmechanik, Prof. Marc Wagner

- WS 2016/2017: Teaching Assistant, Theoretische Physik 3, Prof. Marc Wagner

- SS 2016: Tutor, Theoretische Physik 2, Prof. Marc Wagner

- WS 2015/2016: Tutor, Theoretische Physik 1, Prof. Marc Wagner

- SS 2015: Tutor, Mathematik für Biophysiker, Dr. Joachim Reinhardt

- WS 2014/2015: Tutor, Theoretische Physik 5, Prof. Owe Philipsen

- WS 2012/2013: Tutor, Theoretische Physik 1, Prof. Carsten Greiner

- SS 2012: Tutor, Mathematik für Biophysiker, Dr. Francesco Giacosa